Université de Nice-Sophia Antipolis - UFR Sciences

École Doctorale en Sciences Fondamentales et Appliquées

THESE

Pour obtenir le titre de

Docteur en Sciences

de l'Université de Nice-Sophia Antipolis

Spécialité: MATHÉMATIQUES APPLIQUÉES

Présentée et soutenue par

Maria Laura DELLE MONACHE

Lois de conservation pour la modélisation du trafic routier

(Traffic flow modeling by conservation laws)

Thèse dirigée par Paola GOATIN
soutenue le 18 Septembre 2014

JURY:

M. Florent Berthelin	MDC HDR, UNS	Examinateur
M. Christophe Chalons	Professeur, UVSQ	Examinateur
M. Rinaldo M. Colombo	Professeur, U. de Brescia	Rapporteur
Mme. Paola Goatin	CR HDR, Inria	Dir. de thèse
Mme. Simone Göttlich	Professeur, U. de Mannheim	Rapporteur
M. Jean-Patrick Lebacque	Ingénieur ENPC	Examinateur

To my grandparents
and to my family

Acknowledgments

First of all, I would like to show my gratitude to my supervisor, Paola Goatin. I could not have wished for a better guidance. She was supportive and enthusiastic. She provided me with encouragement, help and advice. I express my gratitude to Rinaldo M. Colombo and Simone Göttlich for accepting to be the reviewers of my manuscript, for the time they devoted me and their advice and suggestions. I thank, also, Florent Berthelin, Christophe Chalons and Jean-Patrick Lebacque for accepting to be part of the jury.

I would like to thank all Opale project-team at Inria for making me feel like home and the "coffee-break/sport" gang: Fatima, Cédric, Marco, Laure, Matteo, Hubert, Montserrat, Matthias and José. They made those three years I spent there remarkable. I am grateful to all the people that welcomed me at UC Berkeley. A special thanks to Professor A. Bayen, who kindly advised and assisted me and to Jack, Samitha, Walid, Tim and Luis for their precious help. Big thanks to Catherine to have welcomed me into her house and her family.

A very big and special thanks goes to my friend Jeaniffer for standing me in my crisis times, keeping me company, helping me and making me feel constantly her support. A heartfelt thanks to my big extended family and to my long life friends, Stefano, Marco, Mariagrazia, Flavia, Silvia and Chiara. Without their support and their comprehension all of this would not have been possible.

At last, I would like to dedicate this work to my parents and my brother, Marco. I thank them for giving me the chances to pursuit my ideas and for making me feel always their support. They are the essence and the driving force of everything I do.

This research was supported by the European Research Council under the European Union's Seventh Framework Program (FP/2007-2013) / ERC Grant Agreement n. 257661.

Abstract

In this thesis we consider two coupled PDE-ODE models. One to model moving bottlenecks and the other one to describe traffic flow at junctions.
First of all, we consider a strongly coupled PDE-ODE system that describes the influence of a slow and large vehicle on road traffic. The model consists of a scalar conservation law accounting for the main traffic evolution, while the trajectory of the slower vehicle is given by an ODE depending on the downstream traffic density. The moving constraint is expressed by an inequality on the flux, which models the bottleneck created in the road by the presence of the slower vehicle. We prove the existence of solutions to the Cauchy problem for initial data of bounded variation. Moreover, two numerical schemes are proposed. The first one is a finite volume algorithm that uses a locally nonuniform moving mesh that tracks the slower vehicle position. The second one uses a reconstruction technique to display the behavior of the vehicle. Some numerical tests are shown.
Next, we consider the Lighthill-Whitham-Richards traffic flow model on a junction composed by one mainline, an onramp and an offramp, which are connected by a node. The onramp dynamics is modeled using an ordinary differential equation describing the evolution of the queue length. The definition of the solution of the Riemann problem at the junction is based on an optimization problem and the use of a right of way parameter. The numerical approximation is carried out using a Godunov scheme, modified to take into account the effects of the onramp buffer. We present the result of some simulations and check numerically the convergence of the method. Moreover, after suitable modification, the model is used to solve an optimal control problem on roundabouts. Two cost functionals (*total travel time* and *total waiting time*) are numerically optimized with respect to the right of way parameter.

Keywords: *Traffic flow modeling, Conservation laws, Finite volume methods, Road traffic on networks, Macroscopic models*

Résumé

Les modèles hydrodynamiques ont été fréquemment utilisé dans la littérature pour décrire l'évolution macroscopique de la densité du trafic routier et ont été généralisés avec succès aux réseaux au cours des dernières années. Dans les années 1950, Lighthill et Whitham [111] et Richards [127], indépendamment, ont proposé un modèle de dynamique des fluides pour le trafic routier sur une route unique infinie, en utilisant une équation aux dérivées partielles hyperbolique non linéaire (EDP). Ensuite, la formulation du problème de Cauchy a été étendue avec succès aux problèmes aux limites en [11], puis développée spécifiquement pour les lois de conservation scalaires avec flux concave dans [102]. Plus récemment, plusieurs auteurs ont inclu plus de fonctionnalités dans les modèles. En particulier, certains modèles proposés permettent de décrire le mouvement d'un seul véhicule dans la circulation routière. Dans ces modèles, la trajectoire du véhicule spécifique est décrite par un équation aux dérivées ordinaires (EDO) produisant des modèles couplés EDP-EDO.

Dans cette thèse, nous considérons deux modèles EDP-EDO couplés: un pour modéliser des goulots d'étranglement mobiles et l'autre pour décrire la distribution du trafic sur une rampe d'accès.

Le premier modèle a été introduit pour décrire le mouvement d'un poids lourd ou un bus, qui roule à une vitesse inférieure à celle des autres voitures, en réduisant la capacité de la route et générant ainsi un goulot d'étranglement.
On peut modéliser cette situation d'un point de vue macroscopique par le système suivant:

$$\begin{cases} \partial_t \rho + \partial_x f(\rho) = 0, & (t,x) \in \mathbb{R}^+ \times \mathbb{R}, \\ \rho(0,x) = \rho_o(x), & x \in \mathbb{R}, \\ f(\rho(t,y(t))) - \dot{y}(t)\rho(t,y(t)) \leq \dfrac{\alpha \rho_{\max}}{4V}(V - \dot{y}(t))^2 & t \in \mathbb{R}^+, \\ \dot{y}(t) = \omega(\rho(t,y(t)+)), & t \in \mathbb{R}^+, \\ y(0) = y_o. \end{cases} \tag{CP1}$$

L'EDP est une loi de conservation scalaire avec une contrainte mobile sur le flux et l'EDO décrit la trajectoire du véhicule plus lent. L'inconnue $\rho(t,x) \in [0, \rho_{\max}]$ représente la quantité scalaire conservée, à savoir la densité moyenne des voitures circulant sur la route. La fonction flux $f : [0, \rho_{\max}] \to \mathbb{R}^+$ est une fonction strictement concave avec $f(0) = f(\rho_{\max}) = 0$. Elle est donnée par la formule $f(\rho) = \rho v(\rho)$, où $v(\rho) = V(1 - \frac{\rho}{\rho_{\max}})$ est la vitesse moyenne des véhicules et V est la leur vitesse maximale. La variable y dénote la position du bus, qui se déplace à une vitesse qui dépend du trafic environnant, c'est-à-dire que le bus se déplace avec une vitesse constante V_b tant qu'il n'est pas ralenti par les conditions de circulation en aval. Lorsque cela se produit, il se déplace à la vitesse moyenne des véhicules. Cela peut être modélisé par la définition suivante de la vitesse

$$\omega(\rho) = \begin{cases} V_b & \text{si } \rho \leq \rho^* \doteq \rho_{\max}(1 - \frac{V_b}{V}), \\ v(\rho) & \text{autrement}, \end{cases} \tag{V}$$

A son tour, la circulation est modifiée par la présence du véhicule plus lent. En particulier, $\alpha \in]0,1[$ est le taux de réduction de la capacité de la route dû à la présence du bus. Il y

a donc un couplage fort entre l'EDP et l'EDO.
Le modèle (CP1) a été introduit dans [75] pour modéliser l'effet des moyens de transport en commun, comme le bus, dans un réseau routier. Des autres modèles macroscopiques pour les goulots d'étranglement mobiles ont été récemment proposé par [15, 69, 100]. Par rapport à ces approches, notre modèle propose une définition plus réaliste de la vitesse du véhicule lent et une description de son impact sur les conditions de circulation qui est plus simple à traiter du point de vue analytique et numérique.
Du point de vue analytique, le modèle que nous proposons peut être vu comme une généralisation aux contraintes mobile du problème consistant en une loi de conservation scalaire avec contrainte (fixée dans l'espace) sur le flux, introduit et étudié dans [3, 37, 43]. L'étude des systèmes couplés EDP-EDO n'est pas nouvelle dans le cadre des lois de conservation, nous renvoyons le lecteur à [29, 14, 46, 100]. Néanmoins, le problème posé ici est légèrement différent. D'un côté, nous traitons un couplage fort dans l'EDP et l'EDO lequel s'affectent mutuellement, contrairement à [29, 46] oú la solution de l'EDP ne dépende pas de l'EDO. De l'autre côté, même si le terme droit de l'EDO est discontinu, la définition spécifique du modèle nous permet de considérer des solutions classiques au sens de Carathéodory au lieu des solutions généralisées au sens de Filippov.
En outre, dans notre cas, la présence de la contrainte qui se déplace en fonction des conditions de circulation environnantes, génère des ondes des chocs non-classique, c'est-à-dire des chocs qui satisfont la condition de Rankine-Hugoniot mais qui ne respectent pas la condition d'admissibilité de Lax.
Nous présenterons un résultat d'existence des solutions du modèle (CP1), obtenu par la méthode d'approximation de suivi des fronts, et nous montrerons des simulations numériques obtenues avec une méthode "front/capturing" et une méthode basée sur une technique de reconstruction des ondes de chocs. Dans le premier cas, les résultats sont obtenus par la combinaison d'un algorithme de suivi dans les coordonnées de Lagrange, qui utilise un maillage localement non-uniforme comme dans [131], et un algorithme de suivi qui calcule la position de bus en prenant en compte son interaction avec les ondes de densité comme dans [33]. En particulier, nous allons décaler les points du maillage prés du bus et, par conséquent, nous aurons un maillage localement non uniforme parce que la seule cellule qui se modifie avec la trajectoire de bus est la cellule qui contient le bus.
Le deuxième schéma présenté utilise une technique de reconstruction effectué dans chaque cellule de calcul pouvant contenir un choc classique ou non classique comme dans [17], et un algorithme de suivi (comme celui de [33]) qui suit à chaque pas de temps la position de l'autobus. Nous comparons aussi les deux méthodes.

Dans la deuxième partie, nous introduisons un nouveau modèle macroscopique de jonction pour les bretelles d'autoroute et une discrétisation de Godunov du modèle pour le contrôle de l'accès. Nous considérons le modèle de trafic de Lighthill-Whitham-Richards sur une jonction composée par une voie principale, une bretelle d'accès et une bretelle de sortie, toutes reliées par un noeud.
Une loi de conservation hyperbolique scalaire décrit l'évolution de la densité des véhicules sur la voie principale et une équation ordinaire différentielle décrit l'évolution de la

longueur de la file d'attente sur la bretelle d'accès, qui est modélisée par un "buffer" à fin de s'assurer que les conditions aux limites soient satisfaites au sens fort:

$$\begin{cases} \partial_t \rho_i + \partial_x f(\rho_i) = 0, & (t,x) \in \mathbb{R}^+ \times I_i,\ i = 1,2 \\ \dfrac{dl(t)}{dt} = F_{\text{in}}(t) - \gamma_{\text{r1}}(t), & t \in \mathbb{R}^+, \\ \rho_i(0,x) = \rho_{i,0}(x), & \text{sur } I_i,\ i = 1,2 \\ l(0) = l_0, \end{cases} \tag{CP2}$$

où I_i, $i = 1,2$ sont les segments sortant et entrant de la voie principale et le flux est $f(\rho) = \rho v(\rho)$, où $v(\rho) = 1 - \rho$ est la vitesse moyenne des véhicules. La variable l dénote la longueur de la file d'attente, $F_{\text{in}}(t)$ et $\gamma_{\text{r1}}(t)$ sont, respectivement, les flux entrant et sortant de la bretelle d'accès, $\rho_{i,0}(x)$ et $l_0 \in [0, +\infty[$ sont les conditions initiales. Le système (CP2) est couplé avec un problème d'optimisation à niveau des jonctions, qui donne la répartition du trafic entre les routes. À chaque jonction, nous définissons la demande de la bretelle d'accès $d(F_{\text{in}}, l)$, la fonction demande sur la voie principale entrante $\delta(\rho_1)$ et la fonction d'offre sur le segment de voie principale sortante $\sigma(\rho_2)$ de la manière suivante:

$$d(F_{\text{in}}, l) = \begin{cases} \gamma_{\text{r1}}^{\max} & \text{si } l(t) > 0, \\ \min\left(F_{\text{in}}(t), \gamma_{\text{r1}}^{\max}\right) & \text{si } l(t) = 0, \end{cases} \tag{0.0.1}$$

$$\delta(\rho_1) = \begin{cases} f(\rho_1) & \text{si } 0 \le \rho_1 < \rho_{\text{cr}}, \\ f^{\max} & \text{si } \rho_{\text{cr}} \le \rho_1 \le 1, \end{cases} \tag{0.0.2}$$

$$\sigma(\rho_2) = \begin{cases} f^{\max} & \text{si } 0 \le \rho_2 \le \rho_{\text{cr}}, \\ f(\rho_2) & \text{si } \rho_{\text{cr}} < \rho_2 \le 1, \end{cases} \tag{0.0.3}$$

où $\gamma_{\text{r1}}^{\max}$ est le débit maximal sur la bretelle d'accès et $f^{\max} = f(\rho_{\text{cr}})$ est le flux maximal sur I_1 et I_2. Nous introduisons aussi le paramètre $\beta \in [0,1]$ qui représente, le taux de sortie de la bretelle de sortie et le flux correspondant $\gamma_{\text{r2}}(t) = \beta f(\rho_1(t, 0-))$. La définition de la solution du problème de Riemann à la jonction est basée sur la résolution d'un problème d'optimisation linéaire et sur l'utilisation d'un paramètre de priorité. Nous démontrons l'existence et l'unicité de la solution du problème de Riemann correspondant. Contrairement à [41], où le flux à travers la jonction est maximisé, notre optimisation linéaire consiste à maximiser le flux sur la voie principale sortante. La bretelle de sortie est traité comme un puits, et le paramètre de priorité est introduit pour assurer l'unicité de la solution. Nous faisons le choix de satisfaire la priorité de façon approximative, c'est à dire, la priorité ne sera pas toujours respectée, au profit de la maximisation du flux. De plus, la présence du "buffer" peut créer des ondes supplémentaires à la jonction qui apparaissent lorsque la file d'attente se vide. Cet effet est observé aussi dans les modèles qui décrivent les chaînes d'approvisionnement et doit être prise en compte pour les simulations numériques

Ensuite, ce modèle est étendu aux réseaux et discrétisé en utilisant un schéma de Godunov qui prend en compte les effets du "buffer" de la bretelle d'accès. En particulier, nous modifions de manière appropriée le schéma de Godunov pour inclure les conditions aux limites à la jonction, comme dans [32, 48], et l'ODE décrivant la file d'attente.

Cela permet de tenir compte de la création éventuelle d'un choc supplémentaire lorsque le "buffer" se vide. Nous montrons des approximations numériques de solutions, qui peuvent être discontinues, obtenues utilisant ce modèle. Le schéma donne des approximations numériques précises, comme le montrent les tests numériques. En suite, ce modèle discrétisé a été utilisé pour des problèmes de contrôle d'accès sur l'autoroute. En particulier, le problème d'optimisation est résolu en utilisant la méthode de l'adjoint discret.

Enfin, nous présentons un modèle d'optimisation de la circulation sur les ronds-points. Les ronds-points peuvent être considérés comme des réseaux routiers particuliers et ils peuvent être modélisés comme une concaténation de jonctions. Nous référons au modèle (CP2) et nous l'appliquons au ronds-points. Chaque jonction est décrite par un système couplé EDP - EDO. Nous nous concentrons sur un rond-point avec trois routes entrantes et trois sortantes. Chaque entrée et sortie du rond-point peut être modélisée comme une jonction 2×2 où le cercle du rond-point est la voie principale. En particulier, chaque jonction a une voie principale entrante et une sortante et une troisième route avec des flux entrants et sortants. Cette dernière est modélisée avec un "buffer" de capacité infinie pour le flux entrant et un puits infini pour le flux sortant. L'évolution de la voie principale est décrite par une loi de conservation scalaire, tandis que la dynamique du "buffer" est décrite avec une EDO qui dépend de la différence entre le flux entrant et sortant sur la troisième voie. A chaque jonction le problème de Riemann est résolu uniquement en utilisant un paramètre de priorité et les solutions sont construites par la méthode de suivi des fronts. Nous visons à réduire au minimum le temps total de parcours des voitures sur le réseau (TTT) et le temps d'attente à l'entrée (TWT), qui sont définis comme suit:

$$\begin{aligned} TTT(T,\vec{P}) = &\sum_{i=1}^{3} \int_0^T \int_{I_i} \rho(t,x)dxdt + \sum_{i=1}^{3} \int_0^T l_i(t)dt + \\ &T \cdot \sum_{i=1}^{3} \int_{I_i} \rho(T,x)dx + T \cdot \sum_{i=1}^{3} l_i(T), \end{aligned} \tag{TTT}$$

$$TWT(T,\vec{P}) = \sum_{i=1}^{3} \int_0^T l_i(t)dt + T \cdot l_i(T), \tag{TWT}$$

où P est le paramètre de priorité et $T > 0$ le temps final. Ces fonctions coût sont optimisées pour un réseau simple composé d'une seule jonction de type 2×2. Une expression analytique des fonctions coût est obtenue et l'optimisation est faite par rapport au paramètre de priorité. Puis, à travers des simulations, le comportement du trafic pour le rond-point complet est étudié. Nous distinguons différents cas de simulations qui varient en fonction de la valeur de F_{in} et de β. Vu les expressions compliquées des fonctions coût, il est difficile d'utiliser une approche analytique pour la mise au point d'un algorithme optimisé pour tout le rond-point. Pour cette raison, nous considérons à chaque jonction et à chaque pas de temps les paramètres optimaux correspondant aux densités de la route près de la jonction. La technique pour le calcul du cas optimal est basée sur l'optimisation locale de chaque jonction de type 2×2, qui forment le rond-point.

Les résultats de ces simulations sont ensuite comparés à ceux obtenus en supposant que le paramètre de priorité soit maintenu fixé pour chaque jonction.

Mots clés: *Modèles de trafic, Lois de conservation, Méthodes des volumes finis, Trafic routier sur réseaux, Modèles macroscopiques*

Contents

Introduction **1**

1 Preliminaries **9**
1.1 Hyperbolic conservation laws . . . 10
1.1.1 Weak solution . . . 10
1.1.2 Riemann Problem . . . 13
1.1.3 Function with bounded variation . . . 15
1.1.4 Wave-front tracking method . . . 16
1.2 Traffic flow modeling . . . 18
1.2.1 LWR model . . . 18
1.2.2 Traffic flow on a road network . . . 19
1.2.3 Bottlenecks and coupled micro-macro models . . . 26
1.3 Numerical methods for hyperbolic conservation laws and traffic flow . . . 29
1.3.1 Godunov scheme . . . 30
1.3.2 Godunov scheme on road networks . . . 31
1.3.3 Numerical methods for non-classical shocks . . . 32
1.3.4 Numerical methods for coupled PDE-ODE models . . . 34

I Modeling of a moving bottleneck **35**

2 A strongly coupled PDE-ODE model with moving constraints **37**
2.1 Mathematical model . . . 38
2.2 The Riemann problem with moving density constraint . . . 42
2.3 The Cauchy problem: existence of solutions . . . 43
2.3.1 Wave-front tracking . . . 44
2.3.2 Bounds on the total variation . . . 45
2.3.3 Convergence of approximate solutions . . . 48
2.4 An approach to the stability of the solutions . . . 50
2.4.1 Estimates on shifts . . . 51
2.5 A front tracking algorithm . . . 57
2.5.1 Godunov-type scheme for hyperbolic PDEs with constraint . . . 57
2.5.2 Numerical method for the ODE . . . 60

2.6 A conservative scheme with reconstruction of non-classical and classical shocks . . . 60
2.7 Numerical results . . . 63

II Modeling of junctions using a PDE-ODE approach 71

3 An application to ramp-metering 73
3.1 Introduction . . . 74
3.2 Fundamental definitions and notations . . . 74
3.3 Riemann problem . . . 77
3.4 Numerical results: modified Godunov . . . 86
3.4.1 Boundary conditions and conditions at the junctions . . . 87
3.4.2 ODE treatment . . . 88
3.4.3 Modified Godunov scheme . . . 88
3.5 Numerical results . . . 89
3.6 Discrete adjoint method for optimization . . . 91

4 An application to roundabouts 97
4.1 Introduction . . . 98
4.2 Mathematical model . . . 98
4.3 Riemann problem at the junction . . . 101
4.4 Optimization on networks . . . 102
4.4.1 $\Gamma_2 = (1-\beta)\delta(\hat{\rho}_1) + d(F_{\text{in}}, l)$ . . . 103
4.4.2 $\Gamma_2 = \sigma(\hat{\rho}_2)$ . . . 108
4.4.3 Local Total Waiting Time and Total Travel Time . . . 113
4.5 Numerical scheme . . . 119
4.5.1 Network topology . . . 119
4.5.2 Numerical scheme . . . 119
4.6 Numerical simulations . . . 120
4.6.1 Simulation results . . . 121

5 Conclusions and perspectives 129

Bibliography 133

List of Figures

1.1.1 Conservation of flux . . . 10
1.1.2 Intersection of characteristics . . . 11
1.1.3 Admissibility for Lax entropy condition . . . 13
1.1.4 An example of rarefaction wave . . . 14
1.1.5 An example of shock wave . . . 15
1.1.6 Wave front tracking up to the first time of interaction . . . 17
1.2.1 Speed of cars: linear decreasing function . . . 19
1.2.2 Fundamental diagram . . . 19
1.2.3 An example of road network . . . 20
1.2.4 An example of a graph representing a road junction . . . 21
1.2.5 Fundamental diagram considered in [41] . . . 21
1.2.6 An example of junction represented with a buffer . . . 25
1.2.7 Fundamental diagram considered in [43] . . . 27
1.2.8 An example of a mollifier for the model introduced in [100] . . . 28
1.3.1 Illustration of the finite volume in the $x-t$ plane . . . 31

2.1.1 A typical example of flux function for traffic flow with several lanes . . . 39
2.1.2 Bus and cars speed . . . 40
2.1.3 Moving bottleneck . . . 40
2.1.4 Flux functions for $\dot{y} = V_b$ . . . 41
2.3.1 Interaction between two waves away from the bus trajectory . . . 46
2.3.2 Interaction between a wave and the bus trajectory . . . 47
2.3.3 Interaction between a shock and the bus trajectory . . . 47
2.3.4 Interaction between a rarefaction and the bus trajectory . . . 48
2.4.1 Changes of ξ_b across a discontinuity in $w = \omega(\rho^n)$ . . . 52
2.4.2 Case I: interaction with a shock . . . 53
2.4.3 Case II: Interaction with a rarefaction . . . 55
2.5.1 Local shifting of a grid point when $\left|x^n_{m+\frac{1}{2}} - y^n\right| > \frac{h^n_m}{2}$ . . . 58
2.5.2 Local shifting of a grid point when $\left|x^n_{m+\frac{1}{2}} - y^n\right| \leq \frac{h^n_m}{2}$ . . . 59
2.5.3 Nonuniform finite volume cells . . . 59
2.6.1 Reconstruction of a non-classical shock . . . 62

2.7.1 Evolution of the density at different times corresponding to initial data (2.7.2) and a mesh grid of 500 points . . . 66
2.7.2 Density and bus trajectory in a $x-t$ plane corresponding to initial data (2.7.2) and a mesh grid of 500 points . . . 66
2.7.3 Evolution of the density at different times corresponding to initial data (2.7.3) and a mesh grid of 500 points . . . 67
2.7.4 Density and bus trajectory in a $x-t$ plane corresponding to initial data (2.7.3) and a mesh grid of 500 points . . . 67
2.7.5 Evolution of the density at different times corresponding to initial data (2.7.4) and a mesh grid of 500 points . . . 68
2.7.6 Density and bus trajectory in a $x-t$ plane corresponding to initial data (2.7.4) and a mesh grid of 500 points . . . 68
2.7.7 Evolution of the density at different times corresponding to initial data (2.7.5) and a mesh grid of 500 points . . . 69
2.7.8 Density and bus trajectory in a $x-t$ plane corresponding to initial data (2.7.5) and a mesh grid of 500 points . . . 69
2.7.9 $\mathcal{L}^1$ convergence. . . . 70

3.2.1 Junction modeled . . . 75
3.2.2 Flux function of equation (3.2.1) . . . 75
3.3.1 Solutions of the Riemann Solver at the junction . . . 79
3.3.2 Solution of the Riemann Problem . . . 80
3.3.3 Instantaneous evolution of the demand in the Riemann problem (incoming road) . . . 82
3.3.4 Instantaneous evolution of the supply in the Riemann problem (outgoing road) . . . 83
3.3.5 Supply constrained junction problems . . . 84
3.3.6 Demand constrained junction problem . . . 85
3.3.7 Comparison between Coclite-Garavello-Piccoli model [41] and our model 86
3.4.1 Junction in the case of emptying buffer . . . 89
3.5.1 Evolution in time of the density in the incoming mainline, on the outgoing mainline and evolution of the flux in the onramp and in the offramp, corresponding to initial data (3.5.3) and a space step discretization $\Delta x = 0.01$ . . . 90
3.5.2 Evolution in time of the density in the incoming mainline, on the outgoing mainline and evolution of the flux in the onramp and in the offramp, corresponding to initial data (3.5.4) and a space step discretization $\Delta x = 0.01$ . . . 92
3.6.1 Triangular fundamental diagram considered in this section . . . 93
3.6.2 A junction considered in the network . . . 94

4.2.1 Sketch of the roundabout considered . . . 99
4.2.2 Detail of the network modeled . . . 99
4.2.3 Flux function considered . . . 100

4.4.1 Solution of the initial-boundary value problem for $t \in [0, t_1]$ 103
4.4.2 Solution of the junction problem for $t \in [0, t_3]$ 104
4.4.3 Solution of the junction problem for $t \in [0, t_3]$ 105
4.4.4 Relationship between P_1 and P_2 105
4.4.5 Solution for $t \in [0, t_4]$ 106
4.4.6 Solution for $t \in [0, t_3]$ in the case $\min(P_2, 1) \leq P < 1$ 107
4.4.7 Complete solution for $t \in [0, t_4]$ 108
4.4.8 Relationship between P_1 and P_2 109
4.4.9 Solution of the problem in $[0, t_5]$ 110
4.4.10 Solution for $t \in [0, t_5]$ with $\bar{P} \leq P \leq P_2$ 110
4.4.11 Solution in the case $P \geq P_2$ 112
4.4.12 Solution in the case $P \leq P_1$ 112
4.4.13 Area of integration in the case $P_1 \leq P \leq P_2$ 113
4.4.14 Area of integration in the case $P_1 \leq P < \bar{P}$ 115
4.4.15 Area of integration in the case $\bar{P} \leq P \leq P_2$ 116
4.4.16 Area of integration in the case $P > P_2$ 117
4.4.17 Area of integration in the case $P < P_1$ 118
4.4.18 Area of integration when the waves collide in the region $[-1, 0]$ 119
4.6.1 TTT as a function of F_{in} computed for a time horizon $T = 50$ 122
4.6.2 TWT as a function of F_{in} computed for a time horizon $T = 50$ 123
4.6.3 TTT as a function of β computed for a time horizon $T = 50$ 124
4.6.4 TWT as a function of β computed for a time horizon $T = 50$ 125

List of Tables

2.7.1 Order of convergence for the reconstruction scheme, corresponding to initial data (2.7.2) and (2.7.3). 65

3.5.1 Errors and order of convergence for the Godunov scheme at time $T = 10$, corresponding to initial data (3.5.3) 91
3.5.2 Errors and order of convergence for the Godunov scheme at time $T = 3$, corresponding to initial data (3.5.4) 91
3.6.1 Notations for Section 3.6 93

4.6.1 Gain in TTT computed with the optimal right of way parameter and a fixed one $P = 0.7$ 121
4.6.2 Gain in TTT computed with the optimal right of way parameter and a fixed one $P = 0.4$ 121
4.6.3 Gain in TTT computed with the optimal right of way parameter and a fixed one $P = 0.2$ 126
4.6.4 Gain in TWT computed with the optimal right of way parameter and a fixed one $P = 0.7$ 126
4.6.5 Gain in TWT computed with the optimal right of way parameter and a fixed one $P = 0.4$ 126
4.6.6 Gain in TWT computed with the optimal right of way parameter and a fixed one $P = 0.2$ 127

Introduction

The aim of this thesis is to investigate some mathematical models arising in traffic flow, from both analytical and numerical points of view. Traffic is a phenomenon that is hard to model and simulate due to the difficulty of reproducing the formation and the presence of traffic jams. Several approaches have been developed during the years, each one focusing on some particular traffic characteristic. In particular, researchers have started looking at traffic for different purposes as, for example, minimization of congestion, accidents, pollution, and safety issues. There are several ways of describing traffic flow and the different methods can be summarized in three big categories: microscopic models, macroscopic models and kinetic models. Microscopic models describe the trajectory of each single car in the road with an ordinary differential equation (ODE). The basic models are the car-following ones or models based on Newton's law. The main assumption of the car-following models is that an individual car's motion only depends on the car ahead; see [10, 18, 39, 59, 70, 87, 128]. Kinetic models, instead, use Boltzmann-like equations and the main quantities describing traffic are expressed with density distribution functions; see [1, 115, 121, 123, 124]. The works in thesis refer to macroscopic models where traffic is considered as a fluid. The first ones to introduce this concept were Lighthill, Whitham [111] and independently Richards [127] in the fifties. They were the first ones to describe traffic flow with equations coming from fluid dynamics, using a non linear hyperbolic partial differential equation (PDE). The Cauchy problem has successfully been extended to initial boundary value problems in [11] and then developed specifically for scalar conservation laws with genuinely nonlinear flux in [102]. More recently, several authors proposed models on networks that take into account different types of solutions at the intersections, see [40, 41, 58, 64, 67, 68, 89, 93, 95, 112] and the references therein. In all these works, the road network is described as a graph, incoming and outgoing roads are the edges while the junctions are described by the nodes. Several models on how to distribute the traffic are proposed: in [40, 41, 58, 67, 68, 95] the traffic is distributed according to an optimization problem, while in [64, 93] the junction dynamics is described by a buffer and finally in [89] the traffic is distributed with a multilane model. Subsequently, different numerical methods that approximate solutions for road networks have been developed, see for example [3, 32, 89, 106, 109, 110].

More recently several authors have been investigating different areas of study in order to include more features in the models. In particular, some models were proposed that track a single vehicle moving in the vehicular traffic. In these models, the single vehicle trajectory is described with an ODE generating coupled PDE-ODE models that are able

to take into account the advantages of a microscopic approach and a macroscopic one, see [14, 15, 46, 57, 69, 75, 100]. And later on, also numerical methods have been developed to tackle this type of problems, see for example [52, 53, 56].

All these models rely on the assumption that at any point of the road the flux of cars is a function of the density. This led to several assumptions on the flux function to consider. Many of these models use a concave flux function, which depends only on the density and on the velocity of the traffic flow, which was introduced in [82]. However, many researchers claim that this relation is valid only in steady state conditions and it is not realistic in some situations [78] because it does not match the experimental data. In order to overcome this issue they proposed new models which couple the equation of mass conservation to a second equation in the spirit of the conservation of momentum. In the traffic flow literature, these models are called "second-order" models. These models have been introduced by Payne [122] and Whitham [130] and then consequently a big literature has been developed in the last decades following the work in [5], see [13, 42, 44, 45, 66, 77, 63].

A line of research that applies optimal control to traffic has been developed thanks to the work of Herty et al. [9, 81, 83, 89, 94, 90, 62, 88] and Piccoli et al.[34, 35, 47]. Several approaches have been used to solve the optimal control: adjoint methods, combinatorial methods, mixed-integer methods and instantaneous control. A separate line of research is the one followed by Bressan et al. that tries to unify the Nash game theory with optimal control for traffic flow [23, 24, 25, 26].

The work presented in this thesis follows two research lines: one regarding coupled PDE-ODE models and their application to moving bottlenecks and traffic flow networks, the other one involving junction modeling and its application to optimal control problem. We are going to present two different coupled PDE-ODE models: a strongly coupled problem to model a large and slow vehicle among the traffic flow that reduces the road capacity and the other one to model the behavior of an entrance of an highway or a roundabout. We provide existence of solution for BV initial data for the first model, and we propose two numerical schemes to solve the problem numerically. Moreover, we propose a new junction model and we show how this model could be used for optimal control problems.

Contribution and organization of the dissertation

After a brief introduction on the theory of traffic flow and hyperbolic partial differential equations, the thesis is divided in two parts which follow the two big lines of research of this PhD: the first one concerning models for moving bottlenecks and their theoretical and numerical aspects and the other one concerning models for junctions in road networks. In particular, the manuscript is organized as follows.

In Chapter 1 we give an introduction to the mathematical modeling of traffic flow using hyperbolic scalar conservation laws. The chapter includes a background on the known results on the theory of hyperbolic conservation laws and their application to traffic flow. Moreover, it includes an introduction to the numerical methods for scalar

conservation laws. Particular attention is reserved to the Godunov finite volume scheme and some of its extension to traffic flow models. We also give a review of the most known traffic flow models and we present some models that are important for the results developed in the thesis.

In Chapter 2 we present a model for moving bottlenecks. The model is a strongly coupled PDE-ODE model that is studied from an analytical and numerical point of view. An existence result for the model is proposed and a strategy for the stability of solution is attempted. Moreover, two different numerical methods are presented: a Lagrangian approach with a front tracking/capturing method and a reconstruction based conservative scheme.

In Chapter 3 a new model for 2×2 junctions on highways is proposed. The model consists on a PDE-ODE system. The conservation law describes the main traffic flow while the ODE describes the behavior of the entrance of the highway. The entrance is modeled as a vertical buffer, allowing us to consider strong boundary conditions. A similar model is then used for control problems simulating a ramp-metering situation. The control problem is solved using the discrete adjoint method. Some numerical simulations obtained with the new junction model are presented.

In Chapter 4 we use the model introduced in Chapter 3 to simulate the dynamics on roundabouts. A roundabout can in fact be seen as a concatenation of 2×2 junctions, each junction representing an entering/exiting point. An optimal control on two cost functionals as the Total Travel Time and the Total Waiting Time is numerically solved with respect of a right of way parameter. Some numerical tests are presented.

List of papers

During this PhD the following articles have been published or submitted:

- ⋆ M.L. Delle Monache, P. Goatin, *Scalar conservation laws with moving constraints arising in traffic flow modeling: an existence result*, Journ. of Differential Equations, (2014). DOI:10.1016/j.jde.2014.07.014
- ⋆ M.L. Delle Monache, P.Goatin. *A front tracking method for a strongly coupled PDE-ODE system with moving density constraints in traffic flow.* Discrete Contin. Dyn. Syst. Ser. S, **7(3)**, (2014), 435-447.
- ⋆ M.L. Delle Monache, J. Reilly, S. Samaranayake, W. Krichene, P. Goatin, A. Bayen. *A PDE-ODE model for a junction with ramp buffer.* SIAM Journ. of Appl. Math. **74(1)**, (2014), 22-39.
- ⋆ L.L. Obsu, M.L. Delle Monache, P. Goatin, S.M. Kassa. *Traffic flow optimization on roundabouts*, Math. Methods Appl. Sci., to appear. http://hal.inria.fr/docs/00/93/99/85/PDF/roundabout.pdf
- ⋆ J. Reilly, W. Krichene, M.L. Delle Monache, S. Samaranayake, P. Goatin, A. Bayen. *Adjoint-based optimization on a network of discretized scalar conserva-*

tion law PDEs with applications to coordinated ramp metering, submitted. http://hal.inria.fr/docs/00/87/84/69/PDF/adjoint.pdf

The following conference proceeding have been accepted for publication:

- M.L. Delle Monache. *Modeling of moving bottlenecks in traffic flow: a PDE-ODE model with moving density constraints*. ESAIM: Proc., to appear. Proceedings of SMAI 2013.
- M.L. Delle Monache, L.L. Obsu, P. Goatin and S.M. Kassa, *Traffic flow optimization on roundabouts*, Procedia - Social and Behavioral Sciences, (2014), 127-136. Proceedings of EWGT2013 - 16th Meeting of the EURO Working Group on Transportation, September 2013, Porto.
- M.L. Delle Monache and P. Goatin, *A strongly coupled PDE-ODE system modeling moving density constraints in traffic flow*, in Hyperbolic Problems: Theory, Numerics, Applications, AIMS on Applied Mathematics, Vol.8, pp.501-508.

And, two INRIA research reports were written:

- L.L. Obsu, M.L. Delle Monache, P. Goatin and S.M. Kassa, *Macroscopic traffic flow optimization on roundabouts*, INRIA Research Report no. 8291, April 2013. http://hal.inria.fr/docs/00/81/82/08/PDF/RR-8291.pdf
- M.L. Delle Monache and P. Goatin, *Scalar conservation laws with moving density constraints arising in traffic flow modeling*, INRIA Research Report no. 8119, October 2012. http://hal.inria.fr/docs/00/74/56/81/PDF/RR-8119.pdf

Introduction

Le but de cette thèse est d'étudier certains modèles mathématiques de trafic routier d'un point de vue analytique et numérique. Le trafic routier est un phénomène qui est compliqué à modéliser et à simuler en raison de la difficulté à reproduire la formation et l'évolution de bouchons. Plusieurs approches ont été développées au cours des dernières décennies, chacun axé sur une caractéristique particulière du trafic. En particulier, les chercheurs ont commencé à examiner le trafic à des fins différentes comme, par exemple, la réduction des encombrements, des accidents, de la pollution et pour des problèmes de sécurité. Il y a plusieurs façons de décrire l'écoulement du trafic et les différentes méthodes peuvent être regroupées en trois grandes catégories: les modèles microscopiques, les modèles macroscopiques et les modèles cinétiques. Les modèles microscopiques décrivent la trajectoire de chaque voiture avec une équation différentielle ordinaire (EDO). Les modèles de base sont les "car-following" ou des modèles basés sur la loi de Newton. La principale hypothèse des ces modèles est que le mouvement de chaque voiture ne dépend que de la voiture précédente; voir [10, 18, 39, 59, 70, 87, 128]. Les modèles cinétiques, à la place, utilisent des équations de type Boltzmann et les quantités principales décrivant le trafic sont exprimées avec des fonctions de distribution de la densité; voir [1, 115, 121, 123, 124]. Les travaux de cette thèse se réfèrent aux modèles macroscopiques, où le trafic est considéré comme un milieu continu. Les premiers à introduire ce concept furent Lighthill, Whitham [111] et, indépendamment, Richards [127] dans les années cinquante. Ils ont été les premiers à décrire le trafic avec des équations provenant de la dynamique des fluides. Ils ont utilisé une équation aux dériveés partielles (EDP) non linéaire. Le problème de Cauchy a été étendu aux problèmes aux limites dans [11], puis développé spécifiquement pour les lois de conservation scalaires avec flux non-linéaire dans [102]. Plus récemment, plusieurs auteurs ont proposé des modèles de trafic sur réseau qui prennent en compte différents solutions aux intersections, voir [40, 41, 58, 64, 67, 68, 89, 93, 95, 112] et les références qu'ils contiennent. Dans tous ces travaux, le réseau routier est décrit sous forme de graphe, les routes (entrantes et sortantes) constituent les arcs, tandis que les jonctions sont décrites par les sommets. Plusieurs modèles, qui décrivent la façon de répartir le trafic aux intersections, sont proposés: en [40, 41, 58, 67, 68, 95] le trafic est distribué selon un problème d'optimisation, en [64, 93] la dynamique de la jonction est décrite par un "buffer" et enfin en [89] le trafic est distribué avec un modèle voies multiples. Ensuite, différentes méthodes numériques pour calculer les solutions approchées pour les réseaux routiers ont été mis au point, voir par exemple [3, 32, 89, 106, 109, 110].

Plusieurs auteurs, dans des domaines différents, ont inclu plus de fonctionnalités dans les modèles. En particulier, certains modèles ont été proposés, permettant de reconstruire la trajectoire d' un seul véhicule en mouvement dans la circulation routière. Dans ces modèles, la trajectoire du véhicule est décrite avec une EDO, donnant lieu ´a des modèles couplés EDP-EDO qui prennent en compte les avantages d'une approche à la fois microscopique et macroscopique, voir [14, 15, 46, 57, 69, 75, 100]. Ensuite, des méthodes numériques ont été développées pour résoudre ce type de problèmes, voir par exemple [52, 53, 56]. Tous ces modèles se basent sur l'hypothèse que, à tout point de la route, le flux de voitures dépend seulement de la densité. Cela a conduit à plusieurs hypothèses sur la fonction flux à considérer. La plupart de ces modèles utilisent une fonction de flux concave, qui ne dépend que de la densité de l'écoulement du trafic, qui a été introduite dans [82]. Cependant, de nombreux chercheurs affirment que cette relation n'est valable que à l'équilibre et elle n'est pas réaliste dans certaines situations [78], car elle ne correspond pas aux données expérimentales. Afin de remédier à ce problème, de nouveaux modèles ont été proposés, qui couplent l'équation de conservation de la masse à une deuxième équation dans l'esprit de la conservation du moment. Dans la littérature, ces modèles sont appelés "modèles de second ordre". Ces modèles ont été introduits par Payne [122] et Whitham [130]. Ensuite, nombreux travails ont été développés au cours des dernières décennies à partir des travaux de Aw and Rascle [5], voir [13, 42, 44, 45, 66, 77, 63].

Une ligne de recherche qui applique le contrôle optimal au trafic routier a été développée grâce au travail de Herty et al. [9, 81, 83, 89, 94, 90, 62, 88] et Piccoli et al. [34, 35, 47]. Plusieurs approches ont été utilisées pour résoudre les problèmes de control optimal: les méthodes de l'adjoint, les méthodes combinatoires, les méthodes "mixted integer" et le contrôle instantané. Une autre ligne de recherche est celle suivie par Bressan et al., qui utilise la théorie des jeux de Nash pour le contrôle optimal du trafic [23, 24, 25, 26].

Le travail présenté dans cette thèse suit deux axes de recherche: l'un concernant les modèles couplés EDP-EDO et leur application aux goulots d'étranglement mobiles et aux réseaux, l'autre concernant l'application des modèles des jonctions à des problèmes de contrôle. Nous allons présenter deux modèles couplés EDP-EDO différents: un problème fortement couplé qui modélise un véhicule gros et lent dans le flux de la circulation et qui réduit la capacité de la route et l'autre qui modélise le comportement d'une bretelle d'accès d'une autoroute ou d'un rond-point. Nous fournissons un résultat d'existence des solutions pour données initiales BV pour le premier modèle, et nous proposons deux schémas numériques pour résoudre le problème numériquement. De plus, nous proposons un nouveau modèle de jonction et nous montrons comment ce modèle pourrait être utilisé pour des problèmes de contrôle optimal.

Plan de la thèse

Après une brève introduction sur la théorie du trafic et des lois de conservation, la thèse est divisée en deux parties qui correspondent aux deux axes de recherche de ce travail: la première partie concerne les modèles pour les goulots d'étranglement mobiles et leurs

aspects théoriques et numériques, l'autre est relative aux modèles de jonction pour les réseaux routiers. Plus précisément, le manuscrit est organisé comme suit.

Dans le Chapitre 1, nous donnons une introduction à la modélisation mathématique de l'écoulement du trafic en utilisant les lois de conservation scalaires. En particulier, le chapitre comprend une introduction aux résultats connus sur la théorie des lois de conservation scalaires. En outre, il comprend une introduction aux méthodes numériques pour les lois de conservation scalaires. Une attention particulière est réservée au schéma de type volumes finis de Godunov et son application aux modèles de trafic. Nous donnons également une revue des principales modèles de trafic et nous présentons quelques modèles qui seront importants pour les résultats développés dans la thèse.

Dans le Chapitre 2, nous présentons un modèle pour des goulots d'étranglement mobiles. Il s'agit d'un modèle EDP-EDO fortement couplé qui est étudié d'un point de vue analytique et numérique. Un résultat d'existence pour les solutions est proposé et une stratégie pour montrer la stabilité des solutions est proposée. En outre, deux méthodes numériques différentes sont présentées: une méthode "front/capturing" et un schéma conservatif basé sur une technique de reconstruction des chocs.

Dans le Chapitre 3, un nouveau modèle de jonction 2×2 pour les autoroutes est proposé. Le modèle se compose d'un système EDP-EDO. La loi de conservation décrit le trafic sur la voie principale, tandis que l'EDO décrit le comportement de la bretelle d'accès. L'entrée est modélisée comme un "buffer" vertical, ce qui nous permet d'utiliser des conditions aux limites fortes. Un modèle similaire est ensuite utilisé dans un problème d'optimisation pour une situation de control d'accès. Le problème de contrôle est résolu en utilisant la méthode de l'adjoint discret. Des simulations numériques obtenues avec le nouveau modèle de jonction sont aussi présentées.

Dans le Chapitre 4, nous utilisons le modèle présenté dans le Chapitre 3 pour simuler la dynamique des ronds-points. Un rond-point peut, en fait, être considéré comme une concaténation de jonctions 2×2. Deux problème d'optimisation relatifs au temps total de parcours et au temps total d'attente sont résolus numériquement par rapport à un paramètre de priorité. Des tests numériques sont présentés.

Chapter 1

Preliminaries

Contents

1.1 Hyperbolic conservation laws 10
1.1.1 Weak solution 10
1.1.2 Riemann Problem 13
1.1.3 Function with bounded variation 15
1.1.4 Wave-front tracking method 16
1.2 Traffic flow modeling 18
1.2.1 LWR model 18
1.2.2 Traffic flow on a road network 19
1.2.3 Bottlenecks and coupled micro-macro models 26
1.3 Numerical methods for hyperbolic conservation laws and traffic flow 29
1.3.1 Godunov scheme 30
1.3.2 Godunov scheme on road networks 31
1.3.3 Numerical methods for non-classical shocks 32
1.3.4 Numerical methods for coupled PDE-ODE models 34

1.1 Hyperbolic conservation laws

The works presented in this thesis are based on hyperbolic conservation laws that are non-linear partial differential equations where the unknown variable is a conserved quantity. In this chapter, we introduce some basic notions about scalar conservation laws.

A scalar conservation law in one space-dimension is a first order partial differential equation of the form:

$$\partial_t u + \partial_x f(u) = 0 \quad (t,x) \in \mathbb{R}^+ \times \mathbb{R}, \tag{1.1.1}$$

where $u : [0,+\infty[\times\mathbb{R} \to \mathbb{R}$ is the conserved quantity and $f : \Omega \subseteq \mathbb{R} \to \mathbb{R}$ is the flux, with t being the time variable and x the one-dimensional space variable. Conservation laws own their name to the fact that if we formally integrate (1.1.1) on an arbitrary space interval $[a,b]$ then we obtain

$$\frac{d}{dt}\int_a^b u(t,x)dx = -\int_a^b f(u(t,x))_x dx = f(u(t,a)) - f(u(t,b)). \tag{1.1.2}$$

This means that the integral of u on any interval $[a,b]$ varies according to the difference between the flux of u that enters at $x = a$ and exits at $x = b$, see Figure 1.1.1. In other words, u is neither created nor destroyed but is conserved.

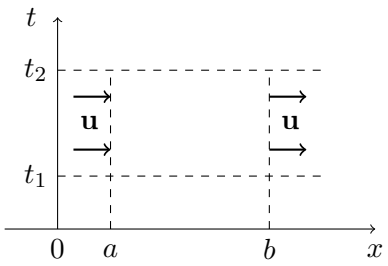


Figure 1.1.1: Flow across two points.

1.1.1 Weak solution

It is known that for non-linear conservation laws, classical solutions may not exist even for very smooth initial data because discontinuities develop in finite time. Consider the scalar Cauchy problem

$$\begin{cases} \partial_t u + \partial_x f(u) = 0, \\ u(0,x) = \bar{u}(x). \end{cases} \tag{1.1.3}$$

Assuming that u is a smooth solution, the equation can be rewritten in the quasi linear form

$$\partial_t u + f'(u)\partial_x u = 0. \tag{1.1.4}$$

For any given point $(\tau,\xi) \in \mathbb{R}^+ \times \mathbb{R}$ we denote by $t \to x(t;\tau,\xi)$ the characteristic line through (τ,ξ), i.e., the solution of the Cauchy problem

$$\dot{x}(t) = f'(u(t,x)), \qquad x(\tau) = \xi. \tag{1.1.5}$$

The function $(t,x_0)\to(t,x(t,x_0))$ is locally invertible and so it is possible to consider the map $u(t,x)=u(t,x(t))$ that satisfies (1.1.4). Observe that the value of u_0 at point x_0 determines the value of the solution u along the entire characteristics $t\to x(t;0,x_0)$, the information contained in the initial data is transported along the characteristic lines.

Nevertheless, for large times t, problem (1.1.5) may not have a unique solution. This happens when the characteristics cross, see Figure 1.1.2. In this condition, it is evident that classical solutions cannot exist. In order to construct solutions globally in time, we

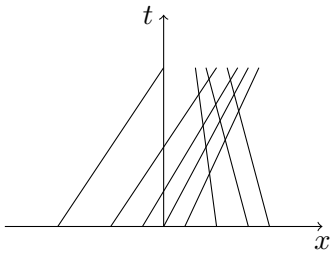


Figure 1.1.2: Intersection of characteristics.

must work in a space of discontinuous functions and consider the conservation law in a distributional sense.

Definition 1.1.1 *Fix $u_0\in\mathcal{L}^1_{\rm loc}(\mathbb{R};\mathbb{R})$ and $T>0$. A function $u:[0,T]\times\mathbb{R}\to\mathbb{R}$ is a weak solution to the Cauchy Problem (1.1.3) if u is continuous as a function from $[0,T]$ into $\mathcal{L}^1_{\rm loc}(\mathbb{R};\mathbb{R})$ and if, for every $\mathcal{C}^1$ function φ with compact support contained in the set $]-\infty,T[\times\mathbb{R}$, it holds*

$$\int_0^T\int_{\mathbb{R}}\{u\cdot\partial_t\varphi+f(u)\cdot\partial_x\varphi\}dxdt+\int_{\mathbb{R}}u_0\cdot\varphi(0,x)dx=0. \tag{1.1.6}$$

Next we look at a discontinuous function and derive some properties that must be respected at jumps. Consider a function u which is piecewise Lipschitz continuous like

$$U(t,x):=\begin{cases}u^- & \text{if } x<\lambda t\\ u^+ & \text{if } x>\lambda t\end{cases} \tag{1.1.7}$$

for some u^-, $u^+\in\mathbb{R}$ and $\lambda\in\mathbb{R}$.

Lemma 1 *The function U in (1.1.7) is a solution of (1.1.1) if and only if*

$$\lambda(u^+-u^-)=f(u^+)-f(u^-). \tag{1.1.8}$$

For the proof of Lemma 1 we refer the reader to [20].
Equation (1.1.8) is called the Rankine-Hugoniot condition and gives a condition on discontinuities of the weak solutions of (1.1.1). In the scalar case (1.1.8) is a single equation and for arbitrary $u^+\neq u^-$ the shock speed is given by

$$\lambda=\frac{f(u^+)-f(u^-)}{u^+-u^-}. \tag{1.1.9}$$

The definition of weak solution alone does not guarantee uniqueness, since it is possible to construct infinitely many weak solutions starting from an initial datum. Therefore, it is necessary to introduce some admissibility conditions, motivated by physical consideration.

- Condition 1 (vanishing viscosity)
  Let us assume that the conservation law can be seen as an approximation of the equation
  $$u_t + f(u)_x = \varepsilon u_{xx} \tag{1.1.10}$$
  for some $\varepsilon > 0$ small.

  Definition 1.1.2 *We say that a weak solution $u(t,x)$ is an admissible solution in the vanishing viscosity sense if there exists a sequence of smooth solutions u^ε to*
  $$u^\varepsilon_t + f(u^\varepsilon)_x = \varepsilon u^\varepsilon_{xx}$$
  which converges to u in $\mathcal{L}^1_{\text{loc}}$ as $\varepsilon \to 0^+$.

- Condition 2 (Entropy)
  From the previous condition, the following can be derived

  Definition 1.1.3 *An entropy for (1.1.1) is any $\mathcal{C}^1$ convex function $\eta : \mathbb{R} \to \mathbb{R}$. Moreover, any $\mathcal{C}^1$ function $q : \mathbb{R} \to \mathbb{R}$ is said an entropy flux for η provided that*
  $$\eta'(u) f'(u) = q'(u) \tag{1.1.11}$$
  for every $u \in \mathbb{R}$. The pair (η, q) is said entropy-entropy flux pair for (1.1.1).

  In particular, by approximation, for each $k \in \mathbb{R}$, $\eta = |u-k|$ and $q(u) = \operatorname{sgn}(u-k) \cdot (f(u) - f(k))$ is an entropy-entropy flux pair and satisfy (1.1.11) at every $u \neq k$.

  Definition 1.1.4 *A weak solution $u = u(t,x)$ to the Cauchy problem (1.1.3) is said entropy admissible if satisfies the Kružhkov entropy condition [99]*
  $$\int_0^T \int_{\mathbb{R}} |u-k| \partial_t \varphi + \operatorname{sgn}(u-k)(f(u) - f(k)) \partial_x \varphi \, dx dt \geq 0 \tag{1.1.12}$$
  for every $k \in \mathbb{R}$ and every $\mathcal{C}^1$ function $\varphi \geq 0$ with compact support in $[0,T[\times\mathbb{R}$.

  We have the following theorem.

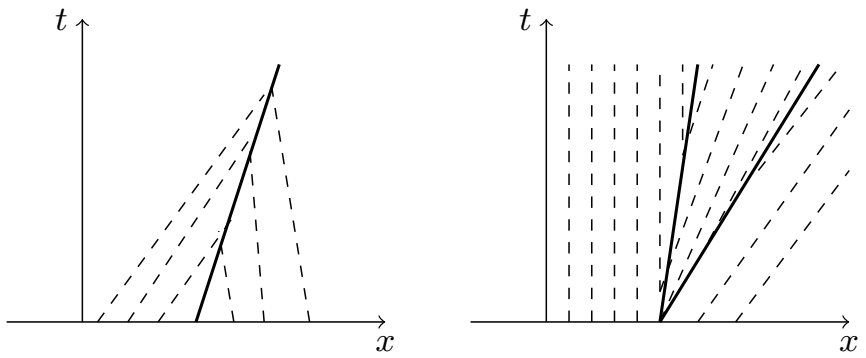
  Theorem 2 *Let $u = u(t,x)$ be a piecewise constant solution to the scalar Cauchy problem (1.1.3). Then u satisfies condition (1.1.12) if and only if along every line of jump $x = \xi(t)$ the following condition holds. For every $\alpha \in [0,1]$*
  $$\begin{cases} f(\alpha u^+ + (1-\alpha)u^-) \geq \alpha f(u^+) + (1-\alpha) f(u^-), & \text{if } u^- < u^+, \\ f(\alpha u^+ + (1-\alpha)u^-) \leq \alpha f(u^+) + (1-\alpha) f(u^-), & \text{if } u^- > u^+, \end{cases} \tag{1.1.13}$$
  where $u^- := u(t, \xi(t)-)$ and $u^+ := u(t, \xi(t)+)$.

For a proof of Theorem 2 and for all the details regarding hyperbolic conservation laws, we refer the reader to [20].
From equation (1.1.13) we can derive the following admissibility condition introduced by P. Lax [101].

- Condition 3 (Lax condition)
  A discontinuity connecting two states u^- and u^+ and traveling with speed λ given by (1.1.9) is entropy if and only if

$$f'(u^-) \geq \lambda \geq f'(u^+).$$

The geometric meaning of this condition is given in Figure 1.1.3. In particular, this condition requires that characteristics run into the jumps and that jumps where characteristics are "created" are not allowed.



(a) Entropy admissible solution. (b) Not entropic solution.

Figure 1.1.3: Geometric explanation for the Lax admissibility condition.

1.1.2 Riemann Problem

A Riemann problem is a Cauchy problem with Heaviside type initial datum.
Let $\Omega \subseteq \mathbb{R}$ be an open set, let $f : \Omega \to \mathbb{R}$ be a smooth and strictly concave flux and consider the scalar conservation law (1.1.1).

Definition 1.1.5 *A Riemann problem for equation (1.1.1) is a Cauchy problem with the initial datum of the form*

$$u_0(x) = \begin{cases} u^-, & \text{if } x < 0, \\ u^+, & \text{if } x > 0, \end{cases} \tag{1.1.14}$$

where u^-, $u^+ \in \Omega$.

The Riemann problem provides the building block for the construction of the solution of Cauchy problems with more general initial data as well as some numerical approximation

schemes (wave-front tracking, Godunov, etc.).
If $u = u(t,x)$ is the unique weak solution of (1.1.1)-(1.1.14), then for every $\theta > 0$ the rescaled function $u^\theta(t,x) = u(\theta t, \theta x)$ provides another solution. By uniqueness, $u = u^\theta$ for every $\theta > 0$. Therefore, we seek for solutions of the type $u(t,x) = v(\frac{x}{t})$. Let us consider the following cases.

1. *Centered rarefaction waves*
   Let us set $\frac{x}{t} = \xi$ and $v = v(\xi)$ smooth such that

$$\partial_t v + \partial_x f(v) = 0$$

   is satisfied. Applying the chain rule we get

$$v'(\xi)\Big(-\frac{x}{t^2}\Big) + v'(\xi) f'(v)\Big(\frac{1}{t}\Big) = 0,$$

   which gives $v'(\xi)\Big(-\frac{x}{t^2} + \frac{f'(v)}{t}\Big) = 0$. Since we are looking for a non constant solution $v' \neq 0$ and hence, $-\frac{x}{t} + f'(v) = 0$ which yields $\xi = f'(v)$. Now, if we assume $f'' < 0$, f' is a decreasing function for each $\xi \in [f'(u^-), f'(u^+)]$, if $u^+ < u^-$ we can find a unique continuous solution of the form

$$u(t,x) = \begin{cases} u^- & \text{if } x < f'(u^-)t, \\ (f')^{-1}(\xi) & \text{if } f'(u^-)t \leq x \leq f'(u^+)t, \\ u^+ & \text{if } x > f'(u^+)t. \end{cases} \tag{1.1.15}$$

   The solution $u(t,x)$ is called a centered rarefaction wave.

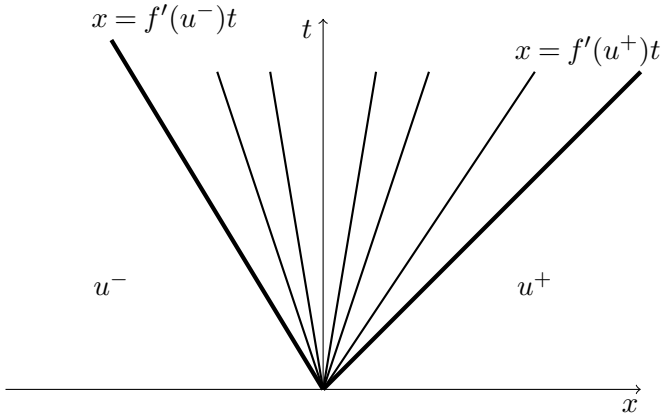


Figure 1.1.4: An example of rarefaction wave.

2. *Shock waves*
   Given equation (1.1.1) and the initial data (1.1.14) if $u^- < u^+$, we define a shock

wave an entropy admissible solution of the form

$$u(t,x) = \begin{cases} u^- & \text{if } x < \lambda t \\ u^+ & \text{if } x > \lambda t \end{cases} \tag{1.1.16}$$

for some λ. By Lemma 1, λ can be found using the Rankine-Hugoniot condition (1.1.8).

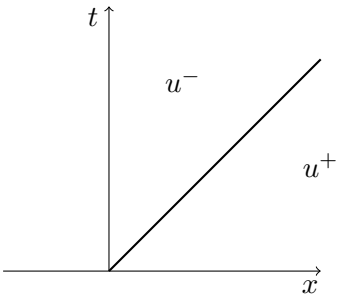


Figure 1.1.5: An example of shock wave.

1.1.3 Function with bounded variation

Consider an interval $J \subseteq \mathbb{R}$ and a function $u : J \to \mathbb{R}$. The total variation of u is defined by

$$\mathrm{TV}(u) = \sup\Big\{ \sum_{j=1}^{N} |u(x_j) - u(x_{j-1})| \Big\}, \tag{1.1.17}$$

the points x_j belongs to J for every $j \in \{0, ..., N\}$, $N \geq 1$ and satisfying $x_0 < x_1 < ... < x_N$.

Definition 1.1.6 *A function $u : J \to \mathbb{R}$ has bounded total variation if $\mathrm{TV}(u) < +\infty$. We denote by $BV(J)$ the set of all functions $u : J \to \mathbb{R}$ with bounded total variation.*

The next theorem provides the key ingredient in the existence proof for weak solutions to scalar conservation laws.

Theorem 3 ([20, Theorem 2.4]) *Consider a sequence of functions $u_\nu : [0, +\infty[\times J \to \mathbb{R}^n$ such that*

$$\mathrm{TV}(u_\nu(t,\cdot)) \leq C, \qquad |u_\nu(t,x)| \leq M \qquad \text{for all } t,\ x,$$

and

$$\int_{\mathbb{R}} |u_\nu(t,x) - u_\nu(s,x)|dx \leq L|t-s| \qquad \text{for all } t,\ s \geq 0.$$

for some constants C, M, L. Then there exists a subsequence u_μ which converges to some function $u \in \mathcal{L}^1_{loc}([0,\infty) \times J; \mathbb{R}^n)$. This limit function satisfies

$$\int_{\mathbb{R}} |u(t,x) - u(s,x)|dx \leq L|t-s| \qquad \text{for all } t,\ s \geq 0.$$

The point values of the limit function u can be uniquely determined requiring that

$$u(t,x) = u(t,x+) \doteq \lim_{y \to x+} u(t,y) \qquad \textit{for all } t,\ x.$$

In this case we have,

$$TV(u(t,\cdot)) \leq C, \qquad |u(t,x)| \leq M \qquad \textit{for all } t,\ x.$$

For the proof see [20, Chapter 2].

1.1.4 Wave-front tracking method

Here we discuss the existence of entropy admissible solutions to the Cauchy problems (1.1.3) , where $\bar{u} \in \mathcal{L}^1(\mathbb{R})$ has bounded total variation. For simplicity, we assume that $f : \Omega \subseteq \mathbb{R} \to \mathbb{R}$ is a strictly concave scalar smooth function.
We introduce at this scope the wave front tracking method. It is a procedure that allows one to prove existence of solutions by following these steps:

1. Approximate the initial condition by piecewise constant functions.
2. At each point of discontinuity solve the corresponding Riemann problem.
3. Approximate the exact solutions to the Riemann problems with piecewise constant functions and piece them together. Solutions can be extended up to the first time t when two waves collide.
4. Repeat steps 2, 3 at the time of interaction.
5. Prove that the approximate solutions so constructed converge to a limit function and that this limit function is an entropy admissible solution.

For a more detailed explanation, we refer the reader to [20, §6].

We will follow these steps to prove the existence of entropy admissible solution to (1.1.3).
We approximate the initial data with piecewise constant functions such that

$$\mathrm{TV}(\bar{u}_\nu) \leq \mathrm{TV}(\bar{u})$$

$$\|\bar{u}_\nu\|_{\mathcal{L}^\infty} \leq \|\bar{u}\|_{\mathcal{L}^\infty}$$

and

$$\|\bar{u}_\nu - \bar{u}\|_{\mathcal{L}^1} < \frac{1}{\nu},$$

for every $\nu \in \mathbb{N}$. By construction, $\bar{u}_\nu$ has a finite number of discontinuities located at $x_1 < ... < x_N$. At each $i = 1, ..., N$, we solve the Riemann problem given by the jump $(\bar{u}_\nu(x_i-), \bar{u}_\nu(x_i+))$. The solution will be exact if we deal with a shock, otherwise if a rarefaction wave appears then it is split in a centered rarefaction fan that contains

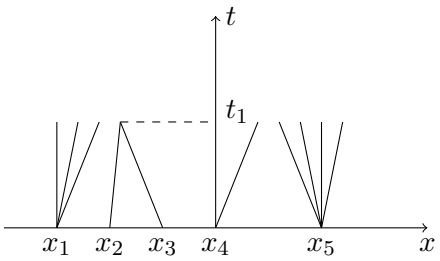


Figure 1.1.6: Construction of approximate solutions constructed by the wave front tracking up to the first time of interaction.

a sequence of jumps of at most size $\frac{1}{\nu}$. At this point, we can construct approximate solutions $u_\nu(t,x)$ up to a time t_1 where two waves interact together, see Figure 1.1.6. At t_1 we repeat the construction up to a second point of interaction $t = t_2$. In order to prove that the approximate solution exists for every $t \in [0,T]$ we have to provide a bound for

1. The number of waves;
2. The number of interactions among the waves;
3. The total variation of the approximate solution.

The first two estimates are concerned with the possibility to construct a piecewise constant approximate solution. The third one is concerned with the convergence of the approximate solutions towards the exact one. The following lemma shows that the number of interactions is finite.

Lemma 4 *For any $\nu \in \mathbb{N}$, the number of wave fronts for the approximate solution u_ν is not increasing with respect to time. Moreover, the number of interaction is bounded by the number of wave fronts.*

We can prove that the total variation is not increasing

Lemma 5 *The total variation of $u_\nu(t,\cdot)$is not increasing with respect to time: for every $t \geq 0$*

$$\mathrm{TV}(u_\nu(t,\cdot)) \leq \mathrm{TV}(\bar{u}).$$

By Theorem 3, the following holds:

Theorem 6 *Let $f : \mathbb{R} \to \mathbb{R}$ be smooth and concave and $\bar{u} \in \mathcal{L}^1(\mathbb{R})$ with bounded variation. Then there exists an entropy-admissible solution $u(t,x)$ to the Cauchy problem (1.1.3) defined for every $t \geq 0$. Moreover,*

$$\|u(t,\cdot)\|_{\mathcal{L}^\infty} \leq \|\bar{u}(\cdot)\|_{\mathcal{L}^\infty}$$

for every $t \geq 0$.

This theorem holds as well for the general class of Lipschitz flux functions f, see [20, Chapter 6].
For the proof of the above theorems and lemmas we refer the reader to [20, 67].

1.2 Traffic flow modeling

1.2.1 LWR model

In the fifties, Lighthill and Whitham [111] and, independently Richards [127] introduced a hydrodynamic model for traffic flow on a single infinite road. They thought of traffic as a fluid and used fluid dynamics equations to describe its behavior. Their model is based on the conservation of cars and it consists of a single conservation law, which describes the traffic evolution in terms of macroscopic variables (density, average speed of cars). This type of models is referred to as macroscopic models in traffic literature.

Let us consider a unidirectional stretch of road which is modeled by an interval $I = [a, b]$ with $a < b$, $a, b, \in \mathbb{R}$ and the possibility of either a and b equal to ∞. The model is based on the equation for the conservation of mass.

$$\partial_t \rho + \partial_x f(\rho) = 0, \quad (t, x) \in \mathbb{R}^+ \times \mathbb{R} \tag{1.2.1}$$

where $\rho = \rho(t, x) \in [0, \rho_{\max}]$ is the conserved quantity representing the density (number of cars per unit length), $\rho_{\max}$ being the maximal density allowed in the car. The flow $f : [0, \rho_{\max}] \to \mathbb{R}$ is a smooth flux function that is usually given by $f(\rho) = \rho v$ where $v = v(\rho)$ is the average speed of cars.
The following hypotheses are made on the flux:

(A1) f is a $\mathcal{C}^2$ function;

(A2) f is a strictly concave function:$f''(\rho) > 0$;

(A3) $f(0) = f(\rho_{\max}) = 0$.

This model is known in the traffic literature as LWR model.
The main assumption for the LWR model is that the velocity depends only on the density of cars. A reasonable supposition is that v is a decreasing function of the density.
In the transportation literature, the graph that links the flux and the density is called fundamental diagram. According to the choice of the velocity function we can have a variety of fundamental diagrams. The simplest choice is a linear function of the density,

$$v(\rho) = v_{\max}\Big(1 - \frac{\rho}{\rho_{\max}}\Big), \tag{1.2.2}$$

see Figure 1.2.1. The corresponding fundamental diagram is obtained by multiplying the density by the speed. This gives a $\mathcal{C}^2$ concave function like the one in Figure 1.2.2. This flow-density relation was introduced by Greenshields [82] and it is one of the most used in the mathematical community in transportation.

Now, let us consider the Riemann problem

$$\begin{cases} \rho_t + f(\rho)_x = 0, \\ \rho(0, x) = \begin{cases} \rho_L & \text{if } x < 0, \\ \rho_R & \text{if } x > 0. \end{cases} \end{cases} \tag{1.2.3}$$

We can define the Riemann Solver for the LWR model as follows:

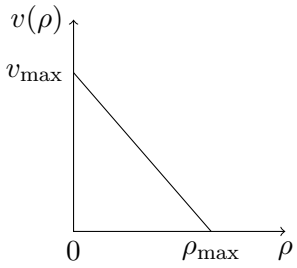


Figure 1.2.1: Speed of cars: linear decreasing function.

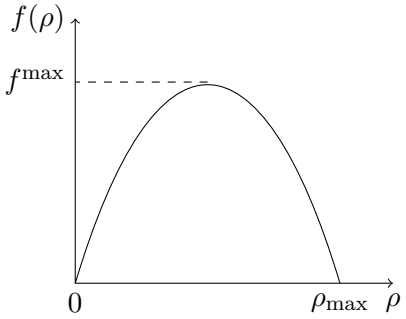


Figure 1.2.2: Fundamental diagram.

Definition 1.2.1 *The Riemann solver $\mathcal{RS}$ for the problem (1.2.3) is the (right continuous) map $\rho(t,x) \to \mathcal{RS}(\rho_L, \rho_R)(\frac{x}{t})$ given by the standard weak entropy solution. It is defined as follows.*

- *If $\rho_L < \rho_R$, then the entropy-admissible solution is given by the shock wave*

$$\rho(t,x) = \begin{cases} \rho_L & \text{if } x < \lambda t, \\ \rho_R & \text{if } x > \lambda t, \end{cases} \tag{1.2.4}$$

  where, by the Rankine-Hugoniot condition, we get $\lambda = \dfrac{f(\rho_R) - f(\rho_L)}{\rho_R - \rho_L}$.

- *If, instead, $\rho_L > \rho_R$ the entropy-admissible solution to the Riemann problem is given by the rarefaction wave*

$$\rho(t,x) = \begin{cases} \rho_L & \text{if } x < f'(\rho_L)t, \\ (f')^{-1}(\frac{x}{t}) & \text{if } f'(\rho_L)t < x < f'(\rho_R)t, \\ \rho_R & \text{if } x > f'(\rho_R)t. \end{cases} \tag{1.2.5}$$

1.2.2 Traffic flow on a road network

The LWR model has been used extensively as the starting point for macroscopic traffic flow models. This model has been extended in the last decades to the network case, see

[41, 67, 68, 80, 89, 93, 95]. In these works, the authors introduce the concept of a road network as a graph with a finite number of vertices and edges. Each vertex describes a road junction and each edge a road, see Figure 1.2.3. In the literature, there are several

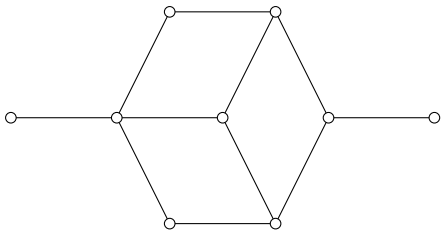


Figure 1.2.3: An example of network. The circles are the vertexes of the graph and they describe the junctions, while the edges represent the roads.

works treating this problem. Hereafter, recall those more closely related to the results presented in the following chapters.

The first work dealing with traffic flow on networks dates back to the nineties when Holden and Risebro [95] introduced the concept of road network and traffic distribution at junctions. The Riemann problem at the junction J for j roads is solved maximizing a concave function of the fluxes of this form $\sum_{\text{roads } j \text{ at } J} g\Big(\frac{f(\rho_j)}{f^{\max}}\Big)$. Their work, which considers only unidirectional networks, has then been extended for general networks by Coclite, Garavello and Piccoli in [41].
In [41], the road network is described as a graph and it can be uniquely determined by a couple (I, J) where I represents a finite collection of edges describing the roads and J a finite collection of nodes representing the road junctions. On each edge the LWR model describes the evolution of the cars density and coupling conditions are given at the nodes to correctly distribute the traffic through the junction. Let us consider a network (I, J) with a single junction J and N incoming roads and M outgoing ones, see Figure 1.2.4. Each road can be described with an interval $I_l = [a_l, b_l]$ for $l = 1, ..., N, N+1, ..., N+M$. On each road consider the equation

$$\partial_t \rho_l + \partial_x f(\rho_l) = 0, \quad l = 1, ..., N+M, \tag{1.2.6}$$

where $\rho_l = \rho_l(t, x) \in [0, \rho_{\max}]$, $(t, x) \in \mathbb{R}^+ \times I_l$ for $l = 1, ..., N+M$ is the density of cars in the road I_l, $f : [0, \rho_{\max}] \to \mathbb{R}$ is the flux function and it is taken equal to $f(\rho) = \rho v(\rho)$, see Figure 1.2.5. $v(\rho)$ is the average speed of cars equal to $v(\rho) = v_{\max}(1 - \frac{\rho}{\rho_{\max}})$. To distribute the traffic at the junction the following assumptions are made:

- The drivers have some prescribed preferences that means that there are some fixed coefficients which distributes the traffic from the incoming roads to the outgoing ones.
- The drivers choose to maximize the flux through the junction, respecting the prescribed preferences.

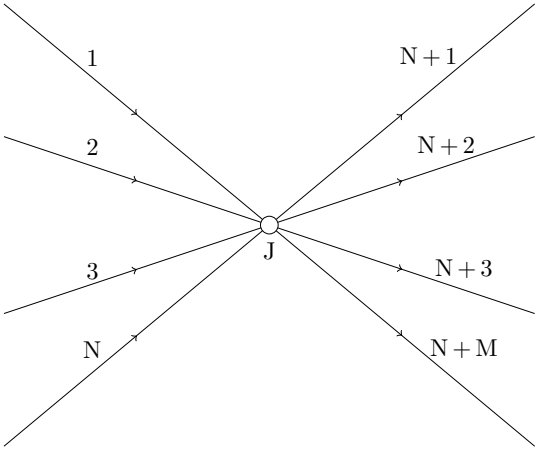


Figure 1.2.4: An example of a graph representing a road junction.

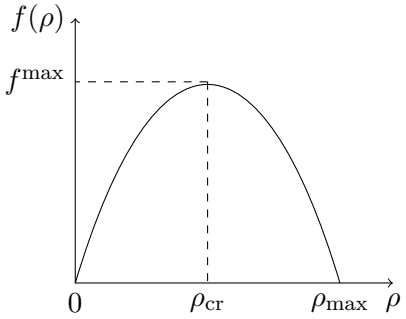


Figure 1.2.5: Fundamental diagram considered in [41].

Moreover, in order to fulfill the conservation of ρ at J mass must be conserved, i.e., the total incoming flux must be equal to the outgoing one:

$$\sum_{i=1}^{N} f(\rho_i(t, b_i-)) = \sum_{j=N+1}^{N+M} f(\rho_j(t, a_j+)). \tag{1.2.7}$$

A traffic distribution matrix is introduced to distribute the traffic among the incoming and outgoing roads.

Definition 1.2.2 *Fix a junction J and I_i incoming roads for $i = 1, ...N$ and I_j outgoing roads for $j = N+1, ..., N+M$. A traffic distribution matrix A is given by*

$$A = \begin{pmatrix} a_{N+1,1} & a_{N+1,2} & \cdots & a_{N+1,N} \\ a_{N+2,1} & a_{N+2,2} & \cdots & a_{N+2,N} \\ \vdots & \vdots & \ddots & \vdots \\ a_{N+M,1} & a_{N+M,2} & \cdots & a_{N+M,N} \end{pmatrix} \tag{1.2.8}$$

where $0 \leq a_{j,i} \leq 1$ *for every* $i = 1, ..., N$ *and for every* $j = N+1, ..., N+M$ *and*

$$\sum_{j=N+1}^{j=N+M} a_{j,i} = 1$$

for every $i = 1, ...N$.

Moreover, the matrix A needs to satisfy the following technical condition in order to have a unique solution of the Riemann problem.

Remark 1 *Let* $\{e_1, ...e_n\}$ *be the canonical basis of* $\mathbb{R}^n$. *Define for every* $i = 1, ...N$, $H_i = \{e_i\}^\perp$ *and for every* $j = N+1, ..., N+M$ *let* $a_j = (a_{j1}, ..., a_{jN}) \in \mathbb{R}^N$ *and define* $H_j = \{a_j\}^\perp$. *Let* $\mathcal{K}$ *be the set of indices* $k = (k_1, ..., k_l)$, $1 \leq l \leq N-1$ *such that* $0 \leq k_1 < k_2 < \cdots < k_l \leq N+M$ *and for every* $k \in \mathcal{K}$ *set* $H_k = \bigcap_{h=1}^{l} H_{k_h}$. *Letting* $\mathbf{1} = (1, ..., 1) \in \mathbb{R}^N$, *then for every* $k \in \mathcal{K}$,

$$\mathbf{1} \notin H_k^\perp.$$

This condition implies, in particular, that it is possible to find a unique solution to the Riemann problem at the junction only if $M \geq N$. In particular, for the case of 2×2 junctions the condition imposes that for every $j = 3, 4$, $a_{j,1} \neq a_{j,2}$.
The Cauchy problem to solve is:

$$\begin{cases} \partial_t \rho_l + \partial_x f(\rho_l) = 0, & (t,x) \in \mathbb{R}^+ \times I_l,\ l = 1, ..., N+M \\ \rho_l(0,x) = \rho_{l,0}(x), & \text{on } I_l\ l = 1, ..., N+M \end{cases} \tag{1.2.9}$$

where $\rho_{l,0}(x)$ represents the initial conditions.
Let us now introduce the definition of admissible solution.

Definition 1.2.3 $\rho = (\rho_1, ..., \rho_{N+M}) \in \prod_{l=1}^{N+M} \mathcal{C}^0\left(\mathbb{R}^+; \mathcal{L}^1 \cap \mathrm{BV}(\mathbb{R})\right)$ *is an admissible solution to* (1.2.6) *if*

1. $\rho = (\rho_1, ..., \rho_{N+M})$ *are weak solutions on* I_l, *for every* $l = 1, ..., N+M$, *i.e.,* $\rho_l : [0, +\infty[\times I_l \to [0,1]$, $l = 1, ..., N+M$, *such that*

$$\int_{\mathbb{R}^+} \int_{I_l} \Big(\rho_l \partial_t \varphi_l + f(\rho_l) \partial_x \varphi_l \Big) dx dt = 0, \quad l = 1, ..., N+M \tag{1.2.10}$$

   for every $\varphi_l \in \mathcal{C}_c^1(\mathbb{R}^+ \times I_l)$.

2. ρ_l *satisfies the Kružhkov entropy condition [99] on* $(\mathbb{R}^+ \times I_l)$, *i.e., for every* $k \in [0,1]$ *and for all* $\varphi_l \in \mathcal{C}_c^1(\mathbb{R} \times I_l)$, $t > 0$,

$$\begin{aligned} &\int_{\mathbb{R}^+} \int_{I_l} (|\rho_l - k| \partial_t \varphi_l + \operatorname{sgn}(\rho_l - k)(f(\rho_l) - f(k)) \partial_x \varphi_l) dx dt \\ &\quad + \int_{I_l} |\rho_{l,0} - k| \varphi_l(0,x) dx \geq 0; \quad l = 1, ..., N+M. \end{aligned} \tag{1.2.11}$$

3. $\sum_{i=1}^{N} f(\rho_i(t,b_i-)) = \sum_{j=N+1}^{N+M} f(\rho_j(t,a_j+))$.

4. $\sum_{i=1}^{N} f(\rho_i(t,b_i-))$ *is maximum subject to*

$$f(\rho_j(\cdot,a_j+)) = \sum_{i=1}^{N} a_{j,1} f(\rho_i(\cdot,b_i-)) \quad \textit{for each } j = N+1,...,N+M, \tag{1.2.12}$$

and to the conservation of mass in 3.

Let us show the procedure to construct solutions to the Riemann problem. Given $\rho_{i,0}, \rho_{j,0} \in [0,\rho_{\max}]$, for $i = 1,..,N$ and $j = 1,..N+M$. The Riemann problem at J is the Cauchy problem (1.2.9) where the initial conditions are given by $\rho_{i,0}, \rho_{j,0}$. Define the map

$$E : (\Gamma_1,..,\Gamma_N) \in \mathbb{R}^N \to \sum_{i=1}^{N} \Gamma_i \tag{1.2.13}$$

and the sets $\Omega_i := [0,\Gamma_i^{\max}] \quad i = 1,....,N$ and $\Omega_j := [0,\Gamma_j^{\max}] \quad j = N+1,....,N+M$ and $\Omega := \{(\Gamma_1,...,\Gamma_N) \in \Omega_1 \times ... \times \Omega_N \mid A(\Gamma_1,...,\Gamma_N)^T \in \Omega_{N+1} \times ... \times \Omega_{N+M}\}$, where

$$\Gamma_i^{\max} = \begin{cases} f(\rho_{i,0}) & \text{if } 0 \le \rho_{i,0} \le \rho_{\mathrm{cr}} \\ f^{\max} & \text{if } \rho_{\mathrm{cr}} < \rho_{i,0} \le \rho_{\max}, \end{cases} \qquad i = 1,...,N, \tag{1.2.14}$$

$$\Gamma_j^{\max} = \begin{cases} f^{\max} & \text{if } 0 \le \rho_{j,0} \le \rho_{\mathrm{cr}} \\ f(\rho_{j,0}) & \text{if } \rho_{\mathrm{cr}} < \rho_{j,0} \le \rho_{\max}, \end{cases} \qquad j = N+1,...,N+M. \tag{1.2.15}$$

The set Ω is closed, convex and not empty. Moreover, due to Remark 1 there exists a unique vector $(\hat{\Gamma}_1,...,\hat{\Gamma}_N) \in \Omega$ such that

$$E(\hat{\Gamma}_1,...,\hat{\Gamma}_N) = \max_{(\Gamma_1,..,\Gamma_N)\in\Omega} E(\Gamma_1,..,\Gamma_N).$$

Once we have the fluxes, we are able to solve the Riemann problem and get the corresponding density. Hence, we can define the Riemann Solver $\mathcal{RS}$ for (1.2.6) with Riemann initial data at a junction J with N incoming roads and M outgoing ones, such that $N \le M$. Let us first introduce the following function:

Definition 1.2.4 *Let $\tau : [0,1] \to [0,1]$ be the map implicitly defined by:*

- $f(\tau(\rho)) = f(\rho)$ *for every* $\rho \in [0,1]$;
- $\tau(\rho) \neq \rho$ *for every* $\rho \in [0,1] \setminus \{\rho_{\mathrm{cr}}\}$.

We recall that ρ_{cr} is the point at which the flux function $f(\rho)$ attains its maximum.

Definition 1.2.5 *Fix a junction J and an initial datum $(\rho_{i,0}, \rho_{j,0})$, for $i = 1, ..., N$ and $j = N+1, ..., N+M$. We define the Riemann solver $\mathcal{RS}$ for (1.2.6):*

$$\mathcal{RS}(\rho_{i,0}, \rho_{j,0}) = (\hat{\rho}_i, \hat{\rho}_j)$$

such that

$$\hat{\rho}_i \in \begin{cases} \{\rho_{i,0}\} \cup]\tau(\rho_{i,0}), 1] & \text{if } 0 \leq \rho_{i,0} \leq \rho_{\text{cr}}, \\ [\rho_{\text{cr}}, 1] & \text{if } \rho_{\text{cr}} \leq \rho_{i,0} \leq \rho_{\max}; \end{cases} \qquad i = 1, ..., M, \qquad f(\hat{\rho}_i) = \hat{\Gamma}_i \tag{1.2.16}$$

and

$$\hat{\rho}_j \in \begin{cases} [0, \rho_{\text{cr}}] & \text{if } 0 \leq \rho_{j,0} \leq \rho_{\text{cr}}, \\ \{\rho_{j,0}\} \cup [0, \tau(\rho_{j,0})[& \text{if } \rho_{\text{cr}} \leq \rho_{j,0} \leq \rho_{\max}; \end{cases} \qquad j = N+1, ..., N+M, \qquad f(\hat{\rho}_j) = \hat{\Gamma}_j \tag{1.2.17}$$

and for $i \in \{1, ..., N\}$ the solution is given by the wave $(\rho_{i,0}, \hat{\rho}_i)$, while for $j \in \{N+1, ..., N+M\}$ the solution is given by the wave $(\hat{\rho}_j, \rho_{j,0})$.

In the case of $N > M$, following [40], some additional parameters can be introduced to find uniquely the solution to the Riemann problem.
In particular, for the case of a 2×1 junction the traffic at the junction is distributed using the following yielding rule. Assume that not all the cars from the incoming roads can enter the outgoing one. Let $f(\rho_j(\cdot, a_j+))$ be the flux of cars that can enter the outgoing link. Then, given any $P \in]0, 1[$, $Pf(\rho_j(\cdot, a_j+))$ is the flux allowed from the first incoming link and $(1-P)f(\rho_j(\cdot, a_j+))$ is the flux coming from the second incoming link. P is called *rigth-of-way* (or priority) parameter and it sets the amount of cars that from each incoming road can go to the outgoing one. Also, in this case, the Riemann problem is solved maximizing the flux at the junction. The feasible set is given by $\Omega = \{(\Gamma_1, \Gamma_2) : 0 \leq \Gamma_i \leq \Gamma_i^{\max}(\rho_{i,0}, 0) \leq \Gamma_1 + \Gamma_2 \leq \hat{\Gamma}_3\}$ where $\hat{\Gamma}_3 = \min\left(\Gamma_1^{\max}(\rho_{i,0}) + \Gamma_2^{\max}(\rho_{i,0}), \Gamma_3^{\max}\right)$ and $\Gamma_i^{\max}$ for $i = 1, 2$ is given by (1.2.14) and $\Gamma_3^{\max}$ is given by (1.2.15). Consider the priority line

$$\Gamma_2 = \frac{1-P}{P}\Gamma_1, \tag{1.2.18}$$

and S the point of intersection of this line with the line $\Gamma_1 + \Gamma_2 = \hat{\Gamma}_3$. If this point belongs to Ω then $(\hat{\Gamma}_1, \hat{\Gamma}_2) = S$ otherwise $(\hat{\Gamma}_1, \hat{\Gamma}_2) = Q$ where Q is the point belonging to Ω on the line $\Gamma_1 + \Gamma_2 = \hat{\Gamma}_3$ closest to the priority line. Once the fluxes are found, it is possible to proceed like in Definition 1.2.5 to find the corresponding densities.

Demand and supply functions

Another way to define the problem at the junction is the one that considers demand and supply functions on the road network that has been introduced independently by Lebacque [106] and Daganzo [50] in the context of vehicular traffic flow. The demand function is described as follows

$$\delta(\rho) = \begin{cases} f(\rho) & \text{if } 0 \leq \rho \leq \rho_{\text{cr}}, \\ f^{\max} & \text{if } \rho_{\text{cr}} < \rho \leq \rho_{\max}; \end{cases} \tag{1.2.19}$$

and the supply function is given by

$$\sigma(\rho) = \begin{cases} f^{\max} & \text{if } 0 \leq \rho \leq \rho_{\mathrm{cr}}, \\ f(\rho) & \text{if } \rho_{\mathrm{cr}} < \rho \leq \rho_{\max}. \end{cases} \tag{1.2.20}$$

These two functions can be seen as the maximal flux that can be sent by the incoming road (demand) and the maximal flux that can be received by the outgoing road (supply). Given those functions, it is possible to define Riemann problems at the junctions that choose as optimal criterion the maximality of either the demand or the supply.

Remark 2 *Note that the works in the context of demand and supply functions can be recast in the framework of the work of [41] setting* $\Gamma_i^{\max} = \delta$ *and* $\Gamma_j^{\max} = \sigma$.

Modeling of junctions with a buffer

An alternative way to describe the dynamics of a junction is to represent it with a buffer as done in [64, 93], see Figure 1.2.6. Usually the junction is represented as a single point with no dynamics, but experience shows that sometimes the geometry of the intersection has a non negligible effect on traffic conditions [93], as for example in the case of roundabouts. The buffer mimics the behavior of this type of junctions. This modeling choice allows to take into account the fact that traffic does not immediately pass through a junction. The buffer, in fact, allows for some storage capacity. Mathematically, the buffer evolution is

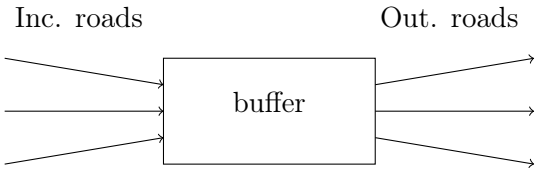


Figure 1.2.6: An example of junction represented with buffer.

described by an ordinary differential equation, which describes the evolution of the total number of cars in the junction at each time. In the works presented in [64, 93] the buffer has a fixed maximal and minimal capacity. In [93], the distribution of fluxes at the junction is done by maximizing the traffic through the junction and setting the outgoing flux $f^{\mathrm{out}} = \min\{\sigma, \mu\}$ and the incoming flux $f^{\mathrm{in}} = \min\{\delta, \mu\}$ where μ is the maximal number of cars that enter or exit the node.
More recently, Bressan et al. [28], introduced a model for junctions with several buffers at the intersection. The goal of the authors is to introduce a model that could be useful in the analysis of global optimization and Nash equilibrium. In fact, in [30] one can find counterexamples to the well-posedness and to the continuity w.r.t. weak convergence of the models introduced in [41, 67, 68], which are the key properties for the use of the model in the framework of global optimization and Nash equilibrium.
The model introduced in [28] has at each road intersection a buffer of limited capacity for every outgoing link. In particular, the buffer of limited capacity is able to model exactly backward propagation of queue along roads like it happens in crowded intersections.

Incoming drivers are admitted to the outgoing links at a rate that depends on the length of the queue at the entrance of the road of their choice. They are able to prove well-posedness for general $\mathcal{L}^\infty$ data and continuity w.r.t. weak convergence.

1.2.3 Bottlenecks and coupled micro-macro models

It is possible to extend the LWR model in order to include many features of traffic flow. Many works that go in this direction have been published in the last years. One particular line of research has been focusing on how to model the effects of a bottleneck among traffic. Bottlenecks may be generated by different reasons. We distinguish between fixed bottlenecks and moving ones. A fixed bottleneck is created by a reduction of the road capacity due to the presence of toll gates or road works, etc. The reduction in the capacity is fixed in one specific position. Moving bottlenecks are, instead, created by the presence of something that moves along the road that can be a slow and large vehicle (bus, trucks, etc.) or a moving road construction site. In this case it becomes necessary, not only, to be able to model the capacity reduction, but also to be able to track a single vehicle among the traffic flow.

During the years several works have focused on modeling these effects. In the engineering framework, we recall the works by C. Daganzo and J.Laval [52, 53] and by L. Leclercq, J.-P. Lebacque, J. B. Lesort and F. Giorgi [75, 76, 86, 107, 108]. All these works are developed in the discrete setting. In the mathematical community, research has focused both on fixed and moving bottleneck [3, 15, 37, 43, 69, 100].

Modeling of a tollgate

Colombo and Goatin [43] model the effect of a tollgate on traffic flow by a conservation law with a time-dependent unilateral constraint. The problem reads

$$\begin{cases} \partial_t \rho + \partial_x f(\rho) = 0 & (t,x) \in (\mathbb{R}^+, \mathbb{R}), \\ \rho(0,x) = \rho_0(x) & x \in \mathbb{R}, \\ f(\rho(t,0)) \leq q(t), & t \in \mathbb{R}^+, \end{cases} \tag{1.2.21}$$

where $q(t)$ is the maximal flux allowed through the toll at time t.
Global well-posedness of (1.2.21) in BV setting is proved. The presence of the constraint imposes the definition of a new type of weak solutions. Indeed, it leads to the creation of shock waves that satisfy the Rankine-Hugoniot equation but violates the Lax entropy condition when the constraint is enforced. These waves are denoted as non-classical shocks. The concept of non-classical shocks has been introduced in the framework of phase transitions by LeFloch and Hayes in the nineties in [84] and after that literature has been developed [2, 6, 7, 8, 85] to apply it to hyperbolic systems. For an extensive reading about non-classical shocks we refer the reader to [103].
The Riemann problem (1.2.21) is studied in [43] under the following assumptions:

1. $f : [0, \rho_{\max}] \to \mathbb{R}$ is Lipschitz, $f(0) = 0 = f(\rho_{\max})$, $f'(\rho)(\rho_{\text{cr}} - \rho)$ for a.e. ρ,
2. $q \in [0, f(\rho_{\text{cr}})]$, $q(t) \equiv q$.

The Constrained Riemann solver is defined by means of the standard one $\mathcal{RS}$, see Definition 1.2.1:

Definition 1.2.6 *The Constrained Riemann Solver $\mathcal{RS}^q$ is defined as follows.*
If $f(\mathcal{RS}(\rho_L,\rho_R))(0)) \leq q$ then $\mathcal{RS}^q(\rho_L,\rho_R) = \mathcal{RS}(\rho_L,\rho_R)$.
Otherwise, $\mathcal{RS}^q(\rho_L,\rho_R)(x) = \begin{cases} \mathcal{RS}(\rho_L,\hat{\rho})(x) & \text{if } x<0, \\ \mathcal{RS}(\check{\rho},\rho_R)(x) & \text{if } x>0, \end{cases}$
where $\check{\rho} < \hat{\rho}$ are the solution to $f(\rho) = q$, see Figure 1.2.7.

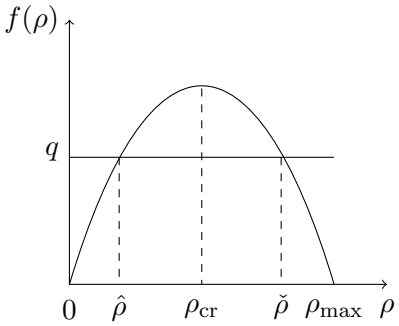


Figure 1.2.7: An example of fundamental diagram considered in [43].

The Riemann solver constrained is consistent, self-similar and the map $\mathcal{RS}^q : [0,\rho_{\max}]^2 \to \mathcal{L}^1$ uniformly continuous. Moreover, existence, uniqueness and stability of solutions for BV initial data are proved. In particular, a new definition of entropy condition is introduced to include non-classical shocks.

Definition 1.2.7 *A weak solution $\rho \in \mathcal{C}^0(\mathbb{R}^+;\mathcal{L}^1(\mathbb{R};[0,\rho_{\max}]))$ is an entropy solution to (1.2.21) if for every $k \in \mathbb{R}$ and for every $\varphi \in \mathcal{C}^1_c(\mathbb{R}^2;\mathbb{R}^+)$*

$$\begin{aligned} &\int_0^T \int_{\mathbb{R}} |\rho - k| \partial_t \varphi + \operatorname{sgn}(\rho - k)(f(\rho) - f(k)) \partial_x \varphi dx dt + \\ &\int_{\mathbb{R}} |\rho_0 - k| \varphi(0,x) dx + 2 \int_0^{+\infty} \left(1 - \frac{q(t)}{f^{\max}}\right) f(k) \varphi(t,0) dt \geq 0 \end{aligned} \tag{1.2.22}$$

We remark that the model (1.2.21) is closely related to conservation laws with space-discontinuous flux, see [4] and reference therein. In particular, in [3] it is recast in the framework of discontinuous fluxes to prove well-posedness for $\mathcal{L}^\infty$ data and convergence of finite volume schemes.

Tracking a car among traffic flow

As mentioned above, in many cases it might be useful to track a vehicle among traffic flow. The first work that goes in this direction is the one by Colombo and Marson [46].

Here, the main traffic flow is described by the LWR model while the ordinary differential equation (1.2.23) accounts for the trajectory of a single driver moving at average speed.

$$\begin{cases} \dot{y} = v(\rho(t,y)) \\ y(0) = y_0, \end{cases} \tag{1.2.23}$$

where y is the position of the driver and it is supposed that the driver is influenced by the traffic surrounding him but it does not influence it.

The ODE is considered in Filippov's sense [60, §4], due to the discontinuity of the right hand side. Well-posedness of the Cauchy problem w.r.t. the initial datum both of the ordinary differential equation and of the conservation law is proved. In particular, Hölder-continuous dependence from the initial position of (1.2.23).

We remark that the model considered in [46] introduces a weak coupling between the LWR and the ODE imposing only a "one-way" influence. In particular, the PDE is independent of the ODE solution.

Moving bottlenecks

The first mathematical model that describes moving bottlenecks is due to Lattanzio, Maurizi and Piccoli [100]. They introduce a fully coupled model where the vehicle described by the ODE interacts with the whole traffic flow, obtaining a micro-macro coupled model. In particular, the situation that the authors refer to is that of a large and slow vehicle that generates a drop of capacity in the road. The model reads

$$\begin{cases} \partial_t \rho + \partial_x f(x, y(t), \rho) = 0, \\ \rho(0,x) = \rho_0(x), \\ \dot{y} = \omega(\rho(t,y)), \\ y(0) = y_0, \end{cases} \tag{1.2.24}$$

where the flux function $f(x, y(t), \rho) = \rho v(\rho)\varphi(x - y(t))$, with $\varphi(\xi)$ being a mollifier representing the capacity dropping of car flow, see Figure 1.2.8. The speed $\omega(\rho) : [0, \rho_{\max}] \to$

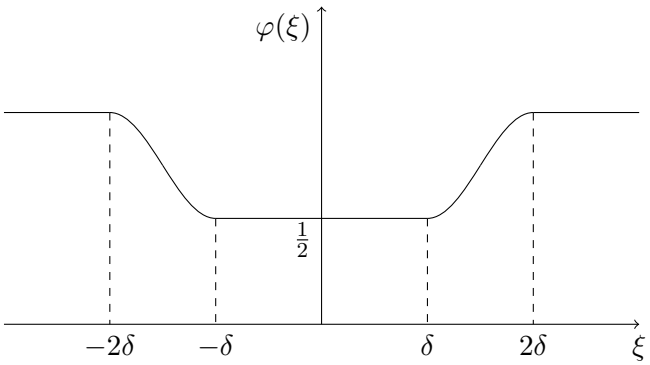


Figure 1.2.8: An example of a mollifier for the model introduced in [100].

$[0,+\infty)$ is a smooth and decreasing function describing the slower vehicle. It is assumed that $\exists\, \zeta \in (0,1)$ such that

$$\sup_{\rho\in(0,1]} \frac{\omega(0)-\omega(\rho)}{\omega(0)-f_\rho(x,y,\rho)} = \sup_{\rho\in(0,1]} \frac{\omega(0)-\omega(\rho)}{\omega(0)-(\rho(v(\rho))'\varphi(x-y)} < 1-\zeta.$$

Existence of solutions are proved with the fractional step method: iteratively in time, it consists of first solving the conservation law with the slower vehicle position fixed, and then solving the ODE using the car density given by the first step. Solutions to the ODE are intended in Filippov's sense [60].

The above model is then extended in [69] to several bus routes on a closed path on networks. Traffic flow is described by the following initial-boundary value problem

$$\begin{cases} \partial_t\rho + \partial_x f(x,y_1,...,y_N,\rho) = g(t,x,\rho), \\ \rho(0,x) = \rho_0(x), \\ \rho(t,0) = \rho(t,L), \end{cases} \tag{1.2.25}$$

where $y_i = y_i(t)$ is the position of the i-th discrete vehicle. The flux function f is given by $f(x,y_1,...,y_N,\rho) = \rho\cdot v(\rho)\cdot\Phi(x,y_1,...,y_N)$. The function $\Phi(y_1,...,y_N) = \min_i \varphi(x-y_i(t))$, with φ the mollifier as in (1.2.24), is responsible for the coupling with the ODEs and $g(t,x,\varphi)$ is a source term that accounts for the junctions. This macroscopic model is then coupled with a microscopic model of a follow-the-leader type, where the behavior of the drivers of the vehicles is influenced by the behavior of the drivers ahead. The coupling guarantees that the velocities of buses is at most the flow velocity, thus depending on the surrounding density, and becomes the maximal possible velocity when the effects of vehicles ahead are negligible.

1.3 Numerical methods for hyperbolic conservation laws and traffic flow

In this section we focus our attention on numerical methods to approximate hyperbolic conservation laws. Usually each mathematical model needs an individual numerical treatment in order to reflect all its physical features. We are going to present a brief overview of the methods used for traffic flow models. In particular, we are going to describe schemes adapted to treat nonlinear fluxes, coupling between equations and road networks.

The most common numerical schemes for hyperbolic partial differential equations are finite volume methods. We refer the reader to [110] for a comprehensive list of the classical numerical schemes. Here we limit our attention to those schemes that we use in the course of this work. In one space dimension, a finite volume method is based on subdividing the spatial domain into intervals called finite volumes (or grid cells) and keeping track of an approximation to the integral of the conserved quantity over each of these volumes. In each time step we update these values using approximations of the fluxes at the cell interfaces.

1.3.1 Godunov scheme

We introduce the following notation: $x^n_{j+\frac{1}{2}}$ are the cell interfaces at time $t^n = t^{n-1} + \Delta t^n$ with $n \in \mathbb{N}$ and $j \in \mathbb{Z}$. A computational cell is given by $C^n_j = [x^n_{j-\frac{1}{2}}, x^n_{j+\frac{1}{2}}]$ where x^n_j is the center of the cell and $\Delta x^n_j = x^n_{j-\frac{1}{2}} - x^n_{j+\frac{1}{2}}$ is the cell width at time t^n. The Godunov scheme [79] is a first order scheme that is based on exact solutions to Riemann problems. Given $u(t,x)$, the cell average of u in the cell C^n_j and at time t^n is defined as

$$u^n_j = \frac{1}{\Delta x^n_j} \int_{x^n_{j-\frac{1}{2}}}^{x^n_{j+\frac{1}{2}}} u(t^n, x)dx. \tag{1.3.1}$$

Then the Godunov scheme consists of two main steps:

1. Solve the Riemann problem at each cell interface $x^n_{j+\frac{1}{2}}$ with initial data (u^n_j, u^n_{j+1}).
2. Compute the cell averages at time t^{n+1} in each computational cell and obtain u^{n+1}_j.

We remark that waves in two neighboring cells do not intersect before Δt^n if the following CFL (Courant-Friedrichs-Lewy) condition holds:

$$\Delta t^n \max_{j\in\mathbb{Z}} \left| f'(u_j) \right| \leq \frac{1}{2} \min_{j\in\mathbb{Z}} \Delta x^n_j. \tag{1.3.2}$$

Classical Godunov scheme can be expressed in conservative form as

$$u^{n+1}_j = u^n_j - \frac{\Delta t^n}{\Delta x^n_j} \Big(F(u^n_j, u^n_{j+1}) - F(u^n_{j-1}, u^n_j) \Big), \tag{1.3.3}$$

where $F(u^n_j, u^n_{j+1}) = F^n_{j+\frac{1}{2}}$ is the Godunov numerical flux and takes in general the following expression:

$$F(u^n_j, u^n_{j+1}) = \begin{cases} \min_{z\in[u^n_j, u^n_{j+1}]} f(z) & \text{if } u^n_j \leq u^n_{j+1}, \\ \max_{z\in[u^n_{j+1}, u^n_j]} f(z) & \text{if } u^n_{j+1} \leq u^n_j. \end{cases} \tag{1.3.4}$$

In order to implement the scheme, boundary conditions need to be imposed on the left and on the right ends of the computational domain. To this end, suppose we have a boundary condition at $x = 0$

$$u(t,0) = u_b(t), \qquad t > 0.$$

Following [32, 110], we add ghost cells, that is we extend the computational domain to include few additional cells at the boundary of the domain and we define

$$u^{n+1}_0 = u^n_0 - \frac{\Delta t^n}{\Delta x^n_j} \Big(F(u^n_0, u^n_1) - F(u^n_b, u^n_0) \Big), \tag{1.3.5}$$

where

$$u^n_b = \frac{1}{\Delta t^n} \int_{t^n}^{t^{n+1}} u_b(t)dt. \tag{1.3.6}$$

replaces u^n_{-1}.

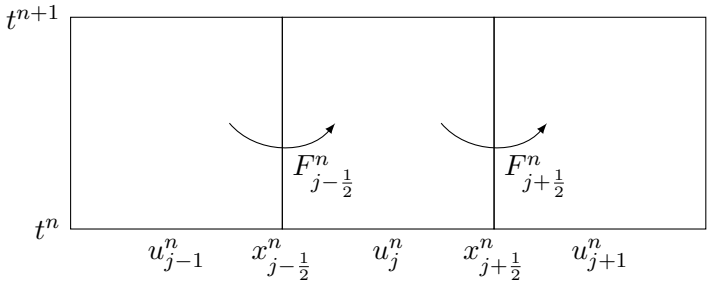


Figure 1.3.1: Illustration of the finite volume in the $x-t$ plane.

1.3.2 Godunov scheme on road networks

Godunov scheme is one of the most common numerical methods used to solve traffic flow problems. Since Godunov scheme uses exact Riemann solver at the cell interfaces then it is one of the preferable scheme for those problems where the Riemann solver can be computed explicitly making it one of the most popular scheme for scalar conservation laws and traffic flow models. For simplicity in the next section we drop the indexes j and n from Δx.
The Godunov scheme for the LWR model (1.2.1) reads:

$$\rho_j^{n+1} = \rho_j^n - \frac{\Delta t^n}{\Delta x}\Big(F(\rho_j^n, \rho_{j+1}^n) - F(\rho_{j-1}^n, \rho_j^n)\Big), \tag{1.3.7}$$

where the numerical flux F for a concave flux function is given by

$$F(u,v) = \begin{cases} \min\left(f(u), f(v)\right) & \text{if } u \le v, \\ f(u) & \text{if } v < u < \rho_{\text{cr}}, \\ f^{\max} & \text{if } v < \rho_{\text{cr}} < u, \\ f(v) & \text{if } \rho_{\text{cr}} < v < u. \end{cases} \tag{1.3.8}$$

In [32] Godunov scheme has been extended to be used also on traffic road networks. In particular, to use Godunov scheme on road network it is necessary to specify the flux at the junction. Let us assume that each road is divided in $J+1$ cells numbered from 0 to J. Since Godunov scheme uses exact Riemann solvers at cell interfaces, at the junction it makes sense to replace the Godunov flux with the exact flux at the junction introduced in Definition 1.2.5. In this way, for each road connected at the junction at the right endpoint, we set

$$\rho_{i,J}^{n+1} = \rho_{i,J}^n - \frac{\Delta t^n}{\Delta x}(\hat{\Gamma}_i - F(\rho_{i,J-1}^n, \rho_{i,J}^n)),$$

while for the roads connected at the junction at the left endpoint, we have

$$\rho_{j,0}^{n+1} = \rho_{j,0}^n - \frac{\Delta t^n}{\Delta x}(F(\rho_{j,0}^n, \rho_{j,1}^n) - \hat{\Gamma}_j),$$

for $i = 1, \ldots N$ and $j = N+1, \ldots, N+M$ where $\hat{\Gamma}_i$ and $\hat{\Gamma}_j$ are the maximized fluxes computed in Section 1.2.2.

Remark 3 *For Godunov scheme there is no need to invert the flux f to compute the densities, as the Godunov flux coincides with the flux at the junction. In this case it suffices to insert the computed maximized fluxes directly into the scheme.*

1.3.3 Numerical methods for non-classical shocks

Non-classical shocks are driven by small-scale effects and they usually require additional conditions to be able to detect them. Over the years several approaches have been proposed, see [17, 38, 104, 105, 131] and references therein. Hereafter, we are going to recall a couple of methods which will be used later on in this work. A way to capture non-classical shocks is to include them directly into the numerical scheme. This is what is done in the case of the random choice and front tracking schemes [38, 104, 105]. These schemes converge to exact solutions even in case of non-classical shocks but they require explicit knowledge of the non-classical Riemann solver which might be expensive numerically.

A Lagrangian algorithm with moving mesh

In 1996 Zhong, Hou and LeFloch [131] introduced a front-tracking capturing method that uses a Lagrangian algorithm to approximate systems of conservation laws with phase boundaries. The phase boundaries, studied in[131], are propagating solid-solid phase boundaries; such waves (as non-classical shocks) are not uniquely determined by the initial condition. In this case, the standard Godunov method does not produce correct results, since it fails to show the presence of the phase boundaries. In [131] the authors develop a front tracking/capturing method that tracks phase boundaries and captures conventional shock waves. The space is discretized in such a way that a cell interface is located at the phase boundary and its speed at the time t^n will be denoted by V^n. The computation will proceed as follows:

1. Compute all quantities at the time t^{n+1} from the approximation at the time t^n including the phase boundary propagation speed and its location.

2. Shift the grid mesh according to the movement of the phase boundary so that the phase boundary remains on a grid point.

To implement this idea one has to use a moving mesh. The algorithm introduced in [131] follows these steps:

1. Compute the speed of propagation of the phase boundary.

2. Shift grid points according to $x^{n+1}_{j+\frac{1}{2}} = x^n_{j+\frac{1}{2}} + V^n \Delta t^n$ for all $j \in \mathbb{Z}$.

3. Compute u^{n+1}_j for all $j \in \mathbb{Z}$.

4. Repeat steps (1)-(3).

When $V^n = 0$ this algorithm corresponds to the Godunov method. The method as it is introduced in [131] shifts uniformly the grid points. However, it is possible to shift the grid only locally. In this way the mesh is locally nonuniform and it moves locally with the phase boundary. Assume that at time t^n the phase boundary is located at $x^n_{m+\frac{1}{2}}$, then at time t^{n+1} it moves to a new position $x^{n+1}_{m+\frac{1}{2}}$. Instead of letting all grid points move with the phase boundary only the point $x_{m+\frac{1}{2}}$ is moved. Consequently the locations of x_m and x_{m+1} change as well as the mesh size.

A convergent and conservative scheme for non-classical solutions

The method introduced in [131] is able to capture non-classical shocks, however it is not easy to implement due to the nonuniform moving mesh. More recently, Boutin, Chalons, Lagoutière and LeFloch in [17] proposed a conservative method that is able to capture non-classical shocks without moving meshes. The method is based on a reconstruction technique that takes place in the cell where a non-classical shock may arise. They propose to reconstruct the non-classical discontinuity in such a way that non-classical shocks are computed exactly while classical shocks suffer moderate numerical diffusion. The main idea of this method is to consider the information u^n_j given in a single cell insufficient to correctly evaluate the Riemann problem whose solution is a phase boundary in that cell. Using a classical Godunov approach, we cannot have any different value from those given by the classical Riemann solver at the interfaces in particular, for example, for shocks, the solution of the Riemann problem is the propagation of the Riemann initial states ($u^n_l = u^n_{j-1}$ and $u^n_r = u^n_{j+1}$) .
So, instead of considering u^n_j as sufficient information for the Riemann solution associated with initial states u^n_{j-1} and u^n_{j+1}, they propose to introduce in the cell C_j the left (right) state $u^n_{j,l}$ ($u^n_{j,r}$) of the non-classical discontinuity which is expected to be present in the Riemann solution associated with u^n_{j-1} and u^n_{j+1}. The position where the reconstruction has to take place is computed using conservation as follows

$$\bar{x}_j = x^n_{j+\frac{1}{2}} + \frac{u^n_{j,r} - u^n_j}{u^n_{j,r} - u^n_{j,l}}\Delta x. \tag{1.3.9}$$

At this point, it is possible to reconstruct the discontinuity given $0 \le d^n_j \le 1$ such that

$$d^n_j = \frac{u^n_{j,r} - u^n_m}{u^n_{j,r} - u^n_{j,l}}. \tag{1.3.10}$$

Then, the numerical flux becomes:

- if the flux function f is non-decreasing

$$\Delta t F^n_{j+\frac{1}{2}} = \begin{cases} \min(\Delta t_{j+\frac{1}{2}}, \Delta t) f(u^n_{j,r}) + \max(\Delta t - \Delta t_{j+\frac{1}{2}}, 0) f(u^n_{j,l}), & \text{if } 0 \le d^n_j \le 1, \\ \Delta t f(u^n_j), & \text{otherwise;} \end{cases} \tag{1.3.11}$$

with $\Delta t_{j+\frac{1}{2}} = \dfrac{1 - d^n_j}{\lambda(u^n_{j,l}, u^n_{j,r})}\Delta x$;

- if f is non-increasing

$$\Delta t F^n_{j-\frac{1}{2}} = \begin{cases} \min\left(\Delta t_{j-\frac{1}{2}}, \Delta t\right) f(u^n_{j,l}) + \max\left(\Delta t - \Delta t_{j-\frac{1}{2}}, 0\right) f(u^n_{j,r}), & \text{if } 0 \leq d^n_j \leq 1, \\ \Delta t f(u^n_j), & \text{otherwise;} \end{cases} \tag{1.3.12}$$

$$\text{with } \Delta t_{j-\frac{1}{2}} = \frac{d^n_j}{-\lambda(u^n_{j,l}, u^n_{j,r})} \Delta x,$$

where $\lambda(u_j, u_{j+1})$ is the phase boundary speed. This scheme is a five-points scheme since u^{n+1}_j depends on u^n_{j-2}, u^n_{j-1}, u^n_j, u^n_{j+1}, u^n_{j+2}.

1.3.4 Numerical methods for coupled PDE-ODE models

Tracking a car on a road network

The work presented in [33] deals with numerical approximation of coupled PDE-ODE systems for traffic flow on a road network. The goal of the numerical scheme is to track a car path among the surrounding traffic flow. The car trajectory is described by an ODE and the surrounding traffic by a scalar conservation laws as in [46] . The algorithm proposed in [33] is divided in two steps:

1. The traffic density values are computed on each road solving Riemann problems. At this step one can use either the wave front tracking method, see Section 1.1.4 or the Godunov scheme, see Section 1.3.1, provided that the condition at junctions are considered.

2. The driver's position is determined solving the ODE by means of an algorithm which, given the densities obtained at the previous step by wave front tracking or the Godunov scheme, determines the car position on the network. They distinguish two situations, according to the position of the car trajectory inside the cell. In both cases, it is necessary to check if the wave starting at the cell interface is a shock or a rarefaction and compute the time of interaction between the wave and the car trajectory. In the case of a rarefaction the initial and final time of interaction is computed and the position of the car is updated by solving explicitly an ordinary differential equation. According to the new position, the cell index of the car position is updated.

Part I

Modeling of a moving bottleneck

Chapter 2

A strongly coupled PDE-ODE model with moving constraints

Contents

2.1 Mathematical model 38
2.2 The Riemann problem with moving density constraint 42
2.3 The Cauchy problem: existence of solutions 43
2.3.1 Wave-front tracking 44
2.3.2 Bounds on the total variation 45
2.3.3 Convergence of approximate solutions 48
2.4 An approach to the stability of the solutions 50
2.4.1 Estimates on shifts 51
2.5 A front tracking algorithm 57
2.5.1 Godunov-type scheme for hyperbolic PDEs with constraint . . 57
2.5.2 Numerical method for the ODE 60
2.6 A conservative scheme with reconstruction of non-classical and classical shocks 60
2.7 Numerical results 63

Introduction

In this chapter, we focus on a strongly coupled PDE-ODE problem that was introduced in [75] to describe the effects of urban transport systems in a road network. A slow moving large vehicle, like a bus or a truck, reduces the road capacity and thus generates a moving bottleneck for the surrounding traffic flow. The main traffic is described by a non-linear transport equation while the bus trajectory is described by an ODE and with an inequality constraint which describes the drop in the capacity of the road due to the presence of the slower vehicle, for example a bus. The solution of the ODE will be intended in Carathéodory sense. Compared to the previous models, the present one gives a more realistic description of the velocity of the slower vehicle and it is easier to handle both from the analytical and the numerical point of view.

The chapter is developed as follows. Section 2.1 gives a description of the model from an analytical point of view. Section 2.2 is dedicated to the solution of the Riemann problem and Section 2.3 shows the existence of solutions for the Cauchy problem. On Section 2.4 we show some partial results on the stability of the solutions. Section 2.5 and 2.6 are dedicated to the numerical schemes and show some numerical tests performed on this model. The results obtained are included in [57, 56].

2.1 Mathematical model

Our aim is to describe the phenomena caused by the presence of a bus in a car flow. Since the macroscopic description of the traffic does not allow to consider single vehicles, we consider the bus as a mobile obstacle that reduces the capacity of the road generating a moving bottleneck for the surrounding traffic. This situation can be modeled by a PDE-ODE strongly coupled system consisting of a scalar conservation law with moving flux constraint accounting for traffic evolution and an ODE describing the slower vehicle motion, i.e.

$$\begin{cases} \partial_t \rho + \partial_x f(\rho) = 0, & (t,x) \in \mathbb{R}^+ \times \mathbb{R}, \\ \rho(0,x) = \rho_o(x), & x \in \mathbb{R}, \\ f(\rho(t,y(t))) - \dot{y}(t)\rho(t,y(t)) \leq \dfrac{\alpha \rho_{\max}}{4V}(V - \dot{y}(t))^2 & t \in \mathbb{R}^+, \\ \dot{y}(t) = \omega(\rho(t,y(t)+)), & t \in \mathbb{R}^+, \\ y(0) = y_o. \end{cases} \tag{2.1.1}$$

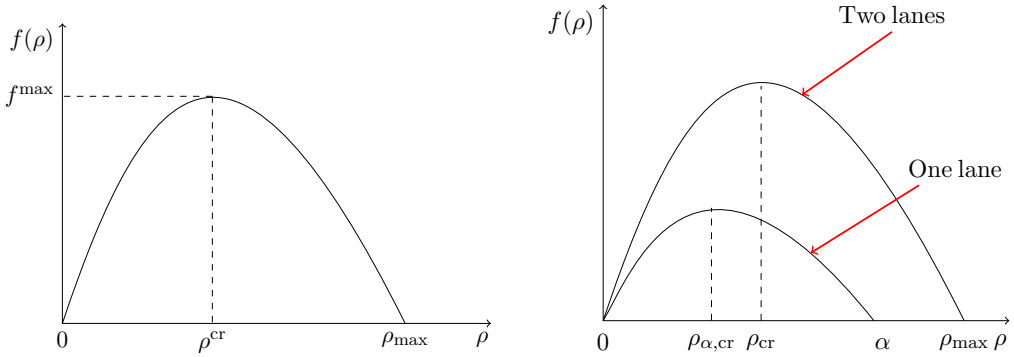
The traffic evolution is described by a scalar hyperbolic conservation law

$$\partial_t \rho + \partial_x f(\rho) = 0, \tag{2.1.2}$$

where the main quantities are the mean traffic density $\rho = \rho(t,x) \in [0, \rho_{\max}]$ which is the scalar conserved quantity, with $\rho_{\max}$ being the maximal density allowed on the road and the flux function $f : [0, \rho_{\max}] \to \mathbb{R}^+$ which is a strictly concave function such that $f(0) = f(\rho_{\max}) = 0$, see Figure 2.1.1a. It is given by the following flux-density relation

$$f(\rho) = \rho v(\rho),$$

where v is a smooth decreasing function denoting the mean traffic speed and here set to be $v(\rho) = V(1 - \frac{\rho}{\rho_{\max}})$, V being the maximal velocity allowed on the road. Every road



(a) One lane (b) Several lanes

Figure 2.1.1: A typical example of flux function for traffic flow (left). Every road has a specific fundamental diagram. For roads with different number of lanes we can consider that the fundamental diagrams are in a ratio corresponding to their maximal capacities (right).

has a specific fundamental diagram. For example, for roads with different number of lanes we can consider as a first approximation that the fundamental diagrams are not affine and in a ratio that depends on the maximal capacities of the different lanes, see Figure 2.1.1b. The bus does not behave like cars hence, it cannot be modeled in the same way. We represent a single bus such that we can track its trajectory at all times. When it is possible, the bus will move at its own maximal speed which, we denote as $V_b < V$. When the surrounding traffic is too dense the bus will adapt its velocity to the one of the cars, so it will not be possible for the bus to overtake the cars, see Figure 2.1.2. From a mathematical point of view, the velocity of the bus can be described by the following function:

$$\omega(\rho) = \begin{cases} V_b & \text{if } \rho \leq \rho^* \doteq \rho_{\max}(1 - \frac{V_b}{V}), \\ v(\rho) & \text{otherwise,} \end{cases} \tag{2.1.3}$$

and the bus trajectory is described by the following ODE

$$\dot{y}(t) = \omega(\rho(t, y(t)+)) \tag{2.1.4}$$

where y denotes the position of the bus.

To describe the interaction between the bus and the traffic we consider the bus as a mobile obstacle, i.e., as a moving restriction of the road. The situation is the following: upstream and downstream with respect to the bus, the cars behave normally while on the side of the bus the road capacity is reduced, generating a bottleneck, see Figure 2.1.3. This discontinuity moves at the bus speed. To better capture the influence of the bus, we

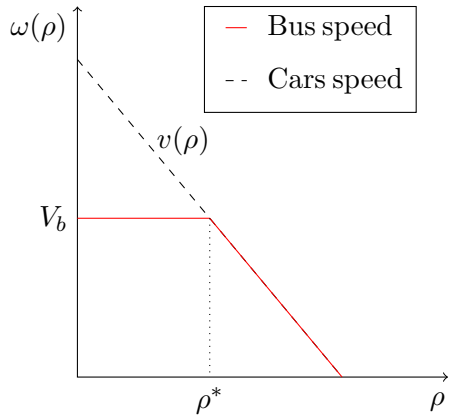


Figure 2.1.2: Bus and cars speed.

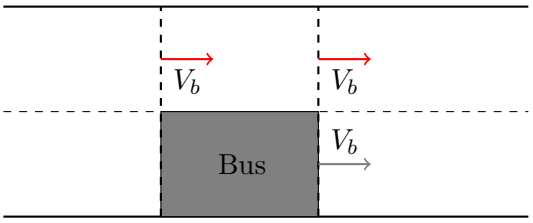


Figure 2.1.3: Moving bottleneck.

choose to study the problem in the bus reference frame. This means setting $X = x - y(t)$. In this coordinate system the velocity of the bus is equal to zero. As a consequence the conservation law can be rewritten as:

$$\partial_t \rho + \partial_X \left(f(\rho) - \dot{y}\rho \right) = 0. \tag{2.1.5}$$

The corresponding constraint on the flux can be written as

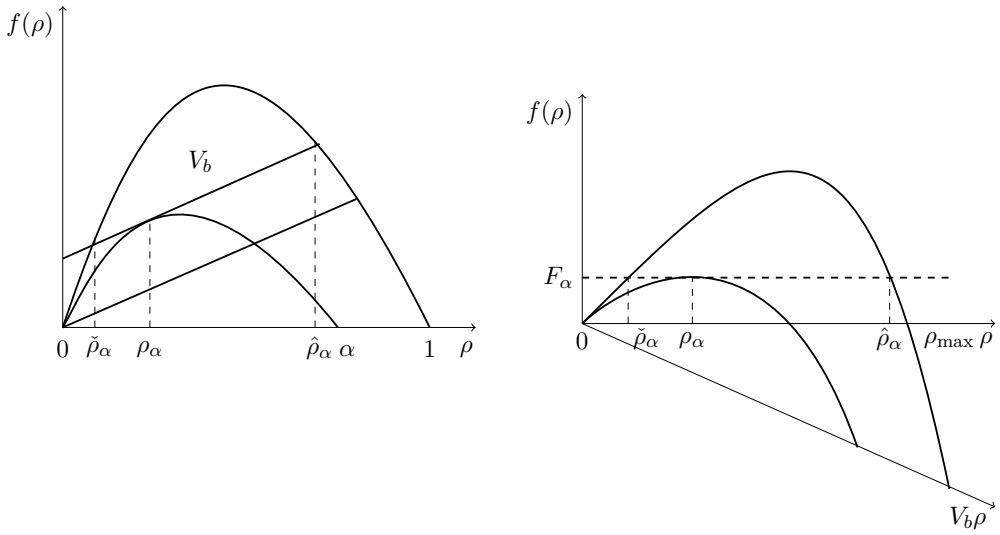
$$f(\rho(t, y(t))) - \dot{y}(t)\rho(t, y(t)) \leq \frac{\alpha \rho_{\max}}{4V}(V - \dot{y}(t))^2, \tag{2.1.6}$$

with the constant coefficient $\alpha \in]0, 1[$ giving the reduction rate of the road capacity due to the presence of the bus. Indeed, let $f_\alpha : [0, \alpha\rho_{\max}] \to \mathbb{R}^+$ be the rescaled flux function describing the reduced flow at $x = y(t)$, i.e.

$$f_\alpha(\rho) = V\rho\left(1 - \frac{\rho}{\alpha\rho_{\max}}\right),$$

and $\rho_\alpha \in]0, \alpha\rho_{\max}/2[$ such that $f'_\alpha(\rho_\alpha) = \dot{y}$, i.e.

$$\rho_\alpha = \frac{\alpha\rho_{\max}}{2}\left(1 - \frac{\dot{y}}{V}\right),$$



(a) Fixed reference frame

(b) Bus reference frame

Figure 2.1.4: Flux functions for $\dot{y} = V_b$. The big fundamental diagram describes the whole road and, the smaller one, the constrained flux at the bus location.

see Figure 2.1.4. Therefore, the right-hand side of (2.1.6) is given by

$$f_\alpha(\rho_\alpha) - \dot{y}\rho_\alpha = \frac{\alpha\rho_\alpha}{4V}(V - \dot{y}(t))^2.$$

Note that inequality (2.1.6) is always satisfied if $\dot{y}(t) = v(\rho)$, since the left hand side is 0. Moreover, it is well defined even if ρ has a jump at $y(t)$ because of the Rankine-Hugoniot conditions. This constraint describes mathematically the reduction of capacity of the road due to the presence of the bus.

For our purposes, it is not restrictive to assume that $\rho_{\max} = V = 1$, so that the full model writes

$$\begin{cases} \partial_t\rho + \partial_x(\rho(1-\rho)) = 0, & (t,x) \in \mathbb{R}^+ \times \mathbb{R}, \\ \rho(0,x) = \rho_o(x), & x \in \mathbb{R}, \\ f(\rho(t,y(t))) - \dot{y}(t)\rho(t,y(t)) \le F_\alpha \doteq \dfrac{\alpha}{4}(1-\dot{y}(t))^2, & t \in \mathbb{R}^+, \\ \dot{y}(t) = \omega(\rho(t,y(t)+)), & t \in \mathbb{R}^+, \\ y(0) = y_o. \end{cases} \tag{2.1.7}$$

2.2 The Riemann problem with moving density constraint

We devote this section to the study of the Riemann problem. Consider (2.1.7) with Riemann type initial data

$$\rho_o(x) = \begin{cases} \rho_L & \text{if } x < 0, \\ \rho_R & \text{if } x > 0, \end{cases} \quad \text{and} \quad y_o = 0. \tag{2.2.1}$$

We aim at defining a Riemann solver for the conservation law with moving flux constraint. Therefore we consider the following Riemann problem

$$\begin{cases} \partial_t \rho + \partial_x f(\rho) = 0, \\ \rho(0,x) = \begin{cases} \rho_L & \text{if } x < 0, \\ \rho_R & \text{if } x > 0, \end{cases} \end{cases} \tag{2.2.2}$$

under the constraint

$$f(\rho(t,y(t))) - \dot{y}(t)\rho(t,y(t)) \leq \frac{\alpha}{4}(1-\dot{y}(t))^2,$$

where the bus velocity $\dot{y}(t)$ is assumed to be constant by self-similarity. The definition of the Riemann solver for (2.1.7), (2.2.1) follows [75, §V]. Denote by $\mathcal{RS}$ the standard (i.e., without the constraint (2.1.6)) Riemann solver for (2.2.2), i.e., the (right continuous) map $(t,x) \mapsto \mathcal{RS}(\rho_L,\rho_R)(x/t)$ given by the standard weak entropy solution to (2.2.2). Moreover, let $\check{\rho}_\alpha$ and $\hat{\rho}_\alpha$, with $\check{\rho}_\alpha \leq \hat{\rho}_\alpha$, be the intersection points of the flux function $f(\rho)$ with the line $f_\alpha(\rho_\alpha) + V_b(\rho - \rho_\alpha)$ (see Figure 2.1.4).

Definition 2.2.1 *The constrained Riemann solver* $\mathcal{RS}^\alpha : [0,1]^2 \to \mathcal{L}^1_{\text{loc}}(\mathbb{R};[0,1])$ *for* (2.1.7), (2.2.1) *is defined as follows.*

1. *If* $f(\mathcal{RS}(\rho_L,\rho_R)(V_b)) > F_\alpha + V_b\mathcal{RS}(\rho_L,\rho_R)(V_b)$, *then*

$$\mathcal{RS}^\alpha(\rho_L,\rho_L)(x/t) = \begin{cases} \mathcal{RS}(\rho_L,\hat{\rho}_\alpha)(x/t) & \text{if } x < V_b t, \\ \mathcal{RS}(\check{\rho}_\alpha,\rho_R)(x/t) & \text{if } x \geq V_b t, \end{cases} \quad \text{and} \quad y(t) = V_b t.$$

2. *If* $V_b\mathcal{RS}(\rho_L,\rho_R)(V_b) \leq f(\mathcal{RS}(\rho_L,\rho_R)(V_b)) \leq F_\alpha + V_b\mathcal{RS}(\rho_L,\rho_R)(V_b)$, *then*

$$\mathcal{RS}^\alpha(\rho_L,\rho_R) = \mathcal{RS}(\rho_L,\rho_R) \quad \text{and} \quad y(t) = V_b t.$$

3. *If* $f(\mathcal{RS}(\rho_L,\rho_R)(V_b)) < V_b\mathcal{RS}(\rho_L,\rho_R)(V_b)$, *then*

$$\mathcal{RS}^\alpha(\rho_L,\rho_R) = \mathcal{RS}(\rho_L,\rho_R) \quad \text{and} \quad y(t) = v(\rho_R)t.$$

Note that, when the constraint is enforced (point 1. in the above definition), a non-classical shock arises, which satisfies the Rankine-Hugoniot condition but violates the Lax entropy condition.

Remark 4 *The above definition is well-posed even if the classical solution* $\mathcal{RS}(\rho_L,\rho_R)(x/t)$ *displays a shock at* $x = V_b t$. *In fact, due to Rankine-Hugoniot equation, we have*

$$f(\rho_L) = f(\rho_R) + V_b(\rho_L - \rho_R)$$

and hence

$$f(\rho_L) > f_\alpha(\rho_\alpha) + V_b(\rho_L - \rho_\alpha) \quad \Longleftrightarrow \quad f(\rho_R) > f_\alpha(\rho_\alpha) + V_b(\rho_R - \rho_\alpha).$$

2.3 The Cauchy problem: existence of solutions

The aim of this section is to study existence of solutions of problems (2.1.1) and (2.1.7). A bus travels along a road whose traffic evolution is modeled by

$$\begin{aligned} &\partial_t \rho + \partial_x(\rho(1-\rho)) = 0, \\ &\rho(0,x) = \rho_o(x), \\ &f(\rho(t,y(t))) - \dot{y}(t)\rho(t,y(t)) \le F_\alpha. \end{aligned} \tag{2.3.1}$$

The bus influences the traffic along the road but it is also influenced by the downstream traffic conditions. The bus trajectory $y = y(t)$ then solves

$$\begin{aligned} &\dot{y}(t) = \omega(\rho(t,y(t)+)), \\ &y(0) = y_o. \end{aligned} \tag{2.3.2}$$

Solutions to (2.3.2) are intended in Carathéodory sense, i.e., as absolutely continuous functions which satisfy (2.3.2) for a.e. $t \ge 0$. Observe that the function $F(t,x) = \omega(\rho(t,x))$ is discontinuous w.r.t. x and it does not satisfy general conditions which imply well-posedness of the Cauchy problem (2.3.2), see [60, §1] for the Carathéodory conditions, and [19, 29] for ODEs which are discontinuous w.r.t. x. In particular, the bus velocity function (2.1.3) does not fulfill the assumptions in [29, (A1)-(A2)] and [46, Eq. (2.1)]. In our setting, due to the strong PDE-ODE coupling, we will prove existence and continuous dependence of both solutions to (2.3.1) and (2.3.2) at the same time.

Definition 2.3.1 *A couple* $(\rho,y) \in \mathcal{C}^0\left(\mathbb{R}^+;\mathcal{L}^1 \cap \mathrm{BV}(\mathbb{R};[0,1])\right) \times \mathcal{W}^{1,1}(\mathbb{R}^+;\mathbb{R})$ *is a solution to* (2.1.7) *if*

1. ρ *is a weak solution of* (2.3.1), *i.e. for all* $\varphi \in \mathcal{C}^1_c(\mathbb{R}^2;\mathbb{R})$

$$\int_{\mathbb{R}^+}\int_{\mathbb{R}} (\rho\partial_t\varphi + f(\rho)\partial_x\varphi)\,dx\;dt + \int_{\mathbb{R}} \rho_o(x)\varphi(0,x)\;dx = 0\;; \tag{2.3.3a}$$

moreover, ρ *satisfies Kružhkov entropy conditions [99] on* $(\mathbb{R}^+\times\mathbb{R}) \setminus \{(t,y(t)) : t \in \mathbb{R}^+\}$, *i.e. for every* $k \in [0,1]$ *and for all* $\varphi \in \mathcal{C}^1_c(\mathbb{R}^2;\mathbb{R}^+)$ *and* $\varphi(t,y(t)) = 0$, $t > 0$,

$$\begin{aligned} \int_{\mathbb{R}^+}\int_{\mathbb{R}} &(|\rho-k|\partial_t\varphi + \mathrm{sgn}(\rho-k)\,(f(\rho)-f(k))\,\partial_x\varphi)\,dx\;dt \\ &+ \int_{\mathbb{R}} |\rho_o - k|\varphi(0,x)\;dx \ge 0\;; \end{aligned} \tag{2.3.3b}$$

2. *y is a Carathéodory solution of (2.3.2), i.e. for a.e. $t \in \mathbb{R}^+$*

$$y(t) = y_o + \int_0^t \omega(\rho(s, y(s)+))\ ds\ ; \tag{2.3.3c}$$

3. *the constraint (2.1.6) is satisfied, in the sense that for a.e. $t \in \mathbb{R}^+$*

$$\lim_{x \to y(t)\pm} (f(\rho)) - \omega(\rho)\rho)\,(t,x) \leq F_\alpha. \tag{2.3.3d}$$

Remark that the above traces exist because $\rho(t,\cdot) \in \mathrm{BV}(\mathbb{R};[0,1])$ for all $t \in \mathbb{R}^+$.

Remark 5 *Our choice of Carathéodory solutions for (2.3.2) is justified by the particular bus velocity defined by (2.1.3). With this choice it is not possible for the bus to end up trapped in a queue unless its speed is equal to V_b, in which case $\omega(\rho(t,y(t)+)) = \omega(\rho(t,y(t)-)) = V_b$. Therefore Carathéodory solutions are always well defined.*

Theorem 7 *Let $\rho_o \in \mathrm{BV}(\mathbb{R};[0,1])$, then the Cauchy problem (2.1.7) admits a solution in the sense of Definition 2.3.1.*

The rest of the section is devoted to the proof of Theorem 7. In particular, we will construct a sequence of approximate solutions via the wave-front tracking method, and prove its convergence. Finally we will check that the limit functions satisfy conditions (2.3.3a)-(2.3.3d) of Definition 2.3.1.

2.3.1 Wave-front tracking

To construct piecewise constant approximate solutions, we adapt the standard wave-front tracking method as described in Section 1.1.4.
Fix a positive $n \in \mathbb{N}$, $n > 0$ and introduce in $[0,1]$ the mesh $\mathcal{M}_n = \{\rho_i^n\}_{i=0}^{2^n}$ defined by

$$\mathcal{M}_n = \left(2^{-n}\mathbb{N} \cap [0,1]\right).$$

In order to include the critical points $\check{\rho}_\alpha, \rho_\alpha$, we modify the above mesh as follows:

- if $\min_i |\check{\rho}_\alpha - \rho_i^n| = 2^{-n-1}$, then we simply add the new point to the mesh:

$$\widetilde{\mathcal{M}}_n = \mathcal{M}_n \cup \{\check{\rho}_\alpha\};$$

- if $|\check{\rho}_\alpha - \rho_l^n| = \min_i |\check{\rho}_\alpha - \rho_i^n| < 2^{-n-1}$, then we replace ρ_l^n by $\check{\rho}_\alpha$:

$$\widetilde{\mathcal{M}}_n = \mathcal{M}_n \cup \{\check{\rho}_\alpha\} \setminus \{\rho_l^n\};$$

- we perform the same operations for $\hat{\rho}_\alpha$.

In this way the distance between two points of the mesh $\widetilde{\mathcal{M}}_n = \{\tilde{\rho}_i^n\}$ satisfies the lower bound $\left|\tilde{\rho}_i^n - \tilde{\rho}_j^n\right| \geq 2^{-n-1}$. Let f_n be the piecewise linear function which coincides with f on $\mathcal{M}_n$, and let ρ_o^n be a piecewise constant function defined by

$$\rho_o^n = \sum_{j\in\mathbb{Z}} \rho_{o,j}^n \, \chi_{]x_{j-1},x_j]} \quad \text{with } \rho_{o,j}^n \in \widetilde{\mathcal{M}}_n,$$

which approximates ρ_o in the sense of the strong $\mathcal{L}^1$ topology, that is

$$\lim_{n\to\infty} \|\rho_o^n - \rho_o\|_{\mathcal{L}^1(\mathbb{R})} = 0,$$

and such that $\mathrm{TV}(\rho_o^n) \leq \mathrm{TV}(\rho_o)$. Above, we have set $x_0 = y_o$.
For small times $t > 0$, a piecewise approximate solution (ρ^n, y_n) to (2.1.7) is constructed piecing together the solutions to the Riemann problems

$$\begin{cases} \partial_t \rho + \partial_x \left(f^n(\rho)\right) = 0, \\ \rho(0,x) = \begin{cases} \rho_{o,0} \text{ if } x < y_o, \\ \rho_{o,1} \text{ if } x > y_o, \end{cases} \\ f(\rho(t,0)) - \dot{y}_n(t)\rho(t,0) \leq \dfrac{\alpha}{4}(1-\dot{y}_n)^2, \end{cases} \qquad \begin{cases} \partial_t \rho + \partial_x \left(f^n(\rho)\right) = 0, \\ \rho(0,x) = \begin{cases} \rho_j \quad \text{if } x < x_j, \\ \rho_{j+1} \text{ if } x > x_j, \end{cases} \\ j \neq 0, \end{cases} \tag{2.3.4}$$

where y_n satisfies

$$\begin{cases} \dot{y}_n(t) = \omega(\rho^n(t, y_n(t)+)), \\ y_n(0) = y_o. \end{cases} \tag{2.3.5}$$

Note that the solutions to the constrained Riemann problem in (2.3.4), left, coupled with (2.3.5), is constructed by means of $\mathcal{RS}^\alpha$, see Definition 2.2.1. The approximate solution ρ^n constructed above can be prolonged up to the first time $\bar{t} > 0$, where two discontinuities collide, or a discontinuity hits the bus trajectory. In both cases, a new Riemann problem arises and its solution, obtained in the former case with $\mathcal{RS}$ and in the latter case with $\mathcal{RS}^\alpha$, allows to extend ρ^n further in time.

2.3.2 Bounds on the total variation

Given an approximate solution $\rho^n = \rho^n(t,\cdot)$ constructed by the wave-front tracking method, we define the Glimm type functional

$$\Upsilon(t) = \Upsilon(\rho^n(t,\cdot)) = \mathrm{TV}(\rho^n) + \gamma = \sum_j \left|\rho_{j+1}^n - \rho_j^n\right| + \gamma, \tag{2.3.6}$$

where γ is given by

$$\gamma = \gamma(t) = \begin{cases} 0 & \text{if } \rho^n(t, y_n(t)-) = \hat{\rho}_\alpha, \ \rho^n(t, y_n(t)+) = \check{\rho}_\alpha \\ 2|\hat{\rho}_\alpha - \check{\rho}_\alpha| & \text{otherwise.} \end{cases} \tag{2.3.7}$$

The value of γ is chosen to get the following interaction estimates.

Lemma 8 *For any $n \in \mathbb{N}$, the map $t \mapsto \Upsilon(t) = \Upsilon(\rho^n(t,\cdot))$ at any interaction either decreases by at least 2^{-n}, or remains constant and the number of waves does not increases.*

Lemma 8 in particular implies that the wave-front tracking procedure can be prolonged to any time $T > 0$.

Proof. In order to obtain a uniform bound on the total variation we will consider the different types of interactions separately. In particular, it is not restrictive to assume that at any interaction time $t = \bar{t}$ either two waves interact or a single wave hits the bus trajectory.

(I1) We consider a classical collision between two waves (see Figure 2.3.1). In this case either two shocks collide (which means that the number of waves diminishes) or a shock and a rarefaction cancel. In any case, $\mathrm{TV}(\rho^n)$ is not increasing and γ is constant and we get $\Upsilon(\bar{t}+) \leq \Upsilon(\bar{t}-)$.

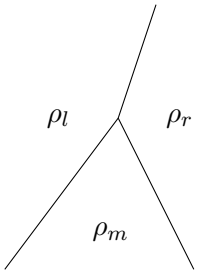


Figure 2.3.1: Interaction between two waves away from the bus trajectory.

A particular case is when the bus trajectory coincides with one of the interacting waves. In this case the wave must be a classical shock between a left state belonging to $[0, \check{\rho}_\alpha]$ and a right state in $[\hat{\rho}_\alpha, \rho^*]$, and it must move with speed equal to V_b. This interaction cannot generate a non-classical shock, therefore it can be treated as the general case above.

(I2) Assume that a wave between two states $\rho_L, \rho_R \in [0, \check{\rho}_\alpha] \cup [\hat{\rho}_\alpha, 1]$ hits the bus trajectory (see Figure 2.3.2). In this case the front crosses the bus trajectory and no new wave is created. Notice that this collision may eventually lead to a modification of the bus trajectory (for example, if $\rho_R > \rho^*$, after the collision the bus takes the velocity $v(\rho_R) \neq \omega(\rho_L)$). In any case, $\mathrm{TV}(\rho^n)$, Υ and the number of waves remain constant.

(I3) Assume that we are in the presence of the non-classical shock along the bus trajectory. Different types of interactions may occur.

(I3.1) Assume the non-classical shock is present at $t < \bar{t}$, and a shock between $\rho_L \in [0, \check{\rho}_\alpha]$ and $\hat{\rho}_\alpha$ hits the bus trajectory on the left (Figure 2.3.3a). After the

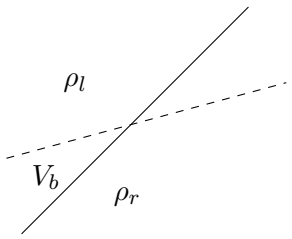


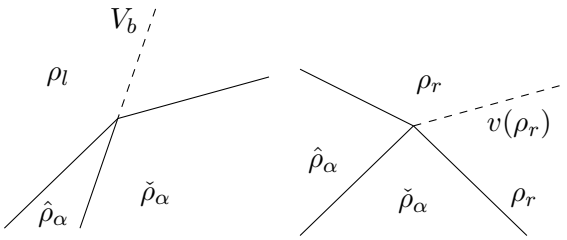
Figure 2.3.2: Interaction between a wave and the bus trajectory.

collision, the number of discontinuities in ρ^n diminishes and the functional Υ remains constant:

$$\begin{aligned}\Delta\Upsilon(\bar{t}) &= \Upsilon(\bar{t}+) - \Upsilon(\bar{t}-)\\ &= |\rho_L - \check{\rho}_\alpha| + 2|\hat{\rho}_\alpha - \check{\rho}_\alpha| - (|\rho_L - \hat{\rho}_\alpha| + |\hat{\rho}_\alpha - \check{\rho}_\alpha|)\\ &= 0.\end{aligned}$$

Assume now a shock between $\check{\rho}_\alpha$ and $\rho_R \in [\hat{\rho}_\alpha, 1]$ hits the bus trajectory on the right (Figure 2.3.3b). Then, after the collision, the bus assumes the velocity $v(\rho_R)$ of the traffic mainstream, the number of discontinuities in ρ^n diminishes and the functional Υ remains constant:

$$\begin{aligned}\Delta\Upsilon(\bar{t}) &= \Upsilon(\bar{t}+) - \Upsilon(\bar{t}-)\\ &= |\hat{\rho}_\alpha - \rho_R| + 2|\hat{\rho}_\alpha - \check{\rho}_\alpha| - (|\check{\rho}_\alpha - \rho_R| + |\hat{\rho}_\alpha - \check{\rho}_\alpha|)\\ &= 0.\end{aligned}$$

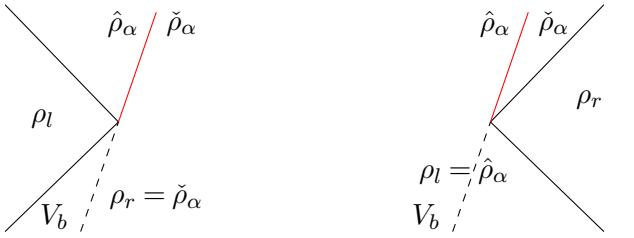


(a) Shock from the left. (b) Shock from the right.

Figure 2.3.3: Interaction between a shock and the bus trajectory.

(I3.2) Consider now the case of a non-classical shock arising at $t = \bar{t}$. We first analyze the case of a rarefaction front hitting the bus trajectory from the left (Figure 2.3.4a). We have $\rho_R = \check{\rho}_\alpha < \rho_L \leq \hat{\rho}_\alpha$. In this case new waves are created at $\bar{t}$ and the total variation is given by:

- $\mathrm{TV}(\bar{t}-) = |\check{\rho}_\alpha - \rho_L| \geq 2^{-n-1}$;
- $\mathrm{TV}(\bar{t}+) = |\hat{\rho}_\alpha - \check{\rho}_\alpha| + |\hat{\rho}_\alpha - \rho_L| \leq 2|\hat{\rho}_\alpha - \check{\rho}_\alpha|$,



(a) Rarefaction from the left.

(b) Rarefaction from the right.

Figure 2.3.4: Interaction between a rarefaction and the bus trajectory.

where the second estimate is obtained by simple algebraic manipulation of the total variation $\mathrm{TV}(\bar{t}+)$. Then we are able to compute the changes in the functional as follows:

$$\begin{aligned}\Delta\Upsilon(\bar{t}) &= \Upsilon(\bar{t}+) - \Upsilon(\bar{t}-)\\ &= (|\hat{\rho}_\alpha - \check{\rho}_\alpha| + |\hat{\rho}_\alpha - \rho_L|) - (|\check{\rho}_\alpha - \rho_L| + 2|\hat{\rho}_\alpha - \check{\rho}_\alpha|)\\ &= 2(\check{\rho}_\alpha - \rho_L) \leq -2^{-n},\end{aligned}$$

hence the functional is strictly decreasing.
Let us consider now the case of a rarefaction front hitting the bus trajectory from the right (Figure 2.3.4, right). In this case we have $\check{\rho}_\alpha \leq \rho_R < \rho_L = \hat{\rho}_\alpha$. A new wave is created at $\bar{t}$ and the total variation is given by:

- $\mathrm{TV}(\bar{t}-) = |\hat{\rho}_\alpha - \rho_R| \geq 2^{-n-1}$;
- $\mathrm{TV}(\bar{t}+) = |\hat{\rho}_\alpha - \check{\rho}_\alpha| + |\check{\rho}_\alpha - \rho_R| \leq 2|\hat{\rho}_\alpha - \check{\rho}_\alpha|$,

The functional changes as follows:

$$\begin{aligned}\Delta\Upsilon(\bar{t}) &= \Upsilon(\bar{t}+) - \Upsilon(\bar{t}-)\\ &= (|\hat{\rho}_\alpha - \check{\rho}_\alpha| + |\check{\rho}_\alpha - \rho_R|) - (|\hat{\rho}_\alpha - \rho_R| + 2|\hat{\rho}_\alpha - \check{\rho}_\alpha|)\\ &= 2(\hat{\rho}_\alpha - \rho_R) \leq -2^{-n},\end{aligned}$$

making the functional strictly decreasing.

□

2.3.3 Convergence of approximate solutions

In this section we prove that the limit of wave-front tracking approximations provides a solution (ρ, y) of the PDE-ODE model (2.1.7) in the sense of Definition 2.3.1.
We start showing the convergence of the wave-front tracking approximations.

Lemma 9 *Let ρ^n and y_n, $n \in \mathbb{N}$, be the wave-front tracking approximations to (2.1.7) constructed as detailed in Section 2.3.1, and assume $\mathrm{TV}(\rho_o) \le C$ be bounded, $0 \le \rho_o \le 1$. Then, up to a subsequence, we have the following convergences*

$$\rho^n \to \rho \qquad \text{in } \mathcal{L}^1_{loc}(\mathbb{R}^+ \times \mathbb{R}; [0,1]); \tag{2.3.8a}$$

$$y_n(\cdot) \to y(\cdot) \qquad \text{in } \mathcal{L}^\infty([0,T]; \mathbb{R}), \text{ for all } T > 0; \tag{2.3.8b}$$

$$\dot{y}_n(\cdot) \to \dot{y}(\cdot) \qquad \text{in } \mathcal{L}^1([0,T]; \mathbb{R}), \text{ for all } T > 0; \tag{2.3.8c}$$

for some $\rho \in \mathcal{C}^0\left(\mathbb{R}^+; \mathcal{L}^1 \cap \mathrm{BV}(\mathbb{R}; [0,1])\right)$ and $y \in \mathcal{W}^{1,1}(\mathbb{R}^+, \mathbb{R})$.

Proof. Lemma 8 gives a uniform bound on the total variation of approximate solutions: $\mathrm{TV}(\rho^n(t,\cdot)) \le \Upsilon(t) \le \Upsilon(0)$. A standard procedure based on Helly's Theorem (see [20, Theorem 2.4]) ensures the existence of a subsequence converging to some function $\rho \in \mathcal{C}^0\left(\mathbb{R}^+; \mathcal{L}^1 \cap \mathrm{BV}(\mathbb{R}; [0,1])\right)$, proving (2.3.8a).
Since $|\dot{y}_n(t)| \le V_b$, the sequence $\{y_n\}$ is uniformly bounded and equicontinuous on any compact interval $[0,T]$. By Ascoli-Arzelà Theorem, there exists a subsequence converging uniformly, giving (2.3.8b).
In order to prove (2.3.8c), we have to show that $\mathrm{TV}(\dot{y}_n; [0,T])$ is uniformly bounded. In fact, the analysis performed in Section 2.3.2 shows that $\dot{y}_n$ can change only at interactions with waves coming from its right. We can estimate the speed variation at interactions times $\bar{t}$ by the size of the interacting front:

$$|\dot{y}_n(\bar{t}+) - \dot{y}_n(\bar{t}-)| = |\omega(\rho_L) - \omega(\rho_R)| \le |\rho_L - \rho_R|.$$

In particular, $\dot{y}_n$ is non-increasing at interactions with shock fronts and non-decreasing at interactions with rarefaction fronts, which must be originated at $t = 0$. In fact, the analysis performed in Section 2.3.2 shows that no new rarefaction front can arise at interactions. Therefore,

$$\mathrm{TV}(\dot{y}_n; [0,T]) \le 2\,\mathrm{PV}(\dot{y}_n; [0,T]) + \|\dot{y}_n\|_{\mathcal{L}^\infty([0,T])} \le 2\,\mathrm{TV}(\rho_o) + V_b$$

is uniformly bounded. Above, $\mathrm{PV}(\dot{y}_n; [0,T])$ denotes the positive variation of $\dot{y}_n$, i.e. the total amount of positive jumps in the interval $[0,T]$. □

Proof of (2.3.3a) and (2.3.3b)

Since ρ^n converge strongly to ρ in $\mathcal{L}^1_{loc}(\mathbb{R}^+ \times \mathbb{R}; [0,1])$, it is straightforward to pass to the limit in the weak formulation of the conservation law, proving that the limit function ρ satisfies (2.3.3a). Kružhkov entropy condition (2.3.3b) can be recovered in the same way.

Proof of (2.3.3c) and (2.3.3d)

We will prove that

$$\lim_{n\to\infty} \rho^n(t, y_n(t)+) = \rho^+(t) = \rho(t, y(t)+) \quad \text{for a.e. } t \in \mathbb{R}^+. \tag{2.3.9}$$

By pointwise convergence a.e. of ρ^n to ρ, there exists a sequence $z_n \geq y_n(t)$ such that $z_n \to y(t)$ and $\rho^n(t, z_n) \to \rho^+(t)$.

For a.e. $t > 0$, the point $(t, y(t))$ is for $\rho(t, \cdot)$ either a continuity point, or it belongs to a discontinuity curve (represented by $y(\cdot)$) that can be either a classical shock or a non-classical discontinuity between $\rho(t, y(t)-) = \hat{\rho}_\alpha$ and $\rho(t, y(t)+) = \check{\rho}_\alpha$.

Fix $\epsilon^* > 0$ and assume $\mathrm{TV}\left(\rho(t, \cdot);]y(t) - \delta, y(t) + \delta[\right) \leq \epsilon^*$, for some $\delta > 0$. Then by weak convergence of measures (see [31, Lemma 15]) we have
$\mathrm{TV}\left(\rho^n(t, \cdot);]y(t) - \delta, y(t) + \delta[\right) \leq 2\epsilon^*$ for n large enough, and we can estimate

$$\left|\rho^n(t, y_n(t)+) - \rho^+(t)\right| \leq |\rho^n(t, y_n(t)+) - \rho^n(t, z_n)| + \left|\rho^n(t, z_n) - \rho^+(t)\right| \leq 3\epsilon^*$$

for n large enough.

If $\rho(t, \cdot)$ has a discontinuity of strength greater then ϵ^* at $y(t)$, then also $|\rho^n(t, y_n(t)+) - \rho^n(t, y_n(t)-)| \geq \epsilon^*/2$ for n sufficiently large, and we proceed as in [31, Section 4]. That is, we set $\rho^{n,+} = \rho^n(t, y_n(t)+)$ and we show that for each $\varepsilon > 0$ there exists $\delta > 0$ such that for all n large enough there holds

$$\left|\rho^n(s, x) - \rho^{n,+}\right| < \varepsilon \quad \text{for } |s - t| \leq \delta,\ |x - y(t)| \leq \delta,\ x > y_n(s). \tag{2.3.10}$$

In fact, if (2.3.10) does not hold, we could find $\varepsilon > 0$ and sequences $t_n \to t$, $\delta_n \to 0$ such that $\mathrm{TV}\left(\rho^n(t_n, \cdot);]y_n(t_n), y_n(t_n) + \delta_n[\right) \geq \varepsilon$. By strict concavity of the flux function f, there should be a uniformly positive amount of interactions in an arbitrarily small neighborhood of $(t, y(t))$, giving a contradiction. Therefore (2.3.10) holds and we get

$$\left|\rho^n(t, y_n(t)+) - \rho^+(t)\right| \leq |\rho^n(t, y_n(t)+) - \rho^n(t, z_n)| + \left|\rho^n(t, z_n) - \rho^+(t)\right| \leq 2\varepsilon$$

for n large enough, thus proving (2.3.9). Combining (2.3.8c) and (2.3.9) we get $\dot{y}(t) = \omega(\rho(t, y(t)+))$ for a.e. $t > 0$.

In order to verify that the limit solutions satisfy the constraint (2.3.3d), we can use directly (2.3.9) and the fact that wave-front tracking approximations satisfy the constraint (2.1.6) by construction.

2.4 An approach to the stability of the solutions

In this section we show a tentative approach to the problem of the stability of solutions for this type of models. In particular, we get some of the bounds necessary to prove stability but, at the moment, we are not able to prove that the shifts are uniformly bounded for all times $t > 0$. We use the technique of generalized tangent vectors, introduced in [21, 22] for systems of conservation laws, and adapted to scalar equations in traffic applications, see [33, 68] for a detailed description. To resume, we introduce a class of curves (pseudo-polygonals) that connect any two initial data in $\mathcal{D}_C^n = \{(\rho, y) : [0, 1] \times \mathbb{R} \to \mathcal{M}_n \times \mathbb{R} \colon \mathrm{TV}(\rho) \leq C\}$.

Let $]a, b[\subset \mathbb{R}$ and $\mathbf{P}C$ denote the set of piecewise constant functions with finitely many jumps. An *elementary path* is a map $\gamma :]a, b[\to \mathbf{P}C$ of the form

$$\gamma(\theta) = \sum_{j=1}^{N} \rho_j \cdot \chi_{[x_{j-1}^\theta, x_j^\theta[} + y^\theta, \quad \text{where } x_j^\theta = x_j + \xi_{w_j}\theta,\ y^\theta = y + \xi_b\theta,$$

with $x_{j-1}^\theta < x_j^\theta$ for all $\theta \in]a,b[$ and $j = 1, \dots, N$.

A *pseudo-polygonal* is a continuous map $\gamma :]a,b[\to \mathcal{D}_C^n$ such that there exist countably many disjoint open intervals $J_h \subseteq]a,b[$ so that $]a,b[\setminus \cup_h J_h$ is countable and the restriction of γ to each J_h is an elementary path. Moreover, any two elements of $\mathcal{D}_C^n$ can be joined by a pseudo-polygonal γ enterely contained in $\mathcal{D}_C^n$.

We define the length of a pseudo-polygonal γ as

$$\|\gamma\|_n = \int_a^b \Gamma_n[\gamma(\theta)]\, d\theta, \quad \text{where } \Gamma_n = \sum_j \left|\sigma_j \xi_{w_j}\right| W_j + \varphi |\xi_b|,$$

for some suitable weights W_j and φ and σ_j denoting the strength of the jump at x_j: $\sigma_j = \rho_{j+1} - \rho_j$. In the next Section 2.4.1 we will show some bounds on the interactions among waves that can be used to construct uniformly bounded weights such that $W_j, \varphi \in [1, W]$ and the map $t \mapsto \Gamma_n(u(t))$ is uniformly bounded for all times $t > 0$ by $\Gamma_n(u(0))$ multiplied by a factor depending only on the total variation of the initial datum and the final time t. The first requirement implies that the metric

$$d^n(u,v) = \inf \{ \|\gamma\|_n : \gamma(a) = u,\ \gamma(b) = v \}$$

is equivalent to the $\mathcal{L}^1$-distance uniformly in n; the latter ensures the Lipschitz continuity of the semigroup.

2.4.1 Estimates on shifts

We aim at estimating the $\mathcal{L}^1$-distance among solutions, studying how the distance between two approximate solutions varies in time through the study of the evolution of norms of tangent vectors along wave-front tracking approximations.
Fix an approximate wave-front tracking solution (ρ^n, y_n) to (2.1.7). Without loss of generality, at any interaction time $\bar{t} > 0$, one of the following cases occurs:

a) two waves interact away from $x = y_n(\bar{t})$ and no other interaction takes place;

b) a wave interacts with the bus trajectory $x = y_n(\bar{t})$ and no other interaction takes place;

c) interaction involving a non-classical shock, either the non-classical shock is created in the interaction or it disappears at the interaction.

Case a) is classical, and it is well known that the $\mathcal{L}^1$-distance is decreasing, see [67, Lemma 2.7.2]. Here we concentrate on case b) and c). We denote by $w(t,x) = \omega(\rho^n(t, x+))$, then w is piecewise constant with jumps along a finite number of Lipschitzean polygonal lines. Following [29, 46], we introduce the bus trajectory tangent vector

$$\xi_b(t) = \lim_{\varepsilon \to 0^+} \frac{y_\varepsilon(t) - y(t)}{\varepsilon}$$

where $t \mapsto y_\varepsilon(t)$ is the solution of (2.3.2) with an initial datum $y_o + \varepsilon$. The map $t \mapsto \xi_b(t)$ is piecewise constant with jumps at those times where y crosses a discontinuity in w. At these points the tangent vector varies according to

$$\xi_b^+ \doteq \xi_b(t+) = \frac{\dot{y}(t+) - \Lambda}{\dot{y}(t-) - \Lambda}\, \xi_b(t-) = \begin{cases} 0 & \text{if } \dot{y}(t+) = \Lambda, \\ \dfrac{w^+ - \Lambda}{w^- - \Lambda}\, \xi^- & \text{if } \dot{y}(t+) \neq \Lambda, \end{cases} \tag{2.4.1}$$

where Λ is the speed of the discontinuity in w and $w^\pm = \omega(\rho^n(t^\pm, y(t^\pm))$ are the values of w on the sides of the discontinuity (see Figure 2.4.1). In the following, we will assume

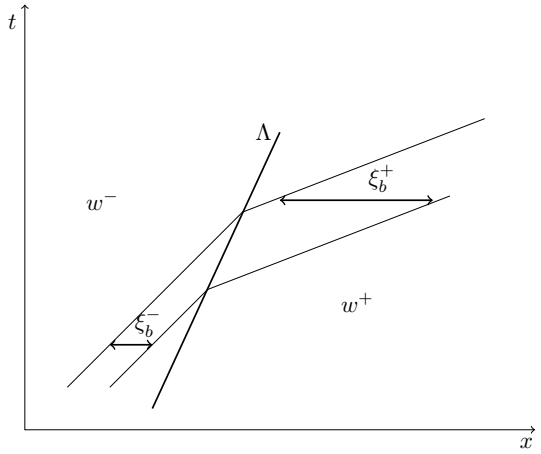


Figure 2.4.1: Changes of ξ_b across a discontinuity in $w = \omega(\rho^n)$.

that both the wave front and the bus trajectory are shifted by ξ_w^- and ξ_b^- respectively. For case b), since the wave speed does not change after the interaction, its shift remains constant, $\xi_w^+ = \xi_w^-$, and we just need to estimate the value of the bus shift ξ_b^+ after the interaction. Following [29, 46], the idea is to find a weight $\varphi = \varphi(t)$ for the bus shift such that the weighted tangent vector $z(t) \doteq \varphi(t)\xi_b(t)$ is not increasing in time. We claim that we can take $\varphi(t) = \varphi(\rho(t, y(t)+))$, where $\varphi(y)$ is defined by

$$\varphi(\rho) \doteq \frac{V_b - f'(\rho)}{\omega(\rho) - f'(\rho)} \in [1, 1 + V_b]\ . \tag{2.4.2}$$

Observe that

$$\frac{d}{d\lambda}\left(\frac{V_b - \lambda}{\omega(\rho) - \lambda}\right) = \frac{V_b - \omega(\rho)}{(\omega(\rho) - \lambda)^2} \geq 0. \tag{2.4.3}$$

We can now define weights $W_i = W_i(t)$ for waves such that the weighted $\mathcal{L}^1$-distance

$$\Gamma_n(t) = \sum_i W_i(t)|\xi_{w_i}(t)\sigma_i(t)| + |z(t)|$$

is not increasing in time. We propose to take

$$W = \begin{cases} \dfrac{2+\rho^*}{\rho^*} & \text{if } \rho^* \le \rho_R + \rho_L \\ 1 & \text{otherwise.} \end{cases} \tag{2.4.4}$$

where $W \in [1, c_0]$.
In order to investigate how tangent vectors vary in time, we have to distinguish different cases.

I. Interaction with a shock: $\rho_R > \rho^*$ and $\rho_L \in [0, \check{\rho}_\alpha] \cup [\hat{\rho}_\alpha, \rho_R]$ (i.e. $w^+ = v(\rho_R) < w^-$). In this case the bus is slowed down by the presence of a queue in front of it. This

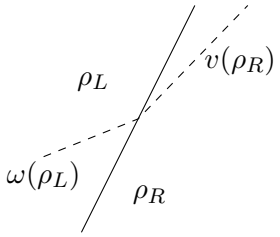


Figure 2.4.2: Case I: interaction with a shock.

creates a discontinuity in its velocity (see Figure 2.4.2). The wave speed does not change across interaction, so we will have $\xi_w^+ = \xi_w^-$. For the bus shift we have the following

$$\xi_b^+ = \frac{v(\rho_R) - \Lambda}{\omega(\rho_L) - \Lambda}\, \xi_b^- + \frac{\omega(\rho_L) - v(\rho_R)}{\omega(\rho_L) - \Lambda}\, \xi_w^-, \tag{2.4.5}$$

where the speed of the discontinuity is given by $\Lambda = 1 - \rho_R - \rho_L$.
If $\rho_L \in [0, \check{\rho}_\alpha] \cup [\hat{\rho}_\alpha, \rho^*]$, then $\omega(\rho_L) = V_b$ and we compute

$$\begin{aligned} z(t+) &= |\varphi(t+)\xi_b(t+)| = \frac{V_b - f'(\rho_R)}{\omega(\rho_R) - f'(\rho_R)}\, \xi_b^+ \\ &= \frac{V_b - f'(\rho_R)}{v(\rho_R) - f'(\rho_R)} \cdot \frac{v(\rho_R) - \Lambda}{V_b - \Lambda}\, \xi_b^- + \frac{V_b - f'(\rho_R)}{v(\rho_R) - f'(\rho_R)} \cdot \frac{V_b - v(\rho_R)}{V_b - \Lambda}\, \xi_w^- \\ &= \frac{1 - \rho^* - 1 + 2\rho_R}{1 - \rho_R - 1 + 2\rho_R} \cdot \frac{1 - \rho_R - 1 + \rho_L + \rho_R}{1 - \rho^* - 1 + \rho_L + \rho_R}\, \xi_b^- + \\ &+ \frac{1 - \rho^* - 1 + 2\rho_R}{1 - \rho_R - 1 + \rho_L + \rho_R} \cdot \frac{1 - \rho^* - 1 + \rho_R}{1 - \rho^* - 1 + \rho_L + \rho_R}\, \xi_w^- \\ &= \frac{2\rho_R - \rho^*}{\rho_R} \cdot \frac{\rho_L}{\rho_L + \rho_R - \rho^*}\, \xi_b^- + \frac{2\rho_R - \rho^*}{\rho_R} \cdot \frac{\rho_R - \rho^*}{\rho_L + \rho_R - \rho^*}\, \xi_w^- \\ &\le \left|\varphi^- \xi_b^-\right| + \frac{2}{\rho_R} |\rho_R - \rho_L| \left|\xi_w^-\right| \\ &\le \left|\varphi^- \xi_b^-\right| + \frac{2}{\rho^*} |\rho_R - \rho_L| \left|\xi_w^-\right|. \end{aligned} \tag{2.4.6}$$

The above inequalities are obtained using the fact that $\varphi(t-)=1$ and $\rho_R>\rho^*$. We then obtain

$$z(t+)\leq\left|\varphi^-\xi_b^+\right|+\frac{2}{\rho^*}\left|\sigma^-\xi_w^-\right|$$

which gives us

$$\begin{aligned}z(t+)+W^+\left|\sigma^+\xi_w^+\right|&\leq z(t-)+\frac{2}{\rho^*}\left|\sigma^-\xi_w^-\right|+W^+\left|\sigma^-\xi_w^-\right|\\&\leq z(t-)+W^-\left|\sigma^-\xi_w^-\right|,\end{aligned}$$

where we used that $W^-=W^++\frac{2}{\rho^*}$ and $\sigma^-=\sigma^+$.
If $\rho_L\in[\rho^*,\rho_R]$,from (2.4.5) we obtain

$$\begin{aligned}z(t+)=|\varphi(t+)\xi_b(t+)|&=\frac{V_b-f'(\rho_R)}{\omega(\rho_R)-f'(\rho_R)}\ \xi_b^+\\&=\frac{V_b-f'(\rho_R)}{v(\rho_R)-f'(\rho_R)}\cdot\frac{v(\rho_R)-\Lambda}{v(\rho_L)-\Lambda}\ \xi_b^-+\frac{V_b-f'(\rho_R)}{v(\rho_R)-f'(\rho_R)}\cdot\frac{v(\rho_L)-v(\rho_R)}{v(\rho_L)-\Lambda}\ \xi_w^-\\&=\frac{1-\rho^*-1+2\rho_R}{1-\rho_R-1+2\rho_R}\cdot\frac{1-\rho_R-1+\rho_L+\rho_R}{1-\rho_L-1+\rho_L+\rho_R}\ \xi_b^-+\\&+\frac{1-\rho^*-1+2\rho_R}{1-\rho_R-1+\rho_L+\rho_R}\cdot\frac{1-\rho_L-1+\rho_R}{1-\rho_L-1+\rho_L+\rho_R}\ \xi_w^-\\&=\frac{2\rho_R-\rho^*}{\rho_R}\cdot\frac{\rho_L}{\rho_R}\ \xi_b^-+\frac{2\rho_R-\rho^*}{\rho_R}\cdot\frac{\rho_R-\rho_L}{\rho_R}\ \xi_w^-\\&\leq\left|\varphi^-\xi_b^-\right|+\frac{2}{\rho_R}|\rho_R-\rho_L|\left|\xi_w^-\right|\\&\leq\left|\varphi^-\xi_b^-\right|+\frac{2}{\rho^*}|\rho_R-\rho_L|\left|\xi_w^-\right|,\end{aligned}\tag{2.4.7}$$

since

$$\frac{2\rho_R-\rho^*}{\rho_R}\cdot\frac{\rho_L}{\rho_R}\leq\frac{2\rho_L-\rho^*}{\rho_L}=\varphi^-$$

for $\rho^*\leq\rho_L\leq\rho_R$.This gives us

$$z(t+)+W^+\left|\sigma^+\xi_w^+\right|\leq z(t-)+\frac{2}{\rho^*}\left|\sigma^-\xi_w^-\right|+W^+\left|\sigma^-\xi_w^-\right|\leq z(t-)+W^-\left|\sigma^-\xi_w^-\right|,\tag{2.4.8}$$

where we used that $W^-=W^++\frac{2}{\rho^*}$ and $\sigma^-=\sigma^+$.

II. Interaction with a rarefaction: $\rho^*\leq\rho_R<\rho_L$ and $|\rho_R-\rho_L|\leq 2^{-n+1}$ (i.e. $\omega^+=v(\rho_R)\geq v(\rho_L)=\omega^-$, see Figure 2.4.3) The bus shift is again given by (2.4.5) and the wave shift shift does not change across the interaction.

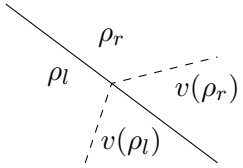


Figure 2.4.3: Case II: Interaction with a rarefaction.

Hence, we have as in (2.4.7)

$$\begin{aligned} z(t+) &= \frac{2\rho_R-\rho^*}{\rho_R}\cdot\frac{\rho_L}{\rho_R}\,\xi_b^- + \frac{2\rho_R-\rho^*}{\rho_R}\cdot\frac{\rho_R-\rho_L}{\rho_R}\,\xi_w^- \\ &= \frac{2\rho_R-\rho^*}{\rho_R}\cdot\frac{\rho_L}{\rho_R}\cdot\frac{2\rho_L-\rho^*}{\rho_L}\cdot\frac{\rho_L}{2\rho_L-\rho^*}\,\xi_b^- + \frac{2\rho_R-\rho^*}{{\rho_R}^2}\cdot|\rho_L-\rho_R|\,\xi_w^- \\ &= \frac{2\rho_R-\rho^*}{2\rho_L-\rho^*}\cdot\frac{{\rho_L}^2}{{\rho_R}^2}\big|\varphi^-\xi_b^-\big| + \frac{2\rho_R-\rho^*}{{\rho_R}^2}\cdot|\rho_L-\rho_R|\,\xi_w^- \\ &\le \left(1+\frac{2^{-n+1}}{\rho^*}\right)^2\big|\varphi^-\xi_b^-\big| + \frac{2}{\rho^*}\big|\sigma^-\xi_w^-\big| \end{aligned}$$

where we used the fact that

$$\frac{{\rho_L}^2}{{\rho_R}^2} = \left(1+\frac{\rho_L-\rho_R}{\rho_R}\right)^2 \le \left(1+\frac{2^{-n+1}}{\rho^*}\right)^2.$$

This gives us

$$\begin{aligned} z(t+)+W^+\big|\sigma^+\xi_w^+\big| &\le \left(1+\frac{2^{-n+1}}{\rho_R}\right)^2 z(t-)+\frac{2}{\rho^*}\big|\sigma^-\xi_w^-\big|+W^+\big|\sigma^-\xi_w^-\big| \\ &\le \left(1+\frac{2^{-n+1}}{\rho^*}\right)^2 z(t-)+W^-\big|\sigma^-\xi_w^-\big|, \end{aligned} \tag{2.4.9}$$

taking $W^- \ge W^+ + \frac{2}{\rho^*}$. Notice that, defining

$$\zeta(t) = z(t) + W(t)|\sigma(t)\xi_w(t)|, \tag{2.4.10}$$

we get

$$\begin{aligned} \zeta(t+) &= z(t+)+W(t+)|\sigma(t+)\xi_w(t+)| \\ &\le \left(1+\frac{2^{-n+1}}{\rho^*}\right)^2 z(t-)+W(t-)|\sigma(t-)\xi_w(t-)| \\ &\le \left(1+\frac{2^{-n+1}}{\rho^*}\right)^2 \zeta(t-). \end{aligned}$$

Since this multiplication factor is applied at each time the bus trajectory hits a rarefaction fan, for any time $T>0$ the total increase can be bounded by

$$\zeta(T) \le \left(1+2\frac{2^{-n}}{\rho^*}\right)^{\frac{2NV(\rho_o)}{2^{-n}}}\zeta(0) \le \exp\left(\frac{4NV(\rho_o)}{\rho^*}\right)\zeta(0), \tag{2.4.11}$$

which gives a bound depending only on the total variation of the initial datum. For case c) we refer to the classification made in Section 2.3.2.

III. The non-classical shock is canceled. We refer here to the interaction I3.1 as shown in Figure 2.3.3.

If the interacting wave is approaching from the left, as in Figure 2.3.3(a), the velocity of the bus does not change along the discontinuity, therefore the shift of the bus remains constant. Moreover, we have $\varphi^- = \varphi^+ = 1$. Concerning the wave shift, we can use the conservation law. Hence, we have

$$\left|\sigma^+\xi_w^+\right| = \left|\sigma^-\xi_w^- + (\hat{\rho}_\alpha - \check{\rho}_\alpha)\xi_b^-\right| \leq \left|\sigma^-\xi_w^-\right| + \left|(\hat{\rho}_\alpha - \check{\rho}_\alpha)\xi_b^-\right|. \tag{2.4.12}$$

This gives us

$$z(t+) + \left|\sigma^+\xi_w^+\right| \leq z(t-) + \left|\sigma^-\xi_w^-\right| + (\hat{\rho}_\alpha - \check{\rho}_\alpha)\left|\xi_b^-\right|. \tag{2.4.13}$$

If the interacting wave is approaching from the right, as shown in Figure 2.3.3(b), the conservation law still hold for the wave shift, but the shift of bus may change, because its speed may decrease. Since the trajectory of the bus is the same as in case I, we can use estimates (2.4.6) or (2.4.7) to bound $z(t+)$. Hence we have

$$z(t+) + W^+\left|\sigma^+\xi_w^+\right| \leq z(t-) + W^-\left|\sigma^-\xi_w^-\right| + (\hat{\rho}_\alpha - \check{\rho}_\alpha)\left|\xi_b^-\right|, \tag{2.4.14}$$

where we have taken $W^- = W^+ + \frac{2}{\rho^*}$.

IV. The non-classical shock arises. We refer here to the interactions I3.2 as shown in Figure 2.3.4. In this case we have an interaction between a rarefaction and the bus trajectory which creates a non-classical shock after $\bar{t}$. The shift of the bus remains the same $\xi_b^+ = \xi_b^-$ and also

$$\varphi^+ = \frac{V_b - f'(\rho_R)}{v(\rho_R) - f'(\rho_R)} = \frac{V_b - f'(\check{\rho}_\alpha)}{V_b - f'(\check{\rho}_\alpha)} = \varphi^- = 1,$$

if the wave is interacting on the left (as in Figure 2.3.4(a)), and

$$\varphi^+ = \frac{V_b - f'(\hat{\rho}_\alpha)}{V_b - f'(\hat{\rho}_\alpha)} = \frac{V_b - f'(\check{\rho}_\alpha)}{V_b - f'(\check{\rho}_\alpha)} = \varphi^- = 1,$$

if the wave is interacting on the right (as in Figure 2.3.4(b)), so we can focus on the wave shift. By merely using the conservation law we have

$$\sigma^+\xi_w^+ + (\check{\rho}_\alpha - \hat{\rho}_\alpha)\xi_b^+ = \sigma^-\xi_w^-,$$

which gives

$$\left|\sigma^+\xi_w^+\right| \leq (\hat{\rho}_\alpha - \check{\rho}_\alpha)\left|\xi_b^-\right| + \left|\sigma^-\xi_w^-\right|.$$

Finally we obtain

$$z(t+) + \left|\sigma^+\xi_w^+\right| \leq z(t-) + |\hat{\rho}_\alpha - \check{\rho}_\alpha|\left|\xi_b^-\right| + \left|\sigma^-\xi_w^-\right|. \tag{2.4.15}$$

The main issue in proving the stability of the solutions is represented by the cases where a rarefaction hits the bus trajectory from the right. In these cases in fact, it is difficult to find an appropriate bound to the $\mathcal{L}^1$-distance. We are not yet able to prove in this case that there exists some suitable bounded weights that ensure the Lipschitz continuity of the semigroup.

2.5 A front tracking algorithm

The aim of this section is to present numerical methods to compute solutions to strongly coupled constrained PDE-ODE problems with moving constraints (2.1.1). We want to be able to track at each time step the bus trajectory and also to reproduce the non-classical solutions generated by the constraint. Since the solutions of the Riemann problem are known explicitly, our first attempt was to develop a Godunov-type method. The standard Godunov method, in principle, could be applied, however, the results produced are not correct, since it will not reproduce all the characteristics of the solutions and it fails to show the presence of the non-classical shock. This can be overcame by applying a front tracking capturing method which uses a Lagrangian algorithm in which the interface is tracked, such as in [131], together with a numerical method that tracks at each time step the slower vehicle trajectory, taken from [33].

2.5.1 Godunov-type scheme for hyperbolic PDEs with constraint

We use the following notation: $x^n_{j+\frac{1}{2}}$ are the cell interfaces at time t^n with $n \in \mathbb{N}$ and $j \in \mathbb{Z}$. A computational cell is given by $[x^n_{j-\frac{1}{2}}, x^n_{j+\frac{1}{2}}]$ where x^n_j is the center of the cell and $h^n_j = x^n_{j-\frac{1}{2}} - x^n_{j+\frac{1}{2}}$ is the cell width at time t^n. Classical Godunov scheme, as seen in Section 1.3, can be expressed in conservative form as

$$\rho^{n+1}_j = \rho^n_j - \frac{\Delta t^n}{\Delta x}\Big(F(\rho^n_j, \rho^n_{j+1}) - F(\rho^n_{j-1}, \rho^n_j)\Big), \tag{2.5.1}$$

where $F(\rho^n_j, \rho^n_{j+1})$ is the numerical flux. Boundary conditions are imposed on the left and on the right ends of the computational domain.

Since our aim is to track the trajectory of the bus using a Lagrangian algorithm, a moving mesh has to be used. In particular, we develop an algorithm which follows at each time step the bus trajectory and modifies the mesh when the inequality

$$f(\mathcal{RS}(\rho_L, \rho_R)(V_b)) > F_\alpha + V_b \mathcal{RS}(\rho_L, \rho_R)(V_b) \tag{2.5.2}$$

holds. In particular, if (2.5.2) is satisfied, then the solution of the Riemann solver is non-classical and hence, classical Godunov scheme cannot be applied. We are going to shift grid points locally and, as a consequence, we will have a locally nonuniform mesh due to a cell interface moving with the bus trajectory. We will use the superscript *new* to indicate the quantities that are modified at time t^n with the grid. Assume that at time t^n, y^n is the bus position and $y^n \in]x^n_{m-\frac{1}{2}}, x^n_{m+\frac{1}{2}}]$ for some m. When (2.5.2) holds, the algorithm for the adaptive mesh reads as follows:

- If $\left|x^n_{m+\frac{1}{2}} - y^n\right| > \dfrac{h^n_m}{2}$ then change the point $x^n_{m-\frac{1}{2}}$ to $x^{new}_{m-\frac{1}{2}} = y^n$ and recompute the cell averages in the cells $m-1$ and m from the formula

$$\rho^{new}_{m-1} = \frac{\Delta x^n_{m-1}\rho^n_{m-1} + (x^{new}_{m-\frac{1}{2}} - x^n_{m-\frac{1}{2}})\rho^n_m}{\Delta x^{new}_{m-1}} \tag{2.5.3}$$

with $\Delta x^{new}_{m-1} = x^{new}_{m-\frac{1}{2}} - x^n_{m-\frac{3}{2}}$, see Figure 2.5.1.

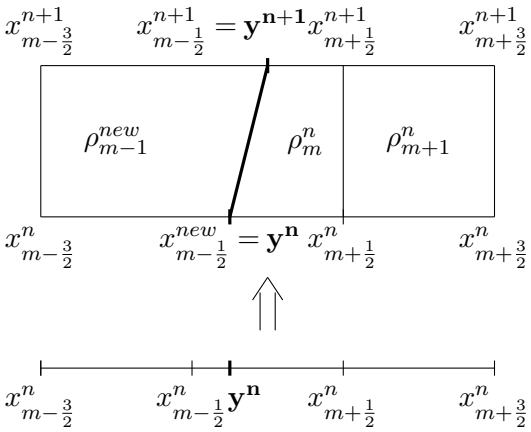


Figure 2.5.1: Local shifting of a grid point when $\left|x^n_{m+\frac{1}{2}} - y^n\right| > \dfrac{h^n_m}{2}$.

- If $\left|x^n_{m+\frac{1}{2}} - y^n\right| \leq \dfrac{h^n_m}{2}$ we adjust the location of the point $x^n_{m+\frac{1}{2}}$ such that $x^{new}_{m+\frac{1}{2}} = y^n$ and then we place the point at the middle distance between $x^n_{m-\frac{3}{2}}$ and $x^{new}_{m+\frac{1}{2}}$, see Figure 2.5.2. We then compute the new cell averages in the cells m and $m+1$ from the formulas

$$\rho^{new}_m = \frac{(x^n_{m-\frac{1}{2}} - x^{new}_{m-\frac{1}{2}})\rho^n_{m-1} + (x^{new}_{m+\frac{1}{2}} - x^n_{m+\frac{1}{2}})\rho^n_m}{\Delta x^{new}_m} \tag{2.5.4}$$

$$\rho^{new}_{m+1} = \frac{\Delta x^n \rho^n_{m+1} + (x^n_{m+\frac{1}{2}} - x^{new}_{m+\frac{1}{2}})\rho^n_m}{\Delta x^{new}_{m+1}} \tag{2.5.5}$$

with $\Delta x^{new}_m = x^{new}_{m+\frac{1}{2}} - x^{new}_{m-\frac{1}{2}}$ and $\Delta x^{new}_{m+1} = x^{new}_{m-\frac{1}{2}} - x^n_{m-\frac{3}{2}}$.

Each time the constraint is enforced the bus position follows the non-classical shock trajectory: $y^{n+1} = x^{n+1}_{m\pm\frac{1}{2}} = x^{new}_{m\pm\frac{1}{2}} + V_b\Delta t^n$. The other cell interfaces are kept unchanged. For simplicity, in the following we replace the superscript new with n to indicate all the quantities at time t^n including the modified ones. An explicit formula for the scheme can be derived in the following way. Consider the finite volume cell T in Figure 2.5.3 (abcd).

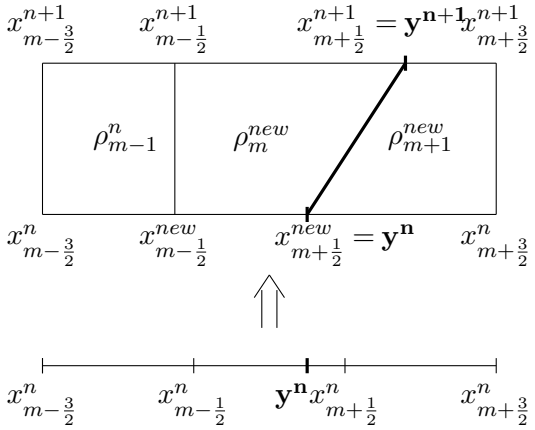


Figure 2.5.2: Local shifting of a grid point when $\left|x^n_{m+\frac{1}{2}} - y^n\right| \leq \frac{h^n_m}{2}$.

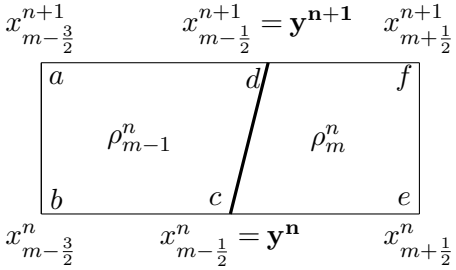


Figure 2.5.3: Nonuniform finite volume cells.

Integrate the conservation law over the finite volume:

$$\int\int_T (\partial_t \rho + \partial_x f(\rho))dxdt = 0$$

From the Green's theorem we have

$$\int_T f(\rho)dt - \rho dx = 0$$

which leads to the following

$$\begin{aligned}\rho_j^{n+1} =& \frac{\Delta x_j^n}{\Delta x_j^{n+1}}\rho_j^n - \frac{\Delta x_j^n}{\Delta x_j^{n+1}}\Big[\Big(\int_{t^n}^{t^{n+1}} f(\mathcal{RS}(\rho_j^n, \rho_{j+1}^n)) - V_b\mathcal{RS}(\rho_j^n, \rho_{j+1}^n)\Big)dt \\ &-\Big(\int_{t^n}^{t^{n+1}} f(\mathcal{RS}(\rho_{j-1}^n, \rho_j^n)) - V_b\mathcal{RS}(\rho_{j-1}^n, \rho_j^n)\Big)dt\Big].\end{aligned}$$

For simplicity we introduce the notation $\tilde{F}(\rho) = F(\rho) - V_b\rho$. Notice that in our case $\tilde{F}$ corresponds to the F_α computed in (2.1.7) when the constraint is active and to $F(\rho)$ with

$V_b = 0$ when the constraint is not enforced. Moreover, one needs to be careful when the bus trajectory is dealt with. In fact, the cell size changes as time increases: one cell will shrink and the other one will be enlarged, and it might be necessary to recompute the averages of the density calculated at a previous time step. When one cell is too small we adjust the location of one grid point. After the mesh has been resized and adjusted we update the cell averages for all cells with the following conservative formula:

$$\rho_j^{n+1} = \frac{\Delta x_j^n}{\Delta x_j^{n+1}} \rho_j^n - \frac{\Delta t^n}{\Delta x_j^{n+1}} \Big(\tilde{F}(\rho_j^n, \rho_{j+1}^n) - \tilde{F}(\rho_{j-1}^n, \rho_j^n) \Big). \tag{2.5.6}$$

2.5.2 Numerical method for the ODE

We detail here how to solve numerically the ODE. At each time t^n we determine the position y^n of the bus by studying the interactions between the bus trajectory and the corresponding density waves within a cell. We distinguish two cases:

- (2.5.2) is satisfied. Then the bus moves always at velocity V_b and we update the bus position $y^{n+1} = V_b \Delta t^n + y^n$.
- (2.5.2) is not satisfied. In this case we implement the tracking algorithm introduced in [33]. We have to distinguish two situations: one when $y^n \in [x^n_{j-\frac{1}{2}}, x^n_j[$ and one when $y^n \in [x^n_j, x^n_{j+\frac{1}{2}}[$. In both cases, we check if the wave starting at the cell interface is a shock or a rarefaction and compute the time of interaction between the wave and the bus trajectory. In the case of the rarefaction the initial and final time of interaction is computed and the position of the bus is updated by solving explicitly an ordinary differential equation. According to the new position of the bus, the cell index is updated.

Numerical algorithm

The steps of the method are described in detail in Algorithm 1.

2.6 A conservative scheme with reconstruction of non-classical and classical shocks

The approach presented in Section 2.5 gives a good approximation of the solutions for our problem, however it is not easy to implement due to the heavy burden represented by the moving mesh. So, we look for another method that could be easily implemented that would be conservative and yet still able to detect non-classical shocks and respect the constraint (2.5.2). We mantain for this section the same notation as in the previous one so: Δx and Δt are the fixed space and time discretization such that we can set $x_{j+\frac{1}{2}} = j\Delta x$ for $j \in \mathbb{Z}$ and $t^n = n\Delta t$ for $n \in \mathbb{N}$, and we assume that at time t^n, y^n is the bus position and $y^n \in C_m = [x_{m-\frac{1}{2}}, x_{m+\frac{1}{2}})$ for some $m \in \mathbb{Z}$. Taking inspiration from

Algorithm 1 Algorithm for the tracking method

Input data: Initial and boundary condition for the PDE and the ODE, m index cell of the bus position y^n

Compute the densities at time t^{n+1} from the density values at time t^n using the Godunov flux F.

if $f(\mathcal{RS}(\rho_m^n, \rho_m^n)(V_b)) > F_\alpha + V_b \mathcal{RS}(\rho_m^n, \rho_m^n)(V_b)$ **then**

  if $\left| x^n_{m+\frac{1}{2}} - y^n \right| > \dfrac{h_m^n}{2}$ **then**

    $x^{new}_{m-\frac{1}{2}} = y^n$, compute the new average for ρ^{new}_{m-1} and update the mesh $x^{n+1}_{m-\frac{1}{2}} = x^{new}_{m-\frac{1}{2}} + V_b \Delta t^n$.

  else

    $x^{new}_{m+\frac{1}{2}} = y^n$, and place the point $x^{new}_{m-\frac{1}{2}} = \dfrac{x^n_{m-\frac{3}{2}} + x^{new}_{m+\frac{1}{2}}}{2}$. Compute the new cell averages for ρ^{new}_m and ρ^{new}_{m+1} and update the mesh $x^{n+1}_{m+\frac{1}{2}} = x^{new}_{m+\frac{1}{2}} + V_b \Delta t^n$.

  end if

end if

Compute the densities averages at time t^{n+1} using formula (2.5.6).

Compute the bus position

if $f(\mathcal{RS}(\rho_m^n, \rho_m^n)(V_b)) > F_\alpha + V_b \mathcal{RS}(\rho_m^n, \rho_m^n)(V_b)$ **then**

  $y^{n+1} = V_b \Delta t^n + y^n$

else

  y^n computed with the tracking algorithm in [33]

end if

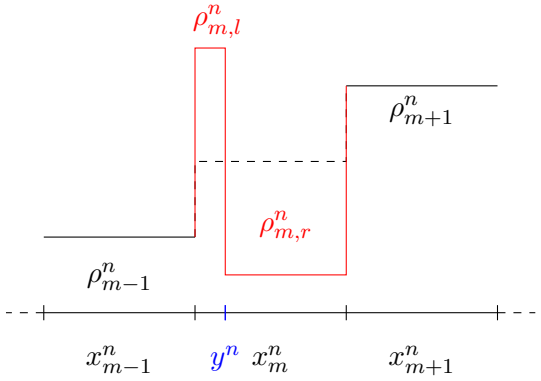


Figure 2.6.1: Reconstruction of a non-classical shock.

[17], we decided to develop a method that using the technique of reconstruction is able to recreate the discontinuity of the non-classical shock. The idea is that, whenever a non-classical shock appears, the information held by the initial data are not enough to correctly generate the exact solution. So it becomes necessary to input in the problem the left (right) trace of the non-classical discontinuity. Moreover, the presence of the bus and condition (2.5.2) tells us exactly when and where the discontinuity is going to appear. So let us suppose that at time t^n a non-classical shock is created at $y^n \in C_m$. Then the sole information ρ^n_m will not be enough to capture it because using, for example, a classical Godunov approach, we cannot have any different value from those given by the classical Riemann solver at the interfaces in particular, for example, for shocks, the solution of the Riemann problem is the propagation of the Riemann initial states ($\rho^n_L = \rho^n_{m-1}$ and $\rho^n_R = \rho^n_{m+1}$). Hence, we propose to introduce in the cell C_m the left (right) state $\rho^n_{m,l} = \hat{\rho}_\alpha$ ($\rho^n_{m,r} = \check{\rho}_\alpha$) of the non-classical discontinuity which is expected to be present in the Riemann solution associated with ρ^n_{m-1} and ρ^n_{m+1} in case inequality (2.5.2) is not satisfied. Since the presence of the non-classical shock is due to the presence of the bus, we require that this reconstructed discontinuity is located inside the cell C_m at a position $\bar{x}_m$. It is possible to reconstruct the discontinuity given $0 \leq d^n_m \leq 1$ such that

$$d^n_m = \frac{\rho^n_{m,r} - \rho^n_m}{\rho^n_{m,r} - \rho^n_{m,l}}. \tag{2.6.1}$$

The method is fully conservative provided that

$$d^n_m \Delta x \rho^n_{m,l} + (1 - d^n_m)\Delta x \rho^n_{m,r} = \rho^n_m.$$

Then, the numerical flux becomes

$$\Delta t F^n_{m+\frac{1}{2}} = \min\left(\Delta t_{m+\frac{1}{2}}, \Delta t\right) f(\rho^n_{m,r}) + \max\left(\Delta t - \Delta t_{m+\frac{1}{2}}, 0\right) f(\rho^n_{m,l}) \tag{2.6.2}$$

where $\Delta t_{m+\frac{1}{2}} = \dfrac{1 - d^n_m}{V_b}\Delta x$.
This method is able to capture non-classical solutions and to produce exact solutions. On

the other hand, with this approach, the classical shocks suffer minor numerical diffusion and this might be problematic in the validation of the solution on the constraint (2.5.2). In fact, if we choose initial data in neighborhood of the values $\hat{\rho}_\alpha$, $\check{\rho}_\alpha$, we notice that the solution generated by this method is not correct. To overcome this problem we reconstruct also the classical shocks, in this way we limit the numerical diffusion and get correct solutions also in this case. The method proceed as follows, we locate the position of the shock $\bar{x}_j \in C_j$, then, it is possible to reconstruct the shock given $0 \leq d_j^n \leq 1$ such that

$$d_j^n = \frac{\rho_R^n - \rho_j^n}{\rho_R^n - \rho_L^n}. \tag{2.6.3}$$

Then, the numerical flux becomes

- if $\lambda(\rho_L^n, \rho_R^n) \geq 0$,

$$\Delta t F_{j+\frac{1}{2}}^n = \begin{cases} \min\left(\Delta t_{j+\frac{1}{2}}, \Delta t\right) f(\rho_R^n) + \max\left(\Delta t - \Delta t_{j+\frac{1}{2}}, 0\right) f(\rho_L^n), & \text{if } 0 \leq d_j^n \leq 1, \\ \Delta t f(\rho_j^n), & \text{otherwise;} \end{cases} \tag{2.6.4}$$

  with $\Delta t_{j+\frac{1}{2}} = \dfrac{1 - d_j^n}{\lambda(\rho_L^n, \rho_R^n)} \Delta x,$

- if $\lambda(\rho_L^n, \rho_R^n) \leq 0$,

$$\Delta t F_{j-\frac{1}{2}}^n = \begin{cases} \min\left(\Delta t_{j-\frac{1}{2}}, \Delta t\right) f(\rho_L^n) + \max\left(\Delta t - \Delta t_{j-\frac{1}{2}}, 0\right) f(\rho_R^n), & \text{if } 0 \leq d_j^n \leq 1, \\ \Delta t f(\rho_j^n), & \text{otherwise;} \end{cases} \tag{2.6.5}$$

  with $\Delta t_{j-\frac{1}{2}} = \dfrac{d_j^n}{-\lambda(\rho_L^n, \rho_R^n)} \Delta x,$

where $\lambda(\rho_L^n, \rho_R^n)$ is the speed of the shock given by the Rankine-Hugoniot condition (1.1.8). With this additional reconstruction we are able also to handle correctly shocks crossing and shocks colliding with non-classical waves.

The ODE is treated as explained in the section 2.5.2. The algorithm follows the steps described in Algorithm 2

2.7 Numerical results

We show some numerical tests obtained with the two method described in Sections 2.5 and 2.6. For illustration, we choose a concave fundamental diagram with the following flux function:

$$f(\rho) = \rho(1 - \rho),$$

with $\rho_{\text{cr}} = 0.5$ the density at which the unique maximum of the flux function is attained such that $f(\rho_{\text{cr}}) = f^{\max}$. Moreover, we introduce for the tracking method $\tilde{F}$ which is given by

$$\tilde{F}(U, V) = \begin{cases} F(U, V) & \text{if } f(\mathcal{RS}(U, V)(V_b)) < F_\alpha + V_b \mathcal{RS}(U, V)(V_b), \\ F_\alpha & \text{otherwise.} \end{cases} \tag{2.7.1}$$

Algorithm 2 Algorithm for the conservative scheme and the bus tracking

Input data: Initial and boundary condition for the PDE and the ODE, m index cell of the bus position y^n.
Compute the densities at time t^{n+1} from the density values at time t^n using the Godunov flux F.
if $\rho_L < \rho_R$ **and** $f(\rho_m^n) \leq F_\alpha + V_b\rho_m^n$, **then**
  Compute $\bar{x}_j$, the index j and d_j^n
  if $0 \leq d_j^n \leq 1$ **then**
    if $\lambda(\rho_L^n, \rho_R^n) \geq 0$ **then**
      Compute $F^n_{j+\frac{1}{2}}$
    else if $\lambda(\rho_L^n, \rho_R^n) \leq 0$ **then**
      Compute $F^n_{j-\frac{1}{2}}$
    end if
  end if
else if $f(u_m^n) > F_\alpha + V_b u_m^n$, **then**
  if $f(\mathcal{RS}(u^n_{m-1}, u^n_{m+1})(V_b)) > F_\alpha + V_b\mathcal{RS}(u^n_{m-1}, u^n_{m+1})(V_b)$ **then**
    Compute d_m^n
    if $0 \leq d_m^n \leq 1$ **then**
      $\Delta t_{m+\frac{1}{2}}$ and F_m with $u^n_{m,l} = \hat{\rho}_\alpha$ and $u^n_{m,r} = \check{\rho}_\alpha$
    end if
  end if
end if
Compute the densities averages at time t^{n+1} using formula (2.5.1).
Compute the bus position
if $f(\mathcal{RS}(u^n_{m-1}, u^n_{m+1})(V_b)) > F_\alpha + V_b\mathcal{RS}(u^n_{m-1}, u^n_{m+1})(V_b)$ **then**
  $y^{n+1} = V_b\Delta t^n + y^n$
else
  y^n computed with the tracking algorithm in [33]
end if

In this section we present some numerical tests performed with the schemes previously described. Here we deal with a road of length 1 parameterized by the interval $[0,1]$. In all the simulations we fix $V_b = 0.3$, $\alpha = 0.6$.
Case I: We consider the following initial data

$$\rho_L(0,x) = 0.4, \quad \rho_R(0,x) = 0.5, \quad y_o = 0.5. \tag{2.7.2}$$

The solution is given by two classical shocks separated by a non-classical discontinuity, as illustrated in Figure 2.7.1 and 2.7.2.
Case II: We consider the following initial data

$$\rho_L(0,x) = 0.8, \quad \rho_R(0,x) = 0.5, \quad y_o = 0.5. \tag{2.7.3}$$

The values of the initial conditions create a rarefaction wave followed by a non-classical and a classical shocks on the density, as illustrated in Figure 2.7.3 and 2.7.4.
Case III: We consider the following initial data

$$\rho_L(0,x) = 0.8, \quad \rho_R(0,x) = 0.4, \quad y_o = 0.4. \tag{2.7.4}$$

In this case, the bus initial position is not aligned with the discontinuity. We can see that the values of the initial conditions create a rarefaction wave followed by a non-classical and a classical shocks on the density that are created when the bus approaches the rarefaction and creates a moving bottleneck, as illustrated in Figure 2.7.5 and 2.7.6.
Case IV: We consider the following initial data

$$\rho_L(0,x) = \hat{\rho}_\alpha, \quad \rho_m(0,x) = \check{\rho}_\alpha, \quad \rho_L(0,x) = 0.95, \quad y_o = 0.25. \tag{2.7.5}$$

The solution is given by a non-classical shock and a classical one that collide. After the collision an third shock is created, as illustrated in Figure 2.7.7 and 2.7.8.

For cases I and II we also show the convergence curves for the reconstruction method in Figure 2.7.9. It represents the log-log $\mathcal{L}^1$ error between the numerical solution and the exact one versus mesh size. The numerical order of convergence, computed with $\frac{\ln(||\rho_{\text{exact}} - \rho_{\text{appr}}||_{\mathcal{L}^1})}{\ln(\Delta x)}$, can be found in Table 2.7.1.

Δx	Order of convergence for Case I	Order of convergence for Case II
0.1	1.1762	0.8212
0.05	0.9928	0.8794
0.025	1.1360	0.9494
0.0125	1.5980	1.4522
0.00625	0.7769	1.0049
0.003125	0.8473	1.0103
0.0015625	0.8871	1.1898

Table 2.7.1: Order of convergence for the reconstruction scheme, corresponding to initial data (2.7.2) and (2.7.3).

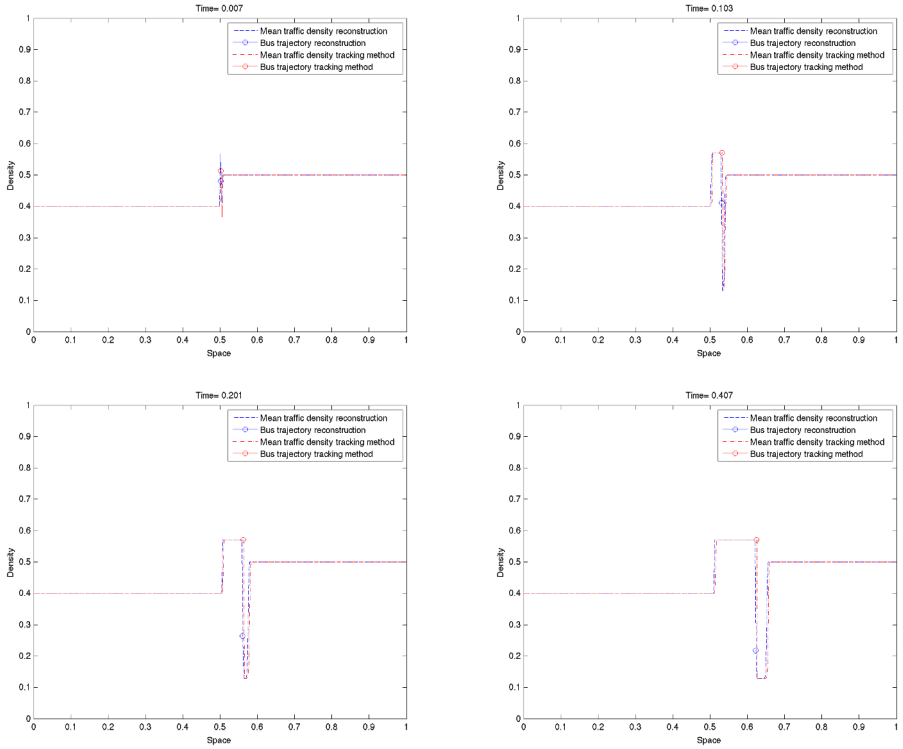


Figure 2.7.1: Evolution of the density at different times corresponding to initial data (2.7.2) and a mesh grid of 500 points.

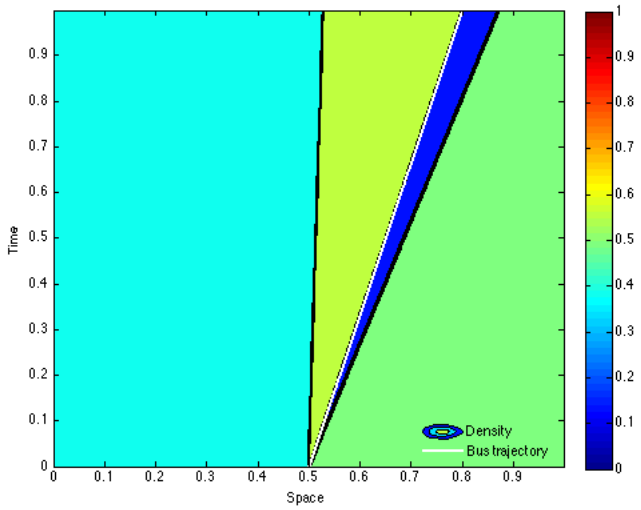


Figure 2.7.2: Density and bus trajectory in a $x-t$ plane corresponding to initial data (2.7.2) and a mesh grid of 500 points.

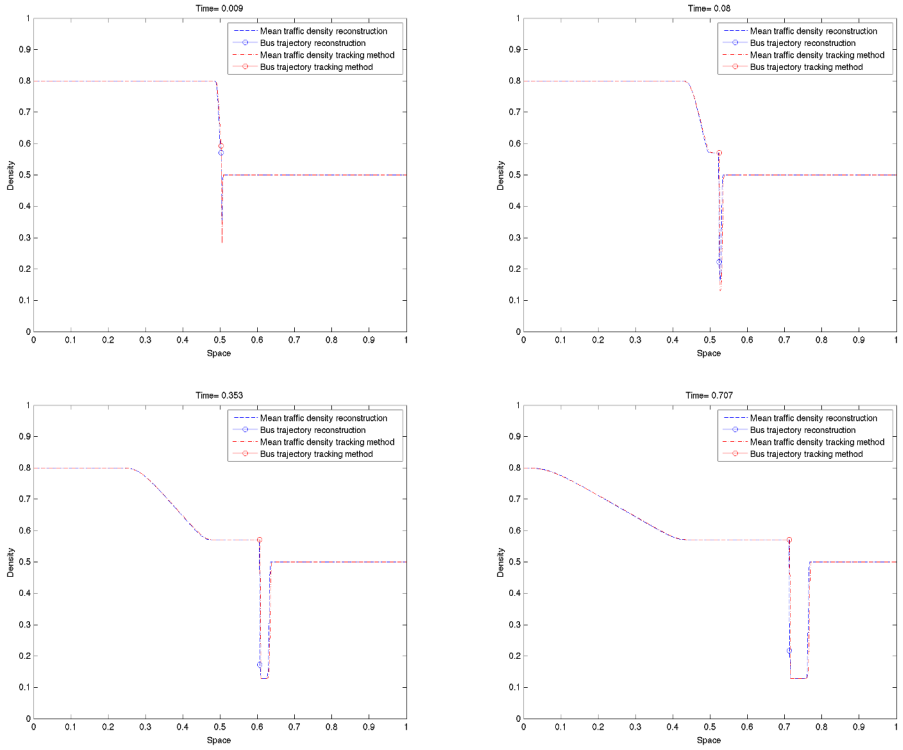


Figure 2.7.3: Evolution of the density at different times corresponding to initial data (2.7.3) and a mesh grid of 500 points.

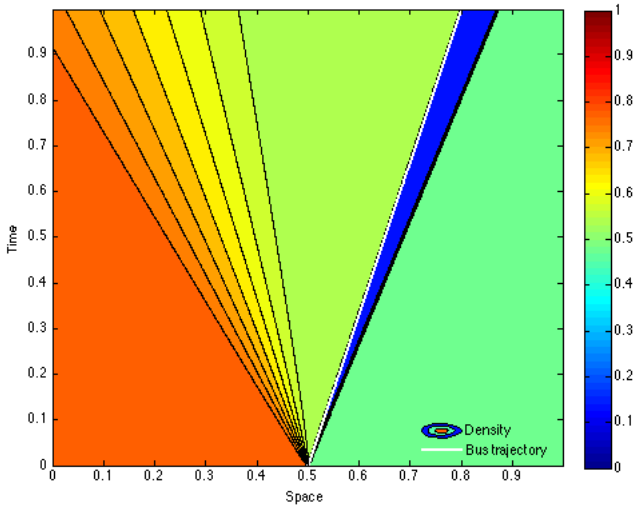


Figure 2.7.4: Density and bus trajectory in a $x-t$ plane corresponding to initial data (2.7.3) and a mesh grid of 500 points.

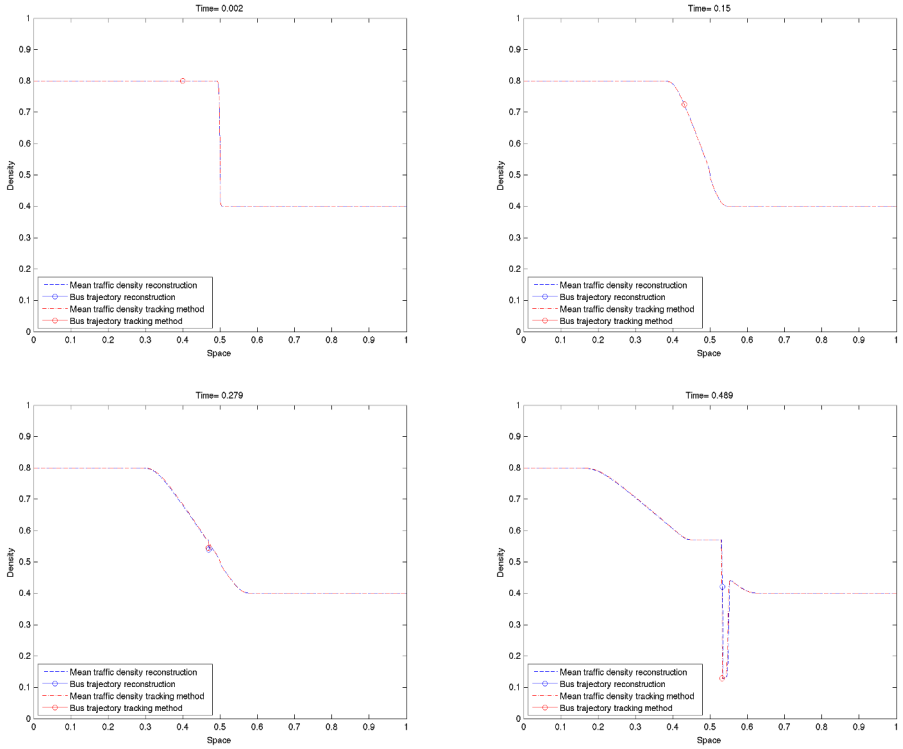


Figure 2.7.5: Evolution of the density at different times corresponding to initial data (2.7.4) and a mesh grid of 500 points.

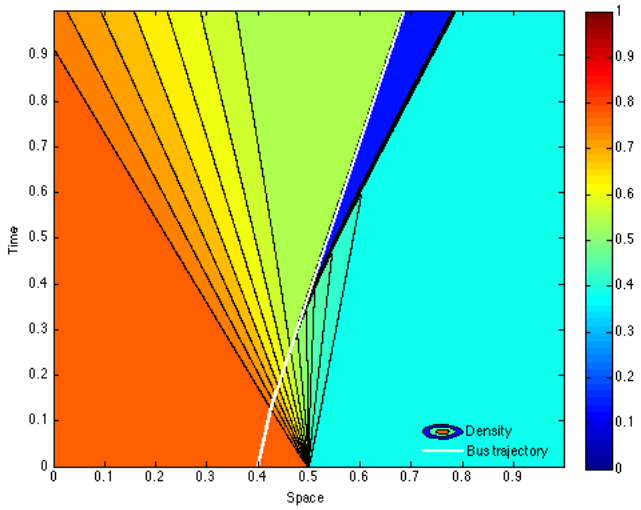


Figure 2.7.6: Density and bus trajectory in a $x-t$ plane corresponding to initial data (2.7.4) and a mesh grid of 500 points.

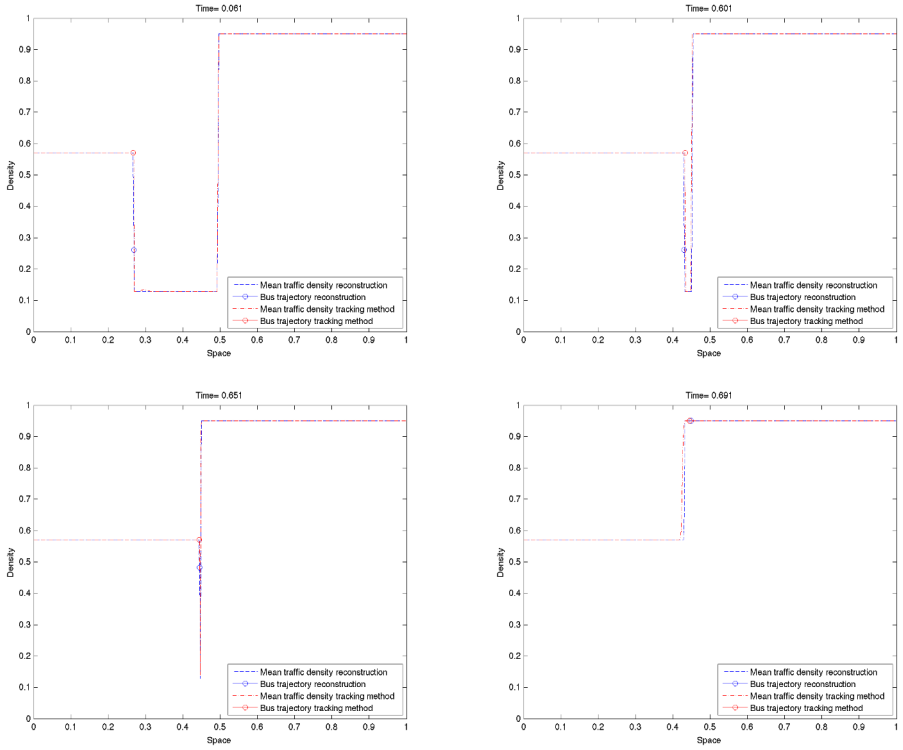


Figure 2.7.7: Evolution of the density at different times corresponding to initial data (2.7.5) and a mesh grid of 500 points.

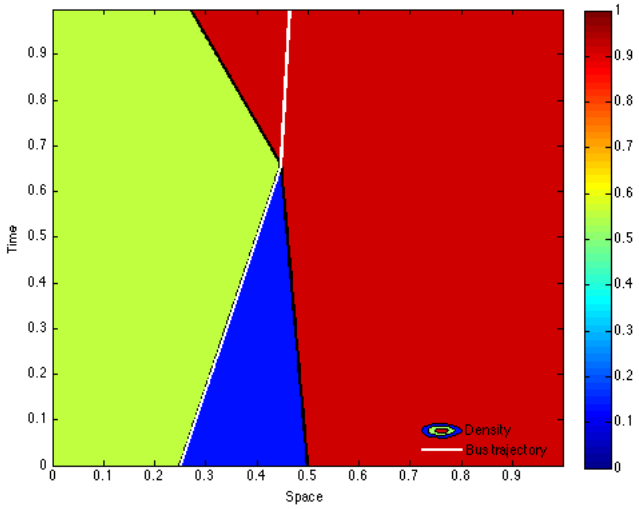
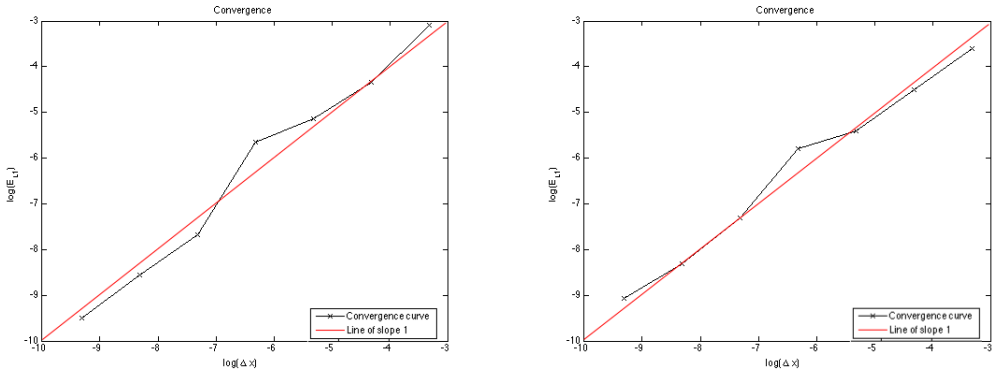


Figure 2.7.8: Density and bus trajectory in a $x-t$ plane corresponding to initial data (2.7.5) and a mesh grid of 500 points.



(a) Classical and non-classical shock - Case I (b) Rarefaction and non-classical shock - Case II

Figure 2.7.9: $\mathcal{L}^1$ convergence.

Both methods show effective results for the problem considered. We were able to obtain good results for the two approaches for several cases with simple Riemann problems and with more complex initial data, involving shocks crossings and bus trajectory not aligned with the density discontinuity. The method with reconstruction is easier to implement compared to the front/capturing method due to the moving mesh but it requires the additional reconstruction of classical shocks for initial data neighboring the values $\hat{\rho}_\alpha$, $\check{\rho}_\alpha$. Moreover, the Lagrangian algorithm uses more iterations to achieve the same results because of the CFL-condition that in this case requires smaller time intervals to counterbalance the presence of smaller cells.

Part II

Modeling of junctions using a PDE-ODE approach

Chapter 3

An application to ramp-metering

Contents

3.1 Introduction 74
3.2 Fundamental definitions and notations 74
3.3 Riemann problem 77
3.4 Numerical results: modified Godunov 86
3.4.1 Boundary conditions and conditions at the junctions 87
3.4.2 ODE treatment 88
3.4.3 Modified Godunov scheme 88
3.5 Numerical results 89
3.6 Discrete adjoint method for optimization 91

3.1 Introduction

In this chapter, we focus on a junction model designed for a ramp metering problem. Ramp metering models have been introduced in the engineering community in a discrete setting, see [116, 117] for details. Here, we apply a continuous approach. We consider the scalar Lighthill-Whitham-Richards model on a network composed of a single junction connecting a mainline, an onramp and an offramp. The mainline evolution is described by a scalar conservation law, while the onramp dynamics is modeled by a buffer of infinite capacity, which is defined by an ordinary differential equation (ODE) depending on the difference between the incoming and outgoing fluxes at the ramp.

In the following sections, we prove the existence and uniqueness of solutions of the Riemann problem at the junction. The results are obtained by solving a Linear Programming (LP) optimization problem. Unlike [67], where the flux through the junction is maximized, our LP-optimization consists in maximizing the flux on the outgoing mainline, see Remark 8 below. The offramp is treated as a sink, and a priority parameter is introduced to ensure uniqueness of the solution. As a modeling choice, the priority is satisfied in an approximate way, i.e., the priority will not always be respected, in benefit of flux maximization.

We present numerical approximations of possibly discontinuous solutions obtained using this model. In particular, we suitably modify the Godunov scheme to include the boundary conditions at the junction, as in [32, 48], and the ODE describing the buffer. This allows one to take into account the possible creation of an additional shock when the buffer empties. The scheme provides accurate numerical approximations, as shown by the numerical tests provided here. Moreover, we chose an adjoint calculus approach to solve optimal control problems.

This chapter is organized as follows. Section 3.2 contains some preliminary notations and definitions, while Section 3.3 describes in details the solution of the Riemann problem at the junction. In Section 3.4 we introduce the numerical scheme with the particular boundary conditions used to compute approximate solutions to the problem. In Section 3.5 we present some numerical tests which show the effectiveness of our approximation. Finally, in Section 3.6 an optimal control problem is introduced and solved with the adjoint method.

The results obtained in this chapter are due to a collaboration with Prof. A. M. Bayen, J. Reilly, S. Samaranayake and W. Krichene from UC Berkeley under the Inria associated team ORESTE (Optimal REroute Strategies for Traffic managEment) and can be found in [58, 125].

3.2 Fundamental definitions and notations

We consider a junction with one mainline I modeled by the real line $]-\infty,+\infty[$, one onramp R_1 and one offramp R_2 at $x=0$, as illustrated in Figure 3.2.1. From a macroscopic point of view, this means that on each mainline segment $I_1 =]-\infty,0[$ and $I_2 =]0,+\infty[$,

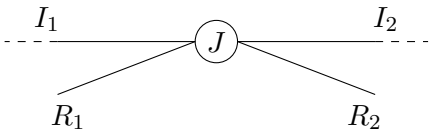


Figure 3.2.1: Junction modeled.

we consider the mass conservation equation:

$$\partial_t \rho + \partial_x f(\rho) = 0, \quad (t,x) \in \mathbb{R}^+ \times I_i, \tag{3.2.1}$$

where $\rho = \rho(t,x) \in [0, \rho_{\max}]$ is the mean traffic density, $\rho_{\max}$ is the maximal density allowed on the road and the flux function $f : [0, \rho_{\max}] \to \mathbb{R}^+$ is given by the following flux-density relation

$$f(\rho) = \rho v(\rho),$$

where $v(\rho)$ is a smooth decreasing function denoting the mean traffic speed.
Throughout the chapter, we assume for simplicity that:

(A1) $\rho_{\max} = 1$;

(A2) $f(0) = f(1) = 0$;

(A3) f is a strictly concave function.

Assumptions (A2) and (A3) ensure existence and uniqueness of a point of maximum of the flux function $\rho_{\text{cr}} \in]0,1[$. A typical example of flux function that satisfies these assumptions is given in Figure 3.2.2.

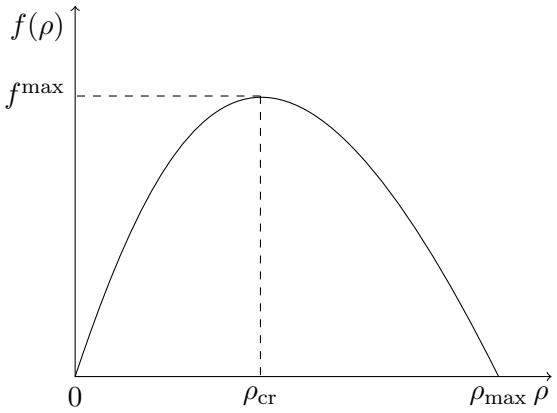


Figure 3.2.2: Flux function of equation (3.2.1).

On the onramp R_1 we consider the presence of a buffer modeled by the following ODE:

$$\frac{dl(t)}{dt} = F_{\text{in}}(t) - \gamma_{\text{r1}}(t), \quad t \in \mathbb{R}^+, \tag{3.2.2}$$

where $l(t) \in [0,+\infty[$ is the length of the queue, $F_{\text{in}}(t)$ is the flux that enters the onramp and $\gamma_{\text{r1}}(t)$ is the flux that exits from the onramp.
This particular choice is taken to avoid backward waves on the onramp boundary, which happens in the case of horizontal queues that consider vehicles arranged over the length of the roadway. In particular, at the left boundary of the onramp, backward moving shock waves can result in lost information on the flux that actually enters the buffer. The presence of the buffer, considered as a vertical queue in which vehicles are stacked one upon the other, helps accounting for all the flow that enters the onramp. For simplicity, we consider the offramp as a sink of infinite capacity that accepts all the flux entering from the mainline I_1, and we assume that no flux from the onramp is allowed in the offramp.
The Cauchy problem to solve is then:

$$\begin{cases} \partial_t \rho_i + \partial_x f(\rho_i) = 0, & (t,x) \in \mathbb{R}^+ \times I_i,\ i = 1,2 \\ \dfrac{dl(t)}{dt} = F_{\text{in}}(t) - \gamma_{\text{r1}}(t), & t \in \mathbb{R}^+, \\ \rho_i(0,x) = \rho_{i,0}(x), & \text{on } I_i,\ i = 1,2 \\ l(0) = l_0, \end{cases} \tag{3.2.3}$$

where $\rho_i(0,x)$ represents the initial condition and $l_0 \in [0,+\infty[$ is the initial load of the buffer. This will be coupled with an optimization problem at the junction which will give the distribution of the traffic among the roads.

We define the demand $d(F_{\text{in}},l)$ of the onramp, the demand function $\delta(\rho_1)$ on the incoming mainline segment corresponding to the density ρ_1, and the supply function $\sigma(\rho_2)$ on the outgoing mainline segment corresponding to the density ρ_2 as follows.

$$d(F_{\text{in}},l) = \begin{cases} \gamma_{\text{r1}}^{\max} & \text{if } l(t) > 0, \\ \min\left(F_{\text{in}}(t), \gamma_{\text{r1}}^{\max}\right) & \text{if } l(t) = 0, \end{cases} \tag{3.2.4}$$

$$\delta(\rho_1) = \begin{cases} f(\rho_1) & \text{if } 0 \le \rho_1 < \rho_{\text{cr}}, \\ f^{\max} & \text{if } \rho_{\text{cr}} \le \rho_1 \le 1, \end{cases} \tag{3.2.5}$$

$$\sigma(\rho_2) = \begin{cases} f^{\max} & \text{if } 0 \le \rho_2 \le \rho_{\text{cr}}, \\ f(\rho_2) & \text{if } \rho_{\text{cr}} < \rho_2 \le 1, \end{cases} \tag{3.2.6}$$

where $\gamma_{\text{r1}}^{\max}$ is the maximal flow on the onramp and $f^{\max} = f(\rho_{\text{cr}})$ is the maximal flux on I_1 and I_2. Moreover, we introduce $\beta \in [0,1]$ the split ratio of the offramp, and $\gamma_{\text{r2}}(t) = \beta f(\rho_1(t,0-))$ its flux.

Definition 3.2.1 *A triple* $(\rho_1,\rho_2,l) \in \prod_{i=1}^{2} \mathcal{C}^0\left(\mathbb{R}^+;\mathcal{L}^1 \cap \text{BV}(\mathbb{R})\right) \times \mathcal{W}^{1,\infty}(\mathbb{R}^+;\mathbb{R}^+)$ *is an admissible solution to (3.2.3) if*

1. ρ_1, ρ_2 *are weak solutions on* I_1, I_2, *i.e.,* $\rho_i : [0,+\infty[\times I_i \to [0,1]$, $i = 1,2$, *such that*

$$\int_{\mathbb{R}^+} \int_{I_i} \left(\rho_i \partial_t \varphi_i + f(\rho_i) \partial_x \varphi_i\right) dx dt = 0, \quad i = 1,2, \tag{3.2.7}$$

for every $\varphi_i \in \mathcal{C}_c^1(\mathbb{R}^+ \times I_i)$.

2. *ρ_i satisfies the Kružhkov entropy condition [99] on $(\mathbb{R}^+ \times I_i)$, i.e., for every $k \in [0,1]$ and for all $\varphi_i \in \mathcal{C}_c^1(\mathbb{R} \times I_i)$, $t > 0$,*

$$\begin{aligned} &\int_{\mathbb{R}^+} \int_{I_i} (|\rho_i - k| \partial_t \varphi_i + \operatorname{sgn}(\rho_i - k)(f(\rho_i) - f(k)) \partial_x \varphi_i) dx dt \\ &\quad + \int_{I_i} |\rho_{i,0} - k| \varphi_i(0,x) dx \geq 0; \quad i = 1,2. \end{aligned} \tag{3.2.8}$$

3. $f(\rho_1(t,0-)) + \gamma_{\mathrm{r}1}(t) = f(\rho_2(t,0+)) + \gamma_{\mathrm{r}2}(t)$.

4. *The flux of the outgoing mainline $f(\rho_2(t,0+))$ is maximum subject to*

$$f(\rho_2(t,0+)) = \min\Big((1-\beta)\delta(\rho_1(t,0-)) + d(F_{\mathrm{in}}(t), l(t)), \sigma(\rho_2(t,0+))\Big) \tag{3.2.9}$$

and 3

5. *l is a solution of (3.2.2) for a.e. $t \in \mathbb{R}^+$.*

Remark 6 *A parameter P is introduced in the next section to ensure uniqueness of the solution. $P \in]0,1[$ is a right of way parameter that defines the amount of flux that enters the outgoing road from the incoming mainline and from the onramp. In particular, $Pf(\rho_2(t,0+))$ is the flux allowed from the incoming mainline into the outgoing mainline, and $(1-P)f(\rho_2(t,0+))$ the flux from the onramp. As described in Section 1.2.2.*

3.3 Riemann problem

In this section, we construct step by step the Riemann Solver at the junction. This will be the building block to construct approximate Godunov scheme (or wave-front tracking) solutions to general Cauchy problems. We fix constants $\rho_{1,0}, \rho_{2,0} \in [0,1]$, $l_0 \in [0,+\infty[$, $F_{\mathrm{in}} \in]0,+\infty[$ and a priority factor $P \in]0,1[$. The Riemann problem at J is the Cauchy problem (3.2.3) where the initial conditions are given by $\rho_{0,i}(x) \equiv \rho_{0,i}$ in I_i for $i = 1,2$. We define the Riemann Solver by means of a Riemann Solver $\mathcal{RS}_{\bar{l}}$, which depends on the instantaneous load of the buffer $\bar{l}$. For each $\bar{l}$ the Riemann Solver $\mathcal{RS}_{\bar{l}}$ is constructed in the following way.

1. Define $\Gamma_1 = f(\rho_1(t,0-))$, $\Gamma_2 = f(\rho_2(t,0+))$, $\Gamma_{\mathrm{r}1} = \gamma_{\mathrm{r}1}(t)$;
2. Consider the space $(\Gamma_1, \Gamma_{\mathrm{r}1})$ and the sets $\mathcal{O}_1 = [0, \delta(\rho_1)]$, $\mathcal{O}_{\mathrm{r}1} = [0, d(F_{\mathrm{in}}, \bar{l})]$;
3. Trace the lines $(1-\beta)\Gamma_1 + \Gamma_{\mathrm{r}1} = \Gamma_2$ and $\Gamma_1 = \frac{P}{1-P}\Gamma_{\mathrm{r}1}$;
4. Consider the region

$$\Omega = \Big\{(\Gamma_1, \Gamma_{\mathrm{r}1}) \in \mathcal{O}_1 \times \mathcal{O}_{\mathrm{r}1} : (1-\beta)\Gamma_1 + \Gamma_{\mathrm{r}1} \in [0, \Gamma_2]\Big\}. \tag{3.3.1}$$

Different situations can occur depending on the value of Γ_2:

- Demand limited case: $\Gamma_2 = (1-\beta)\delta(\rho_1(t,0-)) + d(F_{\text{in}}, \bar{l})$.
  We set Q to be the point $(\hat{\Gamma}_1, \hat{\Gamma}_{\text{r1}})$ such that $\hat{\Gamma}_1 = \delta(\rho_1(t,0-))$, $\hat{\Gamma}_{\text{r1}} = d(F_{\text{in}}, \bar{l})$ and $\hat{\Gamma}_2 = (1-\beta)\delta(\rho_1(t,0-)) + d(F_{\text{in}}, \bar{l})$, as illustrated in Figure 3.3.1(a).

- Supply limited case: $\Gamma_2 = \sigma(\rho_2(t,0+))$.
  We set Q to be the point of intersection of $(1-\beta)\Gamma_1 + \Gamma_{\text{r1}} = \Gamma_2$ and $\Gamma_1 = \frac{P}{1-P}\Gamma_{\text{r1}}$. If $Q \in \Omega$, we set $(\hat{\Gamma}_1, \hat{\Gamma}_{\text{r1}}) = Q$ and $\hat{\Gamma}_2 = \Gamma_2$, see Figure 3.3.1(b); if $Q \notin \Omega$, we set $(\hat{\Gamma}_1, \hat{\Gamma}_{\text{r1}}) = S$ and $\hat{\Gamma}_2 = \Gamma_2$, where S is the point of the segment $\Omega \cap (\Gamma_1, \Gamma_{\text{r1}}) : (1-\beta)\Gamma_1 + \Gamma_{\text{r1}} = \Gamma_2$ closest to the line $\Gamma_1 = \frac{P}{1-P}\Gamma_{\text{r1}}$, obtained solving the problem

$$\begin{aligned} \text{minimize} \quad & \left\| \begin{pmatrix} \gamma_{\text{r1}}(t) \\ f(\rho_1(t,0-)) \end{pmatrix} - \left[\begin{pmatrix} \gamma_{\text{r1}}(t) \\ f(\rho_1(t,0-)) \end{pmatrix} \cdot \alpha^P \right] \alpha^P \right\|_2^2 \\ \text{subject to} \quad & f(\rho_2(t,0+)) = (1-\beta) f(\rho_1(t,0-)) + \gamma_{\text{r1}}(t), \\ & \gamma_{\text{r1}}(t) \le d(F_{\text{in}}, \bar{l}), \\ & f(\rho_1(t,0+)) \le \delta(\rho_1), \end{aligned} \tag{3.3.2}$$

  where α^P is the normalized vector $\alpha^P = \dfrac{1}{\sqrt{P^2 + (1-P)^2}} \begin{pmatrix} P \\ 1-P \end{pmatrix}$, see Figure 3.3.1(c).

As can be seen in Figure 3.3.1(c), it might not be possible to respect the priority given by the parameter P if we want to maximize also the flux. Once we have determined $\hat{\Gamma}_1$ and $\hat{\Gamma}_2$, we can define $\hat{\rho}_1$, $\hat{\rho}_2$ in a unique way as follows. We recall that $\rho = \rho_{\text{cr}} \in]0,1[$ is the unique point of maximum of the flux and we recall the function τ introduced in Chapter 1 in Definition 1.2.4. Given

$$\rho_1(0,\cdot) \equiv \rho_{1,0} \ , \ \rho_2(0,\cdot) \equiv \rho_{2,0},$$

there exists a unique couple $(\hat{\rho}_1, \hat{\rho}_2) \in [0,1]^2$ such that

$$\hat{\rho}_1 \in \begin{cases} \{\rho_{1,0}\} \cup]\tau(\rho_{1,0}), 1] & \text{if } 0 \le \rho_{1,0} \le \rho_{\text{cr}}, \\ [\rho_{\text{cr}}, 1] & \text{if } \rho_{\text{cr}} \le \rho_{1,0} \le 1; \end{cases} \qquad f(\hat{\rho}_1) = \hat{\Gamma}_1, \tag{3.3.3}$$

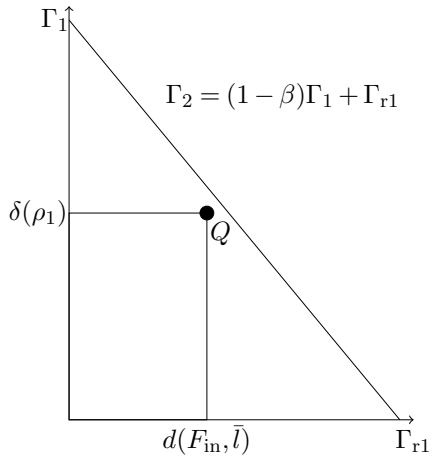
and

$$\hat{\rho}_2 \in \begin{cases} [0, \rho_{\text{cr}}] & \text{if } 0 \le \rho_{2,0} \le \rho_{\text{cr}}, \\ \{\rho_{2,0}\} \cup [0, \tau(\rho_{2,0})[& \text{if } \rho_{\text{cr}} \le \rho_{2,0} \le 1; \end{cases} \qquad f(\hat{\rho}_2) = \hat{\Gamma}_2. \tag{3.3.4}$$

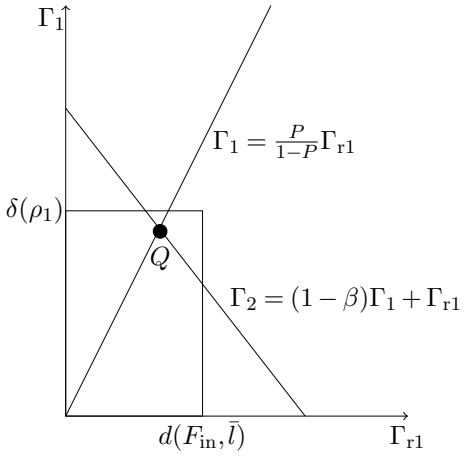
For the incoming road the solution is given by the wave $(\rho_{1,0}, \hat{\rho}_1)$, while for the outgoing road the solution is given by the wave $(\hat{\rho}_2, \rho_{2,0})$. In this setting, given any initial data $\rho_{1,0}$, $\rho_{2,0}$, we can define $\mathcal{RS}_{\bar{l}} : [0,1]^2 \to [0,1]^2$ by

$$\mathcal{RS}_{\bar{l}}(\rho_{1,0}, \rho_{2,0}) = (\hat{\rho}_1, \hat{\rho}_2). \tag{3.3.5}$$

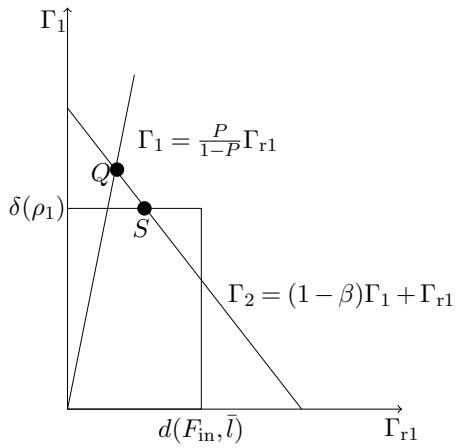
Now given the initial load of the buffer $l_0 = \bar{l}$, the function $l(t)$ at time $t > 0$ is given according to the following possibilities, determined by straight integration of (3.2.2):

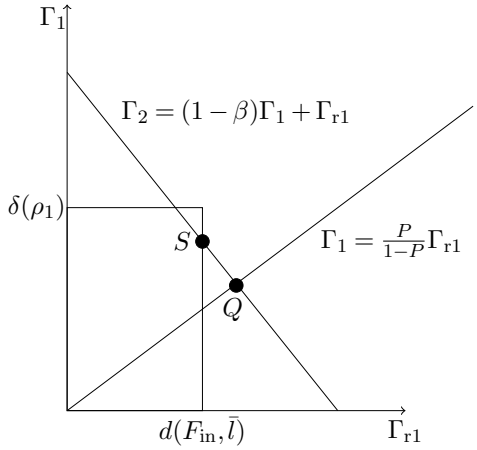


(a) Demand limited case



(b) Supply limited case: intersection inside Ω





(c) Supply limited case: intersection outside Ω

Figure 3.3.1: Solutions of the Riemann Solver at the junction.

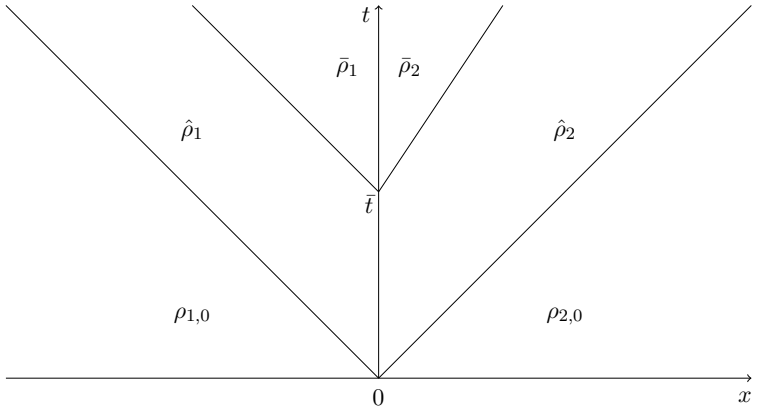


Figure 3.3.2: Solution of the Riemann Problem.

- If $F_{\text{in}} < \hat{\Gamma}_{\text{r1}}$, then

$$l(t) = \begin{cases} l_0 + (F_{\text{in}} - \hat{\Gamma}_{\text{r1}})t & \text{if } 0 < t < \frac{l_0}{\hat{\Gamma}_{\text{r1}} - F_{\text{in}}}, \\ 0 & \text{if } t > \frac{l_0}{\hat{\Gamma}_{\text{r1}} - F_{\text{in}}}. \end{cases} \tag{3.3.6}$$

- If $F_{\text{in}} \geq \hat{\Gamma}_{\text{r1}}$, then

$$l(t) = l_0 + (F_{\text{in}} - \hat{\Gamma}_{\text{r1}})t \quad \forall t > 0. \tag{3.3.7}$$

Remark 7 *The presence of the buffer can create waves when the buffer empties at time* $\bar{t} = -l_0/(F_{\text{in}} - \hat{\Gamma}_{\text{r1}}) > 0$ *(with new values of the densities* $\bar{\rho}_1, \bar{\rho}_2$*) if* $F_{\text{in}} < \hat{\Gamma}_{\text{r1}}$*, see Figure 3.3.2.*
No waves are created instead if $F_{\text{in}} \geq \hat{\Gamma}_{\text{r1}}$*, due to the infinity capacity of the buffer. A similar behavior is found in [80, 91] in a PDE-ODE model for supply chains. However, that model displays only waves with positive speeds, which suits supply chains behavior, and deals with a network which is mainly constituted by* 1×1 *junctions where the queue is fed by the previous link and not by an external inflow. Moreover, when the network is extended to include also* $m \times n$ *junctions, the condition on the positivity of the speed ensures that boundary conditions are well defined without need for additional optimization problems at the nodes.*

The following theorem ensures consistency of $\mathcal{RS}_{\bar{l}}$.

Theorem 10 *Consider a junction* J *and fix a priority parameter* $P \in]0,1[$*. For every* $\rho_{1,0}, \rho_{2,0} \in [0,1]$ *and* $l_0 \in [0, +\infty[$*, there exists a unique admissible solution* $(\rho_1(t,x), \rho_2(t,x), l(t))$ *compatible with the Riemann Solver proposed in Section 3.3 and*

the solution is given by

$$\rho_1(t,x) = \begin{cases} \rho_{1,0} & \text{if } x < \hat{s}_1 t, \\ \hat{\rho}_1 & \text{if } \hat{s}_1 t \le x < \operatorname{sgn}(\bar{t}^+)\cdot\min\Big(0, \bar{s}_1(t-\bar{t})\Big), \\ \bar{\rho}_1 & \text{if } \operatorname{sgn}(\bar{t}^+)\cdot\min\Big(0, \bar{s}_1(t-\bar{t})\Big) \le x < 0, \end{cases} \tag{3.3.8}$$

$$\rho_2(t,x) = \begin{cases} \rho_{2,0} & \text{if } x \ge \hat{s}_2 t, \\ \hat{\rho}_2 & \text{if } \operatorname{sgn}(\bar{t}^+)\cdot\max\Big(0, \bar{s}_2(t-\bar{t})\Big) \le x < \hat{s}_2 t, \\ \bar{\rho}_2 & \text{if } 0 \le x < \operatorname{sgn}(\bar{t}^+)\cdot\max\Big(0, \bar{s}_2(t-\bar{t})\Big), \end{cases} \tag{3.3.9}$$

where $\hat{s}_1, \bar{s}_1, \hat{s}_2, \bar{s}_2$ *are given by the Rankine-Hugoniot condition and* $\bar{t} = -\frac{l_0}{(F_{\text{in}} - \hat{\Gamma}_{\text{r1}})}$. *Moreover, for a.e.* $t > 0$, *it holds*

$$(\rho_1(t,0-), \rho_2(t,0+)) = \mathcal{RS}_{l(t)}(\rho_1(t,0-), \rho_2(t,0+)).$$

In (3.3.8), (3.3.9), $\operatorname{sgn}(\bar{t}^+) = 1$ if $\bar{t} > 0$, otherwise $\operatorname{sgn}(\bar{t}^+) = 0$. The proof of the theorem is deferred after some preliminary results. The mapping $\tau(\rho)$ as defined in (1.2.4) and the functions $\delta(\rho_1)$, $d(F_{\text{in}}, l)$ and $\sigma(\rho_2)$ yield the following properties.

Lemma 11 *If* $(\hat{\rho}_1, \hat{\rho}_2)$ *is a solution of the Riemann problem with initial data* $(\rho_{1,0}, \rho_{2,0})$, *then the following holds:*

$$\begin{aligned} \delta(\rho_{1,0}) &\le \delta(\hat{\rho}_1), \\ \sigma(\rho_{2,0}) &\le \sigma(\hat{\rho}_2), \\ d(F_{\text{in}}, l_0) &\le d(F_{\text{in}}, l). \end{aligned}$$

Proof. For the incoming road it holds:

$$\begin{aligned} \delta(\rho_{1,0}) &\le \delta(\hat{\rho}_1) \quad \text{if } 0 \le \rho_{1,0} \le \rho_{\text{cr}}, \\ \delta(\rho_{1,0}) &= \delta(\hat{\rho}_1) \quad \text{if } \rho_{\text{cr}} \le \rho_{1,0} \le 1. \end{aligned} \tag{3.3.10}$$

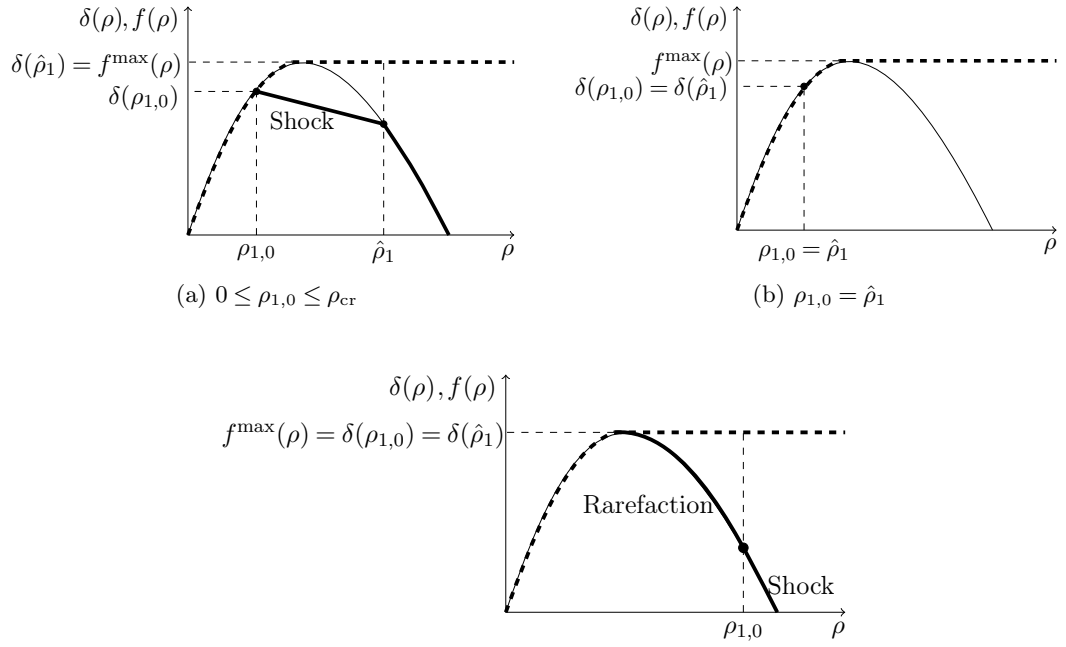
In particular, if $\rho_{1,0} \in [0, \rho_{\text{cr}}]$, either $\hat{\rho}_1 \in]\tau(\rho_{1,0}), 1]$ or $\hat{\rho}_1 = \rho_{1,0}$. In the first case, $\delta(\rho_{1,0}) = f(\rho_{1,0}) \le f^{\max} = \delta(\hat{\rho}_1)$, see Figure 3.3.3(a), while in the second case $\delta(\rho_{1,0}) = f(\rho_{1,0}) = f(\hat{\rho}_1) = \delta(\hat{\rho}_1)$, see Figure 3.3.3(b). On the other hand, if $\rho_{1,0} \in [\rho_{\text{cr}}, 1]$ then $\hat{\rho}_1 \in [\rho_{\text{cr}}, 1]$ and $\delta(\rho_{1,0}) = f^{\max} = \delta(\hat{\rho}_1)$, see Figure 3.3.3(c).

Using the same approach for the outgoing road, we have:

$$\begin{aligned} \sigma(\rho_{2,0}) &= \sigma(\hat{\rho}_2) \quad \text{if } 0 \le \rho_{2,0} \le \rho_{\text{cr}}, \\ \sigma(\rho_{2,0}) &\le \sigma(\hat{\rho}_2) \quad \text{if } \rho_{\text{cr}} \le \rho_{2,0} \le 1, \end{aligned} \tag{3.3.11}$$

In particular, if $0 \le \rho_{2,0} \le \rho_{\text{cr}}$ then $0 \le \hat{\rho}_2 \le \rho_{\text{cr}}$ as well, and $\sigma(\rho_{2,0}) = f^{\max} = \sigma(\hat{\rho}_2)$, see Figure 3.3.4(c). Otherwise $\rho_{\text{cr}} \le \rho_{2,0} \le 1$, and either $\hat{\rho}_2 = \rho_{2,0}$ or $\hat{\rho}_2 \in [0, \tau(\rho_{2,0})[$. In the first case, $\sigma(\rho_{2,0}) = f(\rho_{2,0}) = f(\hat{\rho}_2) = \sigma(\hat{\rho}_2)$, see Figure 3.3.4(b). In the second case, $\sigma(\rho_{2,0}) = f(\rho_{2,0}) \le f^{\max} = \sigma(\hat{\rho}_2)$, see Figure 3.3.4(a).

For the onramp, we consider two different cases, when the buffer is initially empty and when it is not. In both cases different situations can occur.



(a) $0 \leq \rho_{1,0} \leq \rho_{\text{cr}}$ (b) $\rho_{1,0} = \hat{\rho}_1$

(c) $\rho_{\text{cr}} \leq \rho_{1,0} \leq 1$

Figure 3.3.3: Instantaneous evolution of the demand in the Riemann problem (incoming road).

(L1) Initially empty buffer: $l(0) = 0 \Rightarrow d(F_{\text{in}}, l(0)) = \min(F_{\text{in}}, \gamma_{\text{r1}}^{\max})$.

- (L1.1) Buffer increases: $l(0+) > 0 \Rightarrow d(F_{\text{in}}, l(0+)) = \gamma_{\text{r1}}^{\max}$.
  If $d(F_{\text{in}}, l(0)) = F_{\text{in}}$, then $d(F_{\text{in}}, l(0)) \leq d(F_{\text{in}}, l(0+))$.
  If $d(F_{\text{in}}, l(0)) = \gamma_{\text{r1}}^{\max}$, then $d(F_{\text{in}}, l(0)) = d(F_{\text{in}}, l(0+))$.
- (L1.2) Buffer remains empty: $l(0+) = 0 \Rightarrow d(F_{\text{in}}, l(0+)) = \min(F_{\text{in}}, \gamma_{\text{r1}}^{\max})$.
  Hence, $d(F_{\text{in}}, l(0)) = d(F_{\text{in}}, l(0+))$.

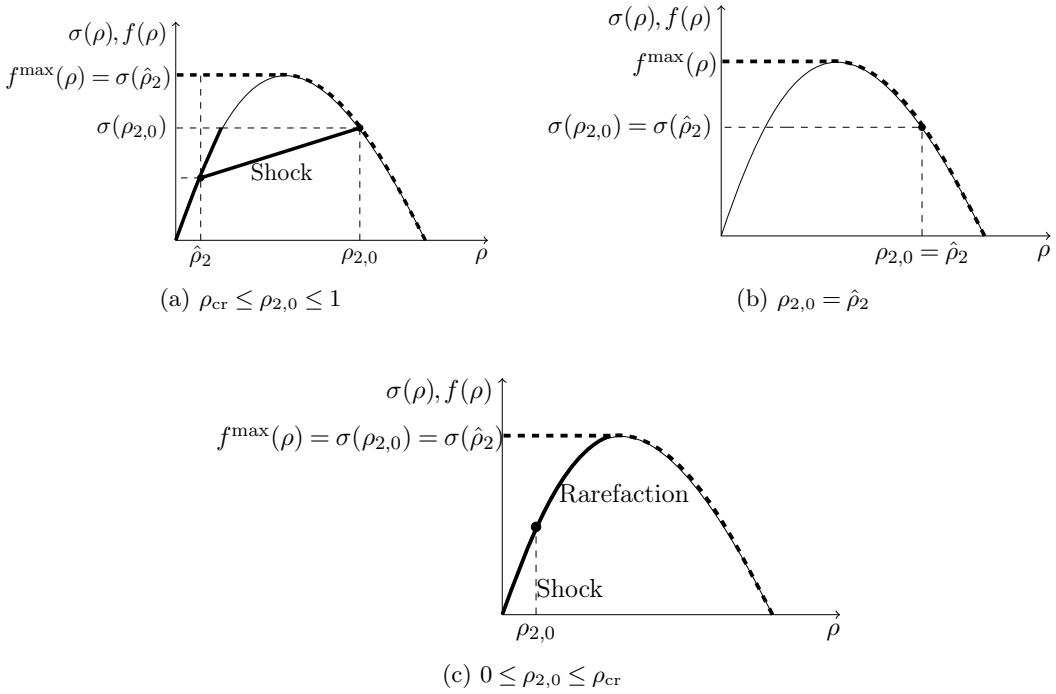
(L2) Buffer initially not empty: $l(0) > 0 \Rightarrow d(F_{\text{in}}, l(0)) = \gamma_{\text{r1}}^{\max}$.

- (L2.1) Buffer grows (decreases) linearly: $0 < l(0) < l(0+)$ $(0 < l(0+) < l(0)) \Rightarrow$ $d(F_{\text{in}}, l(0+)) = \gamma_{\text{r1}}^{\max}$.
  Hence, $d(F_{\text{in}}, l(0)) = d(F_{\text{in}}, l(0+))$.

This concludes the proof. □

Now we are ready to prove Theorem 10.

Proof. Existence and uniqueness follow by construction of the Riemann Solver detailed at the beginning of this section.



(a) $\rho_{\text{cr}} \leq \rho_{2,0} \leq 1$

(b) $\rho_{2,0} = \hat{\rho}_2$

(c) $0 \leq \rho_{2,0} \leq \rho_{\text{cr}}$

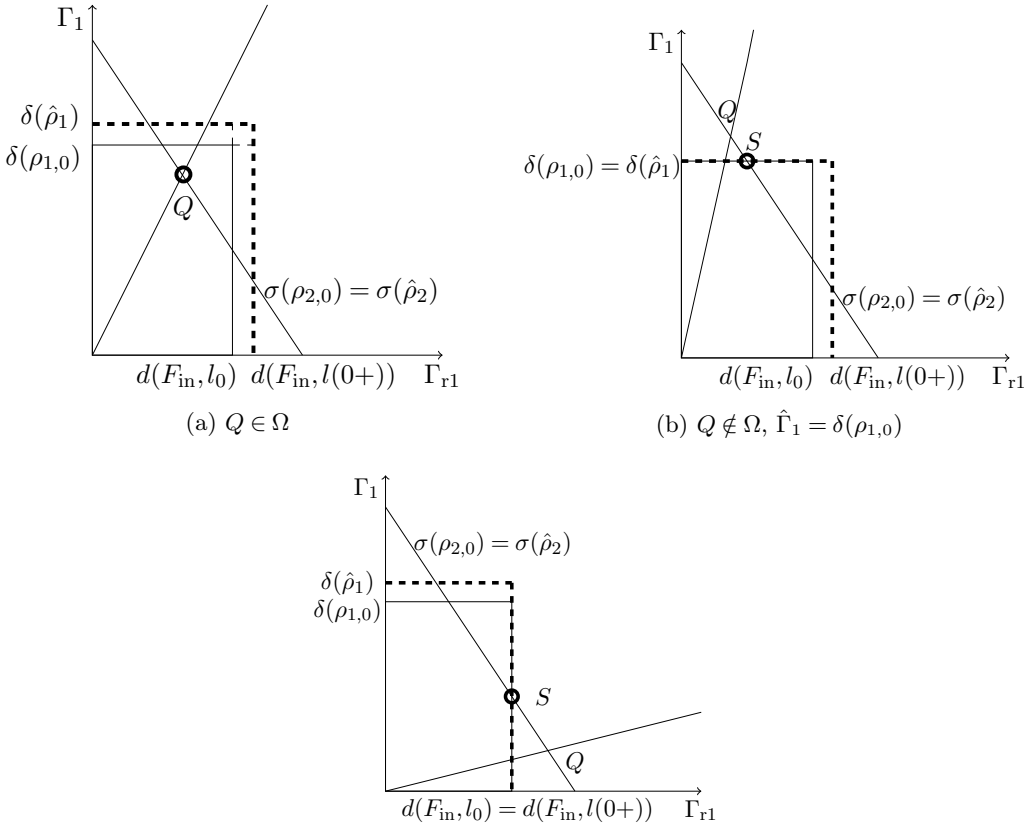
Figure 3.3.4: Instantaneous evolution of the supply in the Riemann problem (outgoing road).

In the following we will show the proof of the consistency of $\mathcal{RS}_{l(t)}$.
Fix $t_0 \geq 0$. If $(\rho_1(t_0,0-),\rho_2(t_0,0+))$ is a solution of the Riemann Solver, corresponding to the same buffer value $l(t_0)$ we need to show that

$$\mathcal{RS}_{l(t_0)}(\rho_1(t_0,0-),\rho_2(t_0,0+)) = (\rho_1(t_0,0-),\rho_2(t_0,0+)).$$

Without loss of generality, we fix $t_0 = 0$ and we keep the same notation used in the proof of Lemma 11.
We show that the optimal point in the feasible set Ω, as defined in (3.3.1), resulting from the Riemann Solver does not change. From the results of Lemma 11 it is straightforward to say that the set Ω either increases between times $t = 0$ and $t > 0$ or does not change, see Figures 3.3.5 and 3.3.6. Now, we need to prove that the optimal point does not change. We treat the supply constrained and the demand limited cases separately.

- Supply constrained junction problem, see Figure 3.3.5.
  We assume that we are supply limited at $t = 0$. In this case, by construction of the Riemann Solver, it holds $\rho_{2,0} = \hat{\rho}_2$ and hence $\sigma(\rho_{2,0}) = \sigma(\hat{\rho}_2)$. The priority line is fixed, the point of intersection Q does not change.



(a) $Q \in \Omega$

(b) $Q \notin \Omega$, $\hat{\Gamma}_1 = \delta(\rho_{1,0})$

(c) $Q \notin \Omega$, $\hat{\Gamma}_{\text{r1}}(0) = d(F_{\text{in}}, l_0)$

Figure 3.3.5: Supply constrained junction problems.

– Optimal solution inside Ω, see Figure 3.3.5(a).
Since Q is determined by the intersection of the two lines and Ω can only increase ($\delta(\rho_{1,0}) \leq \delta(\hat{\rho}_1), d(F_{\text{in}}, l(0)) \leq d(F_{\text{in}}, l(0+))$), we have

$$(\hat{\rho}_1, \hat{\rho}_2) = \mathcal{RS}_{l(0)}(\hat{\rho}_1, \hat{\rho}_2).$$

– Optimal solution on the border of Ω, $\hat{\Gamma}_1 = \delta(\rho_{1,0})$, see Figure 3.3.5(b).
We have to prove that the result of the minimization problem (3.3.2) (the point S in the figure) does not change. In this case, by construction of the Riemann Solver it holds $\rho_{1,0} = \hat{\rho}_1$. This yields $\delta(\rho_{1,0}) = \delta(\hat{\rho}_1)$ by (3.3.10). Since, $d(F_{\text{in}}, l(0))$ can only increase according to the cases (L1) and (L2), it holds

$$(\hat{\rho}_1, \hat{\rho}_2) = \mathcal{RS}_{l(0)}(\hat{\rho}_1, \hat{\rho}_2).$$

– Optimal solution on the border of Ω, $\hat{\Gamma}_{\text{r1}}(0) = d(F_{\text{in}}, l(0))$, see Figure 3.3.5(c).
For the onramp, the only case where the demand can increase is the case (L1.1). In this particular setting, if $d(F_{\text{in}}, l(0)) = F_{\text{in}}$ it holds $\gamma_{r1}(0) = F_{\text{in}}$ and

$F_{\text{in}} \leq \gamma_{\text{r1}}^{\max}$. When the buffer increases we have $\gamma_{\text{r1}}(0+) = d(F_{\text{in}}, l(0+)) = \gamma_{\text{r1}}^{\max}$, which implies $\gamma_{\text{r1}}^{\max} \leq F_{\text{in}}$. Hence, $F_{\text{in}} = \gamma_{\text{r1}}^{\max}$ and $d(F_{\text{in}}, l(0)) = d(F_{\text{in}}, l(0+))$. The mainline demand can only increase. Hence,

$$(\hat{\rho}_1, \hat{\rho}_2) = \mathcal{RS}_{l(0)}(\hat{\rho}_1, \hat{\rho}_2).$$

- Demand constrained junction problem, see Figure 3.3.6.
  $\Omega = \Omega(\rho_{1,0}, l(0)) = \Omega(\hat{\rho}_1, l(0))$. In fact, $\rho_{1,0} = \hat{\rho}_1$ and for the onramp it holds $\gamma_{\text{r1}}^{\max} = F_{\text{in}}$ (as in the previous point), and this yields $\delta(\rho_{1,0}) = \delta(\hat{\rho}_1)$ and $d(F_{\text{in}}, l(0)) = d(F_{\text{in}}, l(0+))$ by (3.3.10) and (L1) and (L2). The supply can only increase by (3.3.11). Hence,
  $$(\hat{\rho}_1, \hat{\rho}_2) = \mathcal{RS}_{l(0)}(\hat{\rho}_1, \hat{\rho}_2).$$

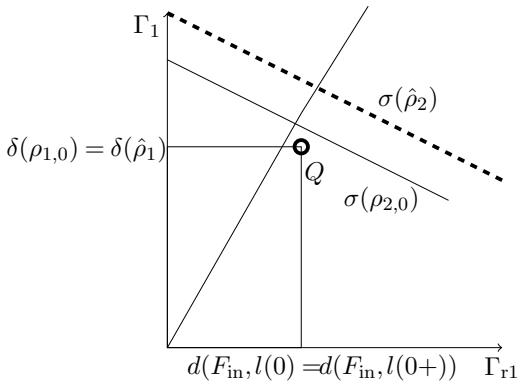


Figure 3.3.6: Demand constrained junction problem.

Moreover, the limiting side of Ω does not change, i.e., it is not possible to pass from a demand constrained junction problem to a supply constrained one and viceversa. This follows for the fact that $\sigma(\rho_{2,0}) = \sigma(\hat{\rho}_2)$ when we have a supply constrained junction problem, Figure 3.3.5 and $d(F_{\text{in}}, l(0)) = d(F_{\text{in}}, l(0+))$, $\delta(\rho_{1,0}) = \delta(\hat{\rho}_1)$ when we have a demand constrained junction problem, Figure 3.3.6.
This concludes the proof. □

Remark 8 *The proposed model is a variant of the junction model considered in [41] and explained in Section 1.2.2 in the 2×2 case. The traffic distribution across the junction is given by the distribution matrix A, subject to technical conditions that ensure uniqueness of the solution. In our case, since we suppose that no flux from the onramp is directed into the offramp, the distribution matrix would look as: $A = \begin{pmatrix} 1-\beta & 1 \\ \beta & 0 \end{pmatrix}$. Clearly, as the offramp gets more congestioned, β decreases. If we solve the model proposed in [41] using this distribution matrix, there can be cases in which the solution gives zero onramp flux, see Figure 3.3.7(a). This is due to the choice of maximizing the flow throughout the*

junction. In fact, in this way, the model tends to satisfy the mainline demand before the onramp one. This does not reflect what happens in reality, since the demand allocation depends on the number of lanes available for each inflow. Hence, we propose a model that fixes this issue balancing the flux between the two incoming roads by the introduction of a right-of-way parameter. In particular, the priority coefficient keeps the maximization point far from the axis, avoiding blocking, see Figure 3.3.7(b).

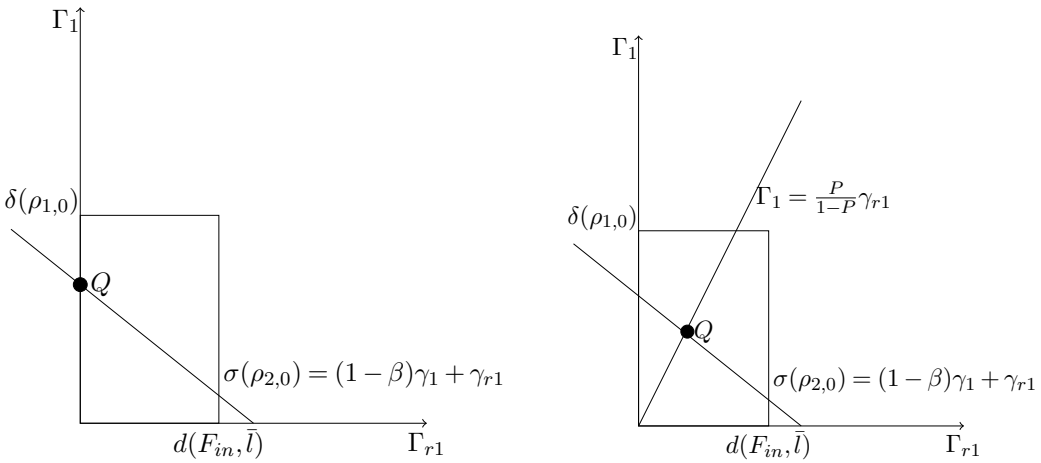


Figure 3.3.7: Comparison between Coclite-Garavello-Piccoli model [41] (left) and our model (right).

Remark 9 *This model extends the use of a priority parameter, as introduced in [40], to the case of* 2×2 *junctions. In [40], the authors use the priority parameter only for* 2×1 *junctions treating* 2×2 *junctions with a traffic distribution matrix which can result, in our setting, in onramp blocking as explained in the previous remark.*

3.4 Numerical results: modified Godunov

In order to find approximate solutions, we adapt the classical Godunov scheme to the problem, with some adjustment due to the presence of the buffer.
We define a numerical grid in $(0,T) \times \mathbb{R}$ using the following notation:

- Δx is the fixed space grid size;
- Δt^n is the nonuniform time grid size given by the CFL condition
- $(t^n, x_j) = (t^{n-1} + \Delta t^n, j\Delta x)$ for $n \in \mathbb{N}$ and $j \in \mathbb{Z}$ are the grid points.

For a function v defined on the grid we write $v_j^n = v(t^n, x_j)$ for j, n varying on a subset of $\mathbb{Z}$ and $\mathbb{N}$ respectively. We also use the notation u_j^n for $u(t^n, x_j)$ when u is a continuous

function on the (t,x) plane. In the following section, we will use the Godunov scheme, introduced in Section 1.3, that under the CFL condition can be written as

$$v_j^{n+1} = v_j^n - \frac{\Delta t^n}{\Delta x}(g(v_j^n, v_{j+1}^n) - g(v_{j-1}^n, v_j^n)), \tag{3.4.1}$$

where numerical flux g is the numerical flux.

3.4.1 Boundary conditions and conditions at the junctions

Here we impose the boundary conditions for the incoming and the outgoing roads at the endpoint not connected to the junction. We also assign boundary conditions at the endpoints of the roads connected to the junction. In both cases we will use the classical approach for road networks as introduced in [32] and shown in Section 1.3.

Boundary conditions

Each road is divided in $J+1$ cells numbered from 0 to J. For the incoming road, in practice, we proceed defining

$$v_0^{n+1} = v_0^n - \frac{\Delta t^n}{\Delta x}(g(v_0^n, v_1^n) - f(v_0^n)),$$

where $f(v_0^n)$ is the value of the flux at the boundary.
An outgoing boundary can be treated analogously,

$$v_J^{n+1} = v_J^n - \frac{\Delta t^n}{\Delta x}(f(v_J^n) - g(v_{J-1}^n, v_J^n)),$$

with $f(v_J^n)$ the outgoing flux.
Since we are dealing with Riemann problems at the junction, the formulation of absorbing boundary conditions is equivalent to the one with the ghost cells which is common in literature.

Conditions at the Junction

For I_1, that is connected at the junction at the right endpoint, we set

$$v_J^{n+1} = v_J^n - \frac{\Delta t^n}{\Delta x}(\hat{\Gamma}_1 - g(v_{J-1}^n, v_J^n)),$$

while for the outgoing road, connected at the junction at the left endpoint, we have

$$v_0^{n+1} = v_0^n - \frac{\Delta t^n}{\Delta x}(g(v_0^n, v_1^n) - \hat{\Gamma}_2),$$

where $\hat{\Gamma}_1$ and $\hat{\Gamma}_2$ are the maximized fluxes computed in Section 3.3.

3.4.2 ODE treatment

Let us consider now the buffer modeled by (3.2.2) on the onramp. At each time step $t^n = t^{n-1} + \Delta t^n$ we compute the new value of the queue length according to two possible cases, with Euler first order integration.

- If $F_{\text{in}}(t^n) < \hat{\Gamma}_{\text{r1}}$

$$l^{n+1} = \begin{cases} l^n + (F_{\text{in}}(t^n) - \hat{\Gamma}_{\text{r1}})\Delta t^n & \text{for } t^{n+1} < \bar{t}, \\ 0 & \text{otherwise .} \end{cases}$$

- If $F_{\text{in}}(t^n) \geq \hat{\Gamma}_{\text{r1}}$

$$l^{n+1} = l^n + (F_{\text{in}}(t^n) - \hat{\Gamma}_{\text{r1}})\Delta t^n.$$

Above, $\hat{\Gamma}_{\text{r1}}$ is the maximized flux described in Section 3.3, $F_{\text{in}}(t^n)$ is the flux entering the onramp at t^n given by

$$F_{\text{in}}(t^n) = \frac{1}{\Delta t^n} \int_{t^n}^{t^{n+1}} F_{\text{in}}(t) dt,$$

and $\bar{t}$ is the time at which the buffer empties. We can calculate the time at which the buffer can empty for each time step Δt^n:

$$\bar{t} = -\frac{l^n}{F_{\text{in}}(t^n) - \hat{\Gamma}_{\text{r1}}} + t^n. \tag{3.4.2}$$

3.4.3 Modified Godunov scheme

Godunov scheme cannot be applied as it is when the buffer empties as noted in [48], because the solution could potentially not be self-similar. If the buffer empties, at some time step Δt^n, we might have multiple shocks at the junction. In this case we divide the time step $\Delta t^n = (t^n, t^{n+1})$ in two sub-intervals $\Delta t_a = (t^n, \bar{t})$ and $\Delta t_b = (\bar{t}, t^{n+1})$, as in Figure 3.4.1, with $\bar{t}$ being defined in (3.4.2). Then, we solve in one time step two different Riemann Problems at the junction. For Δt_a we solve the classical Godunov scheme. For the Δt_b we solve a new Riemann Problem at the junction in which the value of the queue length is $l = 0$. The junction conditions are

$$v_J^{n+1} = v_J^{\bar{t}} - \frac{\Delta t_b}{\Delta x}\left(\hat{\Gamma}_1^{\bar{t}} - g(v_{J-1}^n, v_J^{\bar{t}})\right), \tag{3.4.3}$$

$$v_0^{n+1} = v_0^{\bar{t}} - \frac{\Delta t_b}{\Delta x}\left(g(v_0^{\bar{t}}, v_1^n) - \hat{\Gamma}_2^{\bar{t}}\right), \tag{3.4.4}$$

where with the superscript $\bar{t}$ we indicate the value computed at $t = \bar{t}$ in the previous time step Δt_a.

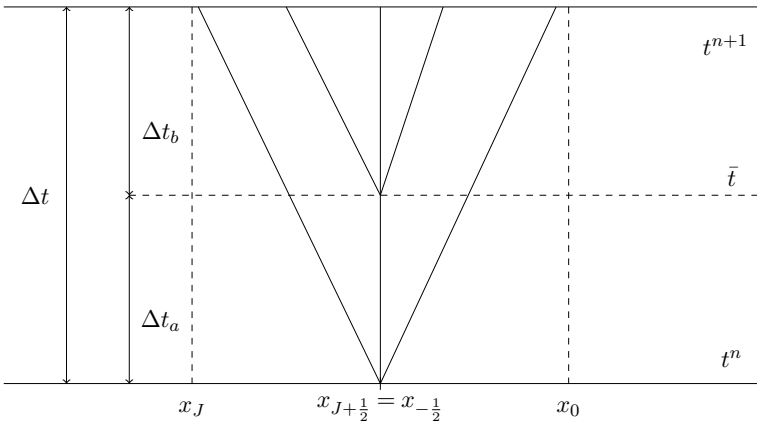


Figure 3.4.1: Junction in the case of emptying buffer.

Remark 10 *We point out that in our case it is not necessary to introduce an explicit correction on the ODE as done in [48] since at time $\bar{t}$ we compute ex novo the Riemann problem at the junction with a queue length equal to zero.*

3.5 Numerical results

In this section we present some numerical tests performed with the scheme previously described. We introduce the formal order of convergence μ of a numerical method

$$\mu = \frac{\ln(\mathrm{TOT}_{\mathrm{err}})}{\ln(\Delta x)}, \tag{3.5.1}$$

where the $\mathcal{L}^1$-norm error is given by

$$\mathrm{TOT}_{\mathrm{err}} = \sum_{i=1}^{2} \|u_e^i - u_c^i\|_{\mathcal{L}^1}. \tag{3.5.2}$$

where u_e^i and u_c^i are the exact solution and the computed solution in each road, respectively. We show some numerical results obtained applying Godunov scheme to problem (3.2.3). Tables 3.5.1 and 3.5.2 provide the values of the $\mathcal{L}^1$-error (3.5.2) and the order of convergence (3.5.1). Here we deal with a mainline of length 8 parametrized by the interval $[-4,4]$ with the node placed at $x=0$, such that $I_1=[-4,0]$ and $I_2=[0,4.]$ In all the simulations we fix $V_{\max}=1$, $P=0.7$, $\beta=0.2$, $\gamma_{\max}=0.5$, $l_0=0.2$ and $F_{\mathrm{in}}=0.05$.

- **Case I**: We consider the following initial data

$$\rho_1(0,x)=0.6, \quad \rho_2(0,x)=0. \tag{3.5.3}$$

  The values of the initial conditions creates a shock on the incoming mainline and a rarefaction on the outgoing one. After a time $t=5.3$ we can see the rarefaction

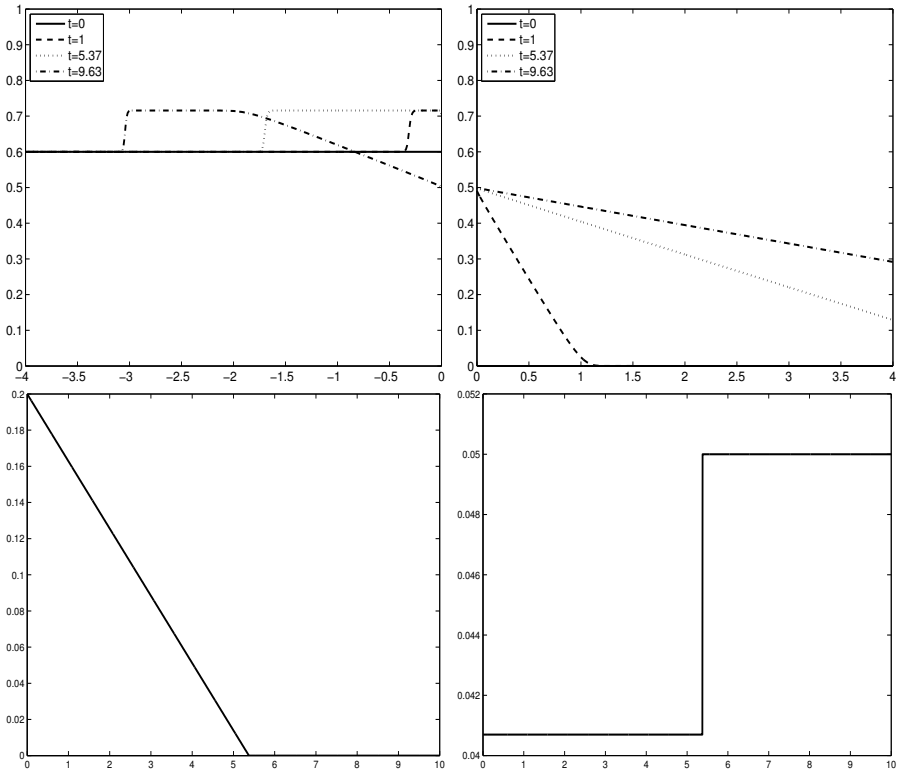


Figure 3.5.1: Evolution in time of the density in the incoming mainline (above, left), on the outgoing mainline (above, right) and evolution of the flux in the onramp (bottom, left) and in the offramp (bottom, right), corresponding to initial data (3.5.3) and a space step discretization $\Delta x = 0.01$.

caused by the buffer that empties in the incoming mainline I_1, as illustrated in Figure 3.5.1. Table 3.5.1 collects the values of the $\mathcal{L}^1$-error and of the order of convergence at time $T = 10$.

- **Case II**: We consider the following initial data

$$\rho_1(0,x) = 0.1, \quad \rho_2(0,x) = 0.6. \tag{3.5.4}$$

In this case, the values of the initial conditions are chosen such that the wave produced by the buffer that empties can be seen in the outgoing mainline. In particular, in this case no waves are generated at initial time. The only wave generated is a shock which appear once that the buffer empties at time $t = 1.53$, as shown in Figure 3.5.2. Table 3.5.2 reports the $\mathcal{L}^1$-error and the order of convergence.

Δx	$\mathcal{L}^1$-error	μ
0.02	$3.69 \cdot 10^{-2}$	0.8432
0.01	$1.49 \cdot 10^{-2}$	0.9133
0.005	$7.21 \cdot 10^{-3}$	0.9322
0.002	$1.10 \cdot 10^{-3}$	1.0962
0.001	$2.23 \cdot 10^{-4}$	1.2170

Table 3.5.1: Errors and order of convergence for the Godunov scheme at time $T = 10$, corresponding to initial data (3.5.3).

Δx	$\mathcal{L}^1$-error	μ
0.02	$1.70 \cdot 10^{-2}$	1.0464
0.01	$1.67 \cdot 10^{-2}$	0.8890
0.005	$1.44 \cdot 10^{-2}$	0.8066
0.002	$9.39 \cdot 10^{-3}$	0.9878
0.001	$3.57 \cdot 10^{-4}$	1.2474

Table 3.5.2: Errors and order of convergence for the Godunov scheme at time $T = 3$, corresponding to initial data (3.5.4).

3.6 Discrete adjoint method for optimization

In this section we show how the model introduced in Section 3.2 can be used in control systems and how to apply it to a ramp metering problem. We give just an idea in a simplified setting without claiming any convergence of the results of this section to the solutions in Section 3.3. In the literature, there are several approaches for the adjoint method for PDEs: continuous adjoint method, discrete adjoint method and automatic differentiation. The first method applies the adjoint directly on the continuous PDE [83, 96, 113, 126], while in the second case the PDE is first discretized and then the adjoint is computed [74, 80, 98]. The third approach uses automatic differentiation to automatically generate an adjoint solver from the numerical representation of the systems of PDEs [71, 114]. For this section we choose a discrete adjoint method. The use of the adjoint method might introduce numerical error at discontinuities if the numerical scheme is not well chosen [73]. There exist results on convergence for Lax-Friedichs type schemes [72] and relaxation methods [9]. In our model though, the presence of junction conditions led us to use of a modified Godunov scheme. Moreover, since analytical results on existence and stability of the solutions for our model are still missing, it is not possible to provide a formal proof of the convergence of the results obtained by the discretized model with the adjoint method to the continuous one.

In this section, we consider a triangular flux function, see Figure 3.6.1 and the density on the onramp is considered to be always in free-flow condition to replicate the behavior of the ODE (3.2.2). In this way we still keep the strong boundary condition and the calculation is simpler. Table 3.6.1 sets the notations for this section.

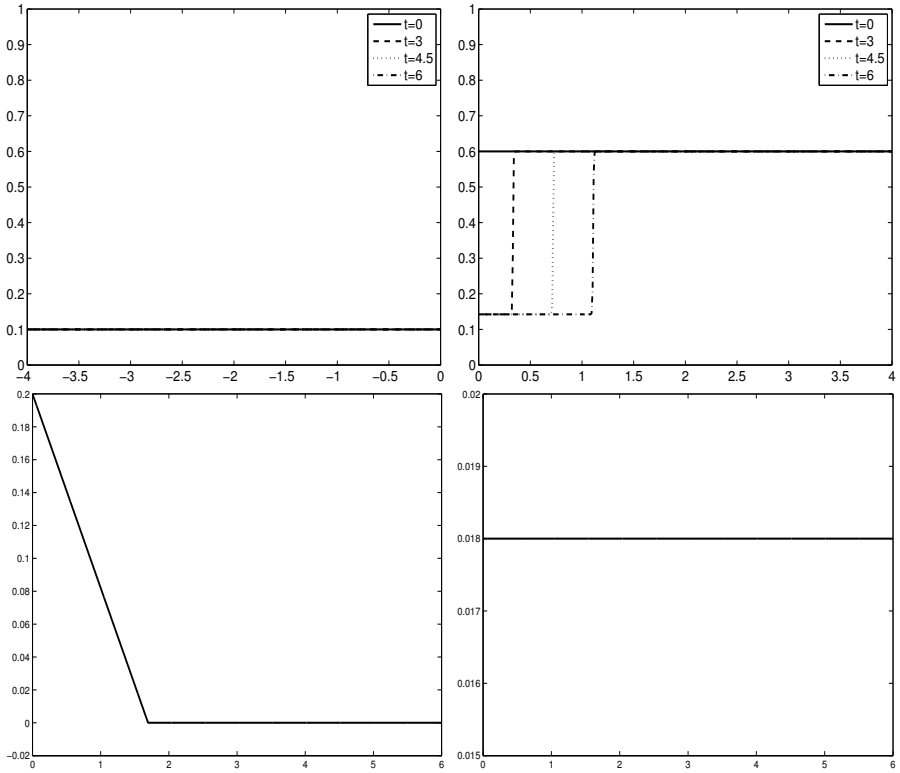


Figure 3.5.2: Evolution in time of the density in the incoming mainline (above, left), on the outgoing mainline (above, right) and evolution of the flux in the onramp (bottom, left) and in the offramp (bottom, right), corresponding to initial data (3.5.4) and a space step discretization $\Delta x = 0.01$.

We consider a network with J links at a discrete time $t = n\Delta t$ for $n = 1, ..., T-1$. Each single junction i for $i = 1, ..., J$ looks like the one in Figure 3.6.2. We take the discretized version of system (3.2.3), given by the Godunov discretization to obtain

$$\rho_{\cdot,i}^{n+1} = \rho_{\cdot,i}^{n} + \frac{\Delta t}{\Delta x}(g_{\cdot}(\rho_{\cdot,i}^{n}, \rho_{\cdot,i+1}^{n}, u_i^n) - g_{\cdot}(\rho_{\cdot,i}^{n}, \rho_{\cdot,i-1}^{n}, u_{i-1}^n)), \quad i = 1, ..., J \; n = 1, ..., T-1 \tag{3.6.1}$$

$$\rho_{\text{onramp},i}^{n+1} = \rho_{\text{onramp},i}^{n} + \frac{\Delta t}{L_i}(f_{\text{onramp}}^{n} - d_i^n), \quad i = 1, ..., J \; n = 1, ..., T-1 \tag{3.6.2}$$

$$d_i^n = u_i^n \min\left(f_{\text{onramp}}^{\max}, \frac{L_i}{\Delta t}\rho_{\text{onramp},i}^{n}\right), \tag{3.6.3}$$

$$\delta_{\text{inc},i}^{n} = \min\left(f^{\max}, v\rho_{\text{inc},i}^{n}\right), \tag{3.6.4}$$

$$\sigma_{\text{out},i}^{n} = \min\left(f^{\max}, w(\rho_{\max} - \rho_{\text{out},i}^{n})\right). \tag{3.6.5}$$

where $u_i^n \in [0,1]$ is our control variable and gives the ramp-metering rate and the subscripts "inc" and "out" describe the incoming and outgoing link of the junction with

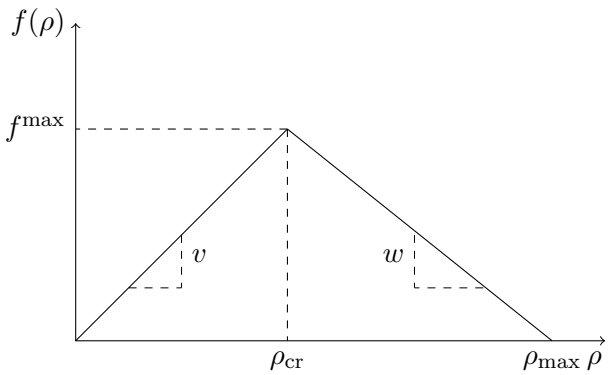


Figure 3.6.1: Triangular fundamental diagram considered in this section.

Notation	
$v = (1 - \rho)$	Free flow speed
$w = \dfrac{f^{\max}}{\rho_{\max} - \rho_{\text{cr}}}$	Congestion wave speed
$\boldsymbol{\rho}$	State variable
$\mathbf{u}$	Control variable
i	index for junctions
n	time index
$\rho^n_{\text{inc},i}$	Density in the incoming link for junction i at time t^n
$\rho^n_{\text{onramp},i}$	Density in the onramp for junction i at time t^n
$\rho^n_{\text{out},i}$	Density in the outgoing link for junction i at time t^n
$g^n_{\text{inc},i}$	Discrete flux in the incoming link for junction i at time t^n
$g^n_{\text{out},i}$	Discrete flux in the outgoing link for junction i at time t^n
$g^n_{\text{onramp},i}$	Discrete flux in the onramp for junction i at time t^n

Table 3.6.1: Notations for Section 3.6.

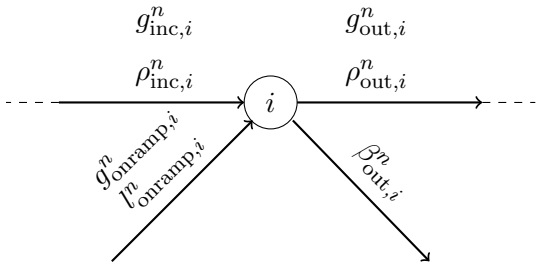


Figure 3.6.2: A junction considered in the network.

$\rho^n_{\text{inc},i+1} = \rho^n_{\text{out},i}$ for every $i = 1, ..., J-1$. The state variable is given by $\rho^n_{\cdot,i} \in [0,1]$ for $i = 1, ..., J$ and $n = 0, ..., T-1$. The state vector is identified with $\boldsymbol{\rho} \in \mathbb{R}^{JT}$ and the control vector with $\mathbf{u} \in \mathbb{R}^{MT}$.
For each state variable $\rho^n_{\cdot,i}$ we consider the state equation $h^n_{\cdot,i} : \mathbb{R}^{JT} \times \mathbb{R}^{MT} \to \mathbb{R}$:

$$h^{n+1}_{\cdot,i} = \rho^{n+1}_{\cdot,i} - \rho^n_{\cdot,i} + \frac{\Delta t}{\Delta x}\Big(g_{\text{inc}}(\rho^n_{\cdot,i}, \rho^n_{\cdot,i+1}, u^n_i) - g_{\text{out}}(\rho^n_{\cdot,i}, \rho^n_{\cdot,i-1}, u^n_{i-1})\Big) = 0 \tag{3.6.6}$$

where

$$\begin{aligned} g_{\text{out}} &= \min\left(\beta^n_{\text{out},i}\delta^n_{\text{inc},i} + d^n_i, \sigma^n_{\text{out},i}\right) \\ g_{\text{inc}} &= \begin{cases} \delta^n_{\text{inc},i} & \text{if } \dfrac{P_i g_{\text{out}}}{\beta^n_{\text{out},i}(1+P_i)} \geq \delta^n_{\text{inc},i} \\ \dfrac{g_{\text{out}} - d^n_i}{\beta^n_{\text{out},i}} & \text{if } \dfrac{g_{\text{out}}}{1+P_i} \geq d^n_i \\ \dfrac{P_i g_{\text{out}}}{\beta^n_{\text{out},i}(1+P_i)} & \text{otherwise} \end{cases} \end{aligned} \tag{3.6.7}$$

for the incoming and outgoing link. And,

$$h^{n+1}_{\text{onramp},i} = \rho^{n+1}_{\text{onramp},i} - \rho^n_{\text{onramp},i} + \frac{\Delta t}{L_i}\Big(f^n_{\text{onramp}} - d^n_i\Big) = 0 \tag{3.6.8}$$

with

$$f^n_{\text{onramp}} = g_{\text{out}} - \beta^n_{\text{out},i} g_{\text{inc}}, \tag{3.6.9}$$

for the onramp.
In addition to the state equations $H(\boldsymbol{\rho}, \mathbf{u}) = 0$ we introduce as well a cost function $C(\boldsymbol{\rho}, \mathbf{u}) : \mathbb{R}^{JT} \times \mathbb{R}^{MT} \to \mathbb{R}$:

$$C(\mathbf{u}, \boldsymbol{\rho}) = \Delta t \sum_{n=1}^{T} \sum_{i=1}^{J} \rho^n_{\cdot,i}. \tag{3.6.10}$$

The objective function represents the total travel time which describes the time spent by the drivers on the road network. We want to minimize the cost functional C over the set of control parameters $\mathbf{u}$, using as constraints the state equations $H(\boldsymbol{\rho}, \mathbf{u}) = 0$. The

optimization problem to solve is the following:

$$\begin{aligned} &\underset{\mathbf{u}\in[0,1]^{JT}}{\text{minimize}} && C(\boldsymbol{\rho},\mathbf{u}) \\ &\text{subject to} && H(\boldsymbol{\rho},\mathbf{u}) = 0. \end{aligned}$$

Remark 11 *We note that both the cost functional and the state equations may be non-convex for this problem.*

To solve this optimization problem we would like to use gradient information in order to find some control variable $\mathbf{u}^*$ that gives local optimal cost $C^*(\boldsymbol{\rho}(\mathbf{u}^*),\mathbf{u}^*)$. However, gradients methods do not guarantee the global optimality of $\mathbf{u}^*$. The gradient of the cost functional is given by:

$$\nabla_{\mathbf{u}} C = \frac{\partial C}{\partial \boldsymbol{\rho}} \nabla_{\mathbf{u}} \boldsymbol{\rho} + \frac{\partial C}{\partial \mathbf{u}}. \tag{3.6.11}$$

Remark 12 *To be able to compute fully* (3.6.11) *all the required partial and full derivatives must be well-defined. This is not necessarily true. For this to hold, one should require that C and H belong to $\mathcal{C}^1$.*

To compute $\nabla_{\mathbf{u}}\boldsymbol{\rho}$ we recall that $\nabla_{\mathbf{u}} H(\boldsymbol{\rho},\mathbf{u}) = 0$ on the trajectories of the systems and thus

$$\frac{\partial H}{\partial \boldsymbol{\rho}} \nabla_{\mathbf{u}} \boldsymbol{\rho} + \frac{\partial \boldsymbol{\rho}}{\partial \mathbf{u}} = 0. \tag{3.6.12}$$

Now, instead of evaluating $\nabla_{\mathbf{u}}\boldsymbol{\rho}$, the adjoint method directly solves the following system:

$$\frac{\partial H^T}{\partial \boldsymbol{\rho}} \lambda = \frac{\partial C}{\partial \boldsymbol{\rho}}. \tag{3.6.13}$$

This system is called the adjoint system and the unknown $\lambda \in \mathbb{R}^{JT}$ is called the adjoint variable. The expression of the gradient becomes then:

$$\nabla_{\mathbf{u}} C = \lambda^T H_{\mathbf{u}} + C_{\mathbf{u}}. \tag{3.6.14}$$

Computing then the partial derivatives in our systems of equations in 3.6.1 we get for the links:

$$\frac{\partial h^n_{\cdot,i}}{\partial \rho^k_{\cdot,j}} = \frac{\partial \rho^{n+1}_{\cdot,i}}{\partial \rho^k_{\cdot,j}} - \frac{\partial \rho^n_{\cdot,i}}{\partial \rho^k_{\cdot,j}} + \frac{\Delta t}{\Delta x}\Big(\frac{\partial}{\partial \rho^k_{\cdot,j}} g_{\text{inc}}(\rho^n_{\cdot,i}, \rho^n_{\cdot,i+1}, u^n_i) - \frac{\partial}{\partial \rho^k_{\cdot,j}} g_{\text{out}}(\rho^n_{\cdot,i}, \rho^n_{\cdot,i-1}, u^n_{i-1}) \Big), \tag{3.6.15}$$

for the state variable and the following result for the control variable:

$$\frac{\partial h^n_{\cdot,i}}{\partial u^k_j} = \frac{\Delta t}{\Delta x}\Big(\frac{\partial}{\partial u^k_j} g_{\text{inc}}(\rho^n_{\cdot,i}, \rho^n_{\cdot,i+1}, u^n_i) - \frac{\partial}{\partial u^k_j} g_{\text{out}}(\rho^n_{\cdot,i}, \rho^n_{\cdot,i-1}, u^n_{i-1}) \Big). \tag{3.6.16}$$

We compute the partial differential equation also for the cost functional (3.6.10), for the equations (3.6.3)-(3.6.5) and for the fluxes (3.6.7) and (3.6.9). For simplicity in the following with s we indicate either the control variable or the state one:

$$\frac{\partial C(\boldsymbol{\rho}, \mathbf{u})}{\partial s} = \begin{cases} \Delta t L_i & \text{if } s = \rho^n_{\cdot,i}, \\ 0 & \text{otherwise,} \end{cases} \tag{3.6.17}$$

$$\frac{\partial d^n_i}{\partial s} = \begin{cases} u^n_i & \text{if } s = \rho^n_{onramp,i} \text{ and } \rho^n_{\text{onramp},i} \leq f^{\max}_{\text{onramp}}, \\ \min\left(f^{\max}_{\text{onramp}}, \rho^n_{\text{onramp},i}\right) & \text{if } s = u^n_i, \\ 0 & \text{otherwise,} \end{cases} \tag{3.6.18a}$$

$$\frac{\partial \delta^n_{\text{inc},i}}{\partial s} = \begin{cases} v & \text{if } s = \rho^n_{\text{inc},i} \text{ and } v\rho^n_{\text{inc},i} \leq f^{\max}, \\ 0 & \text{otherwise,} \end{cases} \tag{3.6.18b}$$

$$\frac{\partial \sigma^n_{\text{out},i}}{\partial s} = \begin{cases} w & \text{if } s = \rho^n_{\text{out},i} \text{ and } w(\rho_{\max} - \rho^n_{\text{out},i} \leq f^{\max}, \\ 0 & \text{otherwise,} \end{cases} \tag{3.6.18c}$$

$$\frac{\partial g_{\text{out}}}{\partial s} = \begin{cases} \beta^n_{\text{out},i} \dfrac{\partial \delta^n_{\text{inc},i}}{\partial s} + \dfrac{\partial d^n_i}{\partial s} & \text{if } \beta^n_{\text{out},i}\delta^n_{\text{inc},i} + d^n_i \leq \sigma^n_{\text{out},i}, \\ \dfrac{\partial \sigma^n_{\text{out},i}}{\partial s} & \text{otherwise,} \end{cases} \tag{3.6.18d}$$

$$\frac{\partial g_{\text{inc}}}{\partial s} = \begin{cases} \dfrac{\partial \delta^n_{\text{inc},i}}{\partial s} & \text{if } \dfrac{P_i g_{\text{out}}}{(1-P_i)} \geq \dfrac{\delta^n_{\text{inc},i}}{\beta^n_{\text{out},i}}, \\ \dfrac{1}{\beta^n_{\text{out},i}}\left(\dfrac{\partial g_{\text{out}}}{\partial s} - \dfrac{\partial d^n_i}{\partial s}\right) & \text{if } \dfrac{g_{\text{out}}}{1+P_i} \geq d^n_i, \\ \dfrac{P_i}{\beta^n_{\text{out},i}(1+P_i)} \dfrac{\partial g_{\text{out}}}{\partial s} & \text{otherwise,} \end{cases} \tag{3.6.18e}$$

$$\frac{\partial f^n_{\text{onramp}}}{\partial s} = \frac{\partial g_{\text{out}}}{\partial s} - \beta^n_{\text{out},i} \frac{\partial g_{\text{inc}}}{\partial s}. \tag{3.6.18f}$$

With these expressions we can then compute fully (3.6.16) and (3.6.15), and hence apply the adjoint method to this problem.

Moreover, in [125] this approach was implemented in a coordinated ramp metering algorithm which uses the previous adjoint method. A field test has been conducted on the I-15 South freeway in California, showing that our approach produces significant improvements compared to existing tools (ALINEA, [120]). The algorithm is now being fully implemented as a component of the traffic simulator module within the Connected Corridor system [12], a project leaded by UC Berkeley and PATH.

Chapter 4

An application to roundabouts

Contents

4.1 Introduction 98
4.2 Mathematical model 98
4.3 Riemann problem at the junction 101
4.4 Optimization on networks 102
4.4.1 $\Gamma_2 = (1-\beta)\delta(\hat{\rho}_1) + d(F_{\text{in}}, l)$ 103
4.4.2 $\Gamma_2 = \sigma(\hat{\rho}_2)$ 108
4.4.3 Local Total Waiting Time and Total Travel Time 113
4.5 Numerical scheme 119
4.5.1 Network topology 119
4.5.2 Numerical scheme 119
4.6 Numerical simulations 120
4.6.1 Simulation results 121

4.1 Introduction

In this chapter, we focus on optimization problems for roundabouts. We consider the model introduced in Chapter 3 and apply it to roundabouts. Roundabouts can be seen as particular road networks and they can be modeled as a concatenation of junctions. Here, we focus on roundabouts with three entrances and three exits that can be modeled as a concatenation of 2x2 junctions with two incoming and two outgoing roads, but the approach can be generalized to more general networks. In particular, each junction has one incoming mainline, one outgoing mainline and a third link with incoming and outgoing fluxes. The third road is modeled with a vertical buffer of infinite capacity for the entering flux and with an infinite sink for the exiting one. The mainline evolution is described by a scalar hyperbolic conservation law, whereas the buffer dynamics is described by an ordinary differential equation (ODE) which depends on the difference between the incoming and outgoing fluxes on the link. The outgoing secondary road is modeled as a sink. At each junction, the Riemann problem is uniquely solved using a right of way parameter, and solutions are constructed exactly via wave-front tracking method.

Our aim is to optimize some cost functionals, such as the Total Travel Time (TTT) and the Total Waiting Time (TWT) through a suitable choice of the right of way parameter for incoming roads. The TTT and the TWT give an estimate of the time spent by drivers in the network sections or in the queues at the buffers, respectively. The cost functionals are computed analytically on a single 2x2 junction. Then, the traffic behavior for the whole roundabout is studied numerically using local optima. Numerical simulations show the effectiveness of the optimization strategy, compared to the case of fixed constant right of way parameters.

The chapter is structured as follows. In Section 4.2 we describe the junction model and the roundabout model. In section 4.3 we give the solution of the Riemann Problem. In Section 4.4 we describe the cost functionals and compute local optimal priority parameters. Section 4.5 and 4.6 are devoted to the description of the numerical scheme and to numerical tests.

The results contained in this chapter are obtained in collaboration with Prof. S. Kassa and L.L. Obsu from the University of Addis Ababa (Ethiopia) and they are included in [119, 118].

4.2 Mathematical model

We consider a roundabout joining three roads as illustrated in Figure 4.2.1, the generalization of the study to an arbitrary number of roads being straightforward. A roundabout can be seen as a periodic sequence of junctions and it can be represented by an oriented graph, in which roads are described by arcs and junctions by vertexes. Each link forming the roundabout is modeled by an interval $I_i = [a_i, b_i] \subset \mathbb{R}$, $i = 1, 2, 3$, $a_i < b_i$. In particular, in our case, each junction can be modeled as a 2×2 junction, see Figure 4.2.2. To recover the behavior of the roundabout, periodic boundary conditions are introduced on

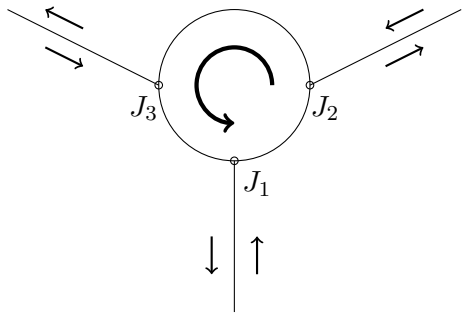


Figure 4.2.1: Sketch of the roundabout considered.

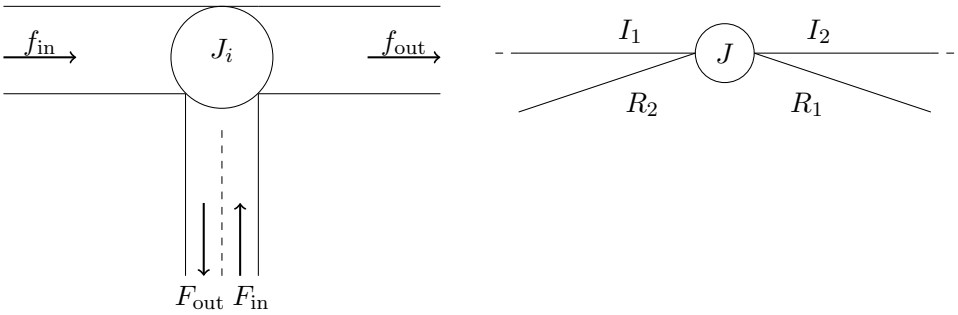
the mainline such that $b_i = a_{i+1}$, $i = 1,2,3$ and $b_3 = a_1$. At each junction we will consider the model introduced in Chapter 3, suitably modified to adapt it to the roundabout structure. The evolution of the traffic flow in the mainline segments is described by a scalar hyperbolic conservation law:

$$\partial_t \rho_i + \partial_x f(\rho_i) = 0, \quad (t,x) \in \mathbb{R}^+ \times I_i \quad i = 1,2,3, \tag{4.2.1}$$

where $\rho_i = \rho_i(t,x) \in [0, \rho_{\max}]$ is the mean traffic density, $\rho_{\max}$ the maximal density allowed on the road and the flux function $f : [0, \rho_{\max}] \to \mathbb{R}^+$ is given by following flux-density relation:

$$f(\rho) = \begin{cases} \rho v_{\mathrm{f}} & \text{if } 0 \le \rho \le \rho_{\mathrm{cr}}, \\ \dfrac{f^{\max}}{\rho_{\max} - \rho_{\mathrm{cr}}}(\rho_{\max} - \rho) & \text{if } \rho_{\mathrm{cr}} \le \rho \le \rho_{\max}, \end{cases} \tag{4.2.2}$$

with v_{f} the maximal speed of the traffic, $\rho_{\mathrm{cr}} = \dfrac{f^{\max}}{v_{\mathrm{f}}}$ the critical density and $f^{\max} = f(\rho_{\mathrm{cr}})$ the maximal flux value, see Figure 4.2.3.



(a) Part of the roundabout. (b) Corresponded junction.

Figure 4.2.2: Detail of the network modeled.

Throughout the chapter, for simplicity, we will assume $\rho_{\max} = 1$ and $v_{\mathrm{f}} = 1$. Figure 4.2.3 gives an example of flux function satisfying the previous hypotheses.

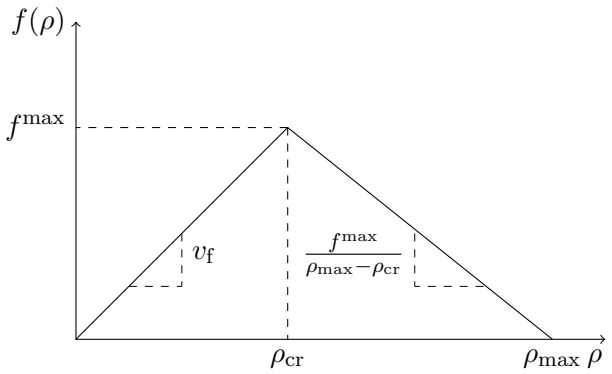


Figure 4.2.3: Flux function considered.

The incoming lanes of the secondary roads entering the junctions are modeled with a buffer of infinite size and capacity.

$$\frac{dl(t)}{dt} = F_{\text{in}}(t) - \gamma_{\text{r1}}(t), \quad t \in \mathbb{R}^+, \tag{4.2.3}$$

The Cauchy problem to solve is then:

$$\begin{cases} \partial_t \rho_i + \partial_x f(\rho_i) = 0, & (t,x) \in \mathbb{R}^+ \times I_i, \\ \dfrac{dl_i(t)}{dt} = F^i_{\text{in}}(t) - \gamma_{\text{r1},i}(t), & t \in \mathbb{R}^+, \\ \rho_i(0,x) = \rho_{i,0}(x), & \text{on } I_i, \\ l_i(0) = l_{i,0} \end{cases} \tag{4.2.4}$$

for $i = 1,2,3$, where $\rho_{i,0}(x)$ are the initial traffic densities and $l_{i,0}$ the initial lengths of the buffers, $l_i(t) \in [0,+\infty[$ is the queue length, $F^i_{\text{in}}(t)$ the flux entering the lane and $\gamma_{\text{r1},i}(t)$ the flux exiting the lane into the roundabout.
This will be coupled with an optimization problem at the junctions that gives the distribution of traffic among the roads.

We define the demand $d(F^i_{\text{in}}, l_i)$ of the incoming lane for the secondary roads, the demand function $\delta(\rho_i)$ on the incoming mainline segment, and the supply function $\sigma(\rho_i)$ on the outgoing mainline segment at each junction as done in Section 3.2. We can define for the roundabout a weak solution

Definition 4.2.1 *Consider a roundabout with three roads $I_i = [a_i, b_i] \subset \mathbb{R}$, $a_i < b_i$, for $i = 1,2,3$, with $b_3 = a_1$, three entrances $R_{1,i}$ $i = 1,2,3$, and three exits $R_{2,i}$ $i = 1,2,3$. A collection of functions $(\rho_i, l_i)_{i=1,2,3} \in \prod_{i=1}^{3} \mathcal{C}^0\left(\mathbb{R}^+; \mathcal{L}^1 \cap \text{BV}(I_i)\right) \times \prod_{i=1}^{3} \mathcal{W}^{1,\infty}(\mathbb{R}^+;\mathbb{R}^+)$ is an admissible solution to (4.2.4) if*

1. *ρ_i is a weak solutions on I_i, i.e., $\rho_i : [0,+\infty[\times I_i \to [0,1]$, such that*

$$\int_{\mathbb{R}^+} \int_{I_i} \Big(\rho_i \partial_t \varphi_i + f(\rho_i) \partial_x \varphi_i \Big) dx dt = 0, \tag{4.2.5}$$

for every $\varphi_i \in \mathcal{C}_c^1(\mathbb{R}^+ \times I_i)$, $i = 1,2,3$.

2. ρ_i *satisfies the Kružhkov entropy condition [99] on* $(\mathbb{R} \times I_i)$, *i.e.,*

$$\int_{\mathbb{R}^+}\int_{I_i} (|\rho_i - k|\partial_t\varphi_i + \operatorname{sgn}(\rho_i - k)(f(\rho_i) - f(k))\partial_x\varphi_i)dxdt + \int_{I_i} |\rho_{i,0} - k|\varphi_i(0,x)dx \geq 0 \tag{4.2.6}$$

for every $k \in [0,1]$ *and for all* $\varphi_i \in \mathcal{C}_c^1(\mathbb{R} \times I_i)$, $i = 1,2,3$.

3. *At each junction* J_i, $f(\rho_i(t,0-)) + \gamma_{\mathrm{r1},i}(t) = f(\rho_{i+1}(t,0+)) + \gamma_{\mathrm{r2},i}(t)$ *for* $i = 1,2,3$ *(where we set* $\rho_4 = \rho_1$*).*

4. *At each junction* J_i, *the flux of the outgoing mainline* $f(\rho_{i+1}(t,0+))$ *is maximum subject to 3 and*

$$f(\rho_{i+1}(t,0+)) = \min\Big((1-\beta)\delta(\rho_i(t,0-)) + d(F_{\mathrm{in}}(t), l_i(t)), \sigma(\rho_{i+1}(t,0+))\Big) \tag{4.2.7}$$

for $i = 1,2,3$, *and* $\rho_4 = \rho_1$.

5. l_i *is a solution of (4.2.3) for almost every* $t \in \mathbb{R}^+$, $i = 1,2,3$.

4.3 Riemann problem at the junction

In this section we describe the construction of the Riemann Solver at a junction and then we apply it to our particular case to recover the expressions of the cost functionals. The Riemann problem at J is the Cauchy problem (4.2.4) where the initial conditions are given by $\rho_{0,i}(x) \equiv \rho_{0,i}$ on I_i for $i = 1,2,3$. In the following, we will focus only on one junction J with two incoming roads and two outgoing ones. We fix constants $\rho_{1,0}, \rho_{2,0} \in [0,1]$, $l_0 \in [0,+\infty[$, $F_{\mathrm{in}} \in]0,+\infty[$ and a priority factor $P \in]0,1[$. We define the Riemann Solver at junction by means of a Riemann Solver $\mathcal{RS}_{\bar{l}} : [0,1]^2 \to [0,1]^2$, which depends on the instantaneous load of the buffer $\bar{l}$. For each $\bar{l}$ the Riemann Solver $\mathcal{RS}_{\bar{l}}(\rho_{1,0}, \rho_{2,0}) = (\hat{\rho}_1, \hat{\rho}_2)$ is constructed as done in Section 3.3. For the sake of clarity we quickly recall the steps to follow.

1. Define $\Gamma_1 = f(\rho_1(t,0-))$, $\Gamma_2 = f(\rho_2(t,0+))$, $\Gamma_{\mathrm{r1}} = \gamma_{\mathrm{r1}}(t)$;
2. Consider the space $(\Gamma_1, \Gamma_{\mathrm{r1}})$ and the sets $\mathcal{O}_1 = [0, \delta(\rho_{1,0})]$, $\mathcal{O}_{\mathrm{r1}} = [0, d(F_{\mathrm{in}}, \bar{l})]$;
3. Trace the lines $(1-\beta)\Gamma_1 + \Gamma_{\mathrm{r1}} = \Gamma_2$; and $\Gamma_1 = \frac{P}{(1-P)(1-\beta)}\Gamma_{\mathrm{r1}}$;
4. Consider the region

$$\Omega = \Big\{(\Gamma_1, \Gamma_{\mathrm{r1}}) \in \mathcal{O}_1 \times \mathcal{O}_{\mathrm{r1}} : (1-\beta)\Gamma_1 + \Gamma_{\mathrm{r1}} \in [0, \Gamma_2]\Big\}. \tag{4.3.1}$$

Different situations can occur depending on the value of Γ_2:

- Demand-limited case.
- Supply-limited case.

Since, on roundabouts exits precede entrances it is necessary that the Riemann Problem for this type of networks has a different junction arrangement. Therefore, the flow coming from the mainline and crossing the junction, interacting with the incoming flow, is $(1-\beta)\Gamma_1$. This leads to consider the priority line as $\Gamma_1 = \frac{P}{(1-P)(1-\beta)}\Gamma_{r1}$ adding a factor of $\frac{1}{1-\beta}$ with respect to the other model. This takes into account the amount of people that leave the roundabout before the entrance. All the proofs in Chapter 3 can be extended and adapted to fit this case.

4.4 Optimization on networks

In this section we define the optimization problem, the cost functionals and derive their expressions. We introduce the Total Travel Time (TTT) on the road network and the Total Waiting Time (TWT) on the incoming lanes of the secondary roads, which are defined as follows:

$$TTT(T,\vec{P}) = \sum_{i=1}^{3}\int_0^T\int_{I_i}\rho(t,x)dxdt + \sum_{i=1}^{3}\int_0^T l_i(t)dt + T\cdot\sum_{i=1}^{3}\int_{I_i}\rho(T,x)dx + T\cdot\sum_{i=1}^{3}l_i(T) \tag{4.4.1}$$

$$TWT(T,\vec{P}) = \sum_{i=1}^{3}\int_0^T l_i(t)dt + T\cdot l_i(T) \tag{4.4.2}$$

for $T>0$ that we will take sufficiently large so that the solution is stabilized. Our aim is to minimize (4.4.1), (4.4.2) with respect to the right of way parameter P. To this end, we derive the explicit expressions of the cost functionals locally at junctions to study their dependence on the right of way parameter P. We consider a single junction as in Figure 4.2.2(b) with $I_1=[-1,0]$ and $I_2=[0,1]$. We suppose that the network and the buffer are empty at $t=0$ and we assume that the following boundary data are given: f^{in} the inflow on the incoming mainline, f^{out} the outflow on the outgoing mainline and F_{in} the incoming flux of the secondary road. Moreover, to reduce the number of cases to be studied, we assume $F_{\text{in}} \le f^{\max} = \gamma_{r1}^{\max}$ and $f^{\text{out}} \le f^{\max}$. Now, we can solve the corresponding initial-boundary value problem.
The first step is to compute the demand and supply functions of the roads. We have $\delta(\rho_{1,0})=0$, $d(F_{\text{in}},l)=\min(F_{\text{in}},\gamma_{r1}^{\max})=F_{\text{in}}$ and $\sigma(\rho_{2,0})=f^{\max}$. Then we can compute Γ_2:

$$\Gamma_2 = \min\Big((1-\beta)\delta(\rho_{1,0}) + d(F_{\text{in}},l), \sigma(\rho_{2,0})\Big) = F_{\text{in}}.$$

It is straightforward to see that the problem is demand limited, hence the optimal point is the point at maximal demands. Thus it follows $\hat{\Gamma}_1 = 0$, $\hat{\Gamma}_2 = F_{\text{in}}$ and $\hat{\Gamma}_{\text{r1}} = F_{\text{in}}$, from which we derive $\hat{\rho}_1 = \rho_{1,0} = 0$ and $\hat{\rho}_2 = F_{\text{in}} < \rho_{\text{cr}}$. Since we are demand limited we also have $l(t) = 0$. The solution in the $x-t$ plane looks as in Figure 4.4.1. The wave produced by the junction problem interacts with the right boundary $x = 1$ at time $t_1 = 1$. Moreover at $x = -1$, the boundary condition enforces the creation of an additional wave at $t = 0$ with speed equal to 1. This gives a density $\hat{\rho}_1 = f^{\text{in}} < \rho_{\text{cr}}$, which reaches the junction at the same time $t_1 = 1$, see Figure 4.4.1.

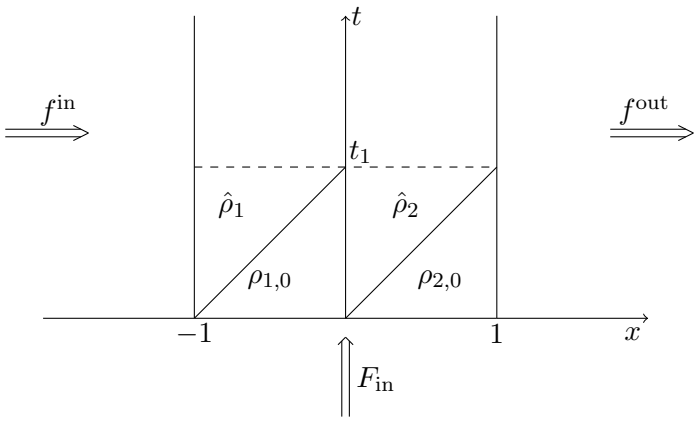


Figure 4.4.1: Solution of the initial-boundary value problem for $t \in [0, t_1]$.

At $t_1 = 1$ we solve a new Riemann problem at the junction with initial densities

$$\rho(1,x) = \begin{cases} \hat{\rho}_1 & \text{if } x < 0, \\ \hat{\rho}_2 & \text{if } x > 0. \end{cases}$$

We assume that the splitting ratio $\beta \in (0,1)$ is the same for all roads and fixed. The demand and supply functions on the respective roads are $\delta(\hat{\rho}_1) = f^{\text{in}}$, $d(F_{\text{in}}, l_0) = \min(F_{\text{in}}, \gamma_{\text{r1}}^{\max}) = F_{\text{in}}$, $\sigma(\hat{\rho}_2) = f^{\max}$. Computing Γ_2 from these values we obtain

$$\Gamma_2 = \min\Big((1-\beta)\delta(\hat{\rho}_1) + d(F_{\text{in}}, l), \sigma(\hat{\rho}_2)\Big)$$

Two cases can occur at this point according to the value of Γ_2:

4.4.1 $\Gamma_2 = (1-\beta)\delta(\hat{\rho}_1) + d(F_{\text{in}}, l)$

In this case the Riemann problem at t_1 is demand limited. No wave is created in the incoming link, and a wave with speed 1 emanates from the junction on the outgoing road with a density $\rho_2 = (1-\beta)f^{\text{in}} + F_{\text{in}}$. The buffer remains empty. At this point we have two different situations according to:

- $F_{\text{in}} < f^{\text{out}}$,

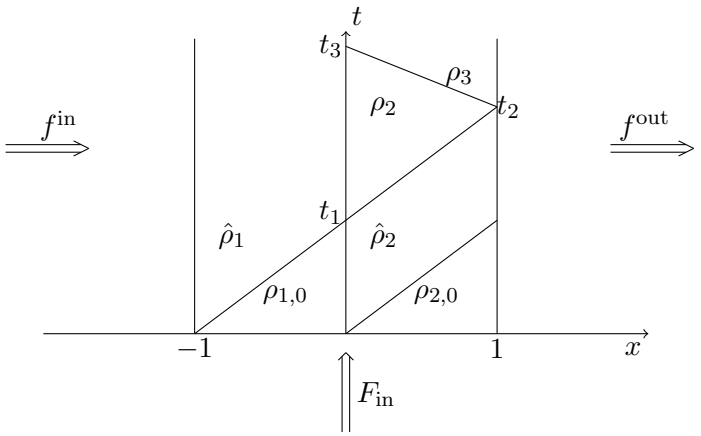


Figure 4.4.2: Solution of the junction problem for $t \in [0, t_3]$.

- $f^{\text{out}} < F_{\text{in}}$.

In the first case ($F_{\text{in}} < f^{\text{out}}$) the wave from the junction interacts with the boundary $x = 1$ at $t_2 = 2$, generating a wave with negative speed and a density $\rho_3 = \dfrac{f^{\max} - (1 - f^{\max}) f^{\text{out}}}{f^{\max}} \in [\rho_{\text{cr}}, 1]$ which reaches the junction at $t_3 = \dfrac{2\lambda(\rho_2, \rho_3) - 1}{\lambda(\rho_2, \rho_3)}$ as shown in Figure 4.4.2.

Above $\lambda(\rho_2, \rho_3) = \dfrac{((1-\beta) f^{\text{in}} + F_{\text{in}} - f^{\text{out}}) f^{\max}}{(1-\beta) f^{\text{in}} f^{\max} + F_{\text{in}} f^{\max} - f^{\max} + (1 - f^{\max}) f^{\text{out}}}$ is given by the Rankine-Hugoniot jump condition. In the second case ($f^{\text{out}} < F_{\text{in}}$) at time t_1 the wave that interacts with the boundary $x = 1$ produces a wave with negative speed and the same density ρ_3 as above. This wave intersect the wave that comes out from the junction at time t_1 generating an additional wave with negative speed. At the point of intersection (t_o, x_o) a new Riemann problem needs to be solved, which creates another wave which reaches the junction at time $t_3 = t_o - \dfrac{1}{\lambda(\rho_2, \rho_3)}$ as shown in Figure 4.4.3. In both cases at t_3

$$f^{\text{out}} \leq (1 - \beta) f^{\text{in}} + F_{\text{in}}.$$

Clearly, at time t_3 the junction problem is supply limited resulting in the following fluxes $\Gamma_2 = f^{\text{out}}$, $\Gamma_1 = \dfrac{P}{1-\beta} f^{\text{out}}$ and $\Gamma_{\text{r1}} = (1 - P) f^{\text{out}}$. Moreover, let us introduce the following values

- $P_1 = \dfrac{f^{\text{out}} - F_{\text{in}}}{f^{\text{out}}}$,
- $P_2 = \dfrac{(1-\beta) f^{\text{in}}}{f^{\text{out}}}$.

Observe that

$$P_2 - P_1 = \frac{(1-\beta) f^{\text{in}}}{f^{\text{out}}} - \frac{f^{\text{out}} - F_{\text{in}}}{f^{\text{out}}} = \frac{(1-\beta) f^{\text{in}} + F_{\text{in}} - f^{\text{out}}}{f^{\text{out}}} \geq 0, \tag{4.4.3}$$

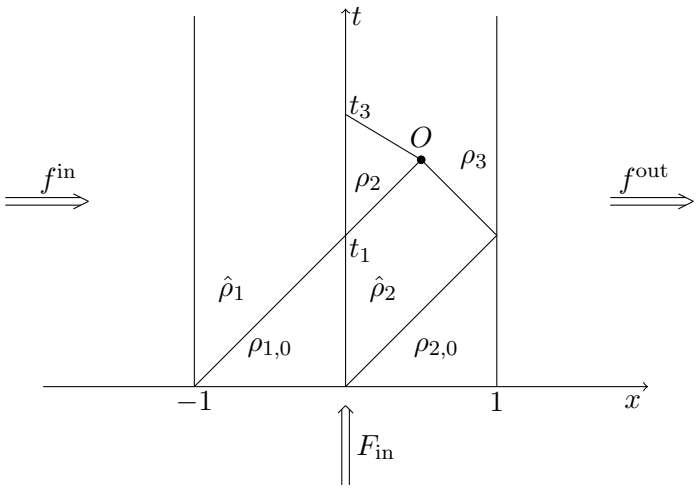


Figure 4.4.3: Solution of the junction problem for $t \in [0, t_3]$.

which implies $P_1 \leq P_2$, see Figure 4.4.4.

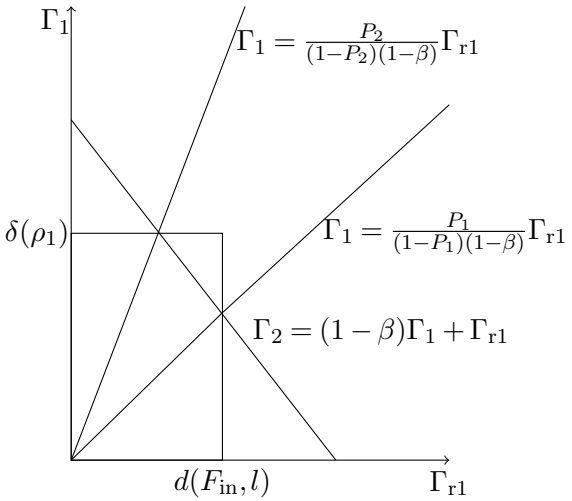


Figure 4.4.4: Relationship between P_1 and P_2.

The solutions of the Riemann problem at the junction are given by:

(1a) If $\max(0, P_1) \leq P \leq \min(P_2, 1)$, then $\left(\dfrac{P}{1-\beta} f^{\text{out}}, (1-P) f^{\text{out}}, f^{\text{out}}\right)$ is the solution of Riemann problem.

(2a) If $1 \geq P > \min(P_2, 1)$, then $\left(f^{\text{in}}, f^{\text{out}} - (1-\beta) f^{\text{in}}, f^{\text{out}}\right)$ is the solution.

(3a) If $0 \leq P < \max(0, P_1)$, then $\left(\dfrac{f^{\text{out}} - F_{\text{in}}}{1-\beta}, F_{\text{in}}, f^{\text{out}}\right)$ is the solution.

According to the different values of P, different cases can occur. For this reason we only sketch the computation of the cost functionals.

Case $\max(0, P_1) \leq P \leq \min(P_2, 1)$.

We solve the Riemann problem at t_3. The solution of the Riemann Problem is given by (1a). From this it follows

$$\rho_1 = \frac{(1-\beta)f^{\max} - (1-f^{\max})Pf^{\text{out}}}{(1-\beta)f^{\max}} \tag{4.4.4}$$

and the wave speed $\lambda(\hat{\rho}_1, \rho_1)$ is

$$\lambda(\hat{\rho}_1, \rho_1) = \frac{\left(f^{\text{in}}(1-\beta) - Pf^{\text{out}}\right)f^{\max}}{(1-\beta)(f^{\text{in}}-1)f^{\max} + (1-f^{\max})Pf^{\text{out}}} \tag{4.4.5}$$

The characteristic $x = \lambda(\hat{\rho}_1, \rho_1)(t - t_3)$ crosses the boundary $x = -1$ at

$$t_4 = t_3 - \frac{1}{\lambda(\hat{\rho}_1, \rho_1)} \tag{4.4.6}$$

On the outgoing road there is no new wave created since $\hat{\Gamma}_2 = f^{\text{out}} = f(\rho_3)$ which can be seen in Figure 4.4.5.

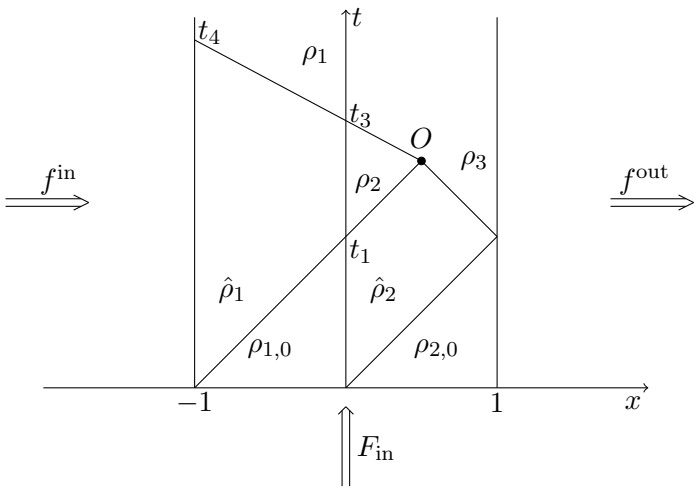


Figure 4.4.5: Solution for $t \in [0, t_4]$.

The buffer length is given by

$$l(t) = (F_{\text{in}} - (1-P)f^{\text{out}})(t - t_3) > 0, \quad \text{for } t > t_3. \tag{4.4.7}$$

Case $\min(P_2, 1) < P \leq 1$.

In this case the solution of the Riemann Problem is given by (2a). On the incoming main road there is no wave with negative speed exiting the junction. Similarly, on the outgoing main road there is no wave since $\hat{\Gamma}_2 = f^{\text{out}}$. The solution is shown in Figure 4.4.6. The buffer increases since $l(t) = (F_{\text{in}} + (1-\beta)f^{\text{in}} - f^{\text{out}})(t - t_3) > 0$.

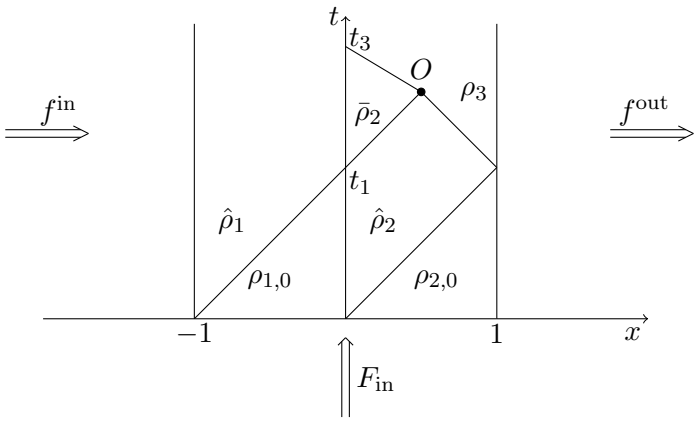


Figure 4.4.6: Solution for $t \in [0, t_3]$ in the case $\min(P_2, 1) \leq P < 1$.

Case $0 \leq P < \max(0, P_1)$.

The solution of the Riemann problem is given by (3a). We get

$$\check{\rho}_1 = \frac{f^{\max}(1 - \beta + f^{\text{out}} - F_{\text{in}}) + F_{\text{in}} - f^{\text{out}}}{(1-\beta)f^{\max}}. \tag{4.4.8}$$

The wave with characteristic speed

$$\lambda(\hat{\rho}_1, \check{\rho}_1) = \frac{f^{\text{in}} - \hat{\Gamma}_1}{\hat{\rho}_1 - \check{\rho}_1} = \frac{\Big((1-\beta)f^{\text{in}} + F_{\text{in}} - f^{\text{out}}\Big)f^{\max}}{(1-\beta)f^{\text{in}}f^{\max} - f^{\max}(1 - \beta + f^{\text{out}} - F_{\text{in}}) + F_{\text{in}} - f^{\text{out}}} \tag{4.4.9}$$

emanating from the junction crosses the boundary $x = -1$ at time $t = t_4$ expressed as:

$$t_4 = t_3 - \frac{1}{\lambda(\hat{\rho}_1, \check{\rho}_1)} \tag{4.4.10}$$

Since $\dfrac{f^{\text{out}} - F_{\text{in}}}{1-\beta} < \delta(\hat{\rho}_1) = f^{\text{in}}$, there is no wave produced by the interaction with the boundary $x = -1$ at time t_4. Also, on the outgoing mainline there is no new wave. The complete solution at t_4 is depicted in Figure 4.4.7.

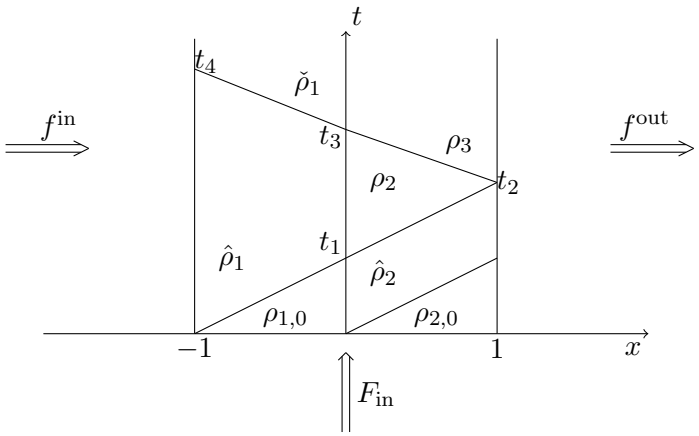


Figure 4.4.7: Complete solution for $t \in [0, t_4]$.

From the value of $\hat{\Gamma}_{r1}$ we can solve the ODE (4.2.3) and find $l(t) = 0$. This conclude the analysis of this subsection.

4.4.2 $\Gamma_2 = \sigma(\hat{\rho}_2)$

In this case we have

$$f^{\max} \leq (1-\beta) f^{\text{in}} + F_{\text{in}} \tag{4.4.11}$$

and hence, it is straightforward to compute the value of $\Gamma_2 = f^{\max}$, $\Gamma_1 = \dfrac{P}{1-\beta} f^{\max}$ and $\Gamma_{\text{r1}} = (1-P) f^{\max}$.
Moreover, let us introduce

- $P_1 = \dfrac{f^{\max} - F_{\text{in}}}{f^{\max}}$,
- $P_2 = \dfrac{(1-\beta) f^{\text{in}}}{f^{\max}}$.

Observe that also in this case it holds

$$P_2 - P_1 = \frac{(1-\beta) f^{\text{in}}}{f^{\max}} - \frac{f^{\max} - F_{\text{in}}}{f^{\max}} = \frac{(1-\beta) f^{\text{in}} + F_{\text{in}} - f^{\max}}{f^{\max}} \geq 0 \tag{4.4.12}$$

because of (4.4.11), which implies $P_1 \leq P_2$, see Figure 4.4.8. Then the solutions of the Riemann problem at the junction are given by

(1b) If $P_1 \leq P \leq P_2$, then $\left(\dfrac{P}{1-\beta} f^{\max}, (1-P) f^{\max}, f^{\max} \right)$ is the solution of Riemann problem.

(2b) If $P \geq P_2$, then $\left(f^{\text{in}}, f^{\max} - (1-\beta) f^{\text{in}}, f^{\max} \right)$ is the solution.

(3b) If $P \leq P_1$, then $\left(\dfrac{f^{\max} - F_{\text{in}}}{1-\beta}, F_{\text{in}}, f^{\max}\right)$ is the solution.

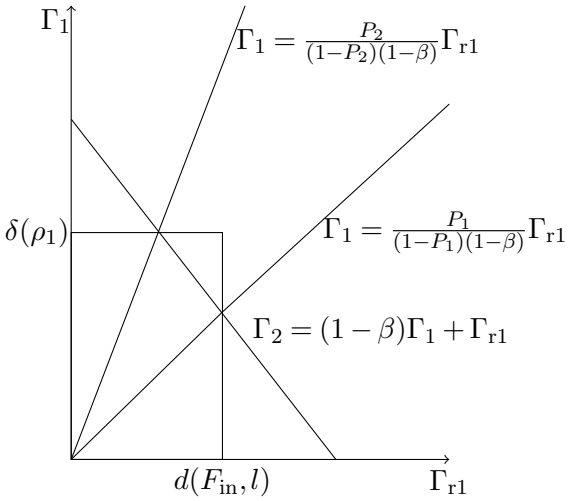


Figure 4.4.8: Relationship between P_1 and P_2.

According to the different values of P different cases can occur. We only sketch the computation of the cost functionals.

Case $P_1 \leq P \leq P_2$.

In this case, at time t_1 the interaction between the wave in the outgoing road and the boundary at $x = 1$ can generate an additional wave if $F_{\text{in}} > f^{\text{out}}$. When this is the case, in fact, there is a wave with negative speed which can interact with other waves between $[0, 1]$. We make the following assumption:

$$F_{\text{in}} > f^{\text{out}}. \tag{4.4.13}$$

In this case, depending on the priority parameter P, the waves emanating from the junction at t_1 and t_4 can collide within the region $-1 < x < 0$. This, in particular, occurs for the value of the priority parameter $P = \bar{P}$, given by

$$\bar{P} = \frac{(1-\beta)\Big((f^{\max})^2 + f^{\max}(2f^{\text{in}} - f^{\text{out}} - f^{\text{in}}F_{\text{in}} + f^{\text{out}}f^{\text{in}}) + 2f^{\text{out}}f^{\text{in}}\Big)}{f^{\max}(F_{\text{in}}f^{\max} - f^{\max} + f^{\text{out}} - f^{\text{out}}f^{\max})} \tag{4.4.14}$$

where $\bar{P}$ is the value at which the waves interact at $x = -1$. We can, then, distinguish two additional cases $P_1 \leq P < \bar{P}$ and $\bar{P} \leq P \leq P_2$.

1. $P_1 \leq P < \bar{P}$. In this case, the waves do not interact in the region $-1 < x < 0$ and no new waves are created. Hence, the study is concluded and the solution is depicted in Figure 4.4.9.

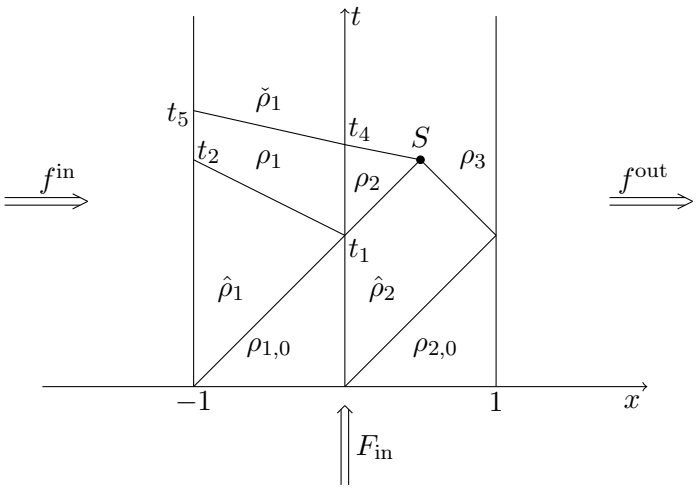


Figure 4.4.9: Solution of the problem in $[0, t_5]$.

2. $\bar{P} \leq P \leq P_2$. In this case there is a collision between the waves emanating from the junction at t_1 and t_4 on the incoming link and the final solution is showed in Figure 4.4.10.

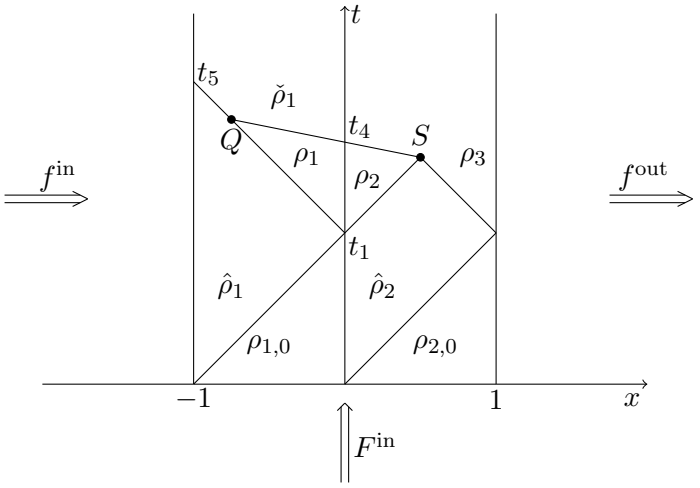


Figure 4.4.10: Solution for $t \in [0, t_5]$ with $\bar{P} \leq P \leq P_2$.

For all cases for $t \geq t_4$ the buffer length increases linearly with a value

$$l(t) = l(t_4) + \left(F_{\text{in}} - (1-P) f^{\text{out}}\right)(t - t_4) > 0. \tag{4.4.15}$$

This concludes the analysis of the case $P_1 \leq P \leq P_2$.

Case $P > P_2$.

The solution of the Riemann problem is given by (2b). In this case, $\rho_1 = \hat{\rho}_1$ and no wave is created in the incoming mainline. On the outgoing link we have $\rho_2 = \rho_{\text{cr}}$, which generates a wave with speed equal to 1. The buffer length increases since $l(t) = (F_{\text{in}} + (1-\beta)f^{\text{in}} - f^{\max})(t-1) > 0$. The wave with positive speed 1 generated at $(t_1, 0)$ interacts with the wave generated from right boundary at point $S = (t_S, x_S)$ at time $t = t_S$ under assumption (4.4.13), see Figure 4.4.11. At the right boundary $f^{\text{out}} = \dfrac{1-\rho_3}{1-f^{\max}} f^{\max}$, hence we obtain that

$$\rho_3 = 1 - \frac{f^{\text{out}}(1-f^{\max})}{f^{\max}}. \tag{4.4.16}$$

At t_4 the Riemann problem at the junction to solve is then

$$\rho(t_4, x) = \begin{cases} \hat{\rho}_1 & \text{if } x < 0, \\ \rho_3 & \text{if } x > 0, \end{cases}$$

coupled with the following demand and supply functions

$$\begin{aligned} &d(F_{\text{in}}, l) = \gamma_{\text{r1}}^{\max} = f^{\max}, \\ &\delta(\hat{\rho}_1) = f^{\text{in}}, \\ &\sigma(\rho_3) = f^{\text{out}}. \end{aligned} \tag{4.4.17}$$

We can now compute

$$\Gamma_2 = \min\Big((1-\beta)\delta(\hat{\rho}_1) + d(F_{\text{in}}, l), \sigma(\rho_3)\Big) = \min\Big((1-\beta)f^{\text{in}} + f^{\max}, f^{\text{out}}\Big) = f^{\text{out}}$$

and

$$\hat{\Gamma}_1 = \frac{P}{1-\beta} f^{\text{out}}.$$

Two cases can occur at this point. If $(1-\beta)f^{\text{in}} < f^{\text{out}}$ the solution of the Riemann Problem at the junction is given by $(\hat{\Gamma}_1, \hat{\Gamma}_{\text{r1}}, \hat{\Gamma}_2) = (f^{\text{in}}, f^{\text{out}} - (1-\beta)f^{\text{in}}, f^{\text{out}})$ for all values of $P > \bar{\bar{P}} = (1-\beta)\dfrac{f^{\text{in}}}{f^{\text{out}}}$. From this it is straightforward to see that $\hat{\rho}_1 = \rho_1$ since $f^{\text{in}} = \hat{\rho}_1$ for $v_{\text{f}} = 1$. No new waves are created.
For $P_2 < P < \bar{\bar{P}}$ we have $(\hat{\Gamma}_1, \hat{\Gamma}_{\text{r1}}, \hat{\Gamma}_2) = \left(\dfrac{P}{1-\beta} f^{\text{out}}, (1-P)f^{\text{out}}, f^{\text{out}}\right)$. The solution of the problem in this case is similar to the case $(1-\beta)f^{\text{in}} > f^{\text{out}}$ hence, we defer its description in the following. If $(1-\beta)f^{\text{in}} > f^{\text{out}}$ the solution of the Riemann problem at the junction becomes

$$(\hat{\Gamma}_1, \hat{\Gamma}_{\text{r1}}, \hat{\Gamma}_2) = \left(\frac{P}{1-\beta} f^{\text{out}}, (1-P)f^{\text{out}}, f^{\text{out}}\right).$$

From this we can uniquely recover the corresponding values of the densities. The solution looks as in Figure 4.4.11.

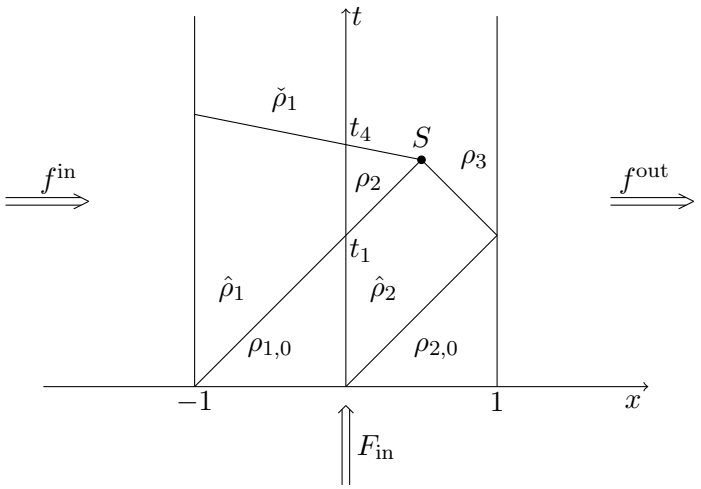


Figure 4.4.11: Solution in the case $P \geq P_2$.

The buffer increases linearly and its expression is given by

$$l(t) = l(t_4) + \left(F_{\text{in}} - (1-P) f^{\text{out}}\right)(t - t_4) > 0. \tag{4.4.18}$$

This completes the analysis for this case.

The case $P \leq P_1$.

The solution of the Riemann problem is given by (3b). In this case, the computations are similar to those of Section 4.4.2. The solution is sketched in Figure 4.4.12. To be noted that the point of intersection N in this case does not depend on the value of P but on the value of the other parameters.

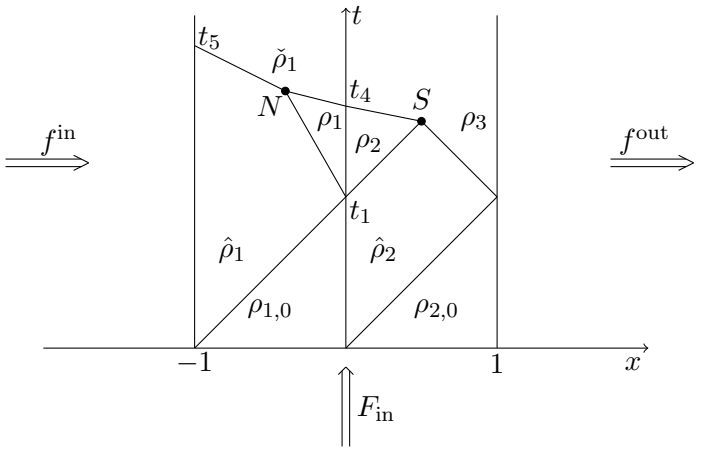


Figure 4.4.12: Solution in the case $P \leq P_1$.

Finally, we compute the queue length at t_4 which is given by

$$l(t) = l(t_4) + \left(F_{\text{in}} - (1-P)f^{\text{out}}\right)(t - t_4) > 0. \tag{4.4.19}$$

4.4.3 Local Total Waiting Time and Total Travel Time

We are now ready to compute the expressions for the Total Travel Time and the Total Waiting Time for each value of P.
Case 4.4.1

- $\max(P_1, 0) \leq P \leq \min(P_2, 1)$

We calculate the TWT_{loc} as follows

$$TWT_{loc}(T,P) = \int_{t_3}^{T} (F_{\text{in}} - (1-P)f^{\text{out}})(t - t_3)dt + T(F_{\text{in}} - (1-P)f^{\text{out}})(T - t_3).$$

while the $TTT_{loc}(T)$ is obtained by a constant term which does not depend on P plus a term depending on the priority, that we denote by $TTT_{loc}(T,P)$:

$$\begin{aligned} TTT_{loc}(T,P) = &\iint_{A_1} \hat{\rho}_1 dtdx + \iint_{A_2} \rho_1(P)dtdx + T\int_0^1 (\rho_1(P) + \rho_3)\,dx \\ &+ \int_{t_3}^{T} (F_{\text{in}} - (1-P)f^{\text{out}})(t - t_3)dt + T(F_{\text{in}} - (1-P)f^{\text{out}})(T - t_3), \end{aligned}$$

where the areas of the integration domains are defined by $A_1 = \frac{1}{2}(t_4(P) - t_3) = A_2$ as shown in Figure 4.4.13.

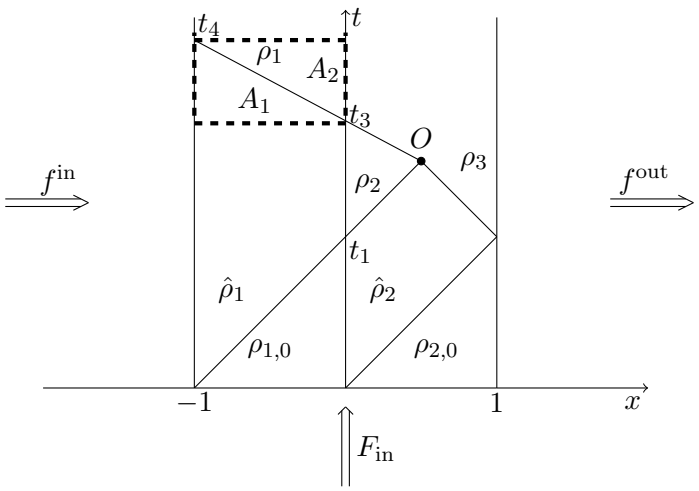


Figure 4.4.13: Area of integration in the case $P_1 \leq P \leq P_2$.

- $\min(P_2, 1) < P \leq 1$

The $TWT_{loc}(T,P)$ is computed as

$$TWT_{loc}(T,P) = \int_{t_3}^{T} (F_{\text{in}} + (1-\beta)f^{\text{in}} - f^{\text{out}})(t-t_3)dt \\ + T(F_{\text{in}} + (1-\beta)f^{\text{in}} - f^{\text{out}})(T-t_3).$$

The $TTT_{loc}(T)$ is given by a constant term plus

$$TTT_{loc}(T,P) = T\int_0^1 (\hat{\rho}_1 + \rho_3)\,dx + \int_{t_3}^{T} (F_{\text{in}} + (1-\beta)f^{\text{in}} - f^{\text{out}})(t-t_3)dt \\ + T(F_{\text{in}} + (1-\beta)f^{\text{in}} - f^{\text{out}})(T-t_3).$$

- $0 \leq P \max(P_1, 0)$

In this case $TWT_{loc} = 0$ since the buffer is empty. The $TTT_{loc}(T)$ is given by a constant term plus

$$TTT_{loc}(T,P) = T\int_0^1 (\check{\rho}_1 + \rho_3)\,dx.$$

Case 4.4.2

- $P_1 \leq P < \bar{P}$ We compute the TWT_{loc} as follows

$$TWT_{loc}(T,P) = \int_{t_1}^{t_4} \left(\left(F_{\text{in}} - (1-P)f^{\max}\right)(t-1)\right)dt + T\left(F_{\text{in}} - (1-P)f^{\text{out}}\right)(T-t_4) \\ + \int_{t_4}^{T} \left(l(t_4) + \left(F_{\text{in}} - (1-P)f^{\text{out}}\right)(t-t_4)\right)dt + Tl(t_4). \tag{4.4.20}$$

Concerning $TTT_{loc}(T)$, it is given by a constant plus

$$TTT_{loc}(T,P) = \int_{A_1} \hat{\rho}_1 dtdx + \int_{A_2} \rho_1(P)dtdx + \iint_{A_3} \check{\rho}_1(P)dtdx \\ + \int_{t_1}^{t_4} \left(\left(F_{\text{in}} - (1-P)f^{\max}\right)(t-1)\right)dt + T\int_0^1 (\check{\rho}_1(P) + \rho_3)\,dx \\ + \int_{t_4}^{T} \left(l(t_4) + \left(F_{\text{in}} - (1-P)f^{\text{out}}\right)(t-t_4)\right)dt + Tl(t_4) \\ + T\left(F_{\text{in}} - (1-P)f^{\text{out}}\right)(T-t_4),$$

where the areas are defined by $A_1 = \frac{1}{2}(t_2(P) - 1)$,
$A_2 = \frac{1}{2}(t_5(P) + t_4 - t_2 - 1)$,
$A_3 = \frac{1}{2}(t_5(P) - t_4)$ and $T = t_5$, as in Figure 4.4.14.

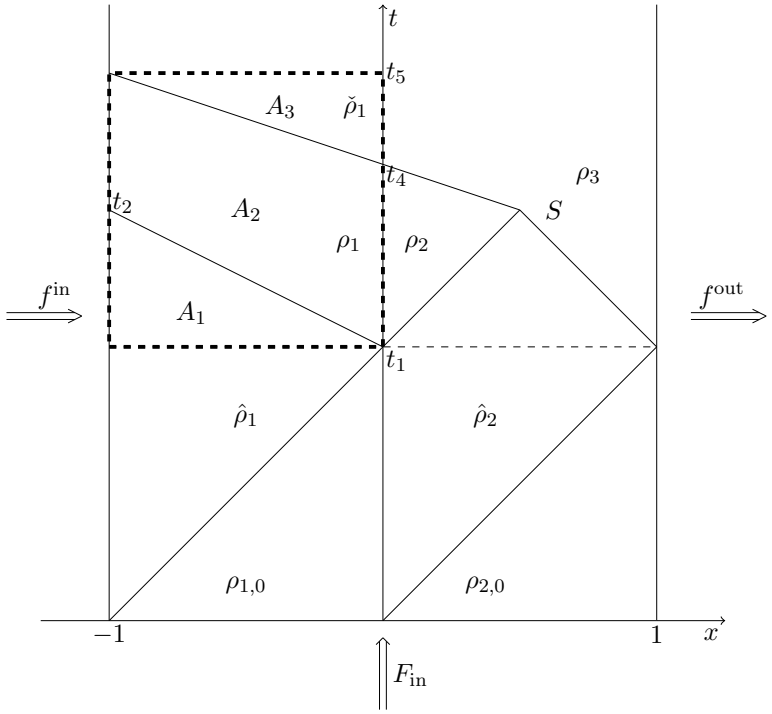


Figure 4.4.14: Area of integration in the case $P_1 \leq P < \bar{P}$.

- $\bar{P} \leq P \leq P_2$ The TWT_{loc} is as in (4.4.20), since it does not depend on the wave interactions but only on the queue length. The $TTT_{loc}(T)$ is given by the constant term plus

$$\begin{aligned} TTT_{loc}(T,P) = &\iint_{A_1+A_2+A_5} \hat{\rho}_1 dtdx + \iint_{A_3} \rho_1(P) dtdx \\ &+ \iint_{A_4+A_6+A_7} \check{\rho}_1(P) dtdx + T\int_0^1 (\check{\rho}_1(P)+\rho_3)\,dx \\ &+ \int_{t_1}^{t_4} ((F_{\text{in}} - (1-P)f^{\max}))(t-1))\,dt \\ &+ \int_{t_4}^{T} \left(l(t_4) + \left(F_{\text{in}} - (1-P)f^{\text{out}}\right)(t-t_4)\right) dt \\ &+ Tl(t_4) + T\left(F_{\text{in}} - (1-P)f^{\text{out}}\right)(T-t_4). \end{aligned}$$

The areas are defined by $A_1 = \frac{1}{2}(t_Q(P)-1)$,
$A_2 = \frac{1}{2}(t_Q(P)-1)(x_Q(P)+1)$,
$A_3 = \frac{1}{2}(x_Q(P) - x_Q(P)t_4)$,
$A_4 = \frac{1}{2}(t_Q(P)-t_4)(-x_Q(P))$,

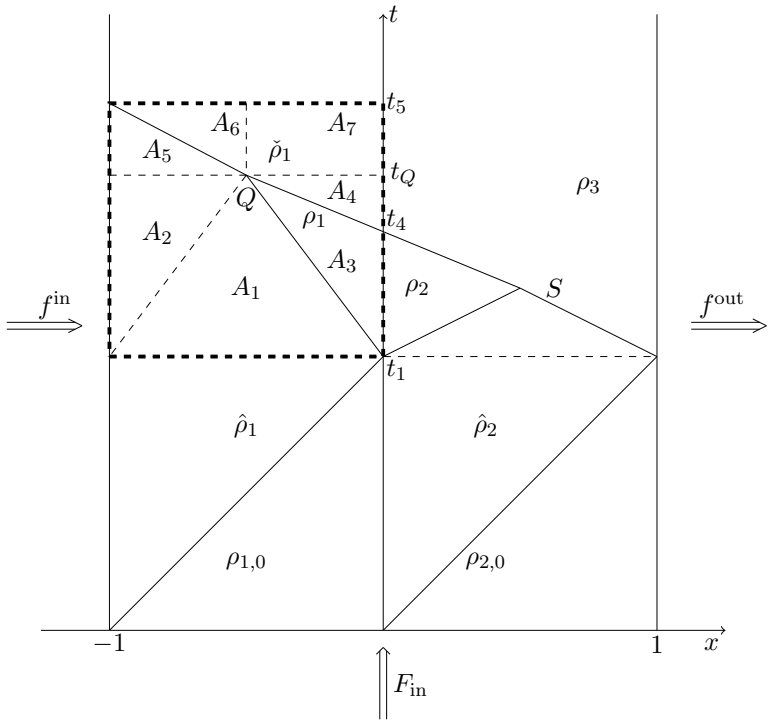


Figure 4.4.15: Area of integration in the case $\bar{P} \leq P \leq P_2$.

$A_5 = \frac{1}{2}(t_5(P) - t_Q(P))(x_Q(P) + 1)$,
$A_6 = \frac{1}{2}(t_5(P) - t_Q(P))(x_Q(P) + 1)$,
$A_7 = (t_5(P) - t_Q(P))(-x_Q(P))$ as in Figure 4.4.15.

- $P > P_2$ In this case we have to consider two different situations according to the value of P. If $P > \bar{\bar{P}}$ and $(1-\beta)f^{\text{in}} < f^{\text{out}}$ then the functionals do not depend on P and hence, we skip it from our analysis. If $P_2 < P < \bar{\bar{P}}$ and $(1-\beta)f^{\text{in}} < f^{\text{out}}$ or $(1-\beta)f^{\text{in}} \geq f^{\text{out}}$ then the TWT_{loc} is given by

$$\begin{aligned} TWT_{loc}(T,P) = &\int_{t_1}^{t_4} \left(F_{\text{in}} + (1-\beta)f^{\text{in}} - f^{\max})(t-1)\right) dt \\ &+ \int_{t_4}^{T} \left((F_{\text{in}} + (1-\beta)f^{\text{in}} - f^{\max})(t_4 - 1) + \left(F_{\text{in}} - (1-P)f^{\text{out}}\right)(t - t_4)\right) dt \\ &+ T(F_{\text{in}} + (1-\beta)f^{\text{in}} - f^{\max})(t_4 - 1) + T\left(F_{\text{in}} - (1-P)f^{\text{out}}\right)(T - t_4). \end{aligned}$$

The $TTT_{loc}(T)$, as usual, is instead calculated by the constant term plus

$$\begin{aligned} TTT_{loc}(T,P) = &\int_{A_1} \hat{\rho}_1(P)dtdx + \int_{A_2} \check{\rho}_1(P)dtdx \\ &+ \int_{t_1}^{t_4} \left(F_{\text{in}} + (1-\beta)f^{\text{in}} - f^{\max})(t-1)\right) dt + T\int_0^1 (\check{\rho}_1(P) + \rho_3)\, dx \\ &+ \int_{t_4}^{T} \left((F_{\text{in}} + (1-\beta)f^{\text{in}} - f^{\max})(t_4-1) + \left(F_{\text{in}} - (1-P)f^{\text{out}}\right)(t-t_4)\right) dt \\ &+ T(F_{\text{in}} + (1-\beta)f^{\text{in}} - f^{\max})(t_4-1) + T\left(F_{\text{in}} - (1-P)f^{\text{out}}\right)(T-t_4) \end{aligned}$$

and the areas for this case are $A_1 = \frac{1}{2}(t_5(P) - t_4)$ and $A_2 = \frac{1}{2}(t_5(P) - t_4)$ as shown in the Figure 4.4.16.

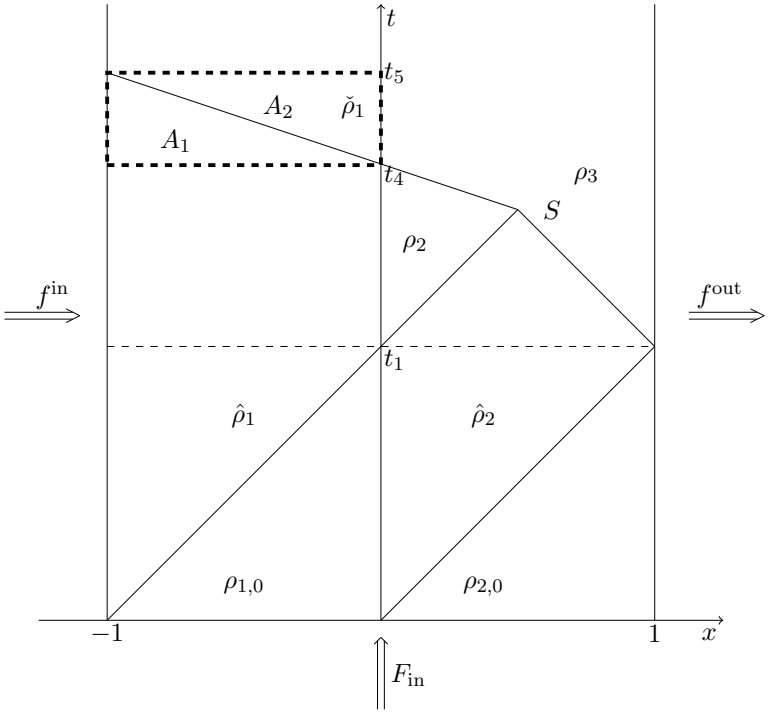


Figure 4.4.16: Area of integration in the case $P > P_2$.

- $P < P_1$ We have two different situations which depend on the intersection of the waves as explained in Section 4.4.2. When the waves do not interact between $x = -1$ and $x = 0$ then the TWT_{loc} is computed as

$$\begin{aligned} TWT_{loc}(T,P) = &\int_{t_4}^{T} \left(F_{\text{in}} - (1-P)f^{\text{out}}\right)(t-t_4)dt \\ &+ T\left(F_{\text{in}} - (1-P)f^{\text{out}}\right)(T-t_4), \end{aligned} \tag{4.4.21}$$

while the $TTT_{loc}(T,P)$ is given by

$$TTT_{loc}(T,P) = \iint_{A_1} \rho_1 dtdx + \iint_{A_2} \check{\rho}_1(P) dtdx + T\int_0^1 (\check{\rho}_1(P)+\rho_3)\,dx + \int_{t_4}^{T} \left(F_{\text{in}} - (1-P)f^{\text{out}}\right)(t-t_4)dt + T\left(F_{\text{in}} - (1-P)f^{\text{out}}\right)(T-t_4),$$

where $A_1 = \frac{1}{2}(t_5 - t_4) = A_2$ as shown in Figure 4.4.17.

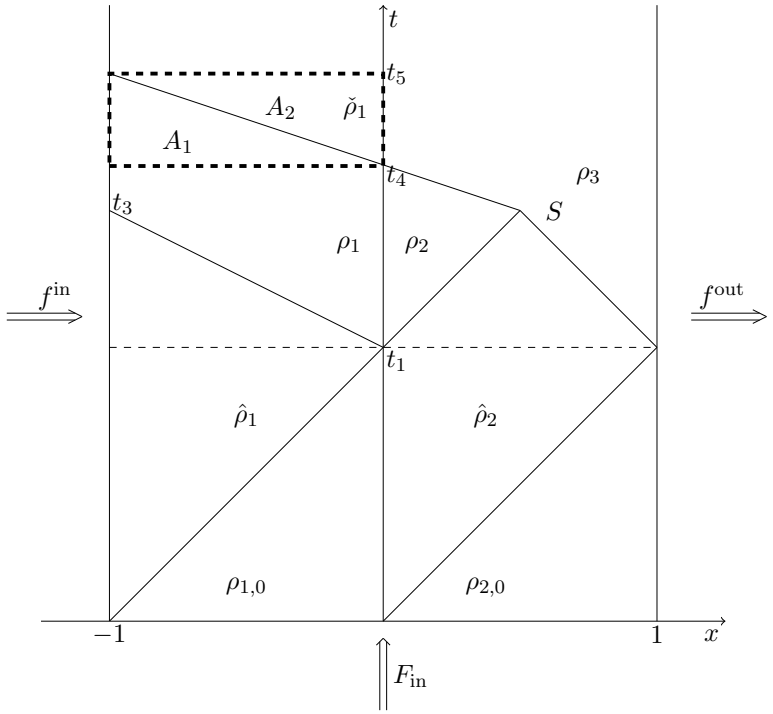


Figure 4.4.17: Area of integration in the case $P < P_1$.

Whereas when the waves interact between $x = -1$ and $x = 0$ then the TWT is computed does not change and the $TTT_{loc}(T,P)$ is computed as follows

$$TTT_{loc}(T,P) = \iint_{A_1} \hat{\rho}_1 dtdx + \iint_{A_2+A_3+A_4} \check{\rho}_1(P) dtdx + \int_{t_4}^{T} \left(F_{\text{in}} - (1-P)f^{\text{out}}\right)(t-t_4)dt + T\int_0^1 (\check{\rho}_1(P)+\rho_3)\,dx + T\left(F_{\text{in}} - (1-P)f^{\text{out}}\right)(T-t_4).$$

The areas are defined by
$A_1 = A_2 = \dfrac{1}{2}(t_5(P) - t_N(P))(x_N(P)+1)$,
$A_3 = (t_5 - t_N(P))(-x_N(P))$,
$A_4 = \dfrac{1}{2}(t_N(P) - t_4)(-x_N(P))$ as in Figure 4.4.18.

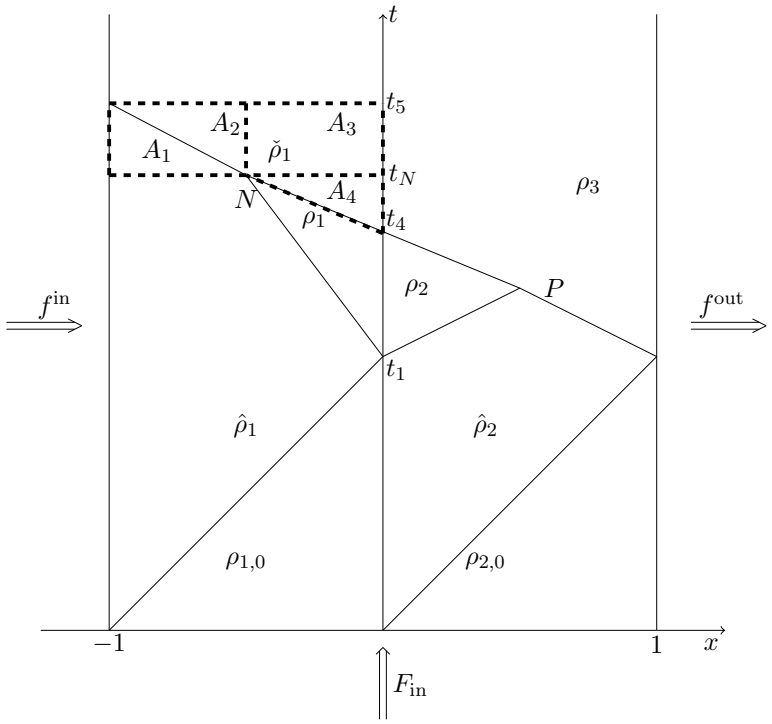


Figure 4.4.18: Area of integration when the waves collide in the region $[-1, 0]$.

4.5 Numerical scheme

In this section we consider the traffic regulation problem for a network as the one in Figure 4.2.1. We analyze the cost functionals introduced in the previous section. In particular, we want to compare the costs corresponding to the instantaneous optimal choice of the right of way parameter and a fixed constant parameter.

4.5.1 Network topology

The roundabout will be modeled by:

- 4 roads from the circle: I_1, I_2, I_3, I_4 with I_1 and I_4 linked with periodic boundary conditions;
- 3 roads connecting the roundabout with the rest of the network: 3 incoming lanes and 3 outgoing ones.

4.5.2 Numerical scheme

From the topology, it can be noted that all the junctions in the roundabout can be represented by 2x2 junctions for which it might be necessary to define a right of way

parameter P. The first step is then to discretize the junction model. We define a numerical grid in $(0,T)\times\mathbb{R}$ using the following notation:

- Δx is the fixed space grid size;
- Δt^n is the grid size, given by the CFL condition;
- $(t^n, x_j) = (t^{n-1} + \Delta t^n, j\Delta x)$ for $n \in \mathbb{N}$ and $j \in \mathbb{Z}$ are the grid points.

Since the model used is the same as the one in Chapter 3, the numerical discretization is done accordingly using the same scheme and the same methods as introduced in 3.4.

4.6 Numerical simulations

In this section we show some simulations results corresponding to different choices of the right of way parameters. We consider approximations obtained by Godunov numerical method, with space step $\Delta x = 0.1$ and the time step determined by the CFL condition. The traffic flow on the road network is simulated in a time interval $[0,T]$, where $T = 50$. As for the initial condition on the roads of the network, we assume that at initial time $t = 0$ all the roads and the buffers are empty, $f^{\text{in}} = f^{\text{out}} = 0$ and we take $F_{\text{in}} \neq 0$. We consider the following parameters for each link: $f^{\max} = 0.66$, $\rho_{\text{cr}} = 0.66$ and $\gamma_{r1}^{\max} = 0.65$. Moreover, we distinguish different cases of simulations which vary according to the value of $F_{\text{in}} \in \{0.1, 0.2, 0.3, 0.4, 0.5, 0.6\}$ and $\beta \in \{0.2, 0.3, 0.4, 0.5, 0.6, 0.7\}$. For each value of F_{in} and β we study different simulations cases:

- Instantaneous right of way parameter that optimizes the cost functionals TTT_{loc} and TWT_{loc}. Given the complicated expressions of the cost functionals it is difficult to use an analytical approach for the development of an optimized algorithm for the whole roundabout. For this reason, we consider at each junction and at each time step the optimal parameters corresponding to the road densities near the junction. The technique for the simulation of the optimal case is based on the local optimization of every junction of 2x2 type, which form the roundabout. To compute the cost functionals, at each time step the values of F_{in}, f^{out} and f^{in} are found as follows:
  - $f^{\text{in}} = \delta(\rho_{\text{inc}})$
  - $f^{\text{out}} = \sigma(\rho_{\text{out}})$
  - $F_{\text{in}} = d(F_{\text{in}}, l^n)$

  The optimal value of the priority parameter is then computed exactly (i.e. analytically as explained in 4.4) at each time step for the corresponding input values.
- Fixed right of way parameter. We analyze the behavior of the cost functionals, assuming that the priority parameter P is the same and kept fixed for each junction.

4.6.1 Simulation results

In Figures 4.6.2, 4.6.1, 4.6.4 and 4.6.3we show some of the simulation results for some representative cases. More precisely we show the value of the functionals TTT (4.4.1) and TWT (4.4.2) computed on the whole roundabout as a function of F_{in} and β. A legend for every picture indicates the different simulation cases. Moreover, the tables 4.6.1, 4.6.2, 4.6.3, 4.6.4, 4.6.5 and 4.6.6 depict the gain in percentage between the optimal case and the constant one for different values of P.

F_{in} \ β	0.2	0.3	0.4	0.5	0.6	0.7
0.1	0.0000%	0.0000%	0.0000%	0.0000%	0.0000%	0.0000%
0.2	-23.9359%	0.0000%	0.0000%	0.0000%	0.0000%	0.0000%
0.3	-19.2538%	0.0000%	0.0000%	0.0000%	0.0000%	0.0000%
0.4	-15.8362%	0.0000%	0.0000%	0.0000%	0.0000%	0.0000%
0.5	-13.3060%	0.0000%	0.0000%	0.0000%	0.0000%	0.0000%
0.6	-11.5724%	0.0000%	0.0000%	0.0000%	0.0000%	0.0000%

Table 4.6.1: Gain in TTT computed with the optimal right of way parameter and a fixed one $P = 0.7$.

F_{in} \ β	0.2	0.3	0.4	0.5	0.6	0.7
0.1	0.0000%	0.0000%	0.0000%	0.0000%	0.0000%	0.0000%
0.2	-26.1638%	-26.7080%	0.0000%	0.0000%	0.0000%	0.0000%
0.3	-21.8880%	-30.3638%	-38.8852%	0.0000%	0.0000%	0.0000%
0.4	-18.2182%	-25.1910%	-32.8044%	-40.3677%	0.0000%	0.0000%
0.5	-15.3961%	-21.1096%	-27.1844%	-32.9931%	0.0000%	0.0000%
0.6	-13.3412%	-18.3294%	-23.2688%	-27.9928%	0.0000%	0.0000%

Table 4.6.2: Gain in TTT computed with the optimal right of way parameter and a fixed one $P = 0.4$.

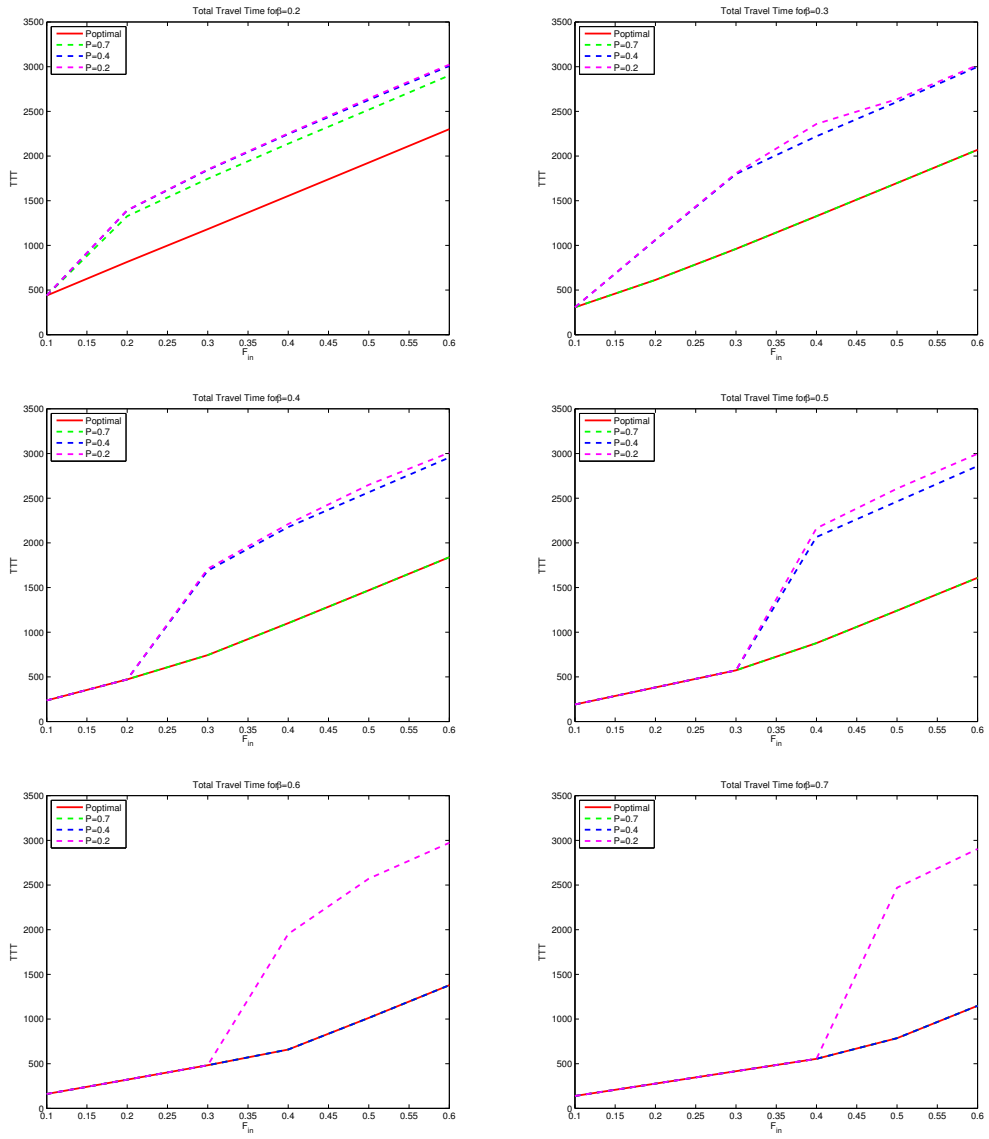


Figure 4.6.1: TTT as a function of F_{in} computed for a time horizon $T = 50$.

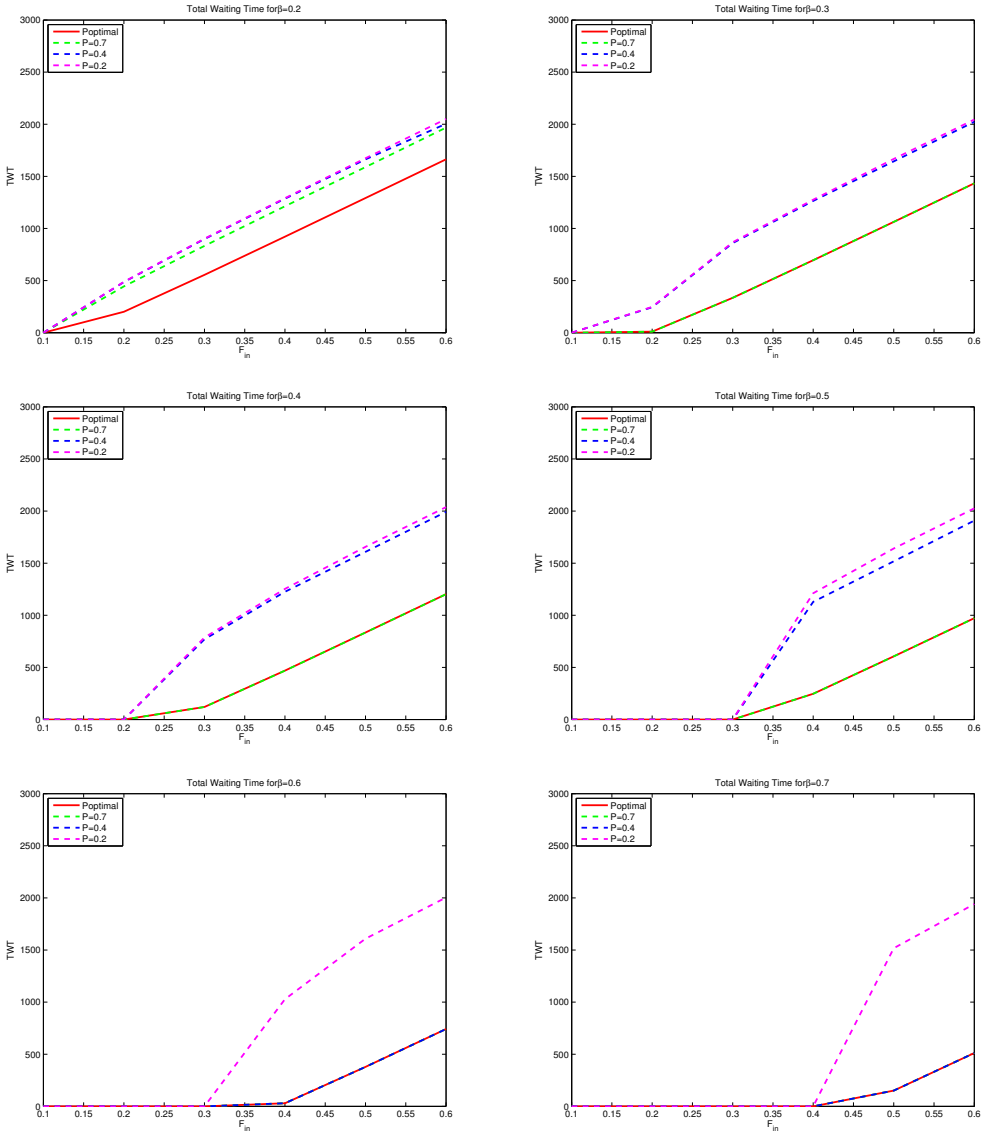


Figure 4.6.2: TWT as a function of F_{in} computed for a time horizon $T = 50$.

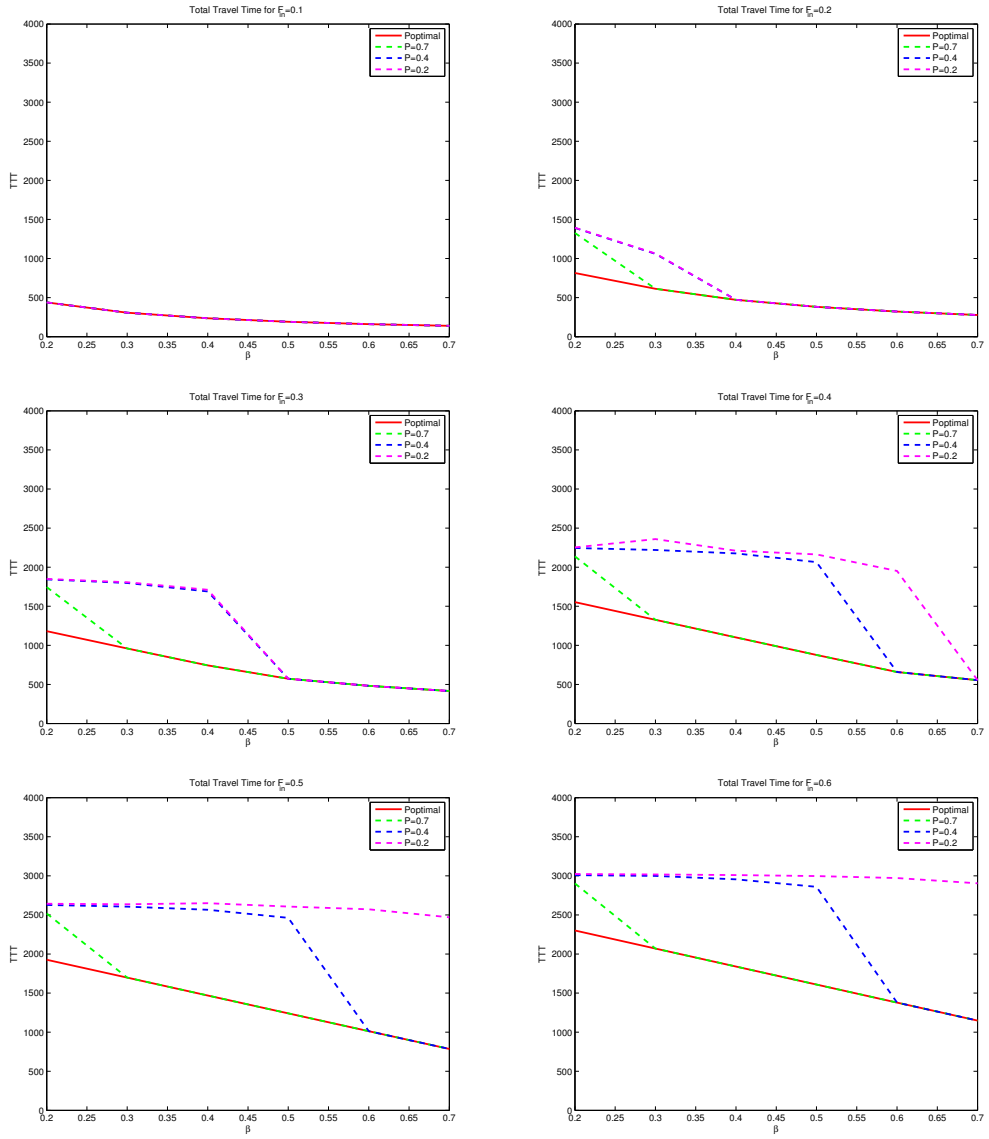


Figure 4.6.3: TTT as a function of β computed for a time horizon $T = 50$.

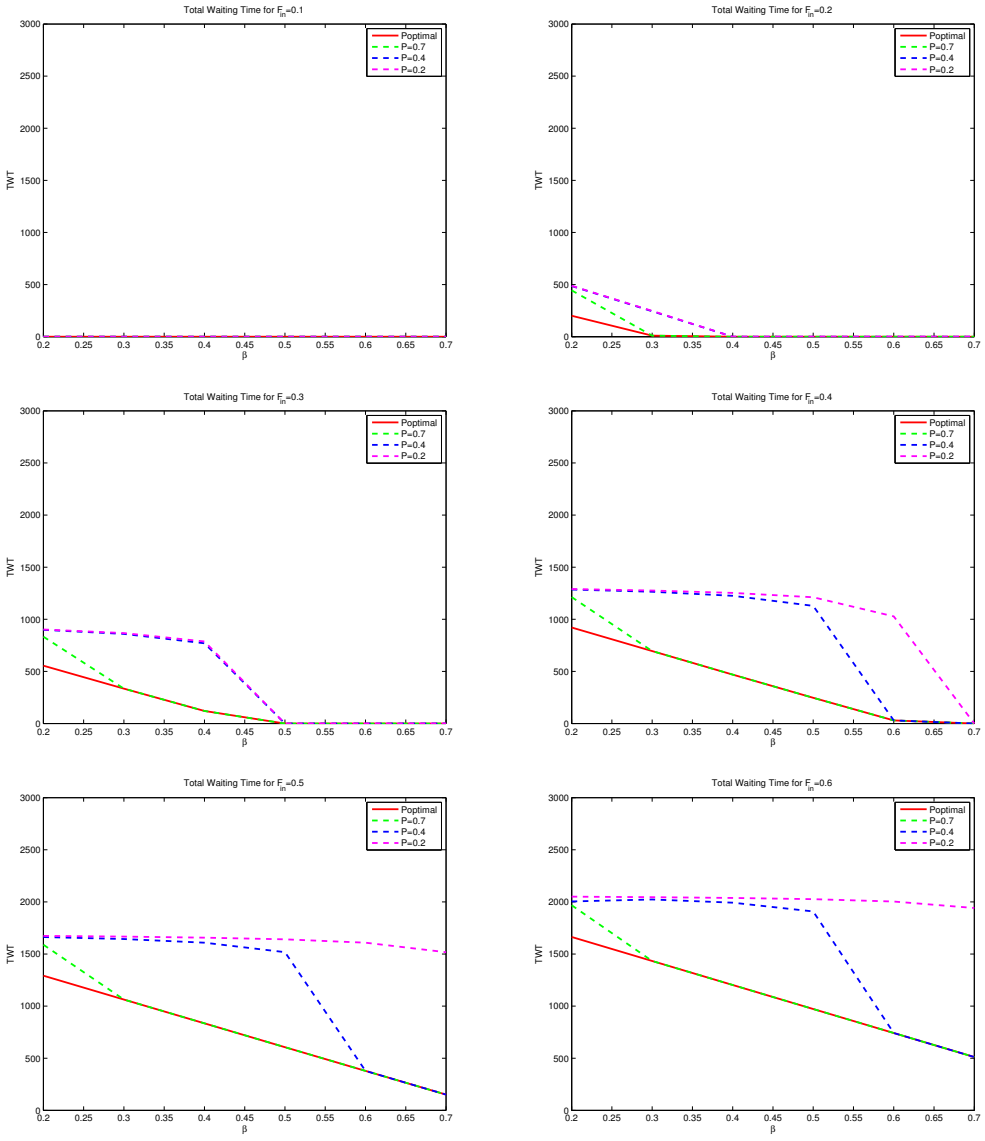


Figure 4.6.4: TWT as a function of β computed for a time horizon $T = 50$.

F_{in} \ β	0.2	0.3	0.4	0.5	0.6	0.7
0.1	0.0000%	0.0000%	0.0000%	0.0000%	0.0000%	0.0000%
0.2	-26.2608%	-26.9396%	0.0000%	0.0000%	0.0000%	0.0000%
0.3	-22.0246%	-30.6028%	-39.4182%	0.0000%	0.0000%	0.0000%
0.4	-18.3772%	-28.0082%	-33.4924%	-42.2899%	-49.5546%	0.0000%
0.5	-15.6867%	-21.6484%	-28.6658%	-35.5027%	-43.4925%	-51.7438%
0.6	-13.5821%	-18.6328%	-24.1359%	-30.1316%	-36.6248%	-43.3260%

Table 4.6.3: Gain in TTT computed with the optimal right of way parameter and a fixed one $P = 0.2$.

F_{in} \ β	0.2	0.3	0.4	0.5	0.6	0.7
0.1	0.0000%	0.0000%	0.0000%	0.0000%	0.0000%	0.0000%
0.2	-37.7363%	0.0000%	0.0000%	0.0000%	0.0000%	0.0000%
0.3	-20.0221%	0.0000%	0.0000%	0.0000%	0.0000%	0.0000%
0.4	-13.6862%	0.0000%	0.0000%	0.0000%	0.0000%	0.0000%
0.5	-10.3010%	0.0000%	0.0000%	0.0000%	0.0000%	0.0000%
0.6	-8.3728%	0.0000%	0.0000%	0.0000%	0.0000%	0.0000%

Table 4.6.4: Gain in TWT computed with the optimal right of way parameter and a fixed one $P = 0.7$.

F_{in} \ β	0.2	0.3	0.4	0.5	0.6	0.7
0.1	0.0000%	0.0000%	0.0000%	0.0000%	0.0000%	0.0000%
0.2	-41.5096%	-92.2568%	0.0000%	0.0000%	0.0000%	0.0000%
0.3	-23.6510%	-43.9810%	-72.9952%	0.0000%	0.0000%	0.0000%
0.4	-16.5219%	-29.0594%	-44.6035%	-64.1409%	0.0000%	0.0000%
0.5	-12.5626%	-21.4584%	-31.6873%	-42.9263%	0.0000%	0.0000%
0.6	-9.2872%	-17.0847%	-24.7253%	-32.5150%	0.0000%	0.0000%

Table 4.6.5: Gain in TWT computed with the optimal right of way parameter and a fixed one $P = 0.4$.

F_{in} \ β	0.2	0.3	0.4	0.5	0.6	0.7
0.1	0.0000%	0.0000%	0.0000%	0.0000%	0.0000%	0.0000%
0.2	-41.6784%	-92.3688%	0.0000%	0.0000%	0.0000%	0.0000%
0.3	-23.8452%	-44.3239%	-73.5147%	0.0000%	0.0000%	0.0000%
0.4	-16.7143%	-29.4949%	-45.5005%	-66.1746%	-94.3553%	0.0000%
0.5	-12.8840%	-22.1229%	-33.0143%	-46.0431%	-61.9339%	-81.8636%
0.6	-10.4278%	-17.6115%	-25.7892%	-35.1576%	-45.9640%	-58.3022%

Table 4.6.6: Gain in TWT computed with the optimal right of way parameter and a fixed one $P = 0.2$.

In both cases, the cost functionals computed with a fixed right of way parameter or with the optimal ones have a different behavior only for those values of F_{in} for which the problem is supply limited. In both cases we have better results for the optimal case. We can see that even when optimizing the TWT, low values of the priority parameters that should favor the entrance with the respect to the mainline are a bad choice. In fact, for these values the roundabout tends to be overly congested blocking, as a matter of fact, the entrances. From our analysis, it seems that in both cases the optimal priority parameters are the ones that favors the mainline compared to the entrances.

Chapter 5

Conclusions and perspectives

In this work we introduced two PDE-ODE-based models to describe traffic flow. First, we set up a mathematical framework for a model for moving bottlenecks on roads. A PDE describes the evolution of the main traffic in time while an ODE describes the bus trajectory. The Riemann problem was defined and solved analytically. Also, we proved the existence of solution for general BV data and give some results concerning stability. Future work will include an effective strategy for the problem of stability of solutions for this model. We showed also two different approaches to the numerical solution of this class of problems. The first one computes the density using a Godunov- type scheme with a locally nonuniform mesh. Then the position of the bus is reconstructed determining the effects of the interactions with density waves as in [33]. Some numerical tests are presented to show the effectiveness of the scheme. To avoid dealing with moving meshes, we focused on the design of a conservative scheme on fixed meshes, following the approach introduced in [17]. The method reconstructs both non-classical and classical shocks in order to reduce numerical diffusion.

In the second part, we introduced a model for a 2×2 junction with an onramp and an offramp. The onramp is modeled by an ODE which represent a vertical buffer. This way of handling boundary conditions makes possible not to lose flow information. The junction flow distribution is solved through a LP-optimization problem, which maximizes the flow in the outgoing mainline. Moreover, a right-of-way parameter is introduced to ensure the uniqueness of the solution and a good representation of field experiences. The model is solved numerically using a modified Godunov scheme that takes into account the waves that can be produced when the buffer empties. Some numerical tests are presented to show the stability and accuracy of the scheme. Moreover, from the analysis of the $\mathcal{L}^1$ error, the convergence of the scheme is demonstrated numerically. We then applied the discrete adjoint approach to the coupled PDE-ODE system to select an optimal ramp-metering strategy on a road network.

Moreover on Chapter 4 we extend the PDE-ODE model to optimize traffic flow on roundabouts. We treat the roundabout as a concatenation of 2×2 junctions. We solve an optimization problem where the optimal control acts on the priority parameters, which assign right of way among incoming roads, for example through traffic lights. Two

cost functionals are introduced, measuring the total waiting time and total travel time. We compute analytically the cost functionals for a single junction, and find the control parameters that locally optimize the flow. The approach is tested on a simple roundabout with three incoming and three outgoing roads. Two different choices of parameters are considered: instantaneously locally optimal and fixed. The local optima outperform the other choice, improving the performances of the network.

Traffic flow modeling is a field in full development, yet many improvements could be achieved starting from the validation of the models to the creation of new models that can add more features. In particular, optimal control of traffic flow is a subject full of potential and a lot of work could be done in this setting to improve performances. Moreover, much work remains to be done to define a soundproof mathematical theory for optimal control of traffic flow which is broadly applicable to hyperbolic conservation laws and traffic flow applications.

Conclusion et perspectives

Dans ce travail, nous avons présenté deux modèles EDP-EDO pour décrire le trafic routier. Tout d'abord, nous avons mis en place un cadre mathématique pour le modèle des goulots d'étranglement mobiles sur les routes. L'EDP décrit l'évolution du trafic global et une EDO décrit la trajectoire du bus. Le problème de Riemann a été défini et résolu analytiquement. En outre, nous avons prouvé l'existence d'une solution pour des données générales BV et nous avons exploré une piste pour prouver la stabilité. Les travaux futurs vont concerner la recherche d'une stratégie efficace pour la question de la stabilité des solutions. Nous avons aussi montré deux approches différentes pour la solution numérique de cette classe de problèmes. Le premier calcule la densité à l'aide d'un schéma de type Godunov avec un maillage localement non uniforme. Ensuite, la position de l'autobus est reconstruite en prenant en compte les effets des interactions avec des ondes de densité comme dans [33]. Quelques tests numériques sont présentés pour montrer l'efficacité du schéma. Pour éviter de travailler avec un maillage adaptatif, nous nous sommes concentrés sur la conception un schéma conservatif basé sur une technique de reconstruction de chocs sur des maillages fixes, suivant l'approche introduite dans [17]. La méthode reconstruit les chocs non-classiques et classiques afin de réduire la diffusion numérique.

Dans la deuxième partie, nous avons présenté un modèle pour une jonction 2×2 avec une bretelle d'accès et une bretelle de sortie. La bretelle d'accès est modélisée par une EDO qui représente un "buffer" vertical. Cette façon de traiter les conditions aux limites permet de ne pas perdre des informations sur le flux en entrée. La répartition du trafic à la jonction est gérée par un problème d'optimisation, qui maximise le débit dans la voie principale sortante. En outre, un paramètre de priorité est introduit afin d'assurer l'unicité de la solution et une bonne représentation des expériences de terrain. Le modèle est résolu numériquement en utilisant un schéma Godunov modifié, qui prend en compte les ondes qui peuvent être produites lorsque le "buffer" se vide. Quelques tests numériques sont présentés pour montrer la stabilité et la précision du schéma. En outre, à partir de l'analyse de l'erreur $\mathcal{L}^1$, la convergence du schéma est démontrée numériquement. Nous avons ensuite appliqué la méthode de l'adjoint discret au système couplé EDP-EDO pour choisir une stratégie de contrôle d'accès optimal sur un réseau routier.

Dans le Chapitre 4, nous appliquons le modèle de jonction couplé EDP-EDO à l'optimisation du flux de trafic sur les ronds-points. Nous traitons le rond-point comme une concaténation des jonctions 2×2. Nous résolvons un problème d'optimisation où

le contrôle agit sur le paramètre de priorité, qui attribue un droit de passage entre les routes entrantes, par exemple par des feux de circulation. Les deux fonctions coût considérées mesurent le temps d'attente total et le temps total de parcours. Nous calculons explicitement les fonctions coût pour une seule jonction, et trouvons les paramètres de contrôle qui permettent d'optimiser localement le trafic. L'approche est testée sur un rond-point simple avec trois routes entrantes et trois routes sortantes. Deux choix différents de paramètres sont pris en compte: localement optimale en temps et fixe. On observe que les optima locaux sont plus performants pour améliorer les performances du réseau.

La modélisation du trafic routier est un domaine en plein développement, toutefois de nombreuses améliorations pourraient être réalisé à partir de la validation des modèles jusqu'à la création de nouveaux modèles ajoutant plus de fonctionnalités. En particulier, le contrôle optimal de la circulation routière est un sujet plein de potentiel et des efforts pourraient être faits dans ce cadre pour améliorer les performances. En outre, beaucoup de travail reste à faire pour développer une théorie mathématique du contrôle optimal de la circulation qui soit applicable aux lois de conservation hyperboliques et au trafic.

Bibliography

[1] E. Alberti and G. Belli. Contributions to the Boltzmann-like approach for traffic flow – A model for concentration dependent driving programs. *Transportation Research*, 12(1):33–42, 1978.

[2] D. Amadori, P. Baiti, P.G. Le Floch, and B. Piccoli. Non classical shocks and the Cauchy problem for non convex conservation laws. *Journal of Differential equations*, 151:345–372, 1999.

[3] B. Andreianov, P. Goatin, and N. Seguin. Finite volume schemes for locally constrained conservation laws. *Numer. Math.*, 115(4):609–645, 2010. With supplementary material available online.

[4] B. Andreianov, K. H. Karlsen, and N.H. Risebro. A theory of $\mathcal{L}^1$-dissipative solvers for scalar conservation laws with discontinuous flux. *Arch. Rational Mech. Anal.*, 201:27–86, 2011.

[5] A. Aw and M. Rascle. Resurrection of "second order" models of traffic flow. *SIAM J. Appl. Math.*, 60:916–938, 2000.

[6] P. Baiti, P.G. Le Floch, and B. Piccoli. Non classical shocks and the Cauchy problem. General conservation laws. *Contemporary Math.*, 238:1–25, 1999.

[7] P. Baiti, P.G. Le Floch, and B. Piccoli. Uniqueness of classical and nonclassical solutions for non linear hyperbolic systems. *J. Differential Equations*, 172:59–82, 2001.

[8] P. Baiti, P.G. Le Floch, and B. Piccoli. Existence theory for nonclassical entropy solutions: scalar conservation laws. *Z. Angew. Math. Phys.*, 55:927–945, 2004.

[9] M. K. Banda and M. Herty. Adjoint IMEX-based schemes for control problems governed by hyperbolic conservation laws. *Comput. Optim. Appl.*, 51:909–930, 2012.

[10] M. Bando, K. Hasebe, A. Nakayama, A. Shibata, and Y. Sugiyama. Dynamical model of traffic congestion and numerical simulations. *Physical Review E*, 51:1035–1042, 1995.

[11] C. Bardos, A. Y. le Roux, and J.-C. Nédélec. First order quasilinear equations with boundary conditions. *Comm. Partial Differential Equations*, 4(9):1017–1034, 1979.

[12] UC Berkeley and Path. Connected corridors. http://connected-corridors.berkeley.edu/, 2013.

[13] S. Blandin, D. Work, P. Goatin, B. Piccoli, and A. M. Bayen. A general phase transition model for vehicular traffic flow. *SIAM J. Appl. Math.*, 71(1):107–127, 2011.

[14] R. Borsche, R. M. Colombo, and M. Garavello. On the coupling of systems of hyperbolic conservation laws with ordinary differential equations. *Nonlinearity*, 23(11):2749–2770, 2010.

[15] R. Borsche, R.M. Colombo, and M. Garavello. Mixed systems: ODEs - balance laws. *Journal of Differential equations*, 252:2311–2338, 2012.

[16] F. Bouchut and F. James. One-dimensional transport equations with discontinuous coefficients. *Nonlinear Anal.*, 32(7):891–993, 1998.

[17] B. Boutin, C. Chalons, F. Lagoutière, and P. G. LeFloch. Convergent and conservative schemes for nonclassical solutions based on kinetic relations. I. *Interfaces and Free Boundaries*, 10(3):399–421, 2008.

[18] Mark Brackstone and Mike McDonald. Car-following: a historical review. *Transportation Research Part F: Traffic Psychology and Behaviour*, 2(4):181–196, 1999.

[19] A. Bressan. Unique solutions for a class of discontinuous differential equations. *Proc. Amer. Math. Soc.*, 104(3):772–778, 1988.

[20] A. Bressan. *Hyperbolic systems of conservation laws*, volume 20 of *Oxford Lecture Series in Mathematics and its Applications*. Oxford University Press, Oxford, 2000. The one-dimensional Cauchy problem.

[21] A. Bressan and R. M. Colombo. Unique solutions of 2×2 conservation laws with large data. *Indiana Univ. Math. J.*, 44(3):677–725, 1995.

[22] A. Bressan, G. Crasta, and B. Piccoli. Well-posedness of the Cauchy problem for $n \times n$ systems of conservation laws. *Mem. Amer. Math. Soc.*, 146(694):viii+134, 2000.

[23] A. Bressan and K. Han. Optimal and equilibria for a model of traffic flow. *SIAM J. Math. Anal.*, 43:2384–2417, 2011.

[24] A. Bressan and K. Han. Nash equilibria for a model of traffic flow with several group of drivers. *ESAIM: Control, Optim. Calc. Var.*, 18:969–986, 2012.

[25] A. Bressan and K. Han. Existence of optima and equilibria for traffic flow on networks. *Netw. Heterog. Media*, 8:627–648, 2013.

[26] A. Bressan, C.J. Liu, W. Shen, and F. Yu. Variational analysis of Nash equilibria for a model of traffic flow. *Quarterly Appl. Math.*, 70:495–515, 2012.

[27] A. Bressan and A. Marson. A variational calculus for discontinuous solutions of systems of conservation laws. *Comm. Partial Differential Equations*, 20(9):1491–1552, 1995.

[28] A. Bressan and K. T. Nguyen. Conservation law models for traffic flow on a network of roads. preprint, http://www.math.ntnu.no/conservation/2014/009.pdf, 2014.

[29] A. Bressan and W. Shen. Uniqueness for discontinuous ODE and conservation laws. *Nonlinear Anal.*, 34(5):637–652, 1998.

[30] A. Bressan and F. Yu. Continuous Riemann solvers for traffic flow at a junction. Discr. Cont. Dyn. Syst., preprint., 2014.

[31] Alberto Bressan and Philippe G. LeFloch. Structural stability and regularity of entropy solutions to hyperbolic systems of conservation laws. *Indiana Univ. Math. J.*, 48(1):43–84, 1999.

[32] G. Bretti, R. Natalini, and B. Piccoli. Numerical approximations of a traffic flow model on networks. *Networks and Heterogeneous Media*, 1(1):57, 2006.

[33] G. Bretti and B. Piccoli. A tracking algorithm for car paths on road networks. *SIAM Journal on Applied Dynamical Systems*, 7:510–531, 2008.

[34] A. Cascone, C. D'Apice, B. Piccoli, and L. Raritá. Optimization of traffic on road networks. *Mathematical Models and Methods in Applied Sciences*, 17:1587–1617, 2007.

[35] A. Cascone, R. Manzo, B. Piccoli, and L. Raritá. Optimization versus randomness for car traffic regulation. *Physical Review E*, 78, 2008.

[36] C. Chalons and P. Goatin. Godunov scheme and sampling technique for computing phase transitions in traffic flow modeling. *Interfaces and Free Boundariese*, 10(2):195–219, 2008.

[37] C. Chalons, P. Goatin, and N. Seguin. General constrained conservation laws. Application to pedestrian flow modeling. *Netw. Heterog. Media*, 8(2):433–463, 2013.

[38] C. Chalons and P.G. Le Floch. Computing undercompressive waves with the random choice method. Nonclassical shock waves. *Interfaces and Free Boundaries*, 5:129–159, 2001.

[39] R. E. Chandler, R. Herman, and E. W. Montroll. Traffic dynamics: Studies in car following. *Operations Research*, 6(2):165–184, 1958.

[40] Yacine Chitour and Benedetto Piccoli. Traffic circles and timing of traffic lights for cars flow. *Discrete and Continuous Dynamical Systems Series B*, 5(3):599, 2005.

[41] G.M. Coclite, M. Garavello, and B. Piccoli. Traffic flow on a road network. *SIAM J. Math. Anal.*, 36(6):1862–1886, 2005.

[42] R. M. Colombo. Hyperbolic phase transitions in traffic flow. *SIAM J. Appl. Math.*, 63(2):708–721, 2002.

[43] R. M. Colombo and P. Goatin. A well posed conservation law with a variable unilateral constraint. *J. Differential Equations*, 234(2):654–675, 2007.

[44] R. M. Colombo, P. Goatin, and B. Piccoli. Road network with phase transition. *Journal of Hyperbolic Differential Equations*, 07(01):85–106, 2010.

[45] R. M. Colombo, P. Goatin, and F. Priuli. Global well posedness of a traffic flow model with phase transitions. *Nonlinear Anal. Ser. A*, 66:2413–2426, 2007.

[46] R. M. Colombo and A. Marson. A Hölder continuous ODE related to traffic flow. *Proc. Roy. Soc. Edinburgh Sect. A*, 133(4):759–772, 2003.

[47] A. Cutolo, C. D'Apice, and R. Manzo. Traffic optimization at junctions to improve vehicular flows. *ISRN Applied Mathematics*, 2011:19, 2011.

[48] A. Cutolo, B. Piccoli, and L. Raritá. An upwind-Euler scheme for an ODE-PDE model of supply chains. *SIAM J. Sci. Comput.*, 33(4):1669–1688, 2011.

[49] C.M. Dafermos. *Hyperbolic Conservation Laws in Continuum Physics.* Springer, 2009.

[50] C.F. Daganzo. The cell transmission model: A dynamic representation of highway traffic consistent with the hydrodynamic theory. *Transportation Research Part B*, 28:269–287, 1994.

[51] C.F. Daganzo. Requiem for high-order fluid approximations of traffic flow. *Transportation Research Part B*, 29(4):277–287, 1994.

[52] C.F. Daganzo and J. A. Laval. Moving bottlenecks: A numerical method that converges in flows. *Transportation Research Part B*, 39:855–863, 2004.

[53] C.F. Daganzo and J. A. Laval. On the numerical treatement of moving bottlenecks. *Transportation Research Part B*, 39:31–46, 2005.

[54] C. D'Apice, S. Göttlich, M. Herty, and B. Piccoli. *Modeling, simulation, and optimization of supply chains: a continuous approach.* SIAM, 2010.

[55] M. L. Delle Monache and P. Goatin. Scalar conservation laws with moving density constraints arising in traffic flow modeling. Technical report, Inria Research Report, n. 8119, 2012.

[56] M. L. Delle Monache and P. Goatin. A front tracking method for a strongly coupled PDE-ODE system with moving density constraints in traffic flow. *Discrete Contin. Dyn. Syst. Ser. S*, 7(3):435–447, 2014.

[57] M. L. Delle Monache and P. Goatin. Scalar conservation laws with moving constraints arising in traffic flow modeling: an existence result. *Journal of Differential equations*, 2014. DOI:10.1016/j.jde.2014.07.014.

[58] M. L. Delle Monache, J. Reilly, S. Samaranayake, W. Krichene, P. Goatin, and A. M. Bayen. A PDE-ODE model for a junction with ramp buffer. *SIAM Journal on Applied Mathematics*, 74(1):22–39, 2014.

[59] L. C. Edie. Car-following and steady-state theory for noncongested traffic. *Operations Research*, 9(1):66–76, 1961.

[60] V. V. Filippov. *Ordinary differential equations with discontinuous right-hand sides*, volume 30. Kluwer academic Publisher, 1994.

[61] A. Fügenschuh, S. Göttlich, M Herty, A Klar, and A. Martin. A discrete optimization approach to large scale supply networks based on partial differential equations. *SIAM J. Sci. Comput.*, 30(3):1490–1507, 2008.

[62] A. Fügenschuh, M. Herty, A. Klar, and A. Martin. Combinatorial and continuous models for the optimization of traffic flows on networks. *SIAM J. Optim.*, 16(4):1155–1176, 2006.

[63] M. Garavello and P. Goatin. The Aw-Rascle traffic model with locally constrained flow. *J. Math. Anal. Appl.*, 378(2):634–648, 2011.

[64] M. Garavello and P. Goatin. The Cauchy problem at a node with buffer. *Discrete Contin. Dyn. Syst.*, 32(6):1915–1938, 2012.

[65] M. Garavello, R. Natalini, B. Piccoli, and A. Terracina. Conservation laws with discontinuous flux. *Netw. Heterog. Media*, 1(3):159–179, 2007.

[66] M. Garavello and B. Piccoli. Traffic flow on a road network using the Aw-Rascle model. *Comm. Partial Differential Equations*, 31:243–275, 2006.

[67] M. Garavello and B. Piccoli. *Traffic flow on networks*, volume 1 of *AIMS Series on Applied Mathematics*. American Institute of Mathematical Sciences (AIMS), Springfield, MO, 2006. Conservation laws models.

[68] M. Garavello and B. Piccoli. Conservation laws on complex networks. *Ann. Inst. H. Poincaré Anal. Non Linéaire*, 26(5):1925–1951, 2009.

[69] I. Gasser, C. Lattanzio, and A. Maurizi. Vehicular traffic flow dynamics on a bus route. *Multiscale Model. Simul.*, 11(3):925–942, 2013.

[70] D. C. Gazis, R. Herman, and R. W. Rhotery. Nonlinear follow-the-leader models of traffic flow. *Operations Research*, 9(4):545–567, 1961.

[71] R. Giering and T. Kaminski. Recipes for adjoint code contruction. *ACM Transactions on mathematical software*, 24(4):437–474, 1998.

[72] M. Giles and S. Ulbrich. Convergence of linearized and adjoint approximations for discontinuous solutions of conservation laws. part 1: linearized approximations and linearized output functionals. *SIAM J. Numer. Anal.*, 48(3):882–904, 2010.

[73] M. Giles and S. Ulbrich. Convergence of linearized and adjoint approximations for discontinuous solutions of conservation laws. part 2: Adjoint approximations and extensions. *SIAM J. Numer. Anal.*, 48(3):905–921, 2010.

[74] M. B. Giles and N. A. Pierce. An introduction to the adjoint approach to design. *Flow, turbulence and combustion*, 65(3-4):393–415, 2000.

[75] F. Giorgi. *Prise en compte des transports en commun de surface dans la modélisation macroscopique de l'écoulement du trafic.* PhD thesis, Institut National des Sciences Appliquées de Lyon, 2002.

[76] F. Giorgi, L. Leclercq, and J. B. Lesort. A traffic flow model for urban traffic analysis: extensions of the LWR model for urban and environmental applications. In *Proceeding of the 15th International Symposium on Transportation and Traffic Theory*, pages 393–416, 2002.

[77] P. Goatin. The Aw-Rascle traffic flow model with phase transition. *Math. Comput. Modeling*, 44:287–303, 2006.

[78] P. Goatin. Analyse et approximation numérique de quelques modès macroscopiques de trafic routier. HDR Thesis, May 2009.

[79] S.K. Godunov. A finite difference method for the numerical computation of discontinuous solutions of the equations of fluid dynamics. *Matematicheskii Sbornik*, 47:271–290, 1959.

[80] S. Göttlich, M. Herty, and A. Klar. Network models for supply chains. *Comm. Math. Sci.*, 3(4):545–559, 2005.

[81] S. Göttlich, M. Herty, and U. Ziegler. Modeling and optimizing traffic light settings on road networks. preprint, 2013.

[82] B. D. Greenshields. A study of traffic capacity. *Proc. Highway Res. Bd.*, 14:448, 1935.

[83] M. Gugat, M. Herty, A. Klar, and G. Leugering. Optimal control for traffic flow networks. *Journal of optimization theory and applications*, 126(3):589–616, 2005.

[84] B.T. Hayes and P.G. Le Floch. Nonclassical shocks and kinetic relations. scalar conservation laws. *Arch. Rational Mech. Anal.*, 139:1–56, 1997.

[85] B.T. Hayes and P.G. Le Floch. Nonclassical shockwaves and kinetic relations. strictly hyperbolic systems. *SIAM J. Math. Anal.*, 31:941–991, 2000.

[86] V. Henn and L. Leclercq. Wave tracking resolution scheme for bus modelling inside the LWR traffic flow model. In *Proceedings of the 5th Triennial Symposium on Transportation Analysis*, 2004.

[87] R. Herman, E. W. Montroll, R. B. Potts, and R. W. Rothery. Traffic dynamics: analysis of stability in car following. *Operations research*, 7(1):86–106, 1959.

[88] M. Herty, C. Kirchner, and A Klar. Instantaneous control for traffic flow. *Mathematical Methods in the Applied Sciences*, 30(2):153–169, 2006.

[89] M Herty and A Klar. Modeling, simulation, and optimization of traffic flow networks. *SIAM Journal on Scientific Computing*, 25(3):1066–1087, 2003.

[90] M. Herty and A. Klar. Simplified dynamics and optimization of large scale traffic flow networks. *Mathematical Models and Methods in Applied Sciences*, 14(4):579–601, 2004.

[91] M. Herty, A. Klar, and B. Piccoli. Existence of solutions for supply chains models based on partial differential equations. *SIAM J. Math. Anal.*, 39(1):160–173, 2007.

[92] M. Herty, A. Klar, A.K. Singh, and P. Spellucci. Smoothed penalty algorithms for optimization of nonlinear models. *Comput. Optim. Appl.*, 37:157–176, 2007.

[93] M. Herty, J. Lebacque, and S. Moutari. A novel model for intersections of vehicular traffic flow. *Netw. Heterog. Media*, 4:813–826, 2009.

[94] M. Herty, S. Moutari, and Rascle A. Optimization criteria for modelling intersections of vehicular traffic flow. *Netw. Heterog. Media*, 1:275–294, 2006.

[95] H. Holden and N.H. Risebro. A mathematical model of traffic flow on a network of unidirectional roads. *SIAM J. Math. Anal.*, 26:999–1017, 1995.

[96] D. Jacquet, C. Canudas de Wit, and D. Koenig. Optimal ramp metering strategy with extended LWR model, analysis and computational methods. In *Proceedings of the 16th IFAC world congress*, 2005.

[97] C. Kirchner, M. Herty, S. Göttlich, and A. Klar. Optimal control for continuous supply network models. *Networks and Heterogeneous Media*, 1(4):675–688, 2006.

[98] A. Kotsialos and M. Papageorgiou. Nonlinear optimal control applied to coordinated ramp-metering. *IEEE Transactions on Control Systems Technology*, 12(6):920–933, 2004.

[99] S. N. Kružhkov. First order quasilinear equations with several independent variables. *Mat. Sb. (N.S.)*, 81 (123):228–255, 1970.

[100] C. Lattanzio, A. Maurizi, and B. Piccoli. Moving bottlenecks in car traffic flow: a PDE-ODE coupled model. *SIAM J. Math. Anal.*, 43(1):50–67, 2011.

[101] P. Lax. Hyperbolic systems of conservation laws II. *Commun. Pure Appl. Math.*, 6:231–258, 1957.

[102] P. G. Le Floch. Explicit formula for scalar non-linear conservation laws with boundary condition. *Mathematical Methods in the Applied Sciences*, 10(3):265–287, 1988.

[103] P. G. Le Floch. *Hyperbolic systems of conservation laws. The theory of classical and noncalssical shockwaves.* Lectures in mathematics ETH Zürich. Birkhäuser, 2002.

[104] P.G. Le Floch. Propagating phase boundaries: formulation of the problem and existence via the Glimm scheme. *Arch. Rational Mech. Anal.*, 123:153–197, 1993.

[105] P.G. Le Floch and M. Shearer. Non classical Riemann solvers with nucleation. *Proc. Roy. Soc. Edinburgh Sect. A*, 134:941–964, 2004.

[106] J.-P. Lebacque. The Godunov scheme and what it means for first order traffic flow models. *Transportation and Traffic Theory*, pages 647–678, 1996.

[107] J.-P. Lebacque, J. B. Lesort, and F. Giorgi. Introducing buses into first-order macroscopic traffic flow models. *Transportation Reasearch Record*, 1644:70–79, 1998.

[108] L. Leclercq, S. Chanut, and J. B. Lesort. Moving bottlenecks in the LWR model: a unified theory. In *Proceedings of the 83rd Transportation Research Board Annual Meeting (TRB)*, 2004.

[109] R.J. LeVeque. *Numerical Methods for Conservation Laws.* Lectures in mathematics ETH Zürich. Birkhäuser, 1992.

[110] R.J. LeVeque. *Finite Volume Methods for Hyperbolic Problems.* Cambridge Texts in Applied Mathematics. Cambridge University Press, 2002.

[111] M. J. Lighthill and G. B. Whitham. On kinematic waves. II. A theory of traffic flow on long crowded roads. *Proc. Roy. Soc. London Ser. A*, 229:317–346, 1955.

[112] A. Marigo and B. Piccoli. A fluid dynamic model for T-junctions. *SIAM Journal on Mathematical Analysis*, 39(6):2016–2032, 2008.

[113] P. Moin and T. Bewley. Feedback control of turbulence. *Applied mechanics reviews*, 47(6S):S3–S13, 1994.

[114] J.-D. Müller and P. Cusdin. On the performance of discrete adjoint CFD codes using automatic differentiation. *International journal for numerical methods in fluids*, 47(8-9):939–945, 2005.

[115] P. Munjal and J. Pahl. An analysis of the Boltzmann-type statistical models for multi-lane traffic flow. *Transportation Research*, 3(1):151 – 163, 1969.

[116] A. Muralidharan, G. Dervisoglu, and R. Horowitz. Freeway traffic flow simulation using the link node cell transmission model. In *American Control Conference*, 2009.

[117] A. Muralidharan and R. Horowitz. Optimal control of freeway networks based on the link node cell transmission model. In *American Control Conference (ACC)*, 2012.

[118] L. L. Obsu, M. L. Delle Monache, P. Goatin, and S. M. Kassa. Macroscopic traffic flow optimization on roundabouts. Technical report, Inria Research Report, n. 8291, April 2013.

[119] L. L. Obsu, M. L. Delle Monache, P. Goatin, and S. M. Kassa. Traffic flow optimization on roundabout. *Mathematical Methods in the Applied Sciences*, to appear. http://hal.inria.fr/docs/00/93/99/85/PDF/roundabout.pdf.

[120] M. Papageorgiou, H. Hadj-Salem, and J. M. Blosseville. ALINEA: A local feedback control law for on-ramp metering. *Transportation Research Board*, 1320:58–64, 1991.

[121] S.L. Paveri-Fontana. On Boltzmann-like treatments for traffic flow: A critical review of the basic model and an alternative proposal for dilute traffic analysis. *Transportation Research*, 9(4):225–235, 1975.

[122] H. J. Payne. Models of freeway traffic and control. In Math. Models Publ. Sys., editor, *Simulation Council Proc.*, volume 28, pages 51–61, 1971.

[123] I. Prigogine and F. C. Andrews. A Boltzmann-like approach for traffic flow. *Operations Research*, 8(6):789–797, 1960.

[124] I. Prigogine and R. Herman. Kinetic theory of vehicular traffic. Technical report, American Elsevier, 1971.

[125] J. Reilly, W. Krichene, M. L. Delle Monache, S. Samaranayake, P. Goatin, and A. M. Bayen. Adjoint-based optimization on a network of discretized scalar conservation law PDEs with applications to coordinated ramp metering. preprint, http://hal.inria.fr/docs/00/87/84/69/PDF/adjoint.pdf, 2014.

[126] J. Reuther, A. Jameson, J. Farmer, L. Martinelli, and D. Saunders. *Aerodynamic shape optimization of complex aircraft configurations via an adjoint formulation.* Research Institute for Advanced Computer Science, NASA Ames Research Center, 1996.

[127] P. I. Richards. Shock waves on the highway. *Operations Research*, 4:42–51, 1956.

[128] A. Schadschneider and M. Schreckenberg. Cellular automaton models and traffic flow. *J. Phys. A Math. Gen.*, 26:L679–L683, 1993.

[129] D. Schrank, B. Eisele, and T. Lomax. The 2012 urban mobility report. Technical report, Texas Transportation Institute, 2012.

[130] G. B. Whitham. *Linear and nonlinear waves*. John Wiley & Sons, Ltd, 1999.

[131] X. Zhong, T. Y. Hou, and P. G. LeFloch. Computational methods for propagating phase boundaries. *Journal of Computational Physics*, 124:192–216, 1996.